UNIVERSITY OF SOUTHAMPTON

Development and application of a three-dimensional water quality model in a partially-mixed estuary, Southampton Water, UK

by

Lei Shi

Thesis submitted to the University of Southampton
For the degree of Doctor of Philosophy

School of Ocean and Earth Science
Faculty of Science

March 2000

UNIVERSITY OF SOUTHAMPTON

ABSTRACT

FACULTY OF SCIENCE
SCHOOL OF OCEAN AND EARTH SCINECE

Doctor of Philosophy

DEVELOPMENT AND APPLICATION OF A THREE-DIMENSIONAL WATER QUALITY MODEL IN A PARTIALLY-MIXED ESTUARY, SOUTHAMPTON WATER, UK

by Lei Shi

The aim of this research was to develop a 'transportable' water quality model for the Solent and Southampton Water estuarine system, as a part of an effort to examine the effects of human activity and natural processes on estuarine water quality. Dissolved oxygen (DO), as a main indicator of water quality, is influenced by physical, chemical and biological processes, and has been chosen as the core parameter to link the different processes to be modelled.

Monthly surveys of DO, planktonic community respiration rates and other water quality parameters (temperature, salinity, chlorophyll, suspended particulate matter, inorganic nutrients etc.) in the Itchen Estuary and Southampton Water were conducted from January 1998 to April 1999. DO data shows that Southampton Water is a relatively healthy estuary, despite receiving considerable loads of oxygen demanding organic sewage effluent discharged from a number of points. A persistent moderate DO sag (DO saturation > 80%) was observed in the upper Itchen Estuary throughout the year. In the lower Itchen Estuary and Southampton Water, the waters were DO saturated during the non-phytoplankton growth season. Surface DO supersaturation was observed during the phytoplankton growth season especially during algal blooms, but no severe DO depletion was detected following the bloom collapse. Community respiration rates maintained a substantial level in the upper Itchen estuary, while in the lower estuary respiration rates were low during the non-phytoplankton season and increased during the phytoplankton growth season. It is suggested that the high winter respiration rate in the upper Itchen Estuary are sustained by inputs from external sources (rivers, sewage and industrial effluents) and that the summer increase in the lower estuary is a consequence of phytoplankton photosynthesis. Nutrients in the Itchen Estuary and Southampton Water show mainly conservative behaviour in a plot of nutrient concentration against salinity. The removal of the nutrients by phytoplankton activity occurred at high salinities during the spring to summer period.

A 3-D finite element baroclinic hydrodynamic model with two-equation q^2-q^2l turbulence closure has been developed including a mass conservation scheme. The model successfully simulated the tides, tidal currents, and estuarine circulation in the Southampton Water and Solent estuarine system. The modelled tidal induced residual currents and water mass transportation in Southampton Water and the Solent have been examined. Model results show the existence of a predominant westward tidal induced residual current in the Solent. The tidal induced residual water mass transport is extremely limited in Southampton Water, except near the entrance to Southampton Water, where it joins the Solent. The estuarine circulation with surface, seaward flowing fresher water and bottom, landward flowing saltier water provides the main mechanism for water mass transport in the model. The short residence time of waters in the estuary estimated from the survey salinity data confirmed how effective the estuarine circulation is for sea water from the Solent to replace the water within Southampton Water. The trapping effect of estuarine circulation is also crucial for the water quality in the estuary.

A water quality model has been developed and coupled with the 3-D hydrodynamic model. The water quality model consists of an external (dissolved oxygen-biochemical oxygen demand) model, which models the direct impact of external inputs (riverine discharge, domestic and industrial effluents) to the water quality, and an internal model, which simulates the impact of local estuarine phytoplankton growth on the water quality. DO and dissolved inorganic nutrients are the 'link substances' between the external model and internal model. The integrated water quality model output has been compared against the survey data for 1998, and has been shown to reproduce the spatial and temporal change in oxygen, nutrients, chlorophyll and planktonic respiration in Southampton Water.

Acknowledgements

Firstly I would like to thank my supervisor Dr. Duncan A. Purdie, for his excellent supervision and guidance and support throughout the duration of my PhD study. Without his support, it would have been impossible to overcome some of the unforeseen non-academic barriers and difficulties experienced during the past three years.

I wish to thank to Dr. Neil Wells for his kind support and constructive criticism, Professor Stephen Hawkins for his encouragement, Professor Paul Tett for his wise advice during our conversations about the microbiological model and parameterisation during the trip to Qingdao, China.

Many thanks to Dr. David Hydes, Sue Holley, of SONUS project for being able to conduct the survey, for the sharing of the data, and Jian Xiong for the days on the rough Southampton Water. I am also grateful to all staff in the Department of Oceanography (now School of Ocean and Earth Science) for their help, especially the technicians and skipper of the Bill Conway.

I would like to thank the British tax-payers for their financial support of the QUID project.

I would also like to thank all UK experts and OUQ staff who were involved in the QUID project especially, project director Mr. Paul Dempsey from WRc, Dr. Gong Yang from WRc, Dr. Jonathan Sharples from SOES, Mrs Jackie Graham from the Environmental Science Centre, Professor Wu, Professor Sun, Professor Xi, and Professor Yu from Ocean University of Qingdao.

Finally, I would like to say special thanks to my family and my wife for their patience, love and support.

Contents list

List of figures

List of tables

Chapter 1 Introduction

Coastal waters throughout the world are subjected to a whole series of human impacts which can lead to their degradation and in extreme cases total ecosystem collapse. Semi-enclosed water bodies such as estuaries are particularly vulnerable suffering from both acute incidents such as oil spills and more chronic pollution from industries and dense populations. Historically, estuaries have been used as a route for disposal of untreated domestic sewage and industrial wastes. More recently these impacts have lessened as pollution controls have been put in place in response to greater environmental awareness. In order to manage water quality of estuaries and maintain ecosystem function, it is necessary to know both the underlying physical processes affecting dispersion of material disposed and the chemical and biological processes that reduce/breakdown non-conservative pollutants.

Estuaries have been prone to problems of low oxygen caused by oxygen demanding human and industrial wastes and the accumulation of organic matter produced by the aquatic plants stimulated by nutrient enrichment (eutrophication). The overall aim of this thesis is to model the physical conditions of an estuary, Southampton Water, and to couple this with a model of water quality.

Southampton Water is an ideal system for such studies because:

1) As a partially-mixed estuary with complex bathymetry it presents a significant challenge to establish a new hydrodynamic model and validate it.
2) Southampton Water is a typical estuarine environment, combining a natural ecosystem with considerable human impact. The system receives a significant nutrient input from riverine discharge and sewage effluents within the catchment area. Regular occurrence of red-tide, phytoplankton blooms have been reported in the estuary causing hypoxia in bottom water during the summer.
3) There is reasonable amount of historical data from Southampton Water and the Solent estuarine system.
4) The recent SOuthern NUtrient Study (SONUS) project provided a platform to carry out a systematic survey of the estuary to collect water quality data, and it also provided access to a shared data base.

1.1 Dissolved oxygen, as an indicator of water quality

Water has the capability to dissolve a certain amount of oxygen and oxygen solubility in sea water is a function of temperature, salinity and pressure (Weiss, 1970; UNESCO, 1973; Riley & Skirrow, 1975; HMSO, 1980). Dissolved oxygen (DO), as a main indictor of the water quality, is very important to aquatic plants and animals. Oxygen deficiency (hypoxia) in sea water may alter the aquatic ecosystem in an undesirable direction. Severe reduction in the DO

concentration to relatively low levels can cause the death of fish and benthic organisms (Officer et al., 1984). Motile organisms may avoid areas of low DO (Gameson, et al., 1973; Officer et al., 1984), for example Salmon will not enter rivers with low oxygen level (Hays, 1988).

Effects of oxygen depletion on benthic organisms can be severe. Howell & Simpson (1994) examined the relationship between bottom DO with catch (finfish, lobster and squid) for effects on abundance of species, numbers of species, and mean length for sites throughout western Long Island Sound. Both species abundance and diversity decreased markedly with bottom DO, with dramatic declines at sites where DO < 2 mg l^{-1}. Similar work on the effects of low DO or hypoxia (< 2 mg l^{-1}) on macrobenthic infaunal community structure and composition in the lower Chesapeake Bay was reported by Dauer et al. (1992). Macrobenthic communities at hypoxia-affected stations were characterised by lower species diversity, low biomass, a lower proportion of deep-dwelling biomass (deeper than 5 cm in the sediment), and change in community composition. Higher dominance in density and biomass of opportunistic species and lower dominance of equilibrium species were observed at hypoxia-affected stations.

In extreme conditions of total oxygen depletion (anoxia), the ecosystem will totally collapse, and the waters become 'dead' with an unpleasant smell from hydrogen sulphide. Since DO is crucial for marine life, there are water quality standards for DO concentration. For example in China, the DO water quality standard for marine sanctuaries and reserves is 5 mgl^{-1}, and the water quality standards outlined by Batelle (1971) recommend that DO concentration should not fall below 4 mgl^{-1} in estuaries and tidal tributaries for the protection of biological resources.

In a healthy water body, the DO is almost saturated. The main cause of DO consumption is oxidation of oxygen-demanding organic matter, and the quantity of DO consumption by organic matter in natural waters was first discussed by Richards (1965). Using the average atomic C:N:P ratio (106:16:1) for marine plankton (Fleming, 1940), and assuming the oxidation state of carbon to be that in carbohydrate i.e.-CH_2O, the amount of oxygen required for the oxidation of the hypothetical composition of plankton tissue $(CH_2O)_{106}(NH_3)_{16}H_3PO_4$ has been given. In waters containing dissolved free oxygen the microbial decomposition of organic debris is then represented by the following overall equation:

$$(CH_2O)_{106}(NH_3)_{16}H_3PO_4+138O_2 \Leftrightarrow 106CO_2+122H_2O+16HNO_3+H_3PO_4.$$

In this reaction oxidation of 1 mol C carbon demands 1 mol O_2 oxygen and oxidation of 1 mol N nitrogen demands 1 mol O_2 oxygen.

If the oxidation of oxygen-demanding material consumes the free oxygen in a water body too rapidly for oxygen replacement, e.g. from the atmosphere or adjacent waters, the DO falls and when it reaches 10% of saturation the oxidation of NH_3 ceases. When it drops further, many aquatic animals die, adding to the oxygen-demanding organic matter load and eventually the water becomes anoxic. Anaerobic bacteria then develop and absorb oxygen, first from NO_3^-

reducing it through NO_2^- to NH_3 or N_2. Finally oxygen is removed from SO_4^{2-} reducing it to H_2S which combines with iron oxides to form FeS and when the available iron is exhausted, H_2S is liberated. When toxic H_2S spreads through the water column all animals die.

It has been suggested (Head, 1976) that in practice the rate of DO consumption does not proceed quickly enough to exceed the supply of oxygen from surrounding water masses and the atmosphere. Under certain circumstances, hypoxia, anoxia and complete removal of DO can occur. These conditions usually result from a contribution of poor water exchange and high organic loading stimulated by nutrient discharge or direct input from riverine and sewage effluents. A report by Malakoff (1998) has shown that oxygen-starved coastal 'dead zones' spawned by human activity have tripled in number world-wide in the last 30 years (and the report does not include the developing countries like China).

The extent of estuarine pollution (DO depletion) by organic matter from sewage effluents and other sources is highly variable. There are several well documented examples: the Thames (Barrett, 1972; Gameson et al., 1975; Head, 1976); the Mersey Estuary (National Rivers Authority, 1995; Hawkins et al., 1999); Baltic Sea (Dybern, 1972; Rosenberg, 1990); Chesapeake Bay (Taft et al., 1980; Officer et al., 1984; Kuo & Neilson, 1987; Kemp, et al., 1992).

The Thames is a very important estuarine system in the UK, it flows through the city of London, one of the most heavily populated areas in the world. Well constructed sewer system discharged untreated sewage into the river from the early 19th century, and by the 1850s the river had became foul smelling and devoid of fish (Gameson, et al., 1973). Although sewage treatment plants began to be operational from the late 19th century, the rapid population growth overran the capacity of the sewage treatment system, and by the 1950's, 30 km of the Thames through London was anoxic in the dry season, and no fish were present for a distance of 70 km (Barrett, 1972).

The Mersey Estuary is probably the most polluted estuary in Europe (National Rivers Authority, 1995). It drains a heavily populated and industrialised area of 13,000 km^2. Pollution of the estuary is a long-standing problem with its roots going back to the days of the industrial revolution in the 18th century. Pollution of the Mersey can be attributed to inadequate sewage treatment facilities, intermittent discharges from combined sewer overflows, industrial discharges, and runoff from agriculture and contaminated land. As long ago as 1865, the government of the day recognised that the problems of pollution created by new industries and their supporting population were severe. In more recent times, the extent of pollution from discharges into the estuary has been reduced as a result of de-industrialisation of the whole catchment and multi-million pound investment in sewage treatment and the sewerage infrastructure. The quality status of the Mersey Estuary is still classified as poor, with a

pronounced DO sag observed throughout most of the estuary and in the upper estuary, anoxia occurs during summer.

Oxygen depletion and anoxia is not restricted to small embayments, but also impacts very large sea areas; the Baltic is naturally oligotrophic (it has small natural organic input and low production), but receives a large quantity of organic waste and shows some sign of eutrophication. As much as one third of the sea floor of the Baltic is now subject to permanent hypoxia, with many regions suffering low oxygen tension on a seasonal basis (Janson, 1972; Rosenberg et al., 1990).

Sometimes the initiation and consequences of DO depletion are linked in an unexpected way. American scientists have traced the origins of a vast hypoxic region in the Gulf of Mexico to inland farmers, living thousands kilometers away, who use fertilizers extensively. The Gulf of Mexico has suffered a long term hypoxic zone near the shore of Louisiana and the delta of Mississippi River, since the early 1970s. The shrimp fishing industry has collapsed since then and scientists have traced the origin of this vast hypoxic region in the Gulf to inland fertiliser use (Malakoff, 1998). The research carried out by Rabalis (1994, 1996) and her colleagues show that a hypoxic zone is a feature of the Mississippi plume. It starts early each year when melting snow and spring rain wash nutrients (nitrate and phosphate) off the land into the river. Except during drought years, the warmer, lighter river plume spills dozens of kilometres outward into the gulf, sliding over the heavier and saltier ocean water, forming a lid like layer. Fuelled by sunlight and dissolved nitrogen, massive algal blooms thrive near the surface, attracting zooplankton that graze on the phytoplankton. Detritus from plankton sink to the bottom, where it is devoured by oxygen-consuming bacteria. Hypoxia sets in when oxygen levels fall below 2 mg l^{-1}, a level that fails to support most marine life; anoxia occurs when the bacteria use up all the oxygen.

A similar seasonal deoxygenation of bottom water and supersaturation of surface water has been detected in the upper Adriatic Sea (Justic, 1987; Vollenweider et al., 1992), where river input and coastal discharges are probably responsible for these conditions.

Johannessen and Dahl (1996) present data on long term trends in the extend and severity of hypoxia along the Norwegian coast of the Skagerrak. Seasonally adjusted oxygen concentrations have declined at all depths over the past 30-40 years, with declines in surface waters beginning in the 1960s. Development of chronic anoxia in deeper waters appeared to be more delayed, dependent on longer-term increases in inputs from surface production, but has subsequently been more severe.

Even a relatively healthy estuary like Southampton Water, may show a DO sag after collapse of phytoplankton blooms such as the annual summer *Mesodinium rubrum* bloom (Rees & Williams, 1982; Soulsby et al., 1984; Crawford et al., 1997).

1.2 DO, an integration of different factors and processes

The level of DO in water is influenced by a combination of different processes, such as re-aeration from the atmosphere, the physical processes of advection and mixing, planktonic community respiration and free oxygen release by algal photosynthesis. In all cases the DO budget is affected by the combination of two or more physical and biological processes.

Atmospheric re-aeration is the main source of free DO, and when water is calm without biological activity, the water will reach its full saturation condition through re-aeration. DO saturation varies with the temperature, salinity and pressure, and empirical equations can be used to predict DO saturation partial pressure (Weiss, 1970; UNESCO, 1973; Riley & Skirrow, 1975; HMSO, 1980) and re-aeration rate (Liss, 1973; Hartman & Hammond, 1985; Wanninkhof, 1992; D'Avanzo & Kremer 1994) which is related to vertical turbulence, mixing coefficient, advection exchange and surface roughness. With the presence of oxygen demanding organic matter, when DO consumption exceeds the supply of free oxygen from the surrounding water mass and the atmosphere, hypoxia or even anoxia may occur.

To define the balance of DO in estuarine, and coastal waters, the effects of physical processes like advection and mixing must be considered. Stratification of the water column is a factor preventing the DO rich surface water mixing with water below the pycnocline.

The Baltic Sea is a large fjord with a shallow narrow entrance. Inside the entrance there are a series of basins, as in the Landsort Deep (459 m), of considerable depth. The shallow entrance to the Baltic Sea restricts the refresh and exchange of bottom waters. There is much fresh water entering the Baltic Sea, so the surface salinity is quite low and the surface water is separated from deeper, more saline water by a halocline. The halocline is so sharp that the wind mixing and winter cooling at the surface are unable to breakdown the halocline, and exchange between surface and deep water is hampered. Since the halocline in the Baltic Sea is permanent, the bottom water is low in DO concentration. The hydrographical conditions in the Baltic Sea (Report of the ICES Working Group on Pollution of the Baltic Sea, 1970) make it extremely vulnerable and sensitive to loading of organic oxygen demanding matter either form internal or external input.

Vertical stratification is mainly caused by either fresh water runoff or surface solar heating, and sometimes both. Vertical stratification intensified by surface solar heating can influence seasonal changes of DO. Research conducted by Kemp et al. (1992) found that seasonal oxygen depletion in Chesapeake Bay was driven by summer stratification when bottom oxygen depleted (due to plankton respiration) water was prevented from mixing with the upper water layers.

Uranouchi Bay, Japan, is a semi-enclosed silled inlet, with summer stratification and weak tidal water exchange. Munekage and Kimura (1990, 1992, 1995) reported that the anoxic

water mass in the lower layer forms with the cessation of DO transport from the upper layer due to a reduction in vertical mixing from June to July, combined with an increase in DO consumption rate and a decrease in DO production by phytoplankton. In the lower layer, most of the DO produced by phytoplankton and transported by tidal exchange is consumed in midsummer, owing to the high respiration activity.

Periodic reoxygenation is closely related to estuarine circulation and spring-neap tidal mixing. Hypoxia and anoxia in bottom waters of the Rappahannock, a tributary estuary of Chesapeake Bay, was observed to persist throughout the summer in the deep basin near the river mouth. The DO in surface waters was always near or at saturation level, while bottom waters exhibited a characteristic spatial pattern. A study conducted by Kuo (1991) revealed that both oxygen demand, either benthic or water column demand, and vertical mixing controlled the longitudinal location of the DO minimum. The strength of gravitational circulation is also shown to affect the occurrence of hypoxia. The initial DO deficiency of bottom water entering an estuary has a strong effect on DO concentration near the mouth of Rappahannock River but the effect diminishes towards the fresher water.

For most estuaries receiving high loading of organic waste, the water mass exchange is crucial to maintain estuarine water quality. An estuary with stronger circulation tends to have less chance for hypoxia to occur. Estuarine circulation normally occurs with fresher water flowing out of the estuary and oxygen saturated saltier water entering the estuary to replace the oxygen depleted bottom water. An estuary with substantial fresh water discharge is unlikely to be subject to serious DO depletion unless there are physical obstacles blocking the development of estuarine circulation or the saltier water entering the estuary is already DO depleted.

Water mass transportation and water mass exchange can be increased radically by tidal currents. Water mass transportation can be estimated by tidally induced Lagrangian residual currents (Longuet-Higgins, 1969; Cheng, et al., 1986), rather than the conventional Eulerian residual. The quantification of the water exchange ratio has been achieved by using the particle tracking method in numerical models (Awaji, 1980).

The hydrographical conditions of estuarine and coastal waters determine if the waters are vulnerable to the loading of oxygen demanding organic matter either directly from external sources or from accumulated organic matter produced by the local aquatic plant communities. Sometimes aerobic bacterial decomposition of large amounts of oxygen-demanding material, directly from sewage effluents or riverine discharge, can cause oxygen depletion in the water column especially near the bottom. This kind of situation is much more frequently seen now in developing countries like China but was historically very common in western countries. Since the huge investment in first construction and high cost of operation, there are few sewage treatment plants in developing countries and most urban sewage waste is discharged untreated directly into receiving waters (e.g. river, estuary, coastal sea).

Due to public awareness of environmental protection, the situation in more developed countries is quite different. Although some sewage is discharged into the environment without secondary treatment (especially in UK), the water exchange in coastal waters is assumed efficient enough to dilute the concentration of sewage down to a certain level by using long outfalls after primary treatment. Most discharged sewage to semi-enclosed waters such as estuaries receives secondary treatment which removes most of the oxygen-demanding material.

The continuous improvement of water quality of the River Thames (UK), has been extensively reported for decades (Barrett, 1972; Gameson et al., 1975; Head, 1976). However more recently the Salmon, a fish very sensitive to the DO concentration, has begun to come back in to the Thames Estuary (Clark et al., 1997).

A long term improvement in water quality due to sewage abatement in the lower Hudson River, New York has been reviewed by Brosnan (1996). Although some water pollution control plants have been in operation in the region since the 1930s the river and estuary have been subject to an enormous loading of oxygen-demanding material, from at least 1922. During the early 1960s, average summer DO percent saturation varied between 35% and 50% in surface waters, and 25% and 49% in bottom waters. Beginning in the late 1970's, most of the existing sewage treatment plants were upgraded to secondary treatment, and additional plants were constructed. Since then, DO concentration in the waters has generally increased through the 1980s and especially in the 1990s, coinciding with the upgrading of a 7.4 $m^3 s^{-1}$ sewage treatment plant to secondary treatment in 1991.

Apart from the direct anthropogenic discharge of oxygen-demanding material, organic oxygen-demanding matter produced locally by photosynthetic aquatic plants (e.g. phytoplankton, phytobenthos) can cause severe DO depletion in estuarine waters. Aquatic plant growth is a natural phenomenon with a regular seasonal pattern. In late winter and early spring nutrient levels, derived from riverine discharge and sewage plant discharge, are high in coastal waters. When light and temperature conditions are optimal for phytoplankton growth, an algal bloom may occur. The phytoplankton take up nutrients, synthesise organic matter by photosynthesis and release free oxygen. An algal bloom will not only release a great amount of oxygen, causing DO super-saturation in surface waters (which may have some adverse effects on marine organisms), but also subsequent degradation of the organic material will deplete the oxygen and sometimes will cause hypoxic conditions in bottom waters and even over the whole water column following decay of the bloom.

Surface primary production in all but the most turbid or nutrient-rich areas is ultimately controlled, or, limited by the availability of one or more nutrients. Primary production in coastal and offshore marine environments is generally assumed to be nitrogen-limited. There is little doubt that anthropogenic nutrient inputs now contribute substantially to the marine nutrient budget. GESAMP (1990) concluded that 'globally, present inputs of nutrients from rivers due to

man's activities are at least as great as those from natural processes' and have led to 'clearly detectable and sustained increases in nutrient concentrations in the receiving water'. The enrichment of the plant nutrients to the marine environment from anthropogenic sources frequently has the effect of increasing primary production (e.g. increased algal growth, algal bloom), a process commonly termed 'cultural eutrophication'. One of the undesirable consequences of eutrophication is the decline of DO saturation of the water column particularly near the sediment-water interface, following the accumulation of oxygen demanding material and elevation of hetrotrophic activity. Numerous studies and reviews have noted an increase in both the frequency and persistence of algal blooms in coastal waters and enclosed sea areas over the past 20-30 years, including the Baltic, Southern North Sea, Black Sea, Adriatic, Mediterranean and the coastal waters of North and South America and Japan (Kerr and Ryder, 1993; Sarokin and Schulkin, 1992; Vollenweider, 1993; McClelland et al., 1997).

The photosynthetic production of organic matter is not only limited by the availability of plant nutrients, but is also forced by solar radiation. Therefore DO variation has a strong seasonal and diel pattern of oscillation which is driven by the seasonal and diel change of solar radiation. Diel oxygen dynamics had been examined by D'Avanzo & Kremer (1994) in an eutrophic estuary of Waquoit Bay, Massachusetts. Waquoit Bay is a shallow (2 m deep) semi-enclosed coastal water body, which is enriched by nutrient loading from septic tank systems. A thick canopy of macroalgae covers the bottom of Waquoit Bay. It was observed that the bottom water was super saturated in the late afternoon, and bottom DO was higher than the surface DO. At dawn, bottom DO, being depleted by respiration of benthic macroalgae at night, was low and also was much less than surface DO. The diel DO variation in bottom waters was larger than that of surface water. Analysis of meteorological records during two anoxic events showed that anoxia developed overnight in midsummer during periods of peak summertime temperatures after several days of cloudy, moderately calm weather. D'Avanzo & Kremer (1994) suggested anoxic events may indicate a chronic increasing problem in these important ecosystems. The diel variation of DO can be used to estimate the community oxygen metabolism (Kemp & Boynton, 1980; Kenney et al., 1988) in coastal waters.

1.3 Modelling DO

As mentioned in section 1.2, the DO balance in coastal waters is influenced by a combination of physical and biological processes. Modelling therefore requires an interdisciplinary approach and modelling DO in an estuarine system requires the modeller to interact with physicists, marine chemists and biologists.

The pioneer DO modelling work on water quality was carried out in streams and rivers where sewage effluent discharge contains oxygen demanding organic matter (e.g. Streeter & Phelps, 1925; O'Connor, 1960; Dobbins, 1964; Koivo & Phillips, 1971; Koivo & Phillips,

1972; Barrett, 1978). This type of model only considered two factors: bacterial decomposition of oxygen-demanding organic matter and re-aeration from the atmosphere.

The more complex DO model is a water quality model (e.g. O'Connor, 1967; DiToro et al., 1971; Chen & Orlob, 1972; Prober et al., 1972; Grenney et al., 1973; O'Connor et al., 1973; Soulsby et al., 1984; Chaudhury et al., 1998) which considers the aquatic plant growth and its consequence to DO balance in stream and river waters. This type of model when used in the context of anthropogenic nutrient enrichment is probably better called a eutrophication model, consistent with the concept of eutrophication (Commission of European Communities, 1991; Justic, 1995; Nixon, 1995). Since they offer easy access and simple physical and biological characteristics, modelling work was first carried out in streams and rivers. To some extent, the water quality modelling approaches used in estuarine and coastal waters are inherited from pervious work in freshwater environments.

The simple DO model is very useful in rivers, or estuaries where heavy loading of oxygen-demanding material discharges into the waters from riverine sources and sewage outfalls. For waters, where a substantial proportion of the oxygen demanding material is derived from the aquatic plant growth, a eutrophication type model should be used.

Since an ecosystem is very complex and processes involved in DO dynamics are poorly understood, it is not surprising that eutrophication type water quality (DO) models have taken many different approaches (e.g. Soulsby et al., 1984; Stigebrandt, et al., 1987; Billen et al., 1988; Bach & Jensen, 1994; Bierman et al., 1994; HR Wallingford, 1995; Chaudhury et al., 1998). Stigebrandt et al. (1988) have modelled the DO and nutrients in the Baltic proper, a highly stratified semi-enclosed sea. Billen et al. (1988) have modelled the DO and microbial processes (phytoplankton and bacterioplankton) in the Schelde Estuary. Huthnance et al. (1993) reviewed the current status of water quality modelling in Europe and summarised processes involved in water quality modelling. Modelling of nutrients, DO and microbiology (plankton, detritus) are considered (Huthnance et al., 1993), and the scope is restricted to the lowest level of food chain and quasi-continuum variable.

One water quality modelling approach should be mentioned that is now fairly widely used that is Tett's L3VMP model (Tett, 1990; Tett & Walne, 1995). The physical structure of the original model is a simple 3-layer vertical structure: surface mixed layer, bottom mixed layer and oxic sediment layer. The distinctiveness of the model is the modelling of the planktonic compartment. Phytoplankton and planktonic microheterotrophs (bacterioplankton and microzooplankton) are combined in a microplankton compartment, described by a cell-quota, threshold-limitation model (Tett & Droop, 1988) in terms of alternative light or nutrient limited growth.

From an environmental management point of view, water quality should be a useful tool for decision making, such as choosing a long sewage outfall, planing of functional zone for

different users, reducing BOD and nutrient loading, improving the water quality etc. A few water quality (DO) models have been integrated in to large scale, multi-disciplinary programs (e.g. North Sea Project; The Chesapeake Bay Program) with the aim of using them for environment management and decision making.

A systemic eutrophication modelling study has been undertaken in Chesapeake Bay (Linker, 1996) as part of Chesapeake Bay Program. By the 1970s, many of Chesapeake Bay's resources were in clear decline. Excess amounts of nutrients overfertilized the bay, feeding the growth of algal blooms which sink to the bottom of the bay and decompose in a process that depletes the water of oxygen. These areas of 'dead water' no longer have oxygen levels sufficient to support fish and other aquatic life.

The Chesapeake Bay Program, a voluntary partnership that includes US Environment Protection Agency and all states within the Chesapeake Bay watershed (64,000 square miles) was created in 1983 to restore the water quality of the bay. An integrated set of models (watershed model, estuary model, airshed model) have been developed. The estuary model examines the effects of loads generated by the watershed model on bay-water quality. The hydrodynamic submodel simulates the flow rates into the bay, the mixing of Chesapeake waters with coastal ocean waters, and the mixing of water within the Chesapeake estuarine system. The water quality submodel calculates the chemical and ecological dynamics of Chesapeake Bay.

The goal of the Chesapeake Bay Program is to reduce the nutrient load entering the bay by 40% by the year 2000. The models have demonstrated that this goal will significantly decrease the 'dead waters' of Chesapeake, and provide guidance to environmental managers and citizens on where the most cost-effective nutrient reduction can be made. Achievement of the goal will enable the water quality in the bay to improve by reducing anoxic water of the bay by 20% by the year 2000. The development of a water quality Chesapeake Bay model has continued for the last 16 years, and four major upgrades have been made (Linker, 1996).

In China, a cross-province Green Bohai Sea Program was launched in early 1999 with the aim of addressing the marine pollution issue in the Bohai Sea. The committee consists of governmental and non-governmental organisations from all 5 provinces of the catchment area of Bohai Sea. Now for the first time in China a large scale multi-disciplinary approach to control the water quality modelling is under way.

1.4 Review of previous research in Southampton Water

Due to the proximity of Southampton Water, scientists from the University of Southampton have conducted regular surveys of this adjacent water body (Dyer, 1973; de Souza Lima & Williams, 1978; Collins, 1978; Bryan, 1979; Rees and Williams, 1982; Crawford & Purdie, 1992; Sylaios, 1994; Kifle & Purdie, 1993; Crawford et al., 1997; Sylaios & Boxall, 1998). Dyer (1973) defined Southampton Water as a partially-mixed estuary following an

extensive survey including measurements of temperature, salinity and currents. The tidal regime in Southampton Water has been described by Webber (1973). The type of tide in Southampton Water is the regular M2 tide, but has a significant M4, M6 shallow water constituents caused by non-linear interaction of the tide. The bathymetry distorts the tidal curve with a double high tide and a young flood stand. The flood tide lasts 2 hours longer than the ebb tide.

The first model applied to Southampton Water was a tidal prism model (Collins, 1978). This model was a modified version (Dyer & Taylor, 1973) of Ketchum's (1951) segment tidal prism method. The model was used to re-produce survey (Byran, 1979; Collins, 1978) results (DOC, nutrients and DO) collected during 1977-1978. Sylaios (1994) developed a simple vertical 2-D hydrodynamic model of Southampton Water, and a series of CTD and ADCP (Acoustic Doppler Current Profiler) data were used to compare with the model results. Using the CTD and ADCP data Sylaios & Boxall (1998) gave a general account of the residual current, and salt balance in Southampton Water. Rees and Williams (1982) undertook a survey in the Test Estuary in order to provide constants for a water quality model, and Soulsby et al. (1984) developed a vertical 2-D water quality model to investigate the effects of the phytoplankton bloom on DO in Southampton Water.

Extensive surveys have been made on the *Mesodinium rubrum* red-tide bloom (Crawford & Purdie, 1992; Kifle & Purdie, 1993; Crawford et al., 1997). The possible factors influencing the initiation and occurrence of the bloom, its continuity, and decay as well as the consequence of the bloom have been considered.

The water quality model of Soulsby et al.'s (1984) is still being used by HR Wallingford with the initial model structure. In 1994 Southern Water contracted HR Wallingford to produce a series of reports about Southampton Water, including a field survey, 2-D hydrodynamic model, and 2-D water quality model.

Beside the academic institutes like the University of Southampton, commercial companies including Associated British Ports (ABP) and Southern Water have their own scientific research and consultancy programmes in Southampton Water and the Solent. Following concern about the negative effects of dredging, ABP have developed a group of 2-D hydrodynamic models with different resolutions, which include sediment transport models. These models can effectively simulate the tidal currents in Southampton Water and the Solent estuary system. There is to date, however, no single physical 3-D hydrodynamic model covering the whole area; the biggest advantage of a single model being that it can minimise the unwanted effects of boundary conditions. Southern Water have mainly focused on water quality and the above mentioned HR Wallingford model is employed by Southern Water. This is the only known systematic water quality model of Southampton Water.

1.5 Research objectives

As part of the Qingdao University Institutional Development Project, supported by Department for International Development, the main task of this research was to develop a water quality model for estuarine and coastal waters. Southampton Water is an ideal location to develop a water quality model, since large observational data set is available, although the data has not been well organised. Monthly surveys of Southampton Water were carried out from January 1998 to April 1999, with the measurement of water temperature, salinity, DO and community respiration rate made at number of positions in the Itchen Estuary and Southampton Water. SONUS core measurements included nutrients, chlorophyll, and suspended particulate matter (SPM) during these surveys.

This research had the following objectives:

1. To develop a 3-D hydrodynamic numerical model of the Southampton Water and Solent estuarine system and validate output against available physical data.
2. To develop a water quality (DO) model for Southampton Water coupled to the 3-D hydrodynamic model.
3. To obtain a data set of water quality parameters from the estuary for comparison to the output of the water quality model.
4. To achieve a better understanding of the mechanism of physical and biological controls on the water quality, particularly the DO, in estuaries and coastal waters.

The thesis is structured as follows. Following the general introduction (Chapter 1), Chapter 2 gives a general account of the Southampton Water estuarine system including the hydrography and tidal environment. Data collected from monthly surveys are presented in Chapter 3, with conclusions drawn from the survey data. In Chapter 4, a brief description of the hydrodynamic model is presented and in Chapter 5 results from the hydrodynamic model are presented and discussed. Chapter 6 gives the structure of the water quality (DO) model, and its application is given in Chapter 7. A final discussion and conclusion are presents in Chapter 8 including a discussion of the limitations of the model and possible further work.

Chapter 2 Southampton Water

2.1 General description

Southampton Water, as an inlet in the southern coast of England on the English Channel (Figure 2.1), forms a northern extension of the Solent estuarine system.

It is widely believed (Geodigest, 1999) that the Solent estuarine system evolved from an ancient river system 'Solent River', which drained much of central south England, although the detail of the evolution may be arguable (Velegrakis et al., 1999). About 17,000 years ago, the sea level was about 100 meters lower than it is today. The coastline was many miles to the south of the Isle Wight and the 'Solent River' ran parallel to the coastline and discharged to the sea, somewhere south of the present position of Littlehampton. Its upper reaches flowed from west to east along a valley, bounded in the south by a chalk ridge, the Purbeck - Isle of Wight Ridge (Figure 2.2). When the ice receded, and sea level rose, gradually the 'Solent River' valley, now the West Solent and East Solent, became submerged beneath the sea surface. The soft chalk ridge on a line between the Needles and Dorset was eroded, and no more than 4000 years ago, the Isle of Wight was isolated and became an Island in the English Channel. With the intrusion of sea water, Southampton Water as a tributary of the old 'Solent River' system then became an estuary. The Solent estuarine system is now highly industrialised and urbanised.

2.2 Bathymetry

Broadly the Southampton Water estuarine system consist of four parts: Southampton Water, the Itchen Estuary, the Test Estuary and the Hamble Estuary. Southampton Water (Figure 2.3a) is about 2.0 km wide and 10.3 km long from Calshot Castle, at the entrance to Southampton Water, to Dockhead, where the Test Estuary and Itchen Estuary meet. The main channel of Southampton Water is maintained to 10-15 m below the local chart datum by regular dredging, and the dredged channel is about 300 meters wide.

Beyond Dockhead the dredging channel extends to the lower part of the Test Estuary for a further 6 km. Above this point, the bed of the Test Estuary rises quickly to the local chart datum level. The tidal limit of the Test Estuary is at Redbridge, about 7.6 km from Dockhead.

The Itchen Estuary is about 2-4 hundred meters wide and 7.8 km long; the tidal limit is at Woodmill. Water depth in the Itchen Estuary rises gradually from 9 m at Dockhead to about 0 m (local Chart Datum) in about 6.2 km. Figure 2.3b shows the water depth of the main channel of Southampton Water, from Woodmill to Calshot Castle.

The Hamble Estuary is much smaller and joins Southampton Water on its eastern side about 2 km north of Calshot Castle.

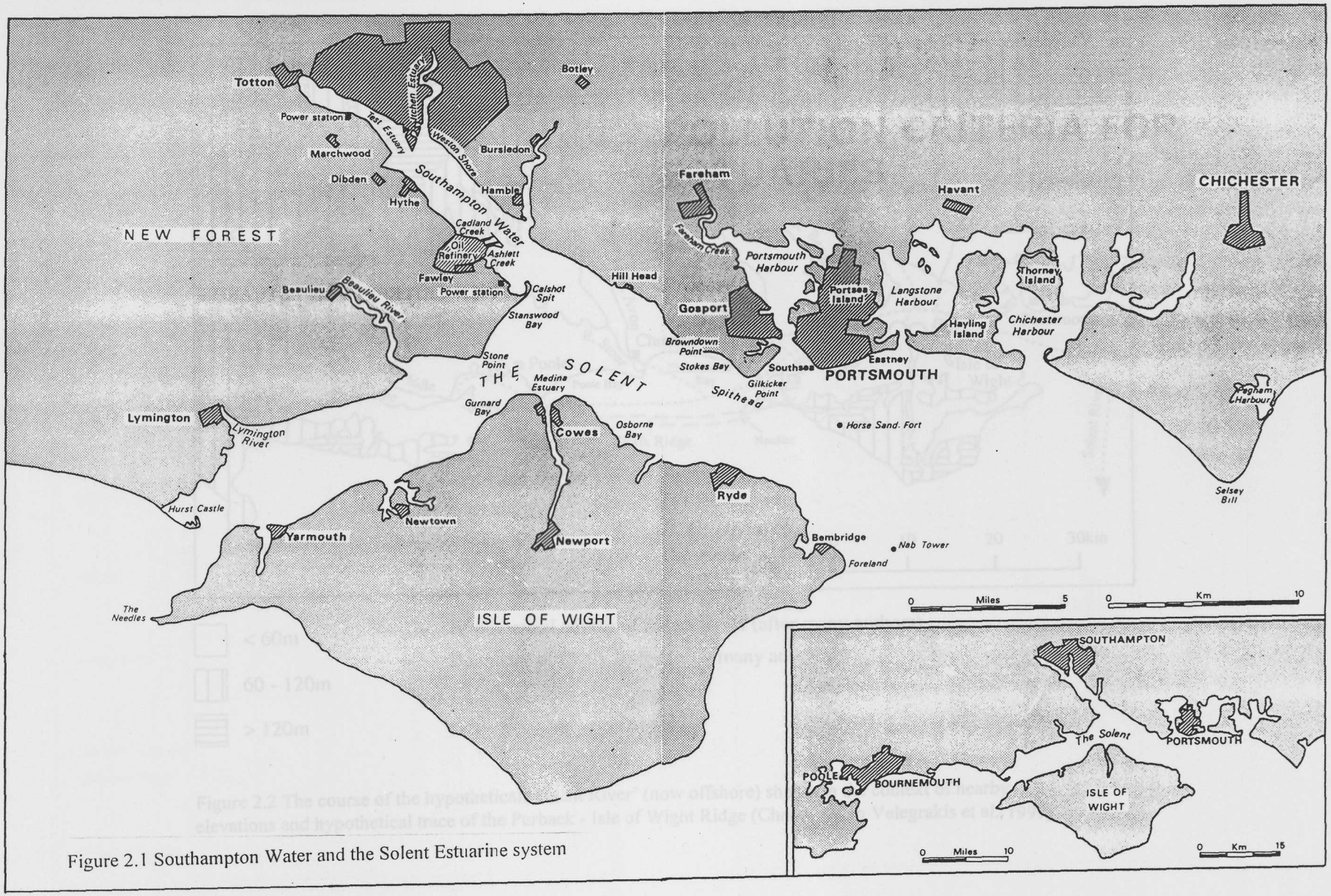

Figure 2.1 Southampton Water and the Solent Estuarine system

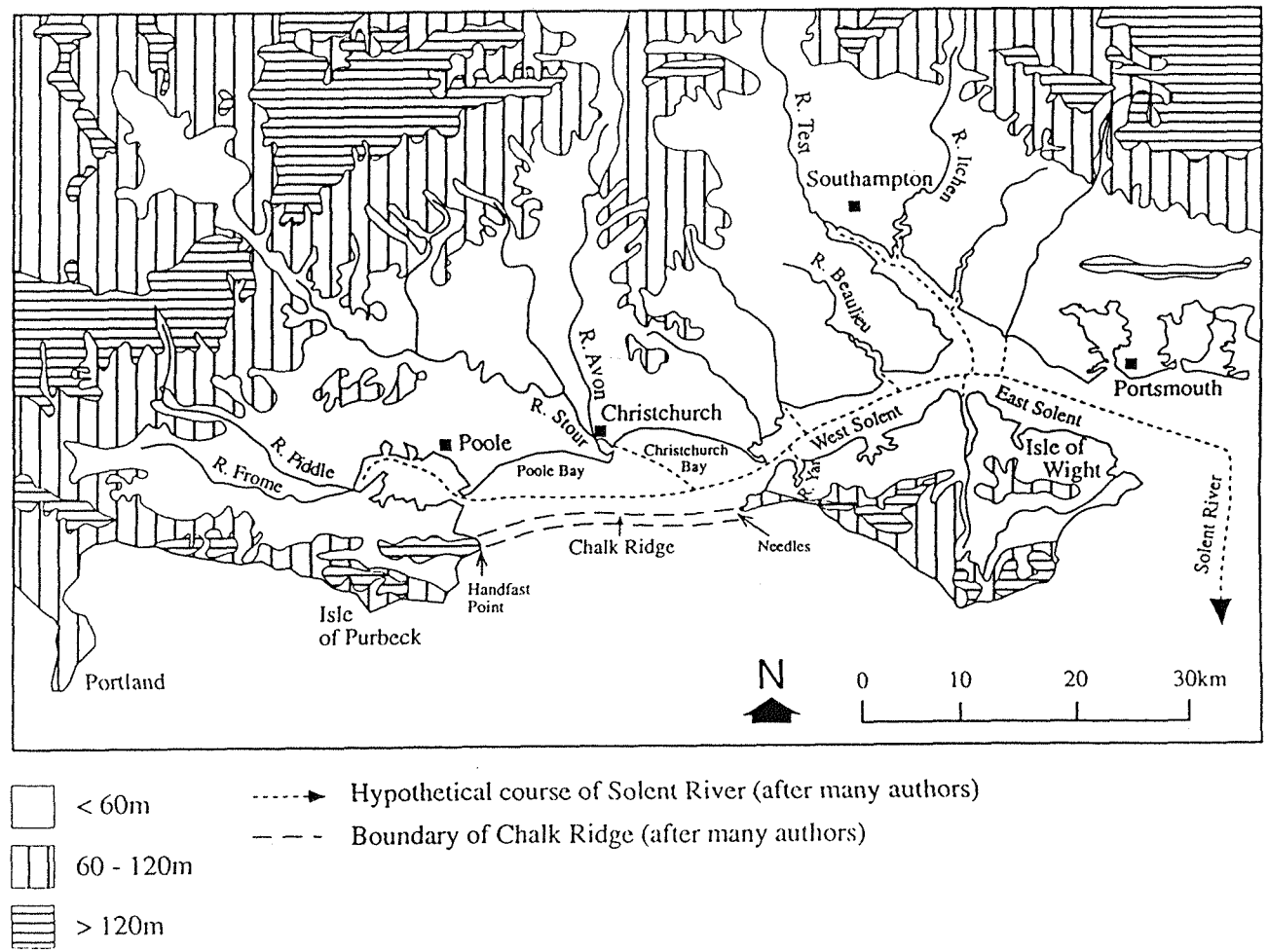

Figure 2.2 The course of the hypothetical 'Solent River' (now offshore) shown in the context of nearby elevations and hypothetical trace of the Purback - Isle of Wight Ridge (Chalk). (from Velegrakis et al., 1999)

Figure 2.3a Southampton Water, Test Estuary, Itchen Estuary and Hamble Estuary

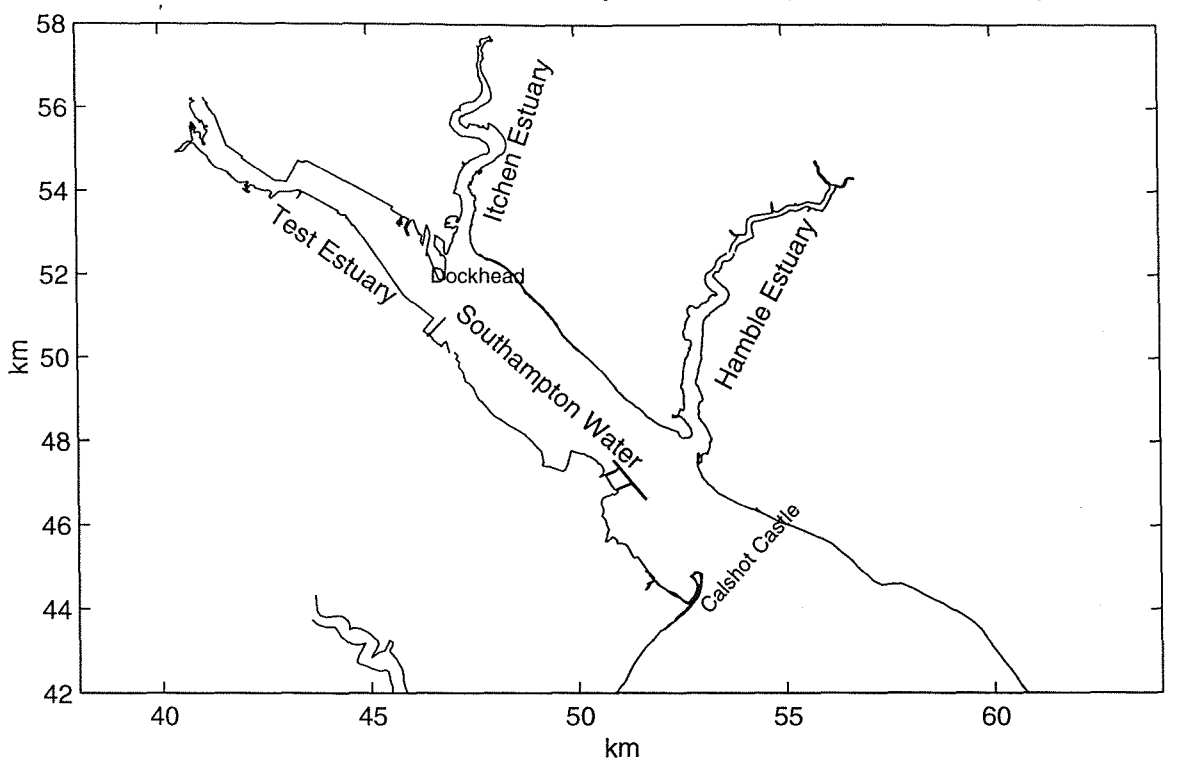

Figure 2.3b Water depth (m) along the main channel of Itchen Estuary and Southampton Water, form Woodmill to Calshot Castle

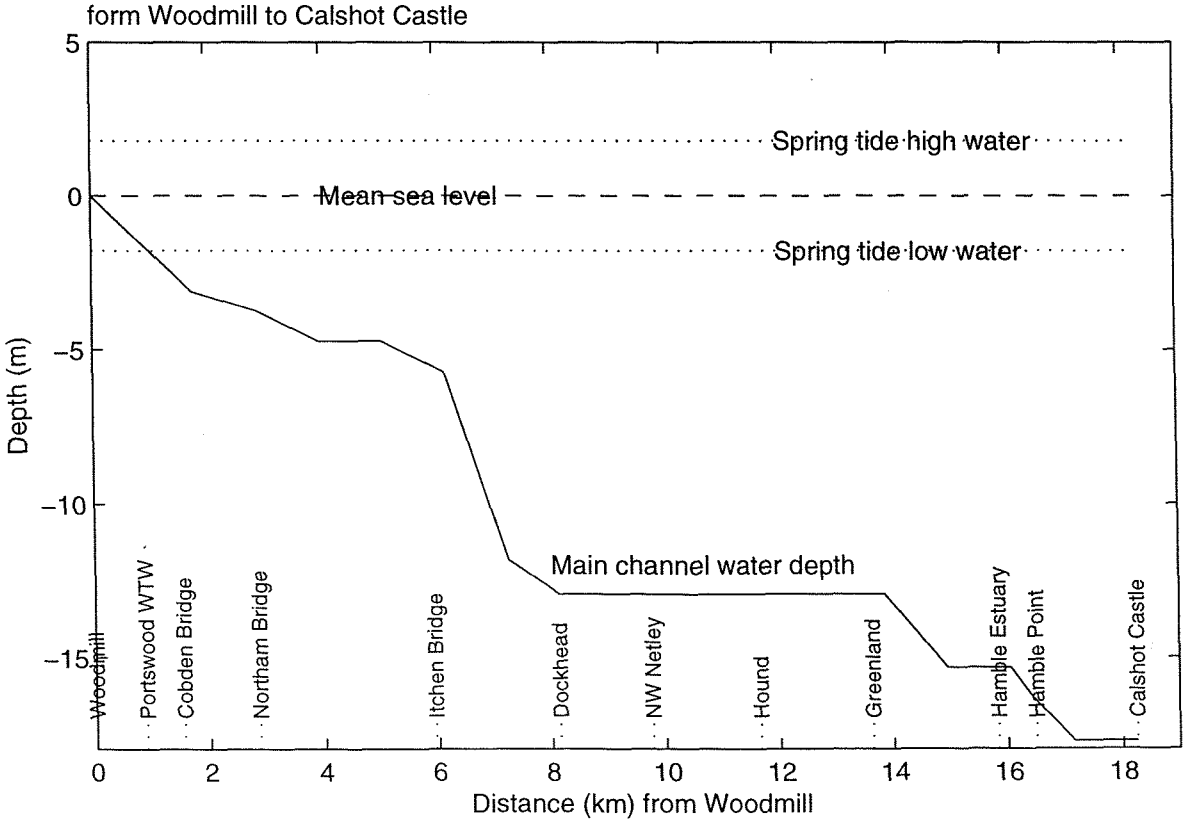

2.3 Tidal regime

A tidal wave is a long wave which is generated by astronomical gravitational forces (Moon and Sun). The tidal wave propagation, regulated by bathymetry, is accomplished by the water movement such as the rise and fall of free sea surface and oscillation of tidal current. For estuaries and coastal seas the tidal regime is dominated by the tidal wave propagated from the open ocean. For Southampton Water and the Solent, the tidal characteristics of the English Channel are the controlling factors.

Figure 2.4 shows the M_2 co-tidal lines for the English Channel. The tidal pattern in the English Channel is a standing wave oscillation, which means the tidal range increases rapidly with distance from the nodal point. According to the M_2 co-tidal lines for the English Channel, Poole Bay, west of the Isle of Wight is in the vicinity of a M_2 node. The close proximity of this node and complex bathymetry in the Solent causes the tide and tidal currents in the Solent estuarine system to be very complex, and the average tidal range (Figure 2.5) in the vicinity of Southampton Water and the Solent changes greatly from west to east; the difference being about 1.5-2.0 m over a distance of about 50 km.

Tide and tidal currents in Southampton Water are dominated by the semi-diurnal M_2 tide (Webber, 1973; Webber, 1980). Tidal range at Dockhead is about 3 m on average. Due to complex bathymetry in the Solent estuarine system and the nonlinear interaction in shallow water, the tidal wave is distorted during its propagation. Non-linear interaction transfers part of the tidal wave energy to the shallow water components (Pugh, 1987). Shallow water constituents M_4 and M_6 have increased significantly, and result in the phenomena of double high tide (Webber, 1980). Flood tides experience a young flood stand, and the flood tide lasts two hours longer than ebb tide (Pugh, 1987).

The M_2 tidal amplitude at Dockhead, Southampton Water, is about 1.38 metre and S_2 tidal amplitude is 0.42 metre. Since the semi-diurnal tides dominate in Southampton Water, the main semi-diurnal constituent M_2 is the average tide. $M_2 + S_2$ is the spring tide, $M_2 - S_2$ represents the neap tide. In Southampton Water Dockhead local datum is 2.74 metres below Ordnance Datum (Newlyn). The approximate maximum astronomical tidal range in Southampton Water is double the local datum of 5.48 metres.

Figure 2.6 shows the tidal volume in Southampton Water under the average tide. The whole of Southampton Water, including the Test Estuary, Itchen Estuary and Hamble Estuary are divided into segments along the main channel of the estuary with the length of every segment being 200 metres. Tidal Volume has been calculated by adding the segment volume from the tidal limit of the Itchen Estuary, Woodmill, down stream to Calshot Castle. Figure 2.6 shows there is a steep increase of tidal volume where the Test Estuary joins the Itchen Estuary

Figure 2.4 Co-tidal line for the English Channel

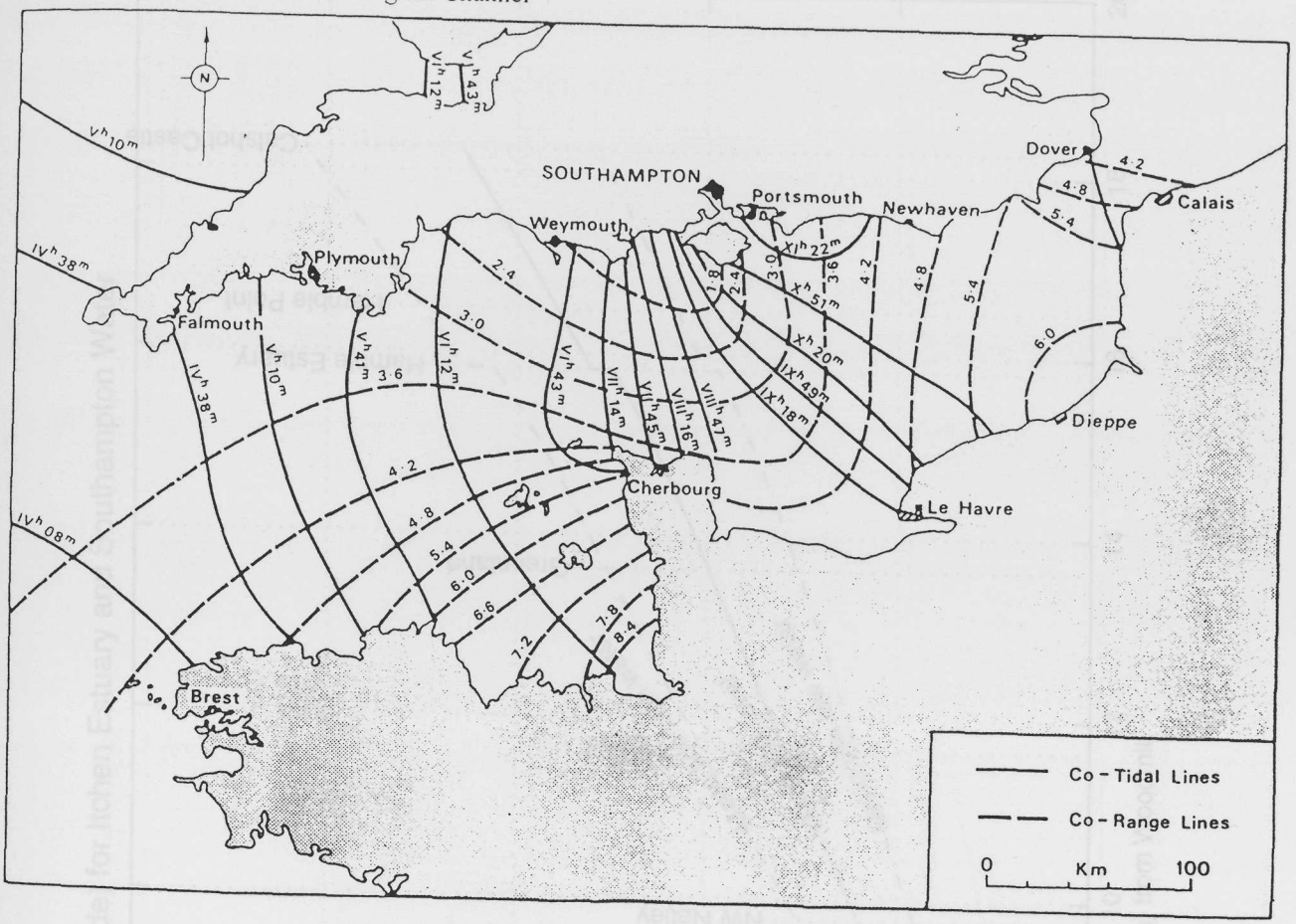

Figure 2.5 Average tidal range (approximate) in Southampton Water and the Solent

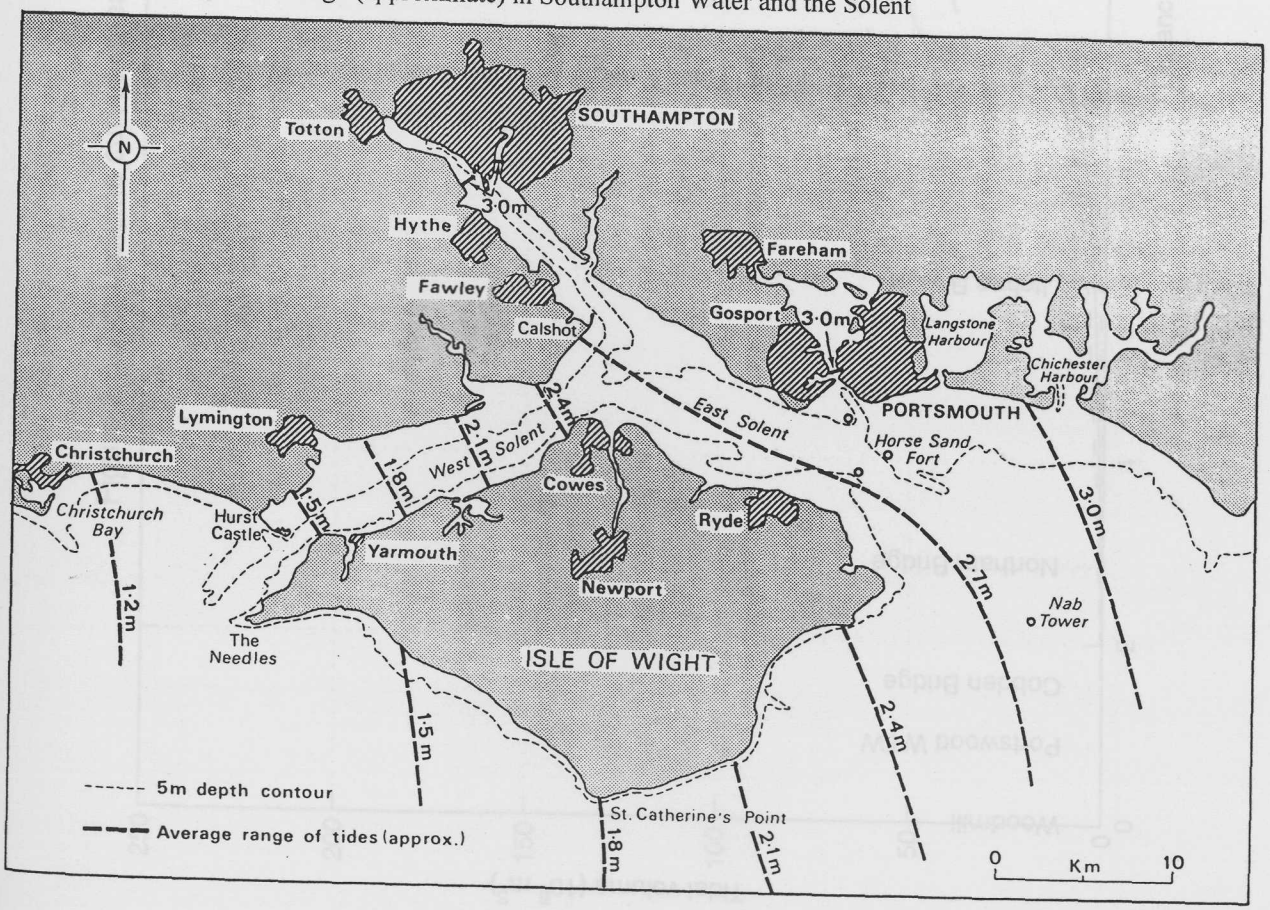

Figure 2.6 Tidal volume curves (mean tide) for Itchen Estuary and Southampton Water

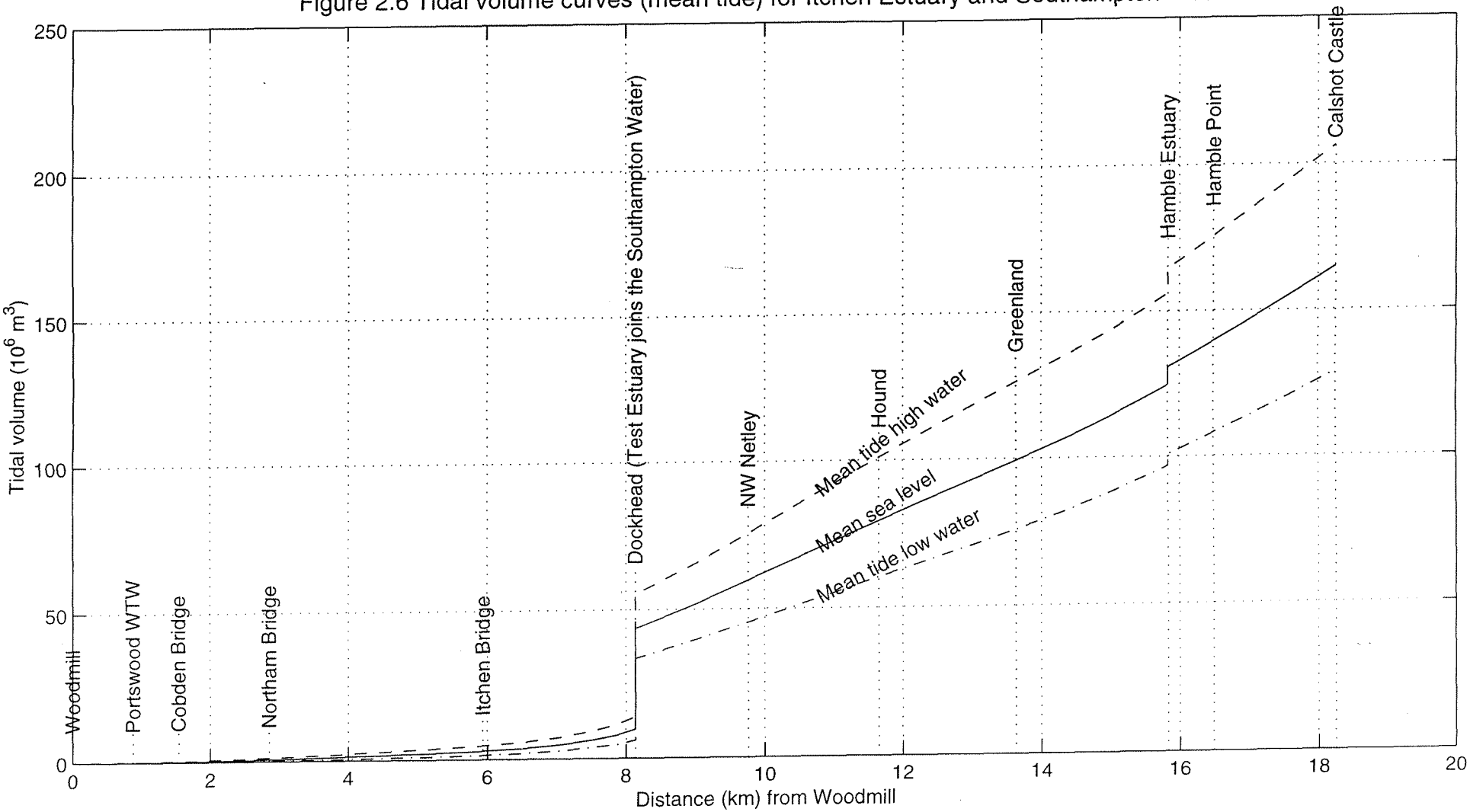

Figure 2.7 Tidal prism for Itchen Estuary and Southampton Water in different tidal conditions

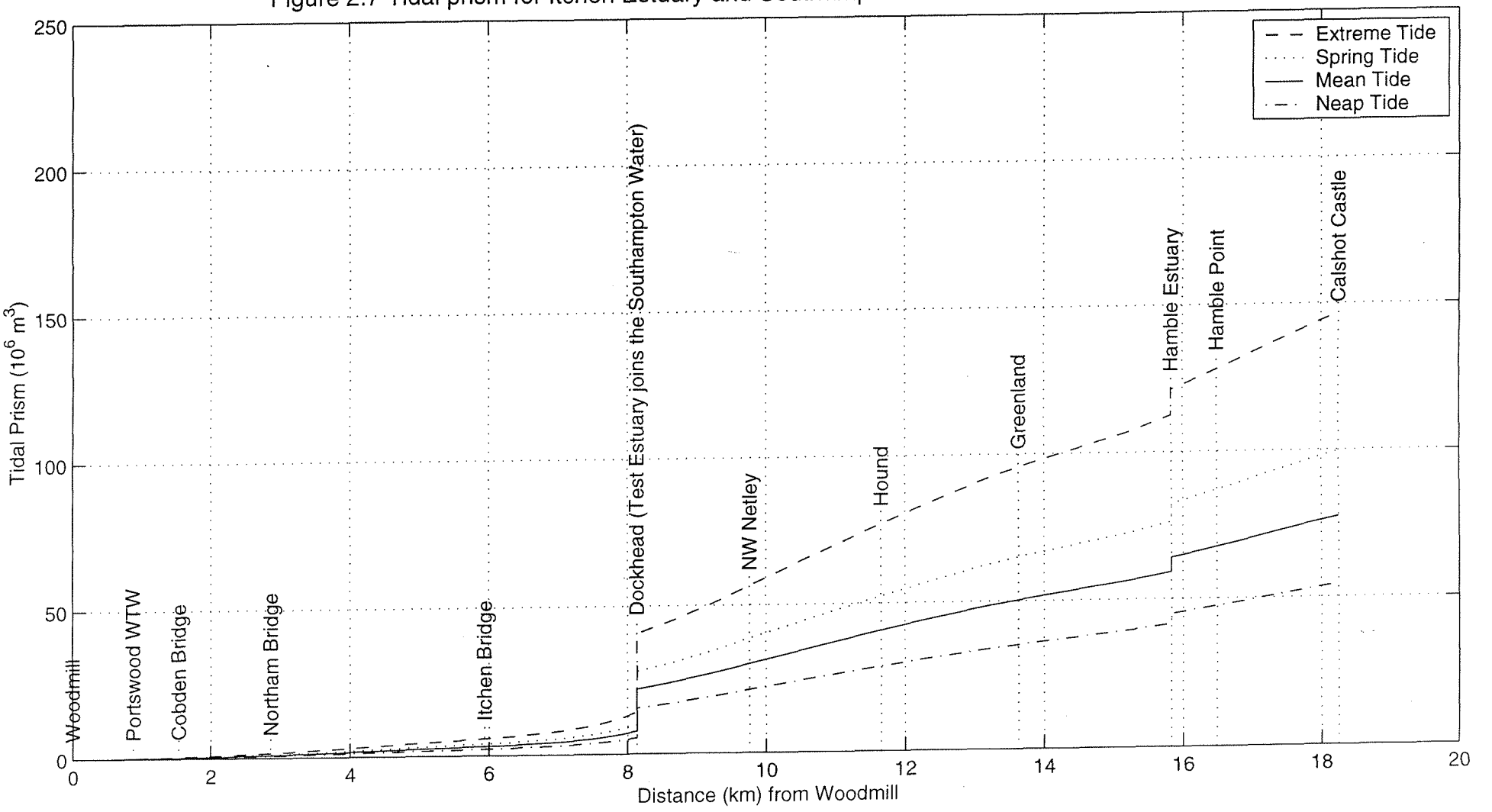

at Dockhead. The total tidal volume at average sea level is about 165×10^6 m^3, and the tidal volume is 206×10^6 m^3 at high water (mean tide), 128×10^6 m^3 at low water (mean tide).

The tidal prism depends on the tidal range. The tidal prism under extreme tidal range, spring tide, average tide, and neap tide is given in Figure 2.7. The tidal prism of Southampton Water is about 100×10^6 m^3 at spring, 50×10^6 m^3 at neaps, and at average tide it is about 78×10^6 m^3, which is about half of the tidal volume at the average sea level. The Test Estuary, Itchen Estuary and Hamble Estuary contribute about 20%, 8%, and 5% of whole tidal prism respectively (Webber, 1973).

Table 2.1 Tidal excursion (released at low water, upstream towards Woodmill) from different stations

Stations	Neap tide (m)	Average tide (m)	Spring tide (m)	Extreme tide (m)
Woodmill	-	-	-	-
Portswood WTW	-	-	-	-
Cobden Bridge	800	900	1,000	-
Northam Bridge	700	1,400	1,800	2,400
Itchen Bridge	1,800	2,400	3,000	4,000
SG No 1	1,000	1,600	2,400	2,600
NW Netley	1,500	1,800	2,300	3,200
Greenland	2,600	3,100	4,000	5,200
Hamble Point	3,000	4,200	5,900	6,600
Calshot Castle	4,000	4,400	6,400	7,400

Using the volumetric method, tidal excursion can be calculated. Table 2.1 is the tidal excursion in the River Itchen and Southampton Water. The normal tidal excursion in Southampton Water is about 4 km, and 900 meters to 2400 meters in the River Itchen on an average tide. Since tidal excursion gives a useful indication of water mass movement (Presuming the tidal current is uniform) in an estuary, the tidal excursion can be used to adjust survey data (Head, 1985).

2.4 River inputs and point sources of pollutants

There are three main rivers discharging fresh water into Southampton Water, the River Test, River Itchen and River Hamble. Table 2.2 shows the average river discharges for the three rivers. However the river flow is highly variable form year to year. Westwood (1982) gave the annual average river discharge for the three rivers as 11.83 m^3 s^{-1} for River Test, 5.33 m^3 s^{-1} for

Table 2.2 River discharge from River Test, River Itchen and River Hamble(1988-1993) (Sylaios, 1994)

	Watershed area (km^2)	Average river discharge (m^3 s^{-1})	Average winter discharge (m^3 s^{-1})	Average summer discharge (m^3 s^{-1})
River Test	1040	8.82	6-9	5.5-6
River Itchen	360	3.26	3-4	2.75-3
River Hamble	56.6	0.29	0.2-0.3	0.1-0.125

River Itchen, and 0.40 m^3 s^{-1} for River Hamble. More recent data (Sylaios, 1994) showed that during 1988-1993, fresh water discharge from the three rivers was reduced by up to 38% over this period. The average annual fresh water discharge during 1988-1993 period from the River Test, River Itchen and River Hamble were 8.82 m^3 s^{-1}, 3.26 m^3 s^{-1} and 0.29 m^3 s^{-1} respectively.

Figure 2.8 River flow (m3/s) from River Test, River Itchen and River Hamble in 1998

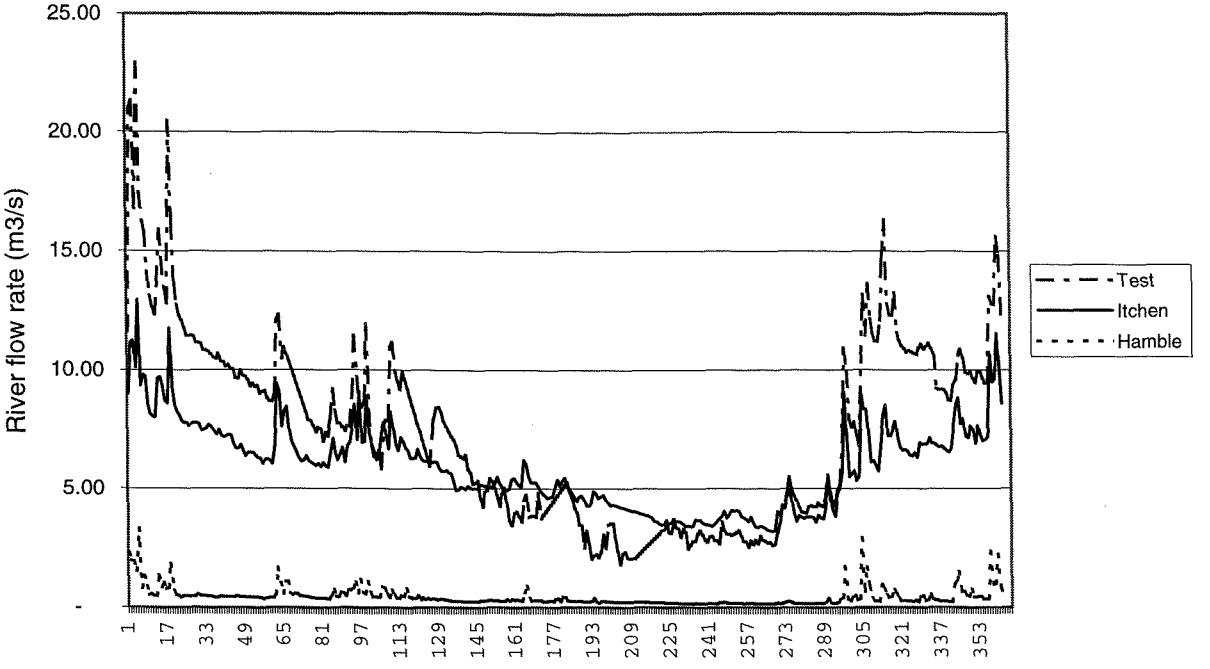

Time in days from January 1, 1998 to December 31, 1998,

The most recent data (Figure 2.8) provided by the Environmental Agency gives the average annual river flow from the River Test, River Itchen and River Hamble as 7.43 $m^3 s^{-1}$, 5.98 $m^3 s^{-1}$ and 0.44 $m^3 s^{-1}$ respectively in 1998. Since Southern Water abstracted up to 136 million litres water per day (equivalent to 1.58 $m^3 s^{-1}$) from River Test, during the summer, the river flow entering the estuary from River Test is less than that from River Itchen.

Riverine load of pollutants (Table 2.3) was given by HR Wallingford in their Report EX 3253 (1995). The load estimates were based on the daily discharge and water quality monitoring for the appropriate gauging station in July 1994.

Table 2.3 Pollutant load of River Test, River Itchen and River Hamble (1994) (HR Wallingford, 1995)

	Test		Itchen		Hamble	
	mg l^{-1}	kg d^{-1}	mg l^{-1}	kg d^{-1}	mg l^{-1}	kg d^{-1}
Total BOD_5	1.5	1,100	2.0	778	2.0	38
Organic Nitrogen	1.5	1,100	1.0	389	1.0	19
Ammonia	0.1	73	0.07	30	0.1	2
Nitrate	6.0	4,410	5.0	1,940	5.0	95
Orthophosphate	0.15	110	0.3	117	0.4	8
DO	100% Sat		100% Sat		100% Sat	
Suspend Solids	15.0	11,000	15.0	5,830	5.0	95
Algal Carbon	0.0	0	0.0	0	0.0	0
Mean Discharge ($m^3 s^{-1}$)	9.27		4.95		0.42	

The water quality of point source effluents and the pollution loads from main point sources are listed in Table 2.4 (HR Wallingford, 1995). Data were estimated from data provided by the National Rivers Authority (now Environmental Agency).

Table 2.4 Point source effluent quality and loads (kg d^{-1}) in 1994 (HR Wallingford, 1995)

	Estuary	Discharge	Total BOD_5		Fast	Dissolved
		$m^3 s^{-1}$	mg l^{-1}	kg d^{-1}		
Bartley water	Test	0.02	2	3.5	50%	50%
Millbrook WTW	Test	0.53	5	229.0	50%	80%
Slowhill Copse WTW	Test	0.22	5	95.0	50%	80%
Portswood WTW	Itchen	0.3	5	130.0	50%	75%
Wolston WTW	Itchen	0.15	5	65.0	50%	80%
Burlesdon WTW	Hamble	0.02	10	17.0	50%	50%
Fawley-Ashlet Creek WTW	Southampton	0.05 (consent)	300	129.6	100%	100%
ISC (Hythe)	Southampton	0.01	1000	864.0	100%	100%
Enichem	Southampton	0.01	25	1382.0	100%	100%
Rechem	Southampton	0.64	25	21.6	100%	100%
Fawley (NationaPower)	Southampton	0.02	2	3.5	100%	100%
Esso 1	Southampton	N/A		490.0	100%	100%
Esso 2	Southampton	N/A		614.0	100%	100%
Essc 3	Southampton	N/A		15.5	100%	100%

Table 2.4 Point source effluent quality and loads (kg d^{-1}) in 1994 (HR Wallingford, 1995)-continued

Suspended solids		Organic nitrogen		Ammonia		Nitrates		Phosphates		DO
mg l^{-1}	kg d^{-1}	mg l^{-1}	kg d^{-1}	mg d^{-1}	kg d^{-1}	mg l^{-1}	kg d^{-1}	mg l^{-1}	Kg d^{-1}	% Sat
10	17.3	2	3.5	0.1	0.2	4	6.9	0.8	1.4	85
6	274.0	4	183	25	1145.0	20	916.0	7	320.0	55
10	190.0	4	76	25	475	0.8	15.2	3	57.0	80
20	518.0	5	13.0	20	518	0.5	13.0	5	130	50
10	130.0	5	65.0	20	259	0.5	6.5	5	65.0	40
20	35	5	8.64	5	8.64	15	25.9	6	10.4	75
250	1080	0	0.0	36	155	0.8	3.5	7.7	33	95
100	86.4	0	0.0	0.5	0.4	5	4.3	0.5	0.4	55
30	1659.0	0.24	13.3	0.3	16.6	1	55.3	0.5	27.6	100
25	21.6	0	0.0	4	3.5	10	8.6	0.3	0.4	95
6	10.4	0	0.0	0.5	0.9	1.8	3.6	0.14	0.0	89
	0		0		116.0		78.0		4.0	N/A
	0		0		135.0		191.0		14.0	N/A
	0		0		1.6		2.4		0.7	N/A

Total pollutant loads into the different areas (Southampton Water, Test Estuary, Itchen Estuary, Hamble Estuary) have been given in Table 2.5. The Test Estuary has the highest nutrients load and the Hamble the lowest.

The river and point sources pollutant loads of 1998 were not available at the time of writing, but the loads are not expected to have significantly changed.

Table 2.5 Total pollutant loads (kg d^{-1}) in 1994 (HR Wallingford, 1995)

	Total BOD_5	Suspended solids	Organic nitrogen	Ammonia	Nitrates	Phosphates
Southampton water	3412.2	1799.0	13.3	277.5	351.8	47.4
Test	1427.5	11481.0	1427.5	1788.2	5348.1	488.4
Itchen	973.0	6478.0	584.0	780.0	1959.5	195.0
Hamble	211.0	441.0	105.4	88.4	354.0	112.0

2.5 Annual algal blooms and red-tides in Southampton Water

Algal blooms are an annual event in Southampton Water, and the 'red-tides' formed by *Mesodinium rubrum* are particularly noteworthy (de Souza Lima & Williams, 1978; Rees & Williams, 1982; Soulsby et al., 1984; Crawford & Purdie, 1992; Kifle, 1992; Kifle & Purdie, 1993; Crawford et al., 1997). The characteristics of these blooms, their initiation, development, decay, dominant species and conversion have been shown to be very different from year to year.

Following a series of surveys of salinity, temperature, dissolved oxygen, chlorophyll and nutrients in the Test Estuary from 4 depths at 6 sites on about 20 occasions annually for 3 years, 1977-1979, Soulsby et al. (1984) summarised the following characteristics:

- A dense phytoplankton bloom developed throughout the estuary each summer with peak chlorophyll level of > 200 $\mu g\ l^{-1}$. The bloom rapidly dispersed and this was generally associated with the period of reduction in DO. Surface DO is supersaturated during periods of blooms, but bottom DO reached a minimum in midsummer of 30%-50% saturation after the bloom collapsed.
- Levels of both nitrate and ammonia were substantially reduced during the phytoplankton bloom period.
- The midsummer phytoplankton bloom was dominated by the phototrophic ciliate *Mesodinium rubrum.*

During the period May-October 1981, detailed analysis of the phytoplankton bloom was undertaken by Rees and Williams (1982) to investigate the phytoplankton photosynthesis and respiration and to provide data for a model to describe the role of photosynthesis in the oxygen budget of the estuary. Two *Mesodinium rubrum* dominated blooms were observed; the first and the larger one was in early July with maximum chlorophyll concentration of 82 $\mu g\ l^{-1}$; the second bloom was in early September. There was a highly significant correlation between levels of chlorophyll and rate of photosynthesis and respiration during the blooms.

The most intensive, continuous survey of algal blooms in Southampton Water was conducted by Kifle (Kifle, 1992; Kifle & Purdie, 1993) in 1988. Seasonal and spatial variation in species composition, abundance, biomass and primary production of phytoplankton were monitored both at the inner estuary station (NW Netley) and outer estuary station (Calshot Buoy).

At Calshot the major bloom event of the year occurred at the beginning of May when chlorophyll levels reached 18 $\mu g\ l^{-1}$ due to a bloom of the diatom *Rhizosolenia delicatula*. A second, broader maximum occurred in June during blooms of *Schroederella delicatula* and *Thalassiosira cf fallax* (centric colonial diatom). Microflagellates, which were present throughout the year, could not be quantified from the chlorophyll figures.

The situation at NW Netley in the mid-estuary region was significantly different. The initial *Skeletonema costatum* bloom (also seen at Calshot) in April resulted in only a small increase in chlorophyll, and this was followed in the first half of May by a chlorophyll peak (15 $\mu g\ l^{-1}$) resulting from the *Rhizosolenia delicatula* bloom. The main chlorophyll peak (70 $\mu g\ l^{-1}$) occurred at the end of June and begining of July, coincident with blooms of the dinoflagellate *Scrippsiella trochoidea* and the autotrophic ciliate *Mesodinium rubrum*. During the *Mesodinium rubrum* bloom, all three nutrients (nitrate, phosphate, silicate) were just above detection levels.

The conditions leading to the initiation, development, duration and decay of blooms in Southampton Water are not well known. Rees and Williams (1982) suggested the development of the bloom appears to be determined, predominantly, by the relationship between growth rate and flushing time, i.e. growth rate has to exceed the flushing time for the bloom to initiate. Neither nutrients nor light appear to be limiting the initiation and development of algal growth in spring, though temperature may be influential. Inorganic nitrogen is the most likely factor limiting the peak and duration of the bloom in summer.

The first known attempt to undertake detailed investigations prior to, and throughout red-tide events caused by *M. rubrum* was provided by Crawford et al. (1997). *Mesodinium rubrum* red-tide events were investigated in detail between 1985-1987 and were characterised by cell numbers which increased to around 1000-3000 ml^{-1}, and chlorophyll levels in excess of 100 $\mu g\ l^{-1}$. Initiation of the blooms did not appear to be triggered by irradiance or nutrients, but coincided with an increase in stability of the water column and increased water temperature.

In some years, *Mesodinium rubrum* blooms have been shown to be maintained in the estuary for several weeks. Nutrient levels are severely depleted during the bloom, with the riverine discharge being the main nutrient supply to maintain the bloom. *Mesodinium rubrum* is a highly motile plankton with rapid swimming speeds of up to 5mm per second. It tends to swim upward to the surface as light increases and downwards as light decreases. This vertical migration behaviour gives the ciliate the ability to swim down to the bottom thus minimising flushing losses from the estuary. Since there was still a significant quantity of nutrients remaining in the water column even at the peak of the bloom, Crawford et al. (1997) suggested that as with bloom initiation, the decline of the red-tides might be linked to declining water column stability.

Mesodinium rubrum blooms were a regular occurrence in the estuary up until 1996 when they seemed to become less frequent. A red-tide bloom occurred in early August 1998. Unlike some dinoflagellate red-tides *Mesodinium rubrum* is not a toxic organism, but blooms can have an impact upon the nutrients and DO concentration in the estuary.

Typical DO saturation values during bloom periods in surface waters are 150% and sometime up to 175%. DO supersaturation is a potential hazard to some organisms, causing, for example, gas-bubble disease in fish. It has been reported (Rees & Williams, 1982; Soulsby et al., 1984; Crawford et al., 1997) that severe depletion down to 20% saturation can occur in regions of the upper estuary during or after *Mesodinium rubrum* blooms. Soulsby et al. (1984) modelled red-tide events and suggested that oxygen depletion resulted from respiration by the ciliate (and presumably bacterioplankton) in the water column, rather than from mass sedimentation of the bloom followed by decomposition. Despite these very low DO saturation values in the estuary, no adverse affects on macroorganisms have been demonstrated to date. However, Horstman (1981) has attributed mass mortalities of macroorganisms, caused by hypoxia and anoxia, to blooms of *M. rubrum* off the coast of South Africa.

Chapter 3 DO and oxygen consumption by planktonic community in Southampton Water

3.1 Introduction

There have been few systemic studies describing the seasonal variation of dissolved oxygen and planktonic community respiration throughout Southampton Water and the Solent estuarine system. Souza Lima and Williams (1978) reported oxygen consumption rates of incubated plankton concentrates collected from stations mainly in the Test Estuary and Southampton Water, from February to September 1972. They suggested winter respiration rates in the upper part of the estuary were sustained by external inputs (domestic and industrial sewage, riverine discharge), whereas summer increases in respiration rates were due to increased phytoplankton abundance. Rees and Williams (1982) reported rates of phytoplankton respiration for May-October 1981 in the Test Estuary, and showed a maximum respiration rate of 178.5 μmol O_2 l^{-1} d^{-1}, which coincided with a *Mesodinium* bloom. During the *Mesodinium* bloom, the surface DO was supersaturated and following the bloom there was a period of oxygen sag with 40.6% saturation in bottom waters. Soulsby et al. (1984) also reported an oxygen sag in bottom waters of the upper Test Estuary during the highly productive months. Crawford et al. (1994) reported a sequence of vertical DO profiles measured in July 1987 at Cracknore in the Test Estuary, showing clear evidence of the oxygen depletion caused by the high respiration rates of planktonic biomass in the water column following a bloom event.

There have been no detailed seasonal spatial surveys of oxygen saturation and plankton respiration measurements made throughout the Itchen Estuary and Southampton Water. A monthly survey programme was conducted as part of the SOuthern NUtrient Study (SONUS) between January 1998 and March 1999 to investigate the water quality status of Southampton Water including the Itchen Estuary and to produce a data set that could be compared with output from a water quality model of the estuary.

The aims of the survey were:

1. To determine the temporal and spatial variation of water quality indicated from measurement of DO in Southampton Water
2. To investigate the main factors or processes controlling the dynamics of dissolved oxygen in the estuary
3. To provide a data set for model parameterisation and to validate the water quality model developed

3.2 Survey details

The dissolved oxygen concentration and oxygen consumption (dark respiration rate) by the planktonic community was measured on each survey at a number of locations throughout the estuary. In addition, the following parameters were determined at each station: vertical temperature (T) and salinity (S) distribution, suspended particulate matter (SPM), chlorophyll concentration, dissolved inorganic nutrient concentration (nitrate, silicate and phosphate) and occasionally light attenuation. Surveys (Table 3.1) were conducted once per month throughout the 15 month period (January 1998-March 1999) and twice per month during phytoplankton growth periods in the spring and summer.

Table 3.1 Summary of surveys and data availability.
+ measured and available. +* measured but not used in data manipulation
- measurement made, but failed to yield reliable data

Date	Tide	T, S profile	DO	Community respiration	DIN	DIP	silicate	SPM	Chlorophyll
16/01/98	spring	+	+	+	+	+	+	+	+
26/02/98	spring	+	+	+	+	+	+	+	+
30/03/98	spring				+	+	+	+	+
21/04/98	neap				+	+	+	+	+
28/04/98	spring				+	+	+	+	+
12/05/98	mid	+	+	+	+	+	+	+	+
19/05/98	neap	+	+	+	+*	+*	+*	+*	+
05/06/98	neap	+	+	+	+	+	+	+	+
12/06/98	spring	+	+	+	+	+	+	+	+
23/07/98	spring	+	+	+	+	+	+	+	+
12/08/98	spring	+	+	+	+	+	+	+	+
24/09/98	spring	+	+	+	+	+	+	+	+
20/10/98	spring	-	+	+	+	+	+	+	+
02/12/98	mid	+	+	+	+	+	+	+	+
19/01/99	spring	-	+	+	+	+	+	+	+
16/02/99	mid	-	-	-	+	+	+	+	+
19/03/99	spring	-	+	+	+	+	+	+	+

Survey stations (Figure 3.1) were selected from Woodmill at the head of the Itchen Estuary (tidal limit) downstream to Calshot Buoy at the junction with the west and the east Solent, near the mouth of Southampton Water. Table 3.2 lists the stations sampled in the transect surveys. A total of 20 stations were routinely sampled, and at each station T and S were measured using a WS Oceans STD at each meter. Water samples were collected for DO and community respiration rate measurements from 10 sites at 1 metre beneath the sea surface and from 1 metre above the bottom. Separated samples were also collected for measurement of chlorophyll a concentration, SPM and inorganic nutrients (nitrate, phosphate and silicate).

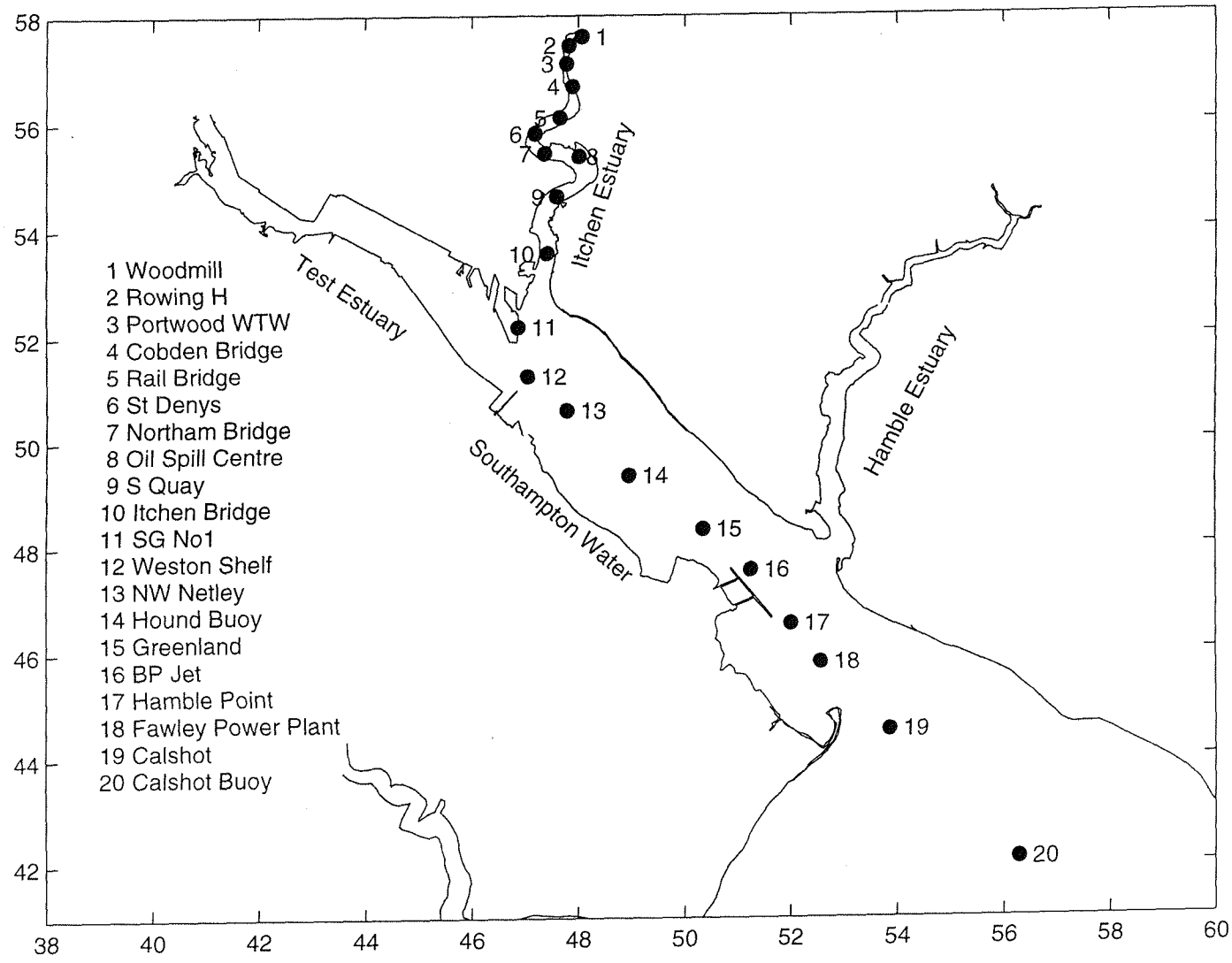

Figure 3.1 Sample stations of monthly transect surveys in the Itchen Estuary and Southampton Water

Table 3.2 Sampling stations of monthly SONUS transect surveys (see Figure 3.1).

Station No	Station	Distance (m) from Woodmill	Distance (m) to next station	DO, respiration rate, S, T profile	Nutrient, SPM, Chlorophyll
1	Woodmill	0	330	+	+
2	Rowing H	330	357		+
3	Portswood WTW	687	441	+	+
4	Cobden Bridge	1,128	694	+	+
5	Rail Bridge	1,822	571		+
6	St Denys	2,393	461		+
7	Northam Bridge	2,854	668	+	+
8	Oil Spill Centre	3,522	1,053		+
9	S Quay	4,575	1,163		+
10	Itchen Bridge	5,738	1,614	+	+
11	SG No 1	7,352	1,244	+	+
12	Weston Shelf	8,596	992		+
13	NW Netley	9,588	1,714	+	+
14	Hound Buoy	11,302	1,727		+
15	Greenland	13,029	1,195	+	+
16	BP Jet	14,224	1,278		+
17	Hamble Point	15,502	926	+	+
18	Fawley Power Plant	16,428	1,820		+
19	Calshot	18,248	3,457		+
20	Calshot Buoy	21,705		+	+

Ideally the survey would have covered the whole of the Southampton Water estuarine system including the Test Estuary, Itchen Estuary and Southampton Water. Practically, however, this was not possible and the Test Estuary was not surveyed above Dockhead. The transect survey was limited to the Itchen Estuary and Southampton Water. Since access to the upper parts of the Itchen Estuary are restricted by water depth, surveys were mainly carried out at high water on spring tides, and the order in which stations were sampled during the survey depended on the time of high water. Occasionally sampling was conducted during neap tides with the aim of comparing the difference between neap and springs. The total time for each survey was about 4-5 hours.

At each DO sample station a surface DO sample and a water sample for surface community respiration measurement were taken, and a vertical profile of salinity and temperature measured. At some stations near bottom DO measurements and samples for bottom community respiration measurements were also taken. Surface nutrients (nitrate, phosphate, silicate), SPM and chlorophyll samples were taken at all 20 stations (Table 3.1, Table 3.2).

Water samples for DO measurement were collected using a 10L Niskin sampler. Once the Niskin sampler was brought on deck, three 50ml DO bottles were filled, and 0.5ml of manganese chloride and 0.5ml alkaline iodine solution added according to Parsons et al. (1984). During the initial surveys (16/01/98, 26/02/98, 12/05/98, 19/05/98), a two litre bottle of surface water sample was collected at each station, and brought back to the laboratory for community respiration measurement. The water sample was redistributed in the laboratory into six 50 ml bottles, of which 3 DO bottle samples were fixed immediately with Winkler reagents, and the

other 3 bottles were incubated in a light proof box in a constant temperature room, set close to the in situ water temperature. After 24 hours incubation, Winkler reagents were added to the incubated bottles, and respiration rate calculated from the difference of DO concentration of the water sample at zero time and after 24 hours incubation.

It was found to be inconvenient and time consuming to redistribute the water samples back in the laboratory following the survey. Therefore during the later surveys, nine 50 ml DO bottles were filled from the Niskin sampler on the boat at the same time. Three duplicate bottles were fixed immediately with Winkler reagents, to define the *in situ* DO concentration, the other six bottles were taken back to the laboratory. Three of these were fixed in the laboratory, the other incubated for 24 hours prior to addition of Winkler reagents.

3.2.1 DO laboratory methods

DO concentration was determined using the Winkler method, and samples analysed using either the manual titration system (described by Bryan, et al., 1979) or the automatic computer controlled system (similar to that described by Williams and Jenkinson, 1982).

3.2.1.1 Standardisation of thiosulphate

Before titration of samples began, the thiosulphate was standardised. Firstly, a 1 litre solution of 0.01N potassium iodate was made up as described in Parsons et al. (1984). 10 ml of this solution was then added using a glass pipette to a clean 50 ml oxygen bottle half filled with milli-Q water. The exact volume dispensed by the 10 ml pipette was determined by weight. 0.5 ml of 10N sulphuric acid was added to the bottle followed by 0.5 ml of alkaline iodide solution and the contents mixed (Parson et al., 1984). Five replicates were produced and each titrated as described below. The normality of the thiosulphate N_T was determined by the following equation:

$$N_T = (V_I * N_I)/V_T \qquad (3.1)$$

where:

N_T = normality of thiosulphate solution (N);

V_T = volume of thiosulphate added (ml);

N_I = normality of iodate solution (N);

V_I = volume of iodate added (ml).

The mean normality from the five replicates was then determined.

3.2.1.2 Manual titration

The apparatus consisted of an endpoint detector connected to a chart recorder and a Metrohm Dosimat 665 automated 1 ml microburette.

To check 100% transmission on the chart recorder, an oxygen bottle containing distilled or sea water was placed in the water bath between the light source and light detector and the chart recorder pen was set at full scale deflection. An opaque card was then placed between the water bath and the light detector to check 0% transmission.

Immediately before titration, 1 ml of 10N sulphuric acid was added to a DO bottle. The bottle was placed into a water bath and a magnetic stirrer bar added to mix the sample. Thiosulphate was then added gradually from the Dosimat until deflection of the chart recorder ceased, indicating that the end point had been reached. The readout of the autotitrator was noted along with the bottle volume.

Oxygen concentrations in $\mu mol\ l^{-1}$ were then calculated using a simple Turbo Basic computer program. This required the *in situ* and fixing temperature of the sample to be given (both were same for DO sample, but different for incubation sample), along with *in situ* salinity, volume of thiosulphate added, bottle volume and normality of thiosulphate. The formulae used in the calculation was given by Iriarte (1991).

3.2.1.3 Computer controlled titration

This method is basically identical to the above method, however, the end point and thiosulphate addition is monitored and controlled by a Hewlett-Packard HP85 microcomputer. When functioning properly, this provides a more accurate and consistent result than the manual method. The dissolved oxygen results were given in % saturation and $\mu mol\ l^{-1}$ calculated from a Basic program running in the microcomputer.

3.2.2 Chlorophyll measurement

During the survey at each station, a 50 ml surface water sample was filtered through a GF/F glass fibre filter (1.45 μm pore size). The filter was then folded with seston inside, placed into a labelled plastic bag and stored in a freezer until analysed. Two replicates were taken from each sample.

The photosynthetic pigments chlorophyll a and phaeo-pigment, were measured using a fluorometric method (Kifle & Purdie, 1993; Mills & Tett, 1990). The spectrophotometric method was used to calibrate the fluorometer (Parson et al., 1984). The whole measurement procedure is a three step procedure.

1. Fluorometric analysis. The filters were placed in a thick walled glass tube and 5 ml of 90% acetone added, the filters were ground using a plastic homogenising tip on a hand operated drill. Once homogenised, the material was placed in a covered plastic tube. Another 5 ml of acetone was then added to the glass tube to wash off the homogenising tip, this was then added to the rest of the material. All samples were labelled and left for 24 hours in a dark refrigerator to allow chlorophyll extraction. Samples then were centrifuged at 2000 r.p.m in

cooled holders. The supernatant was carefully decanted and placed in a similar tube. An AMINCO fluorometer was used for the fluorometric analysis. A subsample was placed in a cuvette and a reading taken, then 2 drops of 10% HCl were added, the cuvette inverted and another reading immediately taken. Periodic blanking, with 90% acetone was carried out during each analysis and the standard remeasured at the end of the analysis.

2. Calibration of fluorometer. Fluorometer readings were calibrated with a pure chlorophyll a solution (Sigma) of known concentration. This was quantified using a spectrophotometer (UNICAM SP500 Series 2), measuring the absorption at different wavelengths (750, 665 nm) before and after acidification. The standard solution was diluted with 90% acetone and the relative intensity was measured in the fluorometer. The concentration of the standard and the subsequent fluorometer reading was used to calculate the chlorophyll a and phaeo-pigment concentration of the natural samples (Parson, et al., 1984), The fluorometer was standardised on the day that samples were analysed.
3. Calculation of chlorophyll a concentration. The readings obtained correspond to relative fluorescence intensity values, and these were converted to chlorophyll a concentration in units of $\mu g\ l^{-1}$ using the Turbo Basic programmes SPCCHL.BAS and CHLLA.BAS. Chlorophyll a, phaeo-pigment concentration and percentage CHLa were determined according to equations given in Parsons et al. (1984) for fluorometric analysis of chlorophyll a.

3.2.3 Suspended particulate matter measurement

Total SPM concentrations were measured from the difference of the dry weight of a GF/F filter before and after filtration of a known volume of sea water sample.

Prior to each survey, the GF/F 47mm diameter filters were soaked in distilled water for approximately 10 minutes. 150 ml of distilled water was then filtered through each filter to remove any loose fibres. The filters were then placed onto pre-combusted foil and dried in an oven at 80 ^{0}C for at least 10 hours. All filters were then taken from the oven immediately to the balance and weighted (W1) to an accuracy of 0.1 mg. The weighed filters were then put into numbered Petri Slides and corresponding filter weight noted.

After each survey, the filters were placed into a freezer until further analysis. The filters were dried in an oven at 80 ^{0}C for at least 10 hours, then weighed (W2) using the same balance. The SPM concentration was then calculated as the difference between weight after and before filtration, and divided by the sea water volume filtered (in litres).

3.2.4 Dissolved inorganic nutrients measurement

All sea water samples were filtered through a GF/F filter into plastic diluvials during the survey. All samples were kept cool in a refrigerator prior to analysis.

In this research all filtered water samples were analysed using a Burkard Scientific SFA-2 Auto-analyser, which is based on the traditional spectrophotomatric Murphy and Riley (1962) method, linked up to a Digital-Analysis Microstream data capture and reduction system. The methods used to determine nitrate, phosphate and silicate were based on colorimetric analysis, and detailed descriptions of the methods was given by Wright and Hydes (1997).

3.2.4.1 Nitrate

The analysis of nitrate requires the reduction of nitrate to nitrite. Nitrite is measured by forming a diazo compound and then an azo dye, which is measured at 540 nm. A Cu/Cd reductor column supplied by Skalar was used to reduce nitrate to nitrite. The nitrite concentration was not measured separately, therefore values reported are for nitrate plus nitrite. Previous studies have shown that nitrite represents less than 5% of total NO_2+NO_3 in Southampton Water (Howard et al., 1995) or about 2% of total NO_2+NO_3 (Collins, 1978).

3.2.4.2 Phosphate

Phosphate is reacted with acidified molybdate reagent to form a phosphomolybdate complex which is then reduced to a highly blue compound. Ascorbic acid is used as the reducing agent with potassium antimonyl tartrate in a single solution reagent. The mixed reagent reacts rapidly with phosphate ions to give a blue-purple complex containing antimony and phosphorous which is measured at 880 nm.

DIP samples were measured using a Burkard Scientific SFA-2 Auto-analyser, which is based on the established spectrophotometric method (Murphy and Riley, 1962). The reagents were all prepared from analytical grade chemicals.

3.2.4.3 Silicate

Dissolved silicate reacts rapidly in acidic molybdate solution to form yellow silicomolybdic acid. This latter may be reduced using a number of reducing agents to give an intense blue coloured compound which is measured at 660 nm. Ascorbic acid was added prior to the reduction step to prevent interference from phosphate.

3.2.5 Light attenuation measurement

During some surveys, at each station, irradiance profiles were measured by recording light levels with a LiCor submarine light sensor attached to a LiCor data logger. Readings were taken at 0.5 meter intervals in the surface 2 meters then at 1 meter intervals to the bottom or until light was undetectable. Light was simultaneously logged with a surface sensor. Assuming that the light attenuation coefficient is the same over the depth interval, then the light attenuation coefficient k is given by:

$$k = \frac{1}{\Delta z} \ln \frac{I_0}{I_1} \qquad (3.2)$$

where I_0 is the light intensity at depth z; I_1 is the light intensity at depth z+Δz; Δz is the depth interval of two measurements.

3.3 Results

3.3.1 Salinity, flushing time and temperature

A typical longitudinal salinity distribution from a survey conducted on 23/07/98 is shown in Figure 3.2a. The data from all surveys are combined in Figure 3.2 b. It is apparent that the high salinity gradients (vertical or longitudinal) occurred in the upper parts of estuary. The surface salinity increases rapidly downstream in the upper parts of the Itchen Estuary from Woodmill (0 km) to Northam Bridge (2.8 km). The average salinity at the Itchen Bridge (5.7 km) is above 30. The salinity increased gradually from Itchen Bridge downstream to Calshot Buoy (average salinity of 34 at 21.7 km).

Surface to bottom salinity differences (Figure 3.2c) show the spatial variation of salinity stratification in the estuary. The water column was always highly stratified in the upper part of the Itchen Estuary. The maximum surface to bottom salinity difference generally occurred at Cobden Bridge (1.1 km) and occasionally at Northam Bridge (2.8 km). The distance from Woodmill to Cobden Bridge is about 1.1 km, and from Cobden Bridge to Northam Bridge is 1.7 km. This suggests that the maximum vertical salinity gradient occurs in a distance of 1.7 km between Cobden Bridge and Northam Bridge.

After Northam Bridge the surface to bottom salinity difference decreases rapidly, at Itchen Bridge (5.7 km) and at SG No 1 (7.3 km) the averaged difference is between 2.0 and 3.0. At Calshot Buoy (21.7 km) the waters were vertically well mixed, with surface to bottom salinity difference always less than 0.5.

Flushing time (time required to replace the existing fresh water at a rate equal to the river discharge), is a very useful indication of the mixing rate whereby material is transported through an estuary, and can be calculated from a knowledge of salinity distribution (e.g. Dyer, 1973, 1981; Bowden, 1967,1980).

Flushing time t_1 is given by:

$$t_1 = F/R \qquad (3.3)$$

where R is the rate of influx of fresh water (mean monthly freshwater flows used for Test and Itchen rivers supplied by Environment Agency) and F is the total volume of fresh water accumulated in the estuary. If S is the salinity at any point within the estuary and S_0 is the salinity of the sea water which is available for mixing, the freshwater content at that point is given by:

$$f=(S_0-S)/S_0 \quad (3.4)$$

To determine F, the estuary is divided into a suitable number of elements of volume ΔV and the appropriate value of f assigned to each element. The total fresh water content is then given by:

$$F = \sum f\Delta V \quad (3.5)$$

where the summation is carried out over the total volume V.

Table 3.3 shows an example of estimated flushing times for regions of Itchen Estuary and Southampton Water calculated from the survey data of 23/07/98 during the summer when freshwater flows are low. The short residence time of water in the upper Itchen Estuary is evident, whereas flushing times of waters between Woodmill and stations in Southampton Water are between 5 an 11 days. The salinity in the estuary ranged form 0.7 at Woodmill to 32.8 at Dockhead. The salinity distribution in the Itchen Estuary covers almost the complete salinity range, which is from 0 to 32.4, while the salinity difference from Dockhead to Calshot Buoy was only 1.2.

Table 3.3 Calculated flushing times for different sections of the estuary bewteen Woodmill and stations listed for 23/07/98.

Stations	Distance from Woodmill (m)	Flushing time (day)	Surface salinity
Woodmill	0	0	0.7
Portswood WTW	687	0.06	0.4
Cobden Bridge	1,128	0.22	2.8
Northam Bridge	2,854	1.30	23.4
Itchen Bridge	5,738	2.30	31.5
SG No 1	7,352	3.30	32.8
NW Netley	9,588	5.35	31.2
Greenland	13,029	8.50	32.4
Hamble Point	15,502	11.3	33.2
Calshot Buoy	21,705		34.0

Due to estuarine circulation, the residence time of surface water is likely to be shorter than bottom water which is trapped by the upstream estuarine circulation. Calculation of flushing times in different sections of the estuary indicate that due to short flushing times in the upper Itchen Estuary, growth of phytoplankton in this region of the estuary is limited.

The main driving force of seasonal changes in water temperature is variation in solar radiation. Figure 3.3a gives the sea surface solar irradiance (two weeks average) in the Southampton area for 1998, and shows a clear pattern of annual variation. This data was mainly obtained from a meteorological station at Thorny Island (W00°55', N50°49'), with some data from Lyminton (W01°33',N50°45'). These are the closest meteorological stations to Southampton Water recording solar irradiance. The spatial averaged water temperature (Figure 3.3.b) varies with a time lag behind the solar elevation. If the time axis of the temperature is shifted to calculate the correlation coefficient between temperature and solar elevation, the maximum correlation coefficient (r^2=0.93) is achieved when the time axis is shifted 26 days

Figure 3.2a Salinity, from Woodmill to Calshot Buoy on 23/07/98 (mean tide high water)

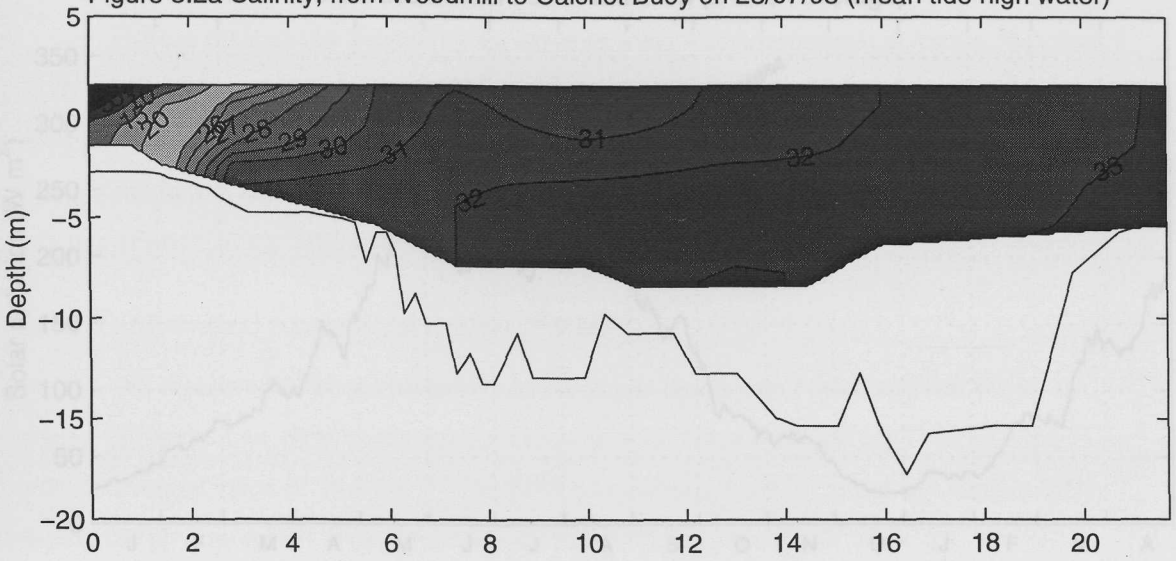

Figure 3.2b Longitudinal distribution of salinity (including all survey results)

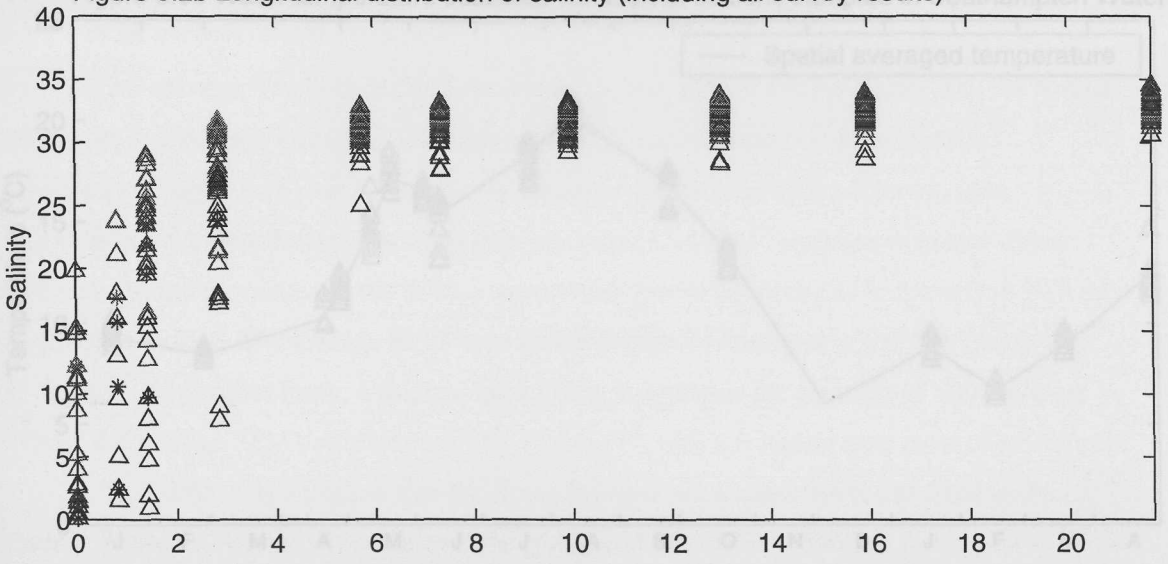

Figure 3.2c Longitudinal distribution of surface to bottom salinity differences

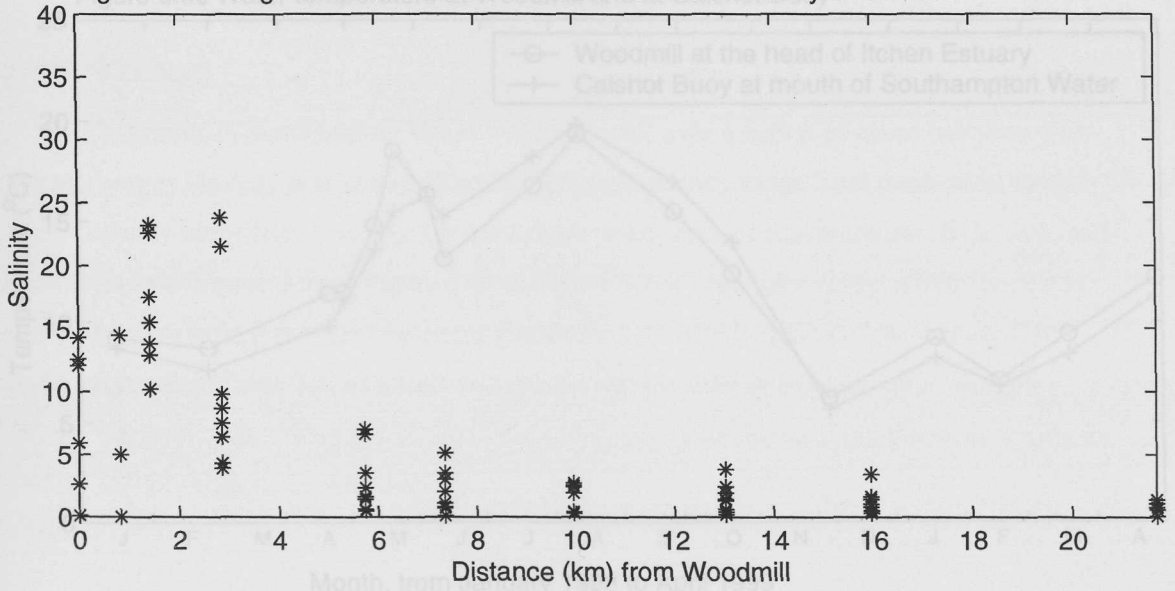

Figure 3.3a Average surface incident solar radiation (2 week average)

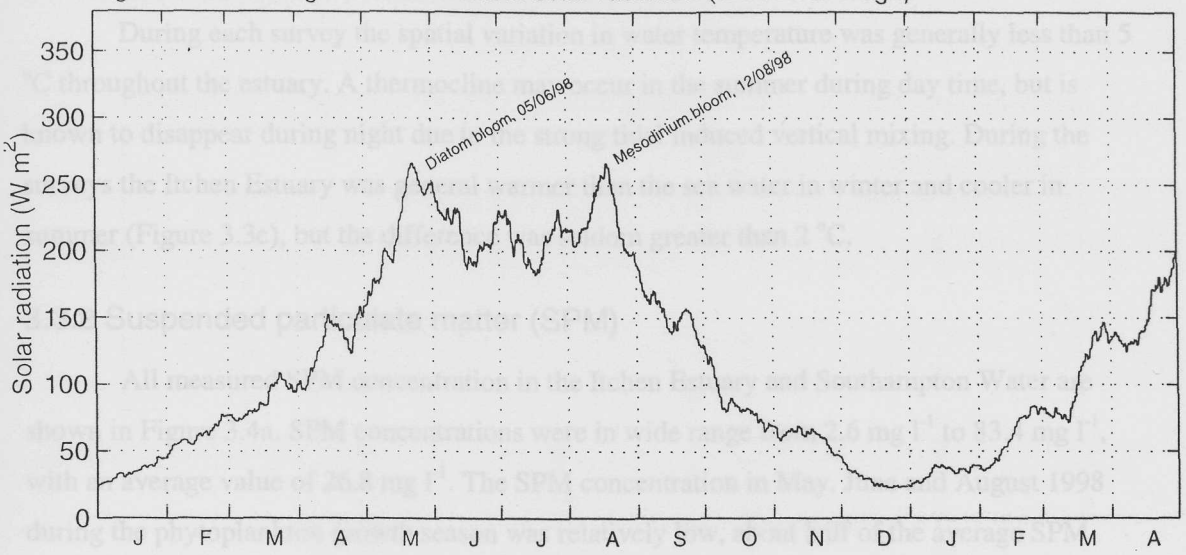

Figure 3.3b Water temperature seasonal variation at stations sampled in Southampton Water

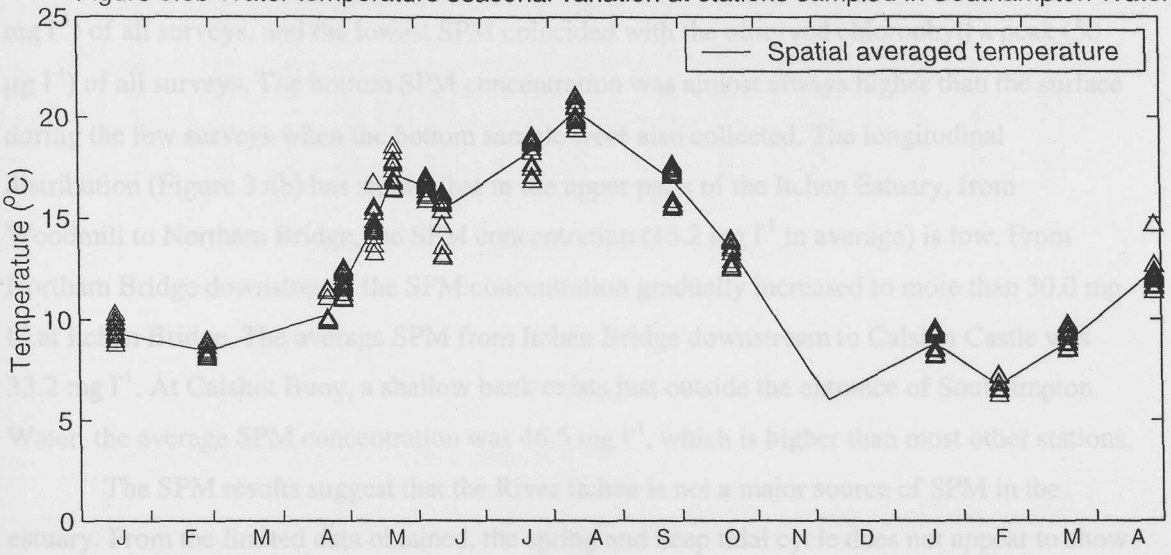

Figure 3.3c Water temperature at Woodmill and at Calshot Buoy

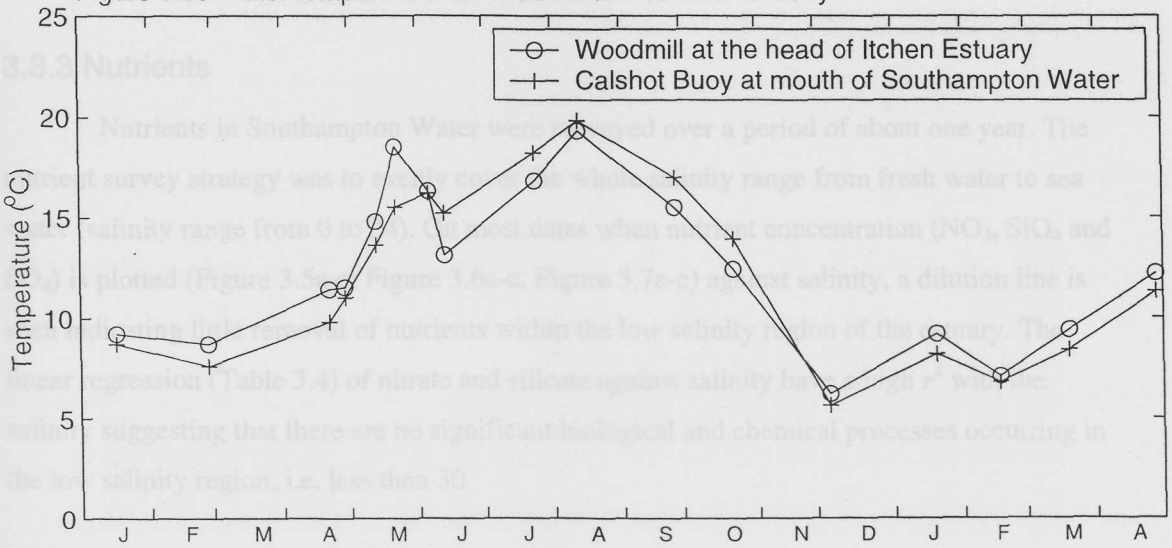

Month, from January 1998 to April 1999

earlier than the real time. This suggests the water temperature lags behind the solar elevation by about a lunar month.

During each survey the spatial variation in water temperature was generally less than 5 °C throughout the estuary. A thermocline may occur in the summer during day time, but is known to disappear during night due to the strong tidal induced vertical mixing. During the surveys the Itchen Estuary was general warmer than the sea water in winter and cooler in summer (Figure 3.3c), but the difference was seldom greater than 2 °C.

3.3.2 Suspended particulate matter (SPM)

All measured SPM concentration in the Itchen Estuary and Southampton Water are shown in Figure 3.4a. SPM concentrations were in wide range from 2.6 mg l^{-1} to 83.4 mg l^{-1}, with an average value of 26.8 mg l^{-1}. The SPM concentration in May, June and August 1998 during the phytoplankton growth season was relatively low, about half of the average SPM concentration. The 05/06/98 survey had the lowest spatial averaged SPM concentration (11.5 mg l^{-1}) of all surveys, and the lowest SPM coincided with the observed chlorophyll a peak (50 μg l^{-1}) of all surveys. The bottom SPM concentration was almost always higher than the surface during the few surveys when the bottom sample were also collected. The longitudinal distribution (Figure 3.4b) has shown that in the upper parts of the Itchen Estuary, from Woodmill to Northam Bridge, the SPM concentration (15.2 mg l^{-1} in average) is low. From Northam Bridge downstream, the SPM concentration gradually increased to more than 30.0 mg l^{-1} at Itchen Bridge. The average SPM from Itchen Bridge downstream to Calshot Castle was 33.2 mg l^{-1}. At Calshot Buoy, a shallow bank exists just outside the entrance of Southampton Water, the average SPM concentration was 46.5 mg l^{-1}, which is higher than most other stations.

The SPM results suggest that the River Itchen is not a major source of SPM in the estuary. From the limited data obtained, the spring and neap tidal cycle does not appear to show a strong correlation with the magnitude of the SPM concentration.

3.3.3 Nutrients

Nutrients in Southampton Water were surveyed over a period of about one year. The nutrient survey strategy was to evenly cover the whole salinity range from fresh water to sea water (salinity range from 0 to 34). On most dates when nutrient concentration (NO_3, SiO_4 and PO_4) is plotted (Figure 3.5a-c, Figure 3.6a-c, Figure 3.7a-c) against salinity, a dilution line is seen indicating little removal of nutrients within the low salinity region of the estuary. The linear regression (Table 3.4) of nitrate and silicate against salinity have a high r^2 with the salinity suggesting that there are no significant biological and chemical processes occurring in the low salinity region, i.e. less than 30.

Figure 3.4a Observed SPM (mg l^{-1}) in the Itchen Estuary and Southampton Water

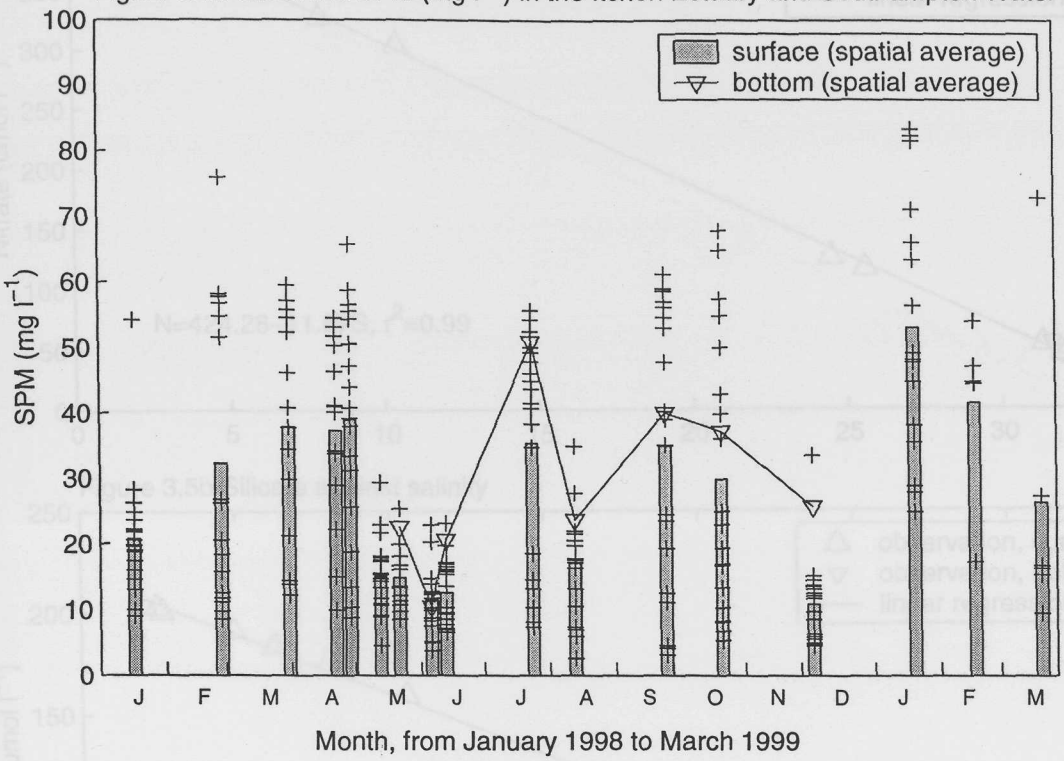

Figure 3.4b Longitudinal distribution of SPM (mg l^{-1})

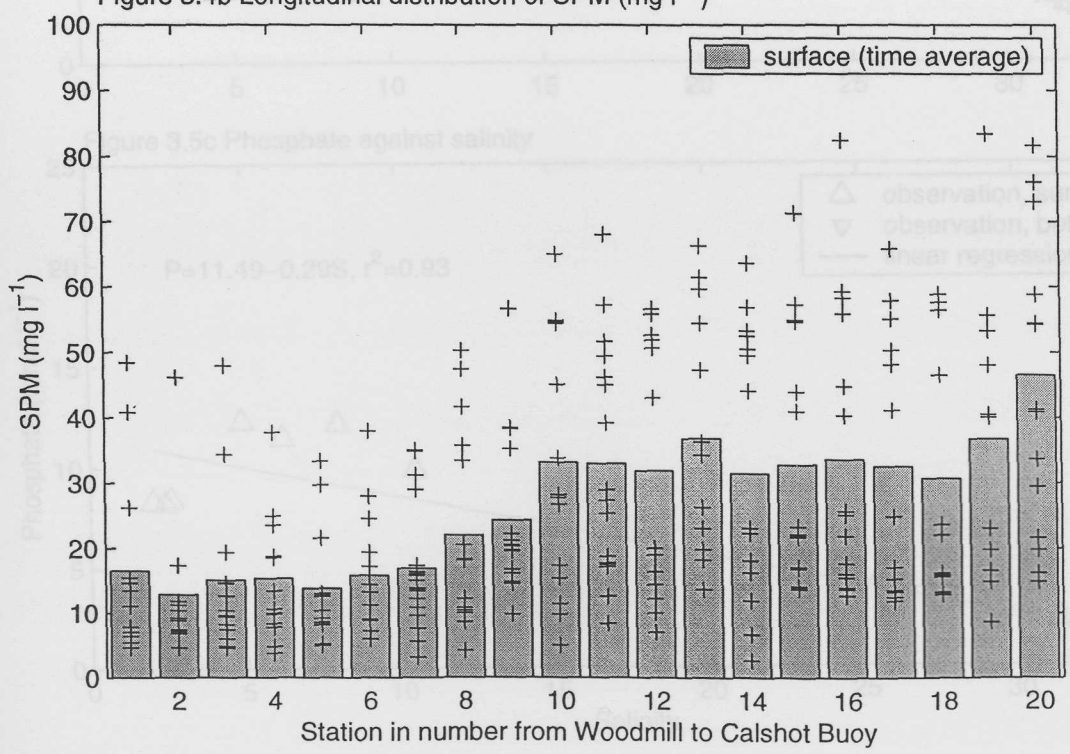

Figure 3.5 Nutrients (observation) plotted against salinity and linear regression line in the Itchen Estuary and Southampton Water, 02/12/98

Figure 3.5a Nitrate against salinity

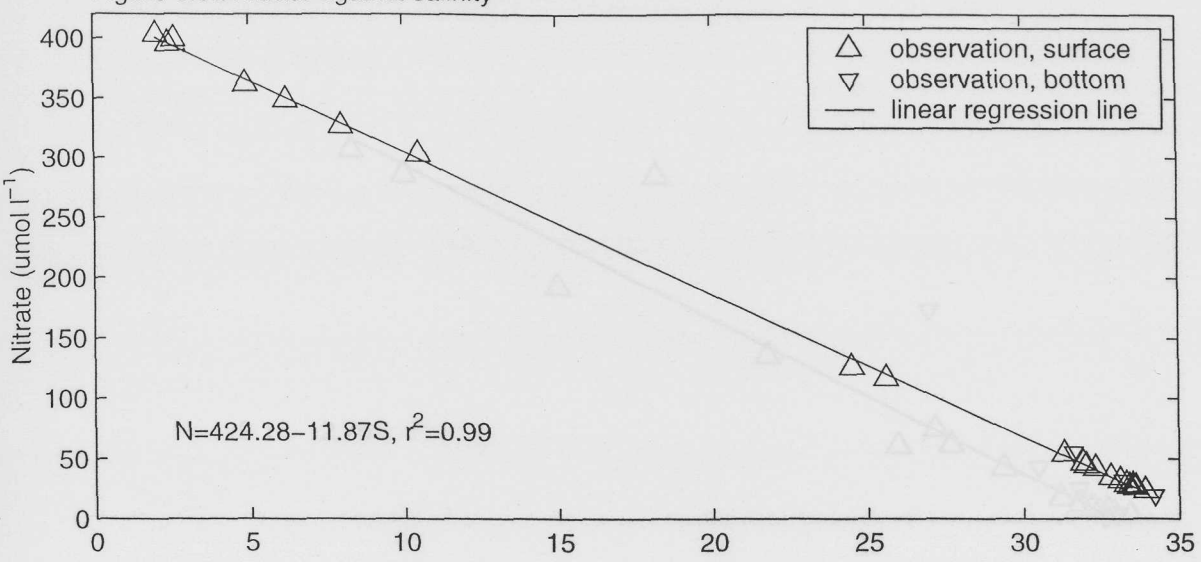

Figure 3.5b Silicate against salinity

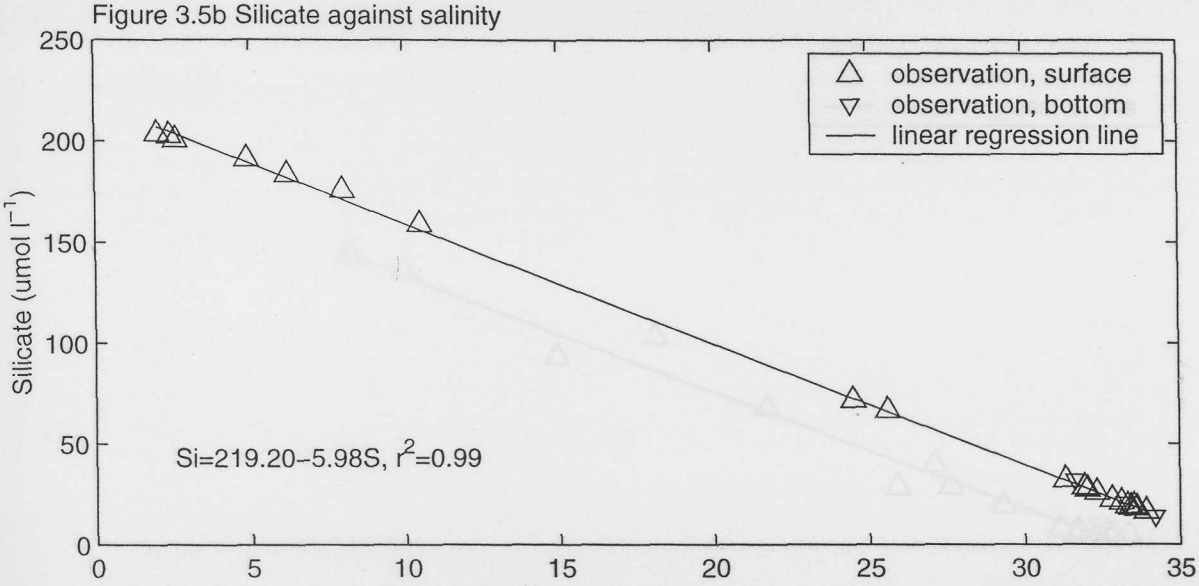

Figure 3.5c Phosphate against salinity

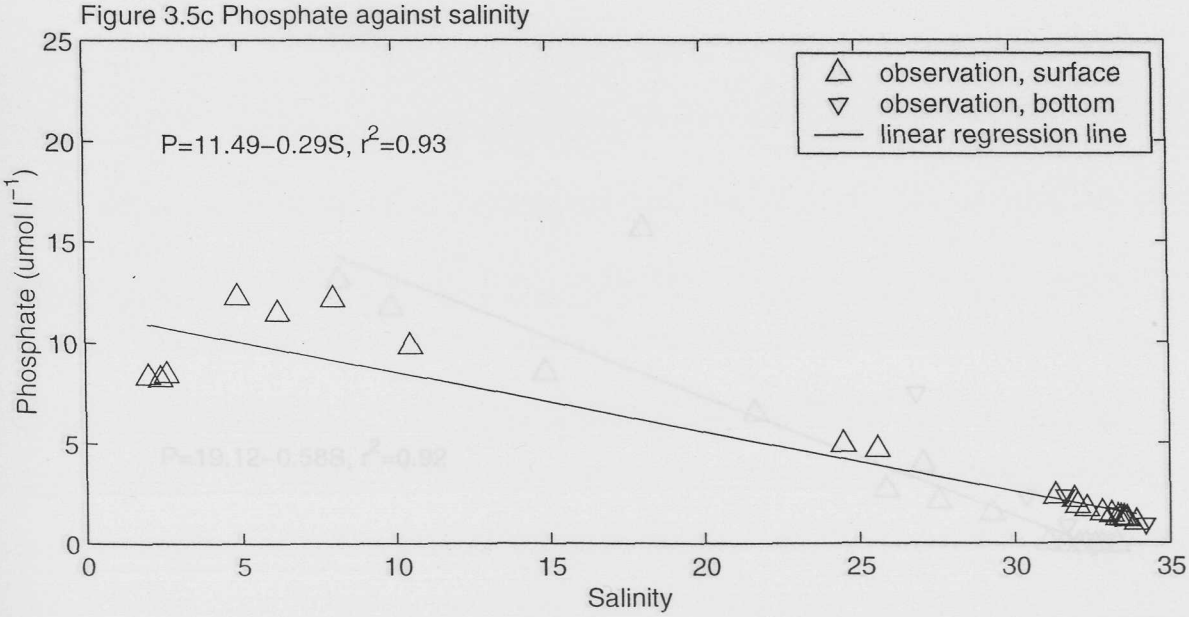

Figure 3.6 Nutrients (observation) plotted against salinity and linear regression line in the Itchen Estuary and Southampton Water, 05/06/98

Figure 3.6a Nitrate against salinity

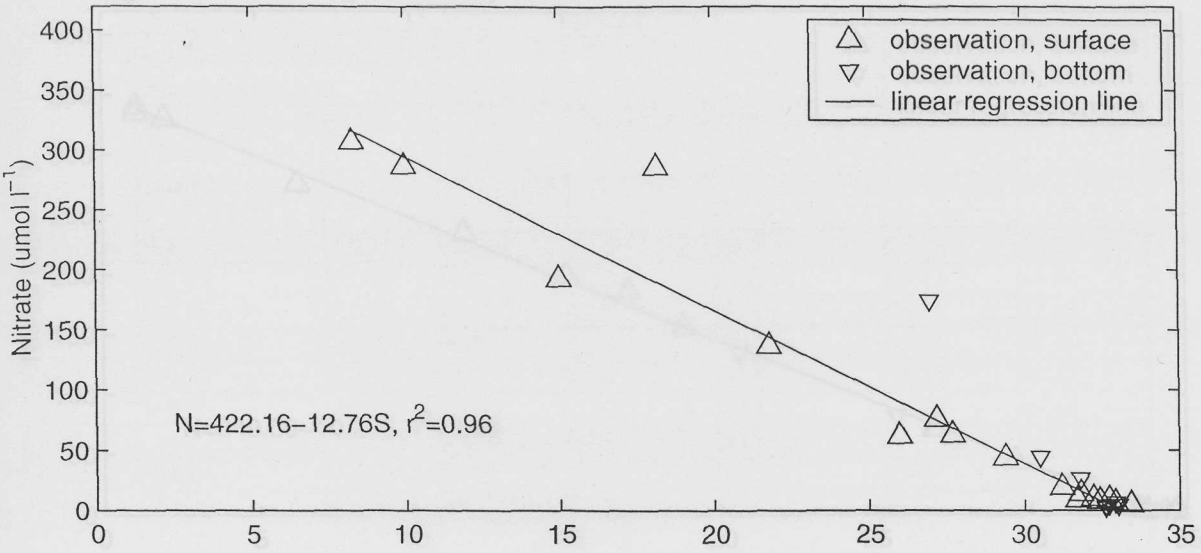

Figure 3.6b Silicate against salinity

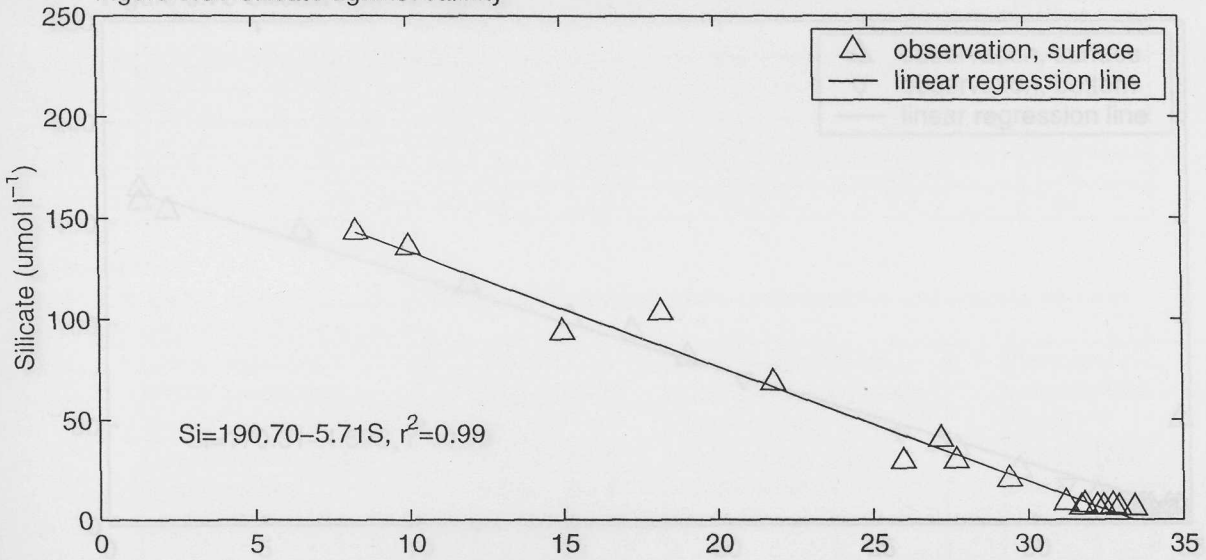

Figure 3.6c Phosphate against salinity

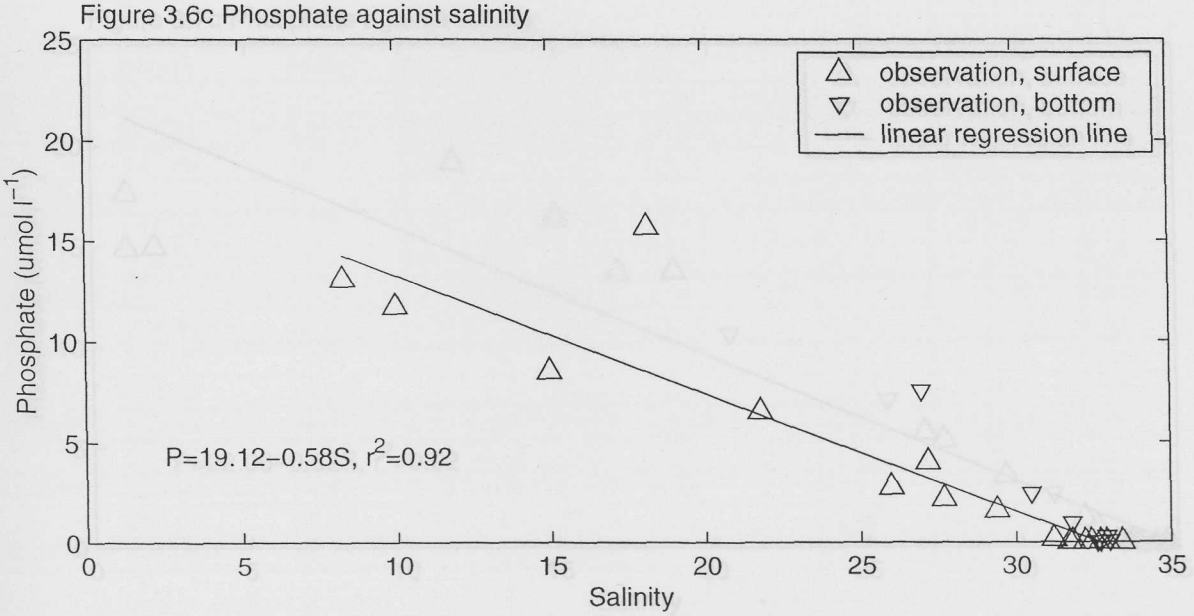

Figure 3.7 Nutrients (observation) plotted against salinity and linear regression line in the Itchen Estuary and Southampton Water, 12/08/98

Figure 3.7a Nitrate against salinity

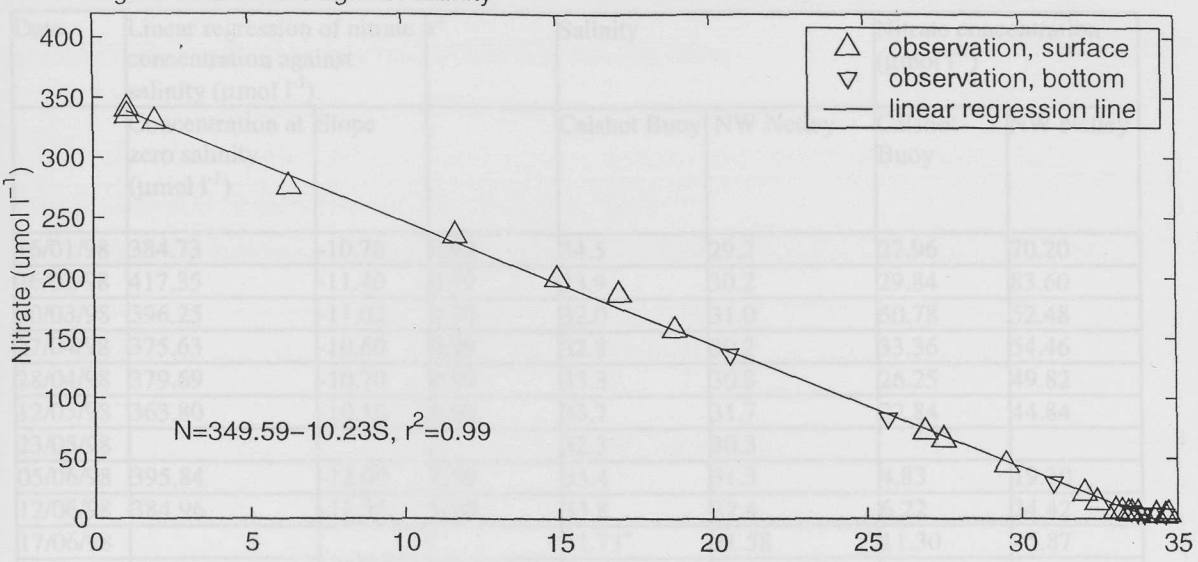

Figure 3.7b Silicate against salinity

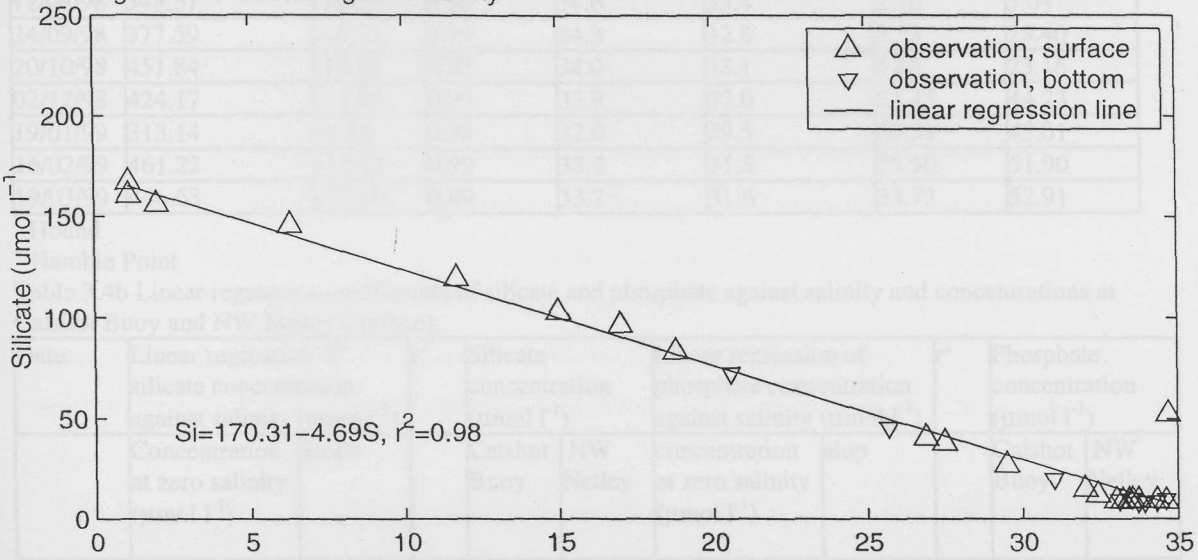

Figure 3.7c Phosphate against salinity

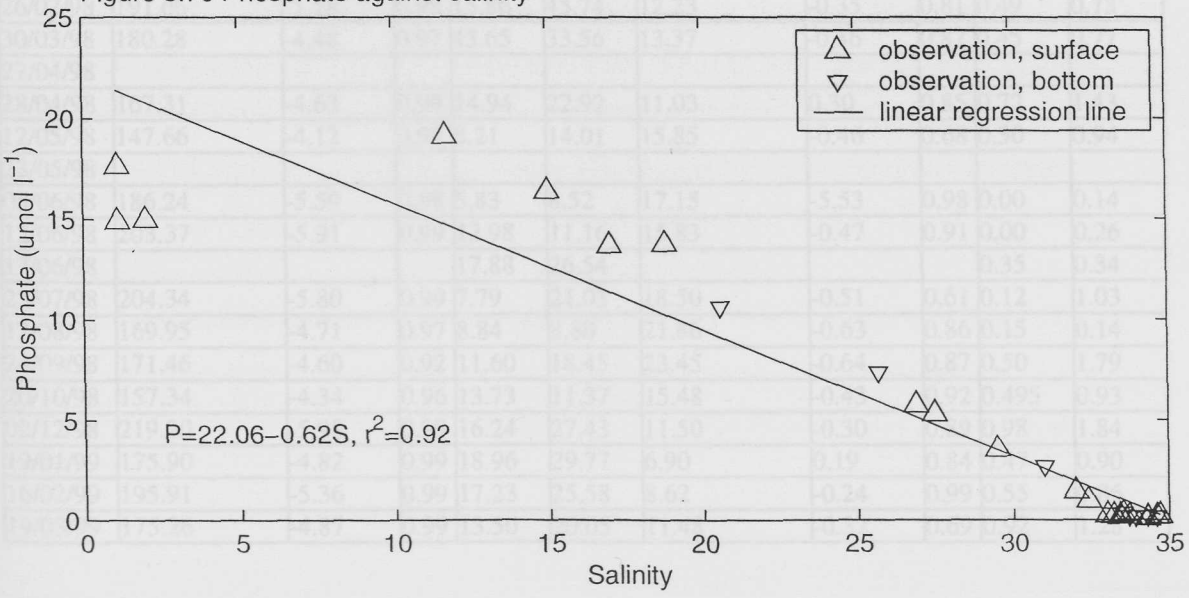

Table 3.4a Linear regression coefficients of nitrate against salinity and concentrations at Calshot Buoy and NW Netley (surface).

Date	Linear regression of nitrate concentration against salinity (μmol l^{-1})		r^2	Salinity		Nitrate concentration (μmol l^{-1})	
	Concentration at zero salinity (μmol l^{-1})	Slope		Calshot Buoy	NW Netley	Calshot Buoy	NW Netley
16/01/98	384.73	-10.78	0.99	34.5	29.2	27.96	70.20
26/02/98	417.35	-11.40	0.99	33.9	30.2	29.84	83.60
30/03/98	396.25	-11.02	0.99	32.0*	31.0	50.78	52.48
27/04/98	375.63	-10.60	0.99	32.8	30.2	33.36	54.46
28/04/98	379.69	-10.70	0.99	33.3	30.8	26.25	49.82
12/05/98	363.80	-10.10	0.99	33.7	31.7	22.84	44.84
23/05/98				32.3	30.3		
05/06/98	395.84	-12.00	0.99	33.4	31.3	4.83	19.30
12/06/98	384.96	-11.35	0.99	33.8	32.4	6.22	24.42
17/06/98				31.73+	31.58	11.30	15.87
23/07/98	366.84	-10.74	0.99	34.5	31.2	2.46	25.82
12/08/98	348.57	-10.20	0.99	34.6	33.4	2.50	5.04
24/09/98	377.59	-10.73	0.99	34.3	32.8	8.53	25.40
20/10/98	451.84	-12.94	0.97	34.0	33.1	5.68	23.16
02/12/98	424.17	-11.85	0.99	33.9	32.0	23.43	44.23
19/01/99	313.14	-8.85	0.98	32.0	29.5	26.31	45.01
16/02/99	461.22	-13.02	0.99	33.2	31.5	29.50	51.90
19/03/99	446.63	-12.39	0.99	33.2	31.6	33.73	52.91

* Hound

+ Hamble Point

Table 3.4b Linear regression coefficients of silicate and phosphate against salinity and concentrations at Calshot Buoy and NW Netley (surface).

Date	Linear regression of silicate concentration against salinity (μmol l^{-1})		r^2	Silicate concentration (μmol l^{-1})		Linear regression of phosphate concentration against salinity (μmol l^{-1})		r^2	Phosphate concentration (μmol l^{-1})	
	Concentration at zero salinity (μmol l^{-1})	Slope		Calshot Buoy	NW Netley	concentration at zero salinity (μmol l^{-1})	slop		Calshot Buoy	NW Netley
16/01/98	192.99	-5.20	0.98	26.50	52.93	9.89	-0.28	0.85	0.32	1.06
26/02/98	191.66	-5.18	0.98	15.86	45.74	12.23	-0.35	0.81	0.49	0.73
30/03/98	180.28	-4.48	0.97	43.65	33.56	13.37	-0.36	0.87	0.45	0.77
27/04/98										
28/04/98	167.31	-4.63	0.99	14.94	22.92	11.03	0.30	0.85	0.72	1.43
12/05/98	147.66	-4.12	0.98	8.21	14.01	15.85	-0.46	0.68	0.30	0.94
23/05/98										
05/06/98	186.24	-5.59	0.98	5.83	8.52	17.15	-5.53	0.98	0.00	0.14
12/06/98	203.37	-5.91	0.99	12.98	11.16	15.83	-0.47	0.91	0.00	0.26
17/06/98				17.88	26.54				0.35	0.34
23/07/98	204.34	-5.80	0.99	7.79	21.03	18.50	-0.51	0.61	0.12	1.03
12/08/98	169.95	-4.71	0.97	8.84	8.80	21.86	-0.63	0.86	0.15	0.14
24/09/98	171.46	-4.60	0.92	11.60	18.45	23.45	-0.64	0.87	0.50	1.79
20/10/98	157.34	-4.34	0.96	13.73	11.37	15.48	-0.43	0.92	0.495	0.93
02/12/98	219.20	-5.98	0.99	16.24	27.43	11.50	-0.30	0.89	0.98	1.84
19/01/99	175.90	-4.82	0.99	18.96	29.77	6.90	0.19	0.84	0.47	0.90
16/02/99	195.91	-5.36	0.99	17.23	25.58	8.62	-0.24	0.99	0.55	0.86
19/03/99	175.26	-4.87	0.99	13.50	20.05	11.48	-0.32	0.69	0.92	1.28

The linear regression of phosphate against salinity (Figure 3.5c, Figure 3.6c, Figure 3.7c) indicates more scatter due to point inputs of phosphate associated with sewage effluents into the Itchen Estuary mainly from Portswood Sewage Works.

Nutrient concentrations in bottom waters were shown to fit the linear regression line quite well. Where vertical salinity stratification is detected, the fresher surface waters have higher nutrient concentrations than saltier bottom water.

The nutrient concentration of fresh water from Itchen River has been extrapolated from the linear regression equation. Environmental Agency data (Year 1996/7) shows that the riverine sources from River Test, River Itchen and River Hamble do not show significant differences in nutrient concentrations.

3.3.4 Chlorophyll

The spatial and temporal distribution of chlorophyll a concentration in Southampton Water during the surveys is shown in Figure 3.8. On two dates high chlorophyll concentrations were detected indicating significant algal blooms (Figure 3.8a), one detected on 05/06/98 and the another on 12/08/98.

During the winter and early spring (from January to March 1998) chlorophyll a concentration was below 2 $\mu g\ l^{-1}$ at all stations. An increase in chlorophyll a concentration occurred from April when solar radiation increased (Figure 3.8a). Prior to the first diatom bloom on 05/06/98, an increase in chlorophyll concentration on 12/05/98 at Woodmill (Station 1) suggests the presence of fresh water phytoplankton or macrophyte debris. On 19/05/98, chlorophyll concentration reached a relatively high level of between 5-10$\mu g\ l^{-1}$ for the whole estuary.

On 05/06/98 a maximum chlorophyll concentration of 50.0 $\mu g\ l^{-1}$ was detected, and dominant phytoplankton species were shown to be diatoms. The diatom bloom was observed in the main channel of Southampton Water with a salinity of more than 30. Chlorophyll a concentration (Figure 3.8a) reached a maximum of 50.0 $\mu g\ l^{-1}$ at NW Netley (Station 13), and remained high at Hound Buoy (Station 14) and Greenland (Station 15), then decreased gradually to 17.1 $\mu g\ l^{-1}$ at Calshot Buoy (Station 16). Chlorophyll a concentration decreased sharply in the upper part of the Itchen Estuary from Itchen Bridge (Station 10) with salinity less than 25.

A maximum chlorophyll a concentration of 12.1 $\mu g\ l^{-1}$ was observed on 12/06/98 during a neap tide survey shortly after the 05/06/98 spring diatom bloom. The relatively high chlorophyll a concentration on 05/06/98 suggested that the diatom bloom had not completely collapsed.

Figure 3.8a Seasonal and spatial variation of chlorophyll a throughout the Itchen Estuary and Southampton Water, from January 1998 to March 1999
(bloom events indicated on 05/06/98 and 12/08/98)

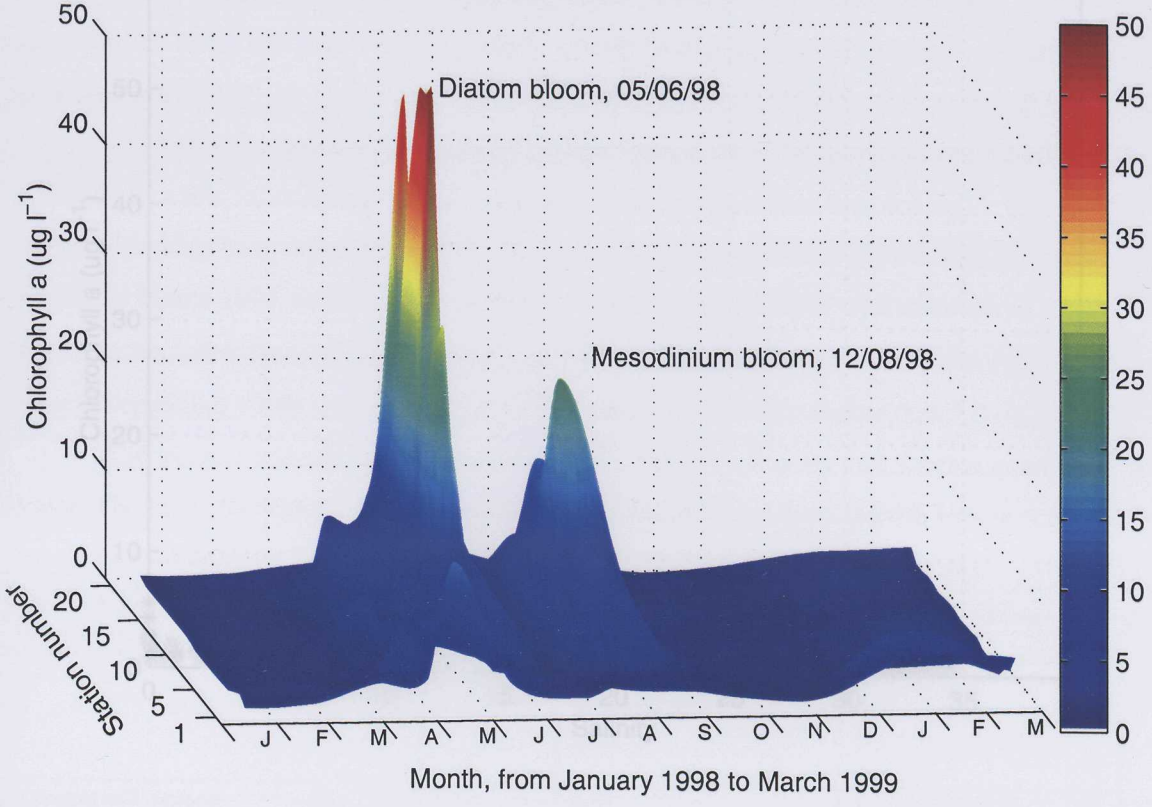

Figure 3.8b Spatially averaged chlorophyll a concentration

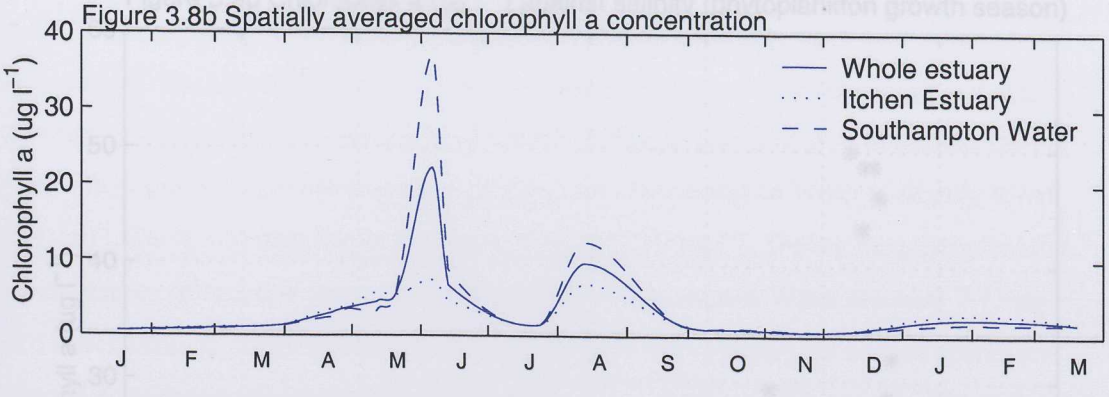

Figure 3.8c Temporally averaged chlorophyll a concentration

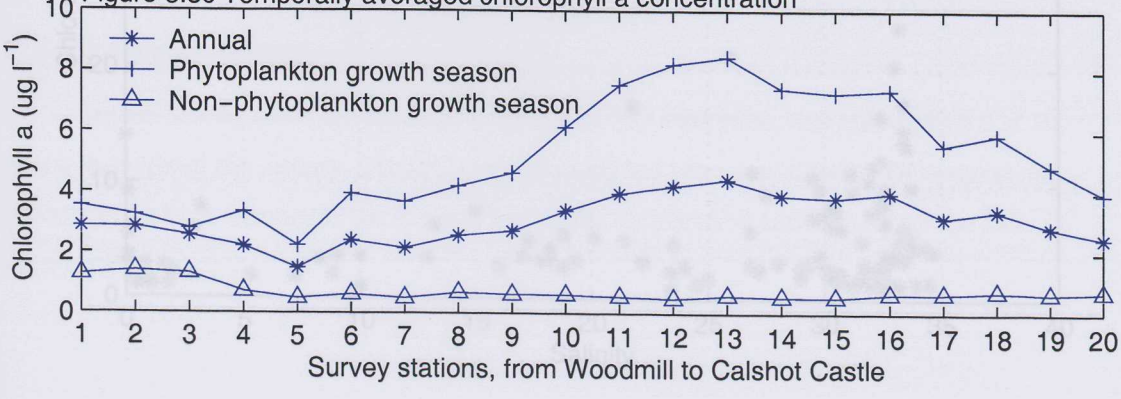

Figure 3.9a Chlorophyll a (ug l^{-1}) against salinity (non–phytoplankton growth season)

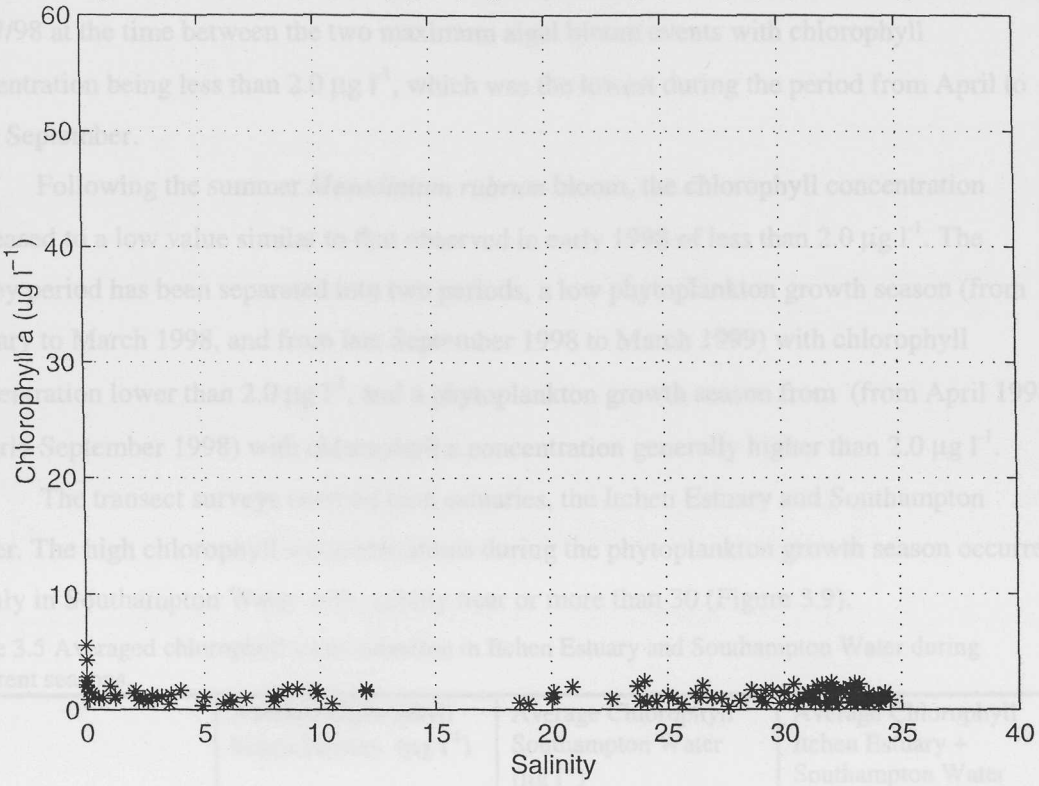

Figure 3.9b Chlorophyll a (ug l^{-1}) against salinity (phytoplankton growth season)

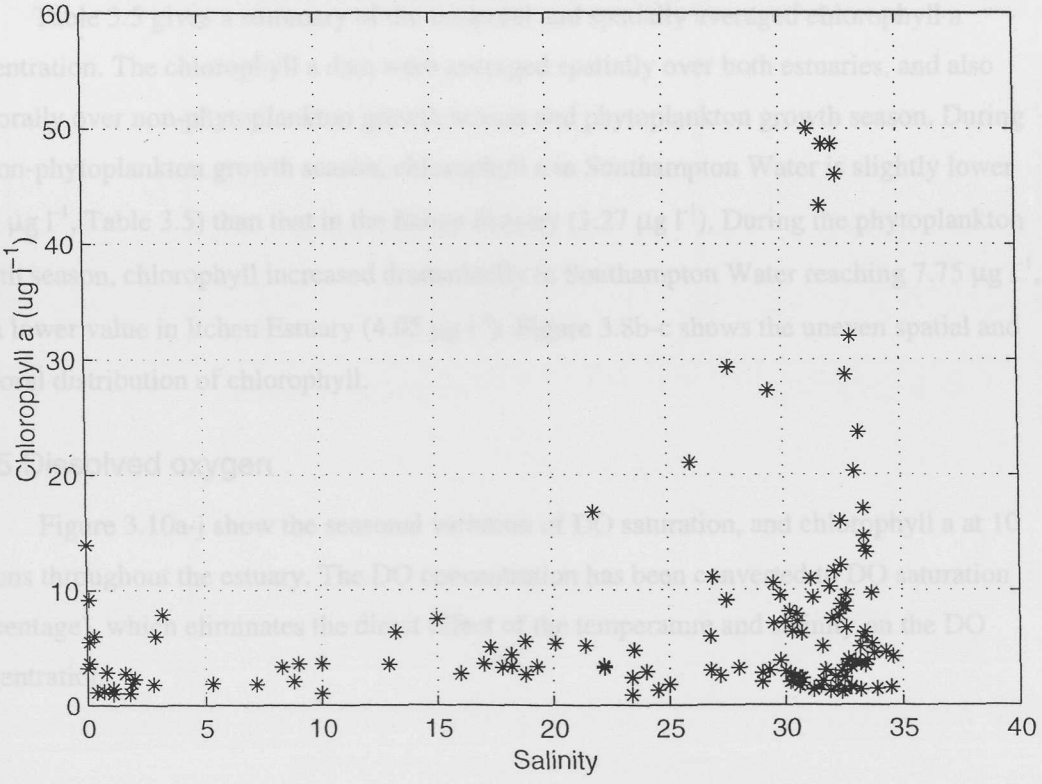

A second peak in phytoplankton biomass occurred on 12/08/98, and the coloured water was shown to be due to *Mesodinium rubrum* with maximum chlorophyll 20.3 $\mu g\ l^{-1}$ at NW Netley. There was no significant phytoplankton biomass detected during the survey made on 23/07/98 at the time between the two maximum algal bloom events with chlorophyll concentration being less than 2.0 $\mu g\ l^{-1}$, which was the lowest during the period from April to early September.

Following the summer *Mesodinium rubrum* bloom, the chlorophyll concentration decreased to a low value similar to that observed in early 1998 of less than 2.0 $\mu g\ l^{-1}$. The survey period has been separated into two periods, a low phytoplankton growth season (from January to March 1998, and from late September 1998 to March 1999) with chlorophyll concentration lower than 2.0 $\mu g\ l^{-1}$, and a phytoplankton growth season from (from April 1998 to early September 1998) with chlorophyll a concentration generally higher than 2.0 $\mu g\ l^{-1}$.

The transect surveys covered both estuaries, the Itchen Estuary and Southampton Water. The high chlorophyll a concentrations during the phytoplankton growth season occurred mainly in Southampton Water with salinity near or more than 30 (Figure 3.9).

Table 3.5 Averaged chlorophyll a concentration in Itchen Estuary and Southampton Water during different seasons.

	Average Chlorophyll Itchen Estuary ($\mu g\ l^{-1}$)	Average Chlorophyll Southampton Water ($\mu g\ l^{-1}$)	Average Chlorophyll Itchen Estuary + Southampton Water ($\mu g\ l^{-1}$)
Low-growth Season	1.27	0.98	1.13
Growth Season	4.05	7.75	5.90
Year Averaged	2.56	3.86	3.19

Table 3.5 gives a summary of the temporal and spatially averaged chlorophyll a concentration. The chlorophyll a data were averaged spatially over both estuaries, and also temporally over non-phytoplankton growth season and phytoplankton growth season. During the non-phytoplankton growth season, chlorophyll a in Southampton Water is slightly lower (0.98 $\mu g\ l^{-1}$, Table 3.5) than that in the Itchen Estuary (1.27 $\mu g\ l^{-1}$). During the phytoplankton growth season, chlorophyll increased dramatically in Southampton Water reaching 7.75 $\mu g\ l^{-1}$, and a lower value in Itchen Estuary (4.05 $\mu g\ l^{-1}$). Figure 3.8b-c shows the uneven spatial and temporal distribution of chlorophyll.

3.3.5 Dissolved oxygen

Figure 3.10a-j show the seasonal variation of DO saturation, and chlorophyll a at 10 stations throughout the estuary. The DO concentration has been converted to DO saturation (percentage), which eliminates the direct effect of the temperature and salinity on the DO concentration.

Figure 3.10 Seasonal variation of DO saturation, and chlorophyll a at 10 survey stations

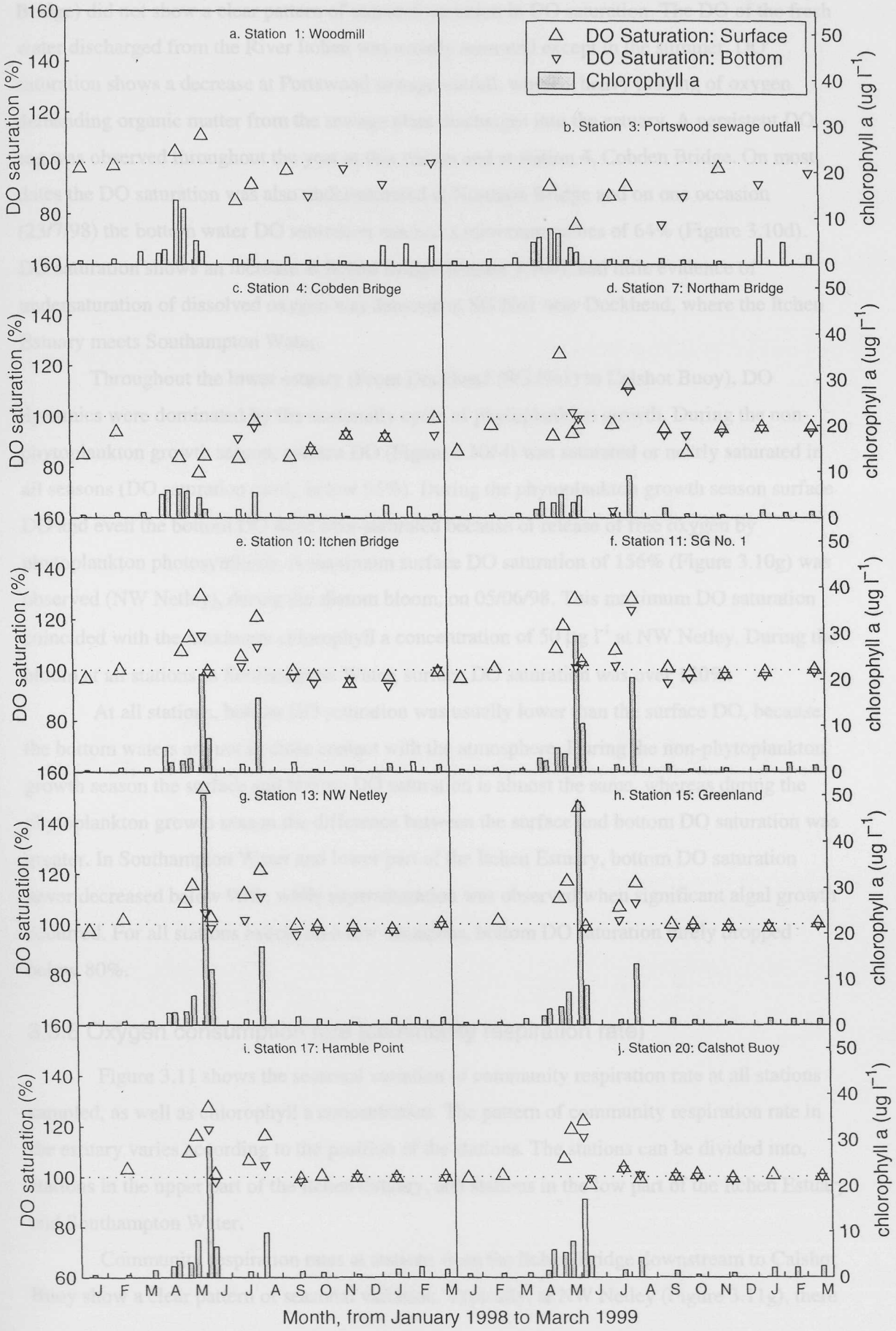

The upper part of the Itchen Estuary (Figure 3.10a-d, From Woodmill to Northam Bridge) did not show a clear pattern of seasonal variation in DO saturation. The DO of the fresh water discharged from the River Itchen was usually saturated except in the summer. DO saturation shows a decrease at Portswood sewage outfall, where a heavy loading of oxygen demanding organic matter from the sewage plant discharges into the estuary. A persistent DO sag was observed throughout the year at this station and at station 4, Cobden Bridge. On most dates the DO saturation was also undersaturated at Northam Bridge and on one occasion (23/7/98) the bottom water DO saturation reached a minimum values of 64% (Figure 3.10d). DO saturation shows an increase at Itchen Bridge (Figure 3.10e), and little evidence of undersaturation of dissolved oxygen was detected at SG No1 near Dockhead, where the Itchen Estuary meets Southampton Water.

Throughout the lower estuary (From Dockhead (SG No1) to Calshot Buoy), DO dynamics were dominated by the seasonally cycle of phytoplankton growth. During the non-phytoplankton growth season, surface DO (Figure 3.10f-j) was saturated or nearly saturated in all seasons (DO saturation rarely below 95%). During the phytoplankton growth season surface DO and even the bottom DO were over-saturated because of release of free oxygen by phytoplankton photosynthesis. A maximum surface DO saturation of 156% (Figure 3.10g) was observed (NW Netley), during the diatom bloom, on 05/06/98. This maximum DO saturation coincided with the maximum chlorophyll a concentration of 50 $\mu g\ l^{-1}$ at NW Netley. During the bloom at all stations in Southampton Water, surface DO saturation was over 120%.

At all stations, bottom DO saturation was usually lower than the surface DO, because the bottom waters are not in close contact with the atmosphere. During the non-phytoplankton growth season the surface and bottom DO saturation is almost the same, whereas during the phytoplankton growth season the difference between the surface and bottom DO saturation was greater. In Southampton Water and lower part of the Itchen Estuary, bottom DO saturation never decreased below 90%, while supersaturation was observed when significant algal growth occurred. For all stations except on a few occasions, bottom DO saturation rarely dropped below 80%.

3.3.6 Oxygen consumption rate (community respiration rate)

Figure 3.11 shows the seasonal variation of community respiration rate at all stations sampled, as well as chlorophyll a concentration. The pattern of community respiration rate in the estuary varies according to the position of the stations. The stations can be divided into, stations in the upper part of the Itchen Estuary, and stations in the low part of the Itchen Estuary and Southampton Water.

Community respiration rates at stations from the Itchen Bridge downstream to Calshot Buoy show a clear pattern of seasonal variation. Typically, at NW Netley (Figure 3.11g), there

Figure 3.11 Seasonal variation of community respiration rate, and chlorophyll a at 10 DO survey stations

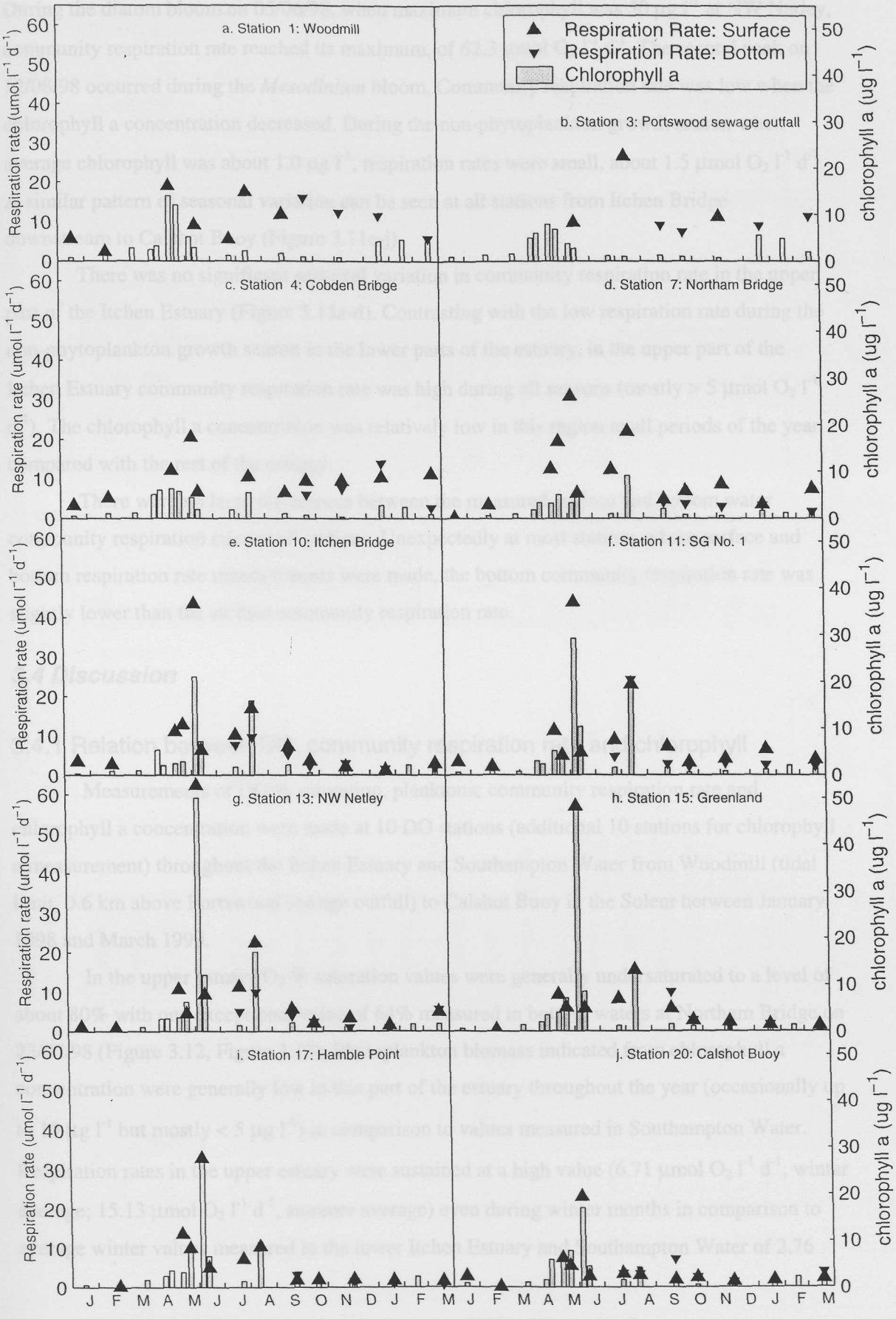

are two peaks of community respiration rate, and each peak coincided with the algal bloom. During the diatom bloom on 05/06/98, when maximum chlorophyll was 50 μg l^{-1} at NW Netley, community respiration rate reached its maximum, of 62.3 μmol O_2 l^{-1} d^{-1}. The second peak on 12/08/98 occurred during the *Mesodinium* bloom. Community respiration rate was low when the chlorophyll a concentration decreased. During the non-phytoplankton growth season when average chlorophyll was about 1.0 μg l^{-1}, respiration rates were small, about 1.5 μmol O_2 l^{-1} d^{-1}. A similar pattern of seasonal variation can be seen at all stations from Itchen Bridge downstream to Calshot Buoy (Figure 3.11e-j).

There was no significant seasonal variation in community respiration rate in the upper part of the Itchen Estuary (Figure 3.11a-d). Contrasting with the low respiration rate during the non-phytoplankton growth season in the lower parts of the estuary, in the upper part of the Itchen Estuary community respiration rate was high during all seasons (mostly > 5 μmol O_2 l^{-1} d^{-1}). The chlorophyll a concentration was relatively low in this region at all periods of the year compared with the rest of the estuary.

There were no large differences between the measured surface and bottom water community respiration rates at all stations. Unexpectedly at most stations where surface and bottom respiration rate measurements were made, the bottom community respiration rate was slightly lower than the surface community respiration rate.

3.4 Discussion

3.4.1 Relation between DO, community respiration rate and chlorophyll

Measurements of DO % saturation, planktonic community respiration rate and chlorophyll a concentration were made at 10 DO stations (additional 10 stations for chlorophyll a measurement) throughout the Itchen Estuary and Southampton Water from Woodmill (tidal limit, 0.6 km above Portswood sewage outfall) to Calshot Buoy in the Solent between January 1998 and March 1999.

In the upper estuary O_2 % saturation values were generally undersaturated to a level of about 80% with one exceptional value of 64% measured in bottom waters at Northam Bridge on 23/07/98 (Figure 3.12, Figure 3.13). Phytoplankton biomass indicated from chlorophyll a concentration were generally low in this part of the estuary throughout the year (occasionally up to 10 μg l^{-1} but mostly < 5 μg l^{-1}) in comparison to values measured in Southampton Water. Respiration rates in the upper estuary were sustained at a high value (6.71 μmol O_2 l^{-1} d^{-1}, winter average; 15.13 μmol O_2 l^{-1} d^{-1}, summer average) even during winter months in comparison to average winter values measured in the lower Itchen Estuary and Southampton Water of 2.76

Figure 3.12 Transect surveys results during phytoplankton growth season: longitudinal distribution of DO saturation, community respiration rate and chlorophyll a

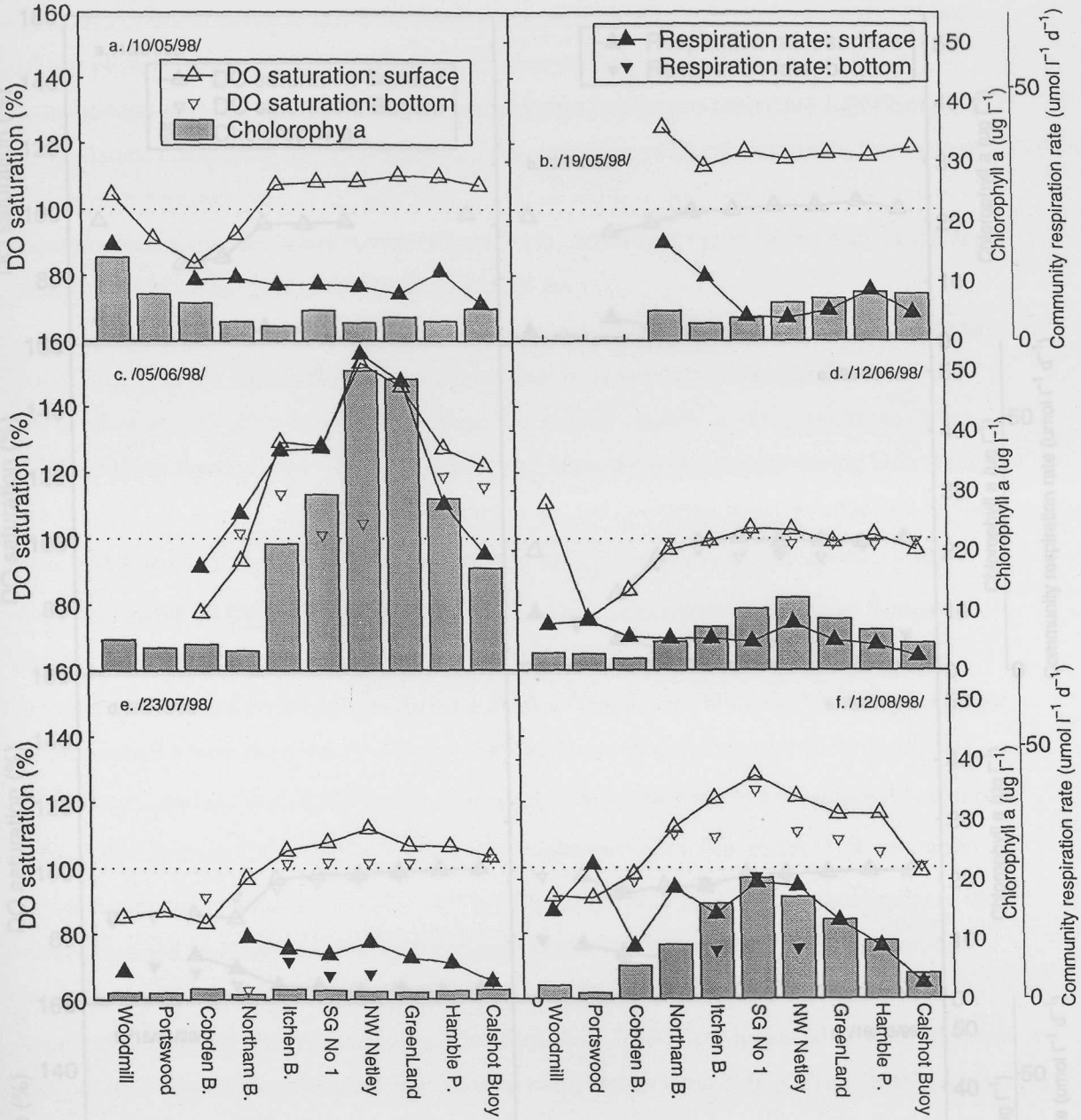

Figure 3.13 Transect surveys results during non-phytoplankton growth season: longitudinal distribution of DO saturation, community respiration rate and chlorophyll a

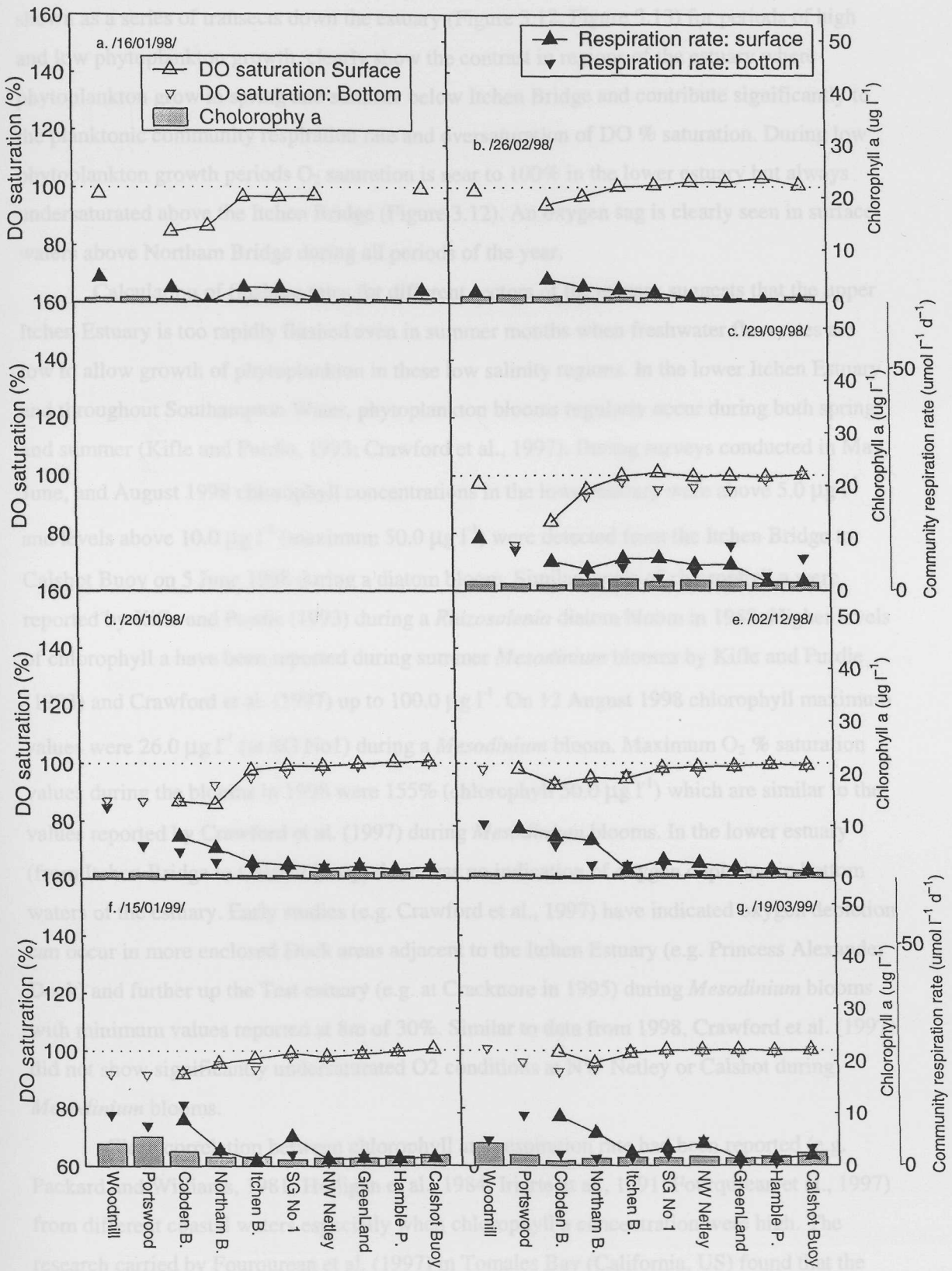

μmol O_2 l^{-1} d^{-1} (Figure 3.12). These high rates of respiration in the low salinity regions of the estuary were sustained by organic inputs from the Portswood Sewage Plant and River Itchen.

A comparison of DO % saturation, respiration rates and chlorophyll a concentration, shown as a series of transects down the estuary (Figure 3.12, Figure 3.13) for periods of high and low phytoplankton growth, clearly show the contrast in regions of the estuary where phytoplankton grow in spring and summer below Itchen Bridge and contribute significantly to the planktonic community respiration rate and oversaturation of DO % saturation. During low phytoplankton growth periods O_2 saturation is near to 100% in the lower estuary but always undersaturated above the Itchen Bridge (Figure 3.12). An oxygen sag is clearly seen in surface waters above Northam Bridge during all periods of the year.

Calculation of flushing rates for different sectors of the estuary suggests that the upper Itchen Estuary is too rapidly flushed even in summer months when freshwater flow rates are low to allow growth of phytoplankton in these low salinity regions. In the lower Itchen Estuary and throughout Southampton Water, phytoplankton blooms regularly occur during both spring and summer (Kifle and Purdie, 1993; Crawford et al., 1997). During surveys conducted in May, June, and August 1998 chlorophyll concentrations in the lower estuary were above 5.0 μg l^{-1} and levels above 10.0 μg l^{-1} (maximum 50.0 μg l^{-1}) were detected from the Itchen Bridge to Calshot Buoy on 5 June 1998 during a diatom bloom. Similar levels of chlorophyll a were reported by Kifle and Purdie (1993) during a *Rhizosolenia* diatom bloom in 1988. Higher levels of chlorophyll a have been reported during summer *Mesodinium* blooms by Kifle and Purdie (1993) and Crawford et al. (1997) up to 100.0 μg l^{-1}. On 12 August 1998 chlorophyll maximum values were 26.0 μg l^{-1} (at SG No1) during a *Mesodinium* bloom. Maximum O_2 % saturation values during the blooms in 1998 were 155% (chlorophyll 50.0 μg l^{-1}) which are similar to the values reported by Crawford et al. (1997) during *Mesodinium* blooms. In the lower estuary (from Itchen Bridge to Calshot Buoy) there was no indication of oxygen depletion in bottom waters of the estuary. Early studies (e.g. Crawford et al., 1997) have indicated oxygen depletion can occur in more enclosed Dock areas adjacent to the Itchen Estuary (e.g. Princess Alexander Dock) and further up the Test estuary (e.g. at Cracknore in 1995) during *Mesodinium* blooms with minimum values reported at 8m of 30%. Similar to data from 1998, Crawford et al. (1997) did not show significantly undersaturated O2 conditions at NW Netley or Calshot during *Mesodinium* blooms.

Close correlation between chlorophyll and respiration rate had been reported (e.g. Packard and Williams, 1981; Holligan et al., 1984; Iriarte et al., 1991; Fourqurean et al., 1997) from different coastal waters especially when chlorophyll a concentration were high. The research carried by Fourqurean et al. (1997) in Tomales Bay (California, US) found that the chlorophyll had a very high correlation with respiration rate and water temperature. To predict

Figure 3.14a Chlorophyll a concentration against respiration rate (all season)

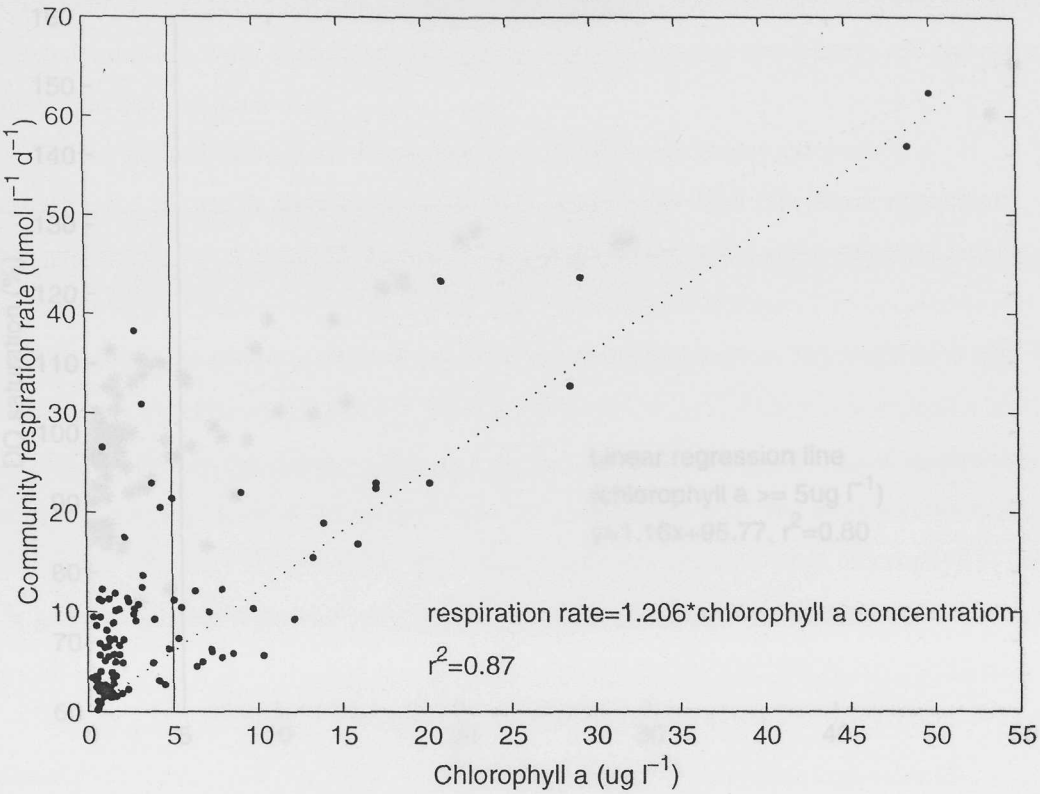

Figure 3.14b Chlorophyll a concentration against specific respiration rate (all season)

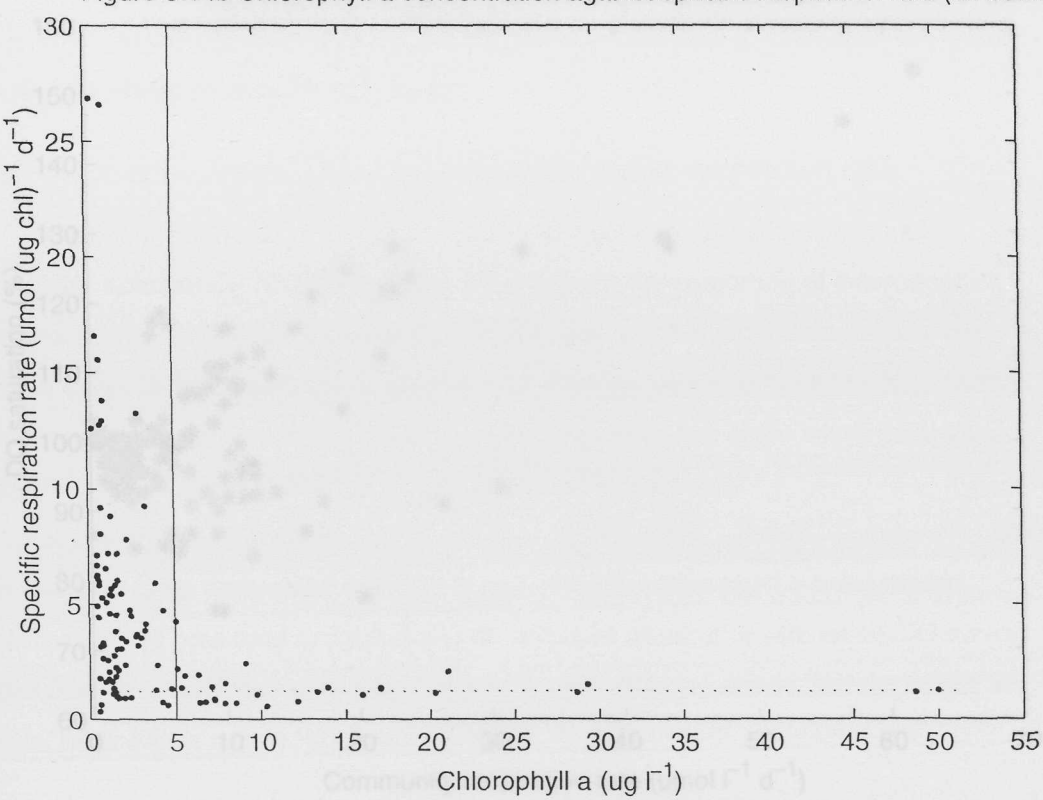

Figure 3.15a DO saturation against chlorophyll a concentration

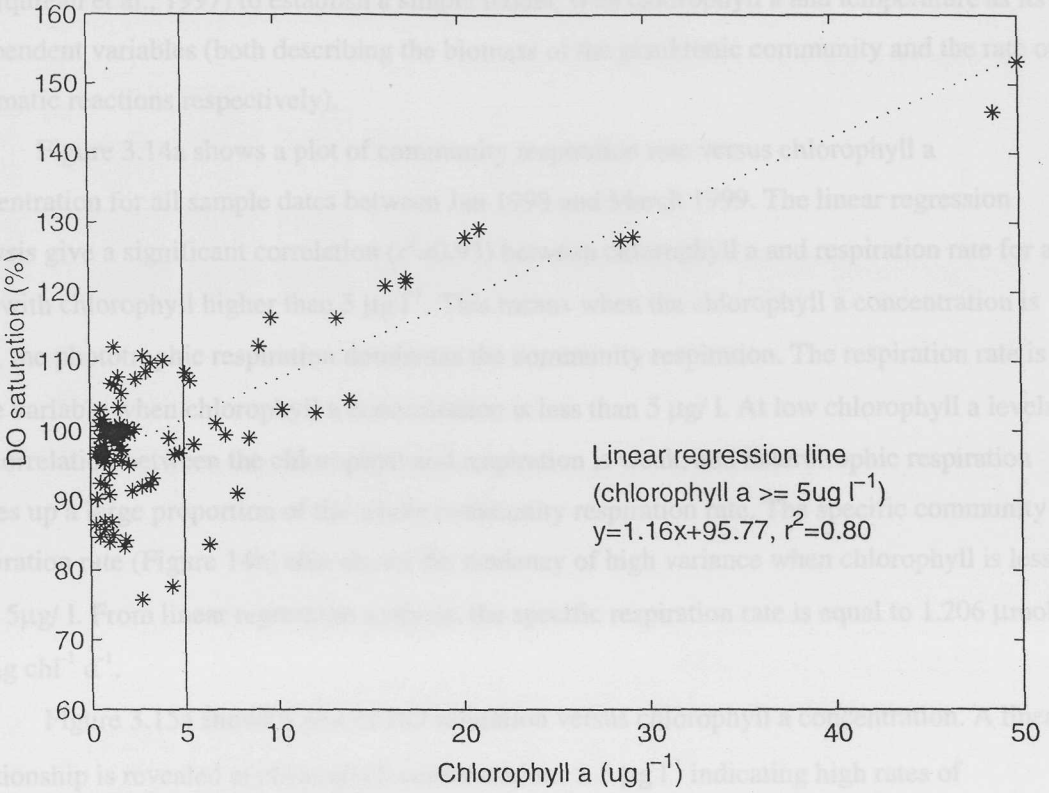

Figure 3.15b DO saturation against community respiration rate

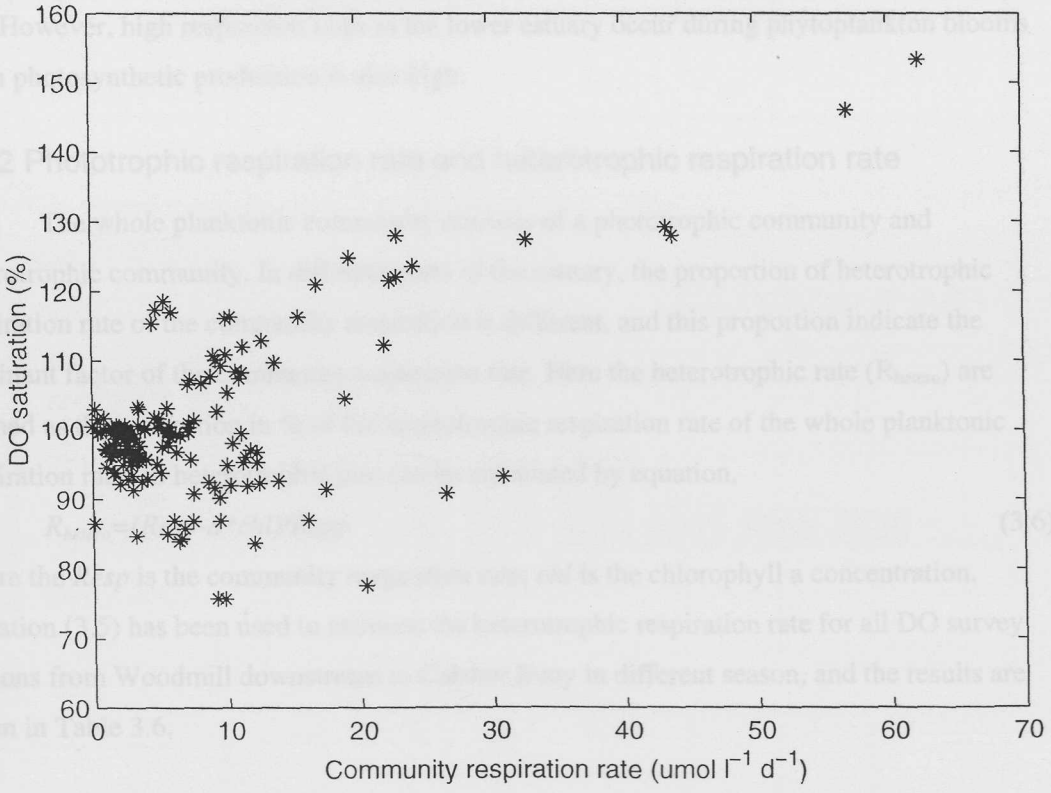

the planktonic community respiration rate, a multiple linear regression method was imployed (Fourqurean et al., 1997) to establish a simple model, with chlorophyll a and temperature as its independent variables (both describing the biomass of the planktonic community and the rate of enzymatic reactions respectively).

Figure 3.14a shows a plot of community respiration rate versus chlorophyll a concentration for all sample dates between Jan 1998 and March 1999. The linear regression analysis give a significant correlation (r^2=0.93) between chlorophyll a and respiration rate for all data with chlorophyll higher than 5 $\mu g\ l^{-1}$. This means when the chlorophyll a concentration is high, the phototrophic respiration dominates the community respiration. The respiration rate is more variable when chlorophyll a concentration is less than 5 μg/ l. At low chlorophyll a levels, the correlation between the chlorophyll and respiration is weak, and heterotrophic respiration makes up a large proportion of the whole community respiration rate. The specific community respiration rate (Figure 14b) also shows the tendency of high variance when chlorophyll is less than 5μg/ l. From linear regression analysis, the specific respiration rate is equal to 1.206 μmol O_2 $\mu g\ chl^{-1}\ d^{-1}$.

Figure 3.15a shows a plot of DO saturation versus chlorophyll a concentration. A linear relationship is revealed at chlorophyll concentrations > 5 $\mu g\ l^{-1}$ indicating high rates of photosynthesis leading to supersaturation of dissolved oxygen in surface waters. When DO saturation is compared with community respiration rate a less clear relationship is evident (Figure 3.15b). It might be expected that high respiration rates will lead to undersaturation of DO. However, high respiration rates in the lower estuary occur during phytoplankton blooms when photosynthetic production is also high.

3.4.2 Phototrophic respiration rate and heterotrophic respiration rate

The whole planktonic community consists of a phototrophic community and heterotrophic community. In different parts of the estuary, the proportion of heterotrophic respiration rate of the community respiration is different, and this proportion indicate the dominant factor of the community respiration rate. Here the heterotrophic rate (R_{hetero}) are defined as the proportion in % of the heterotrophic respiration rate of the whole planktonic respiration rate, so heterotrophic rate can be calculated by equation,

$$R_{hetero}=(Resp-a*chl)/Resp \qquad (3.6)$$

where the *Resp* is the community respiration rate; *chl* is the chlorophyll a concentration. Equation (3.5) has been used to estimate the heterotrophic respiration rate for all DO survey stations from Woodmill downstream to Calshot Buoy in different season, and the results are given in Table 3.6.

Figure 3.16a Heterotrophic rate(%) at 10 DO stations (non–phytoplankton growth season)

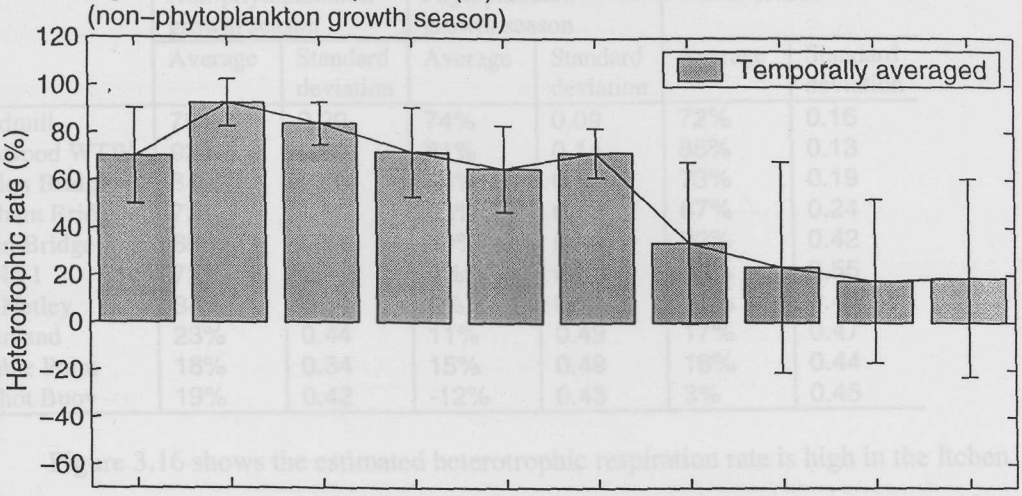

Figure 3.16b Heterotrophic rate (%) at 10 DO stations (phytoplankton growth season)

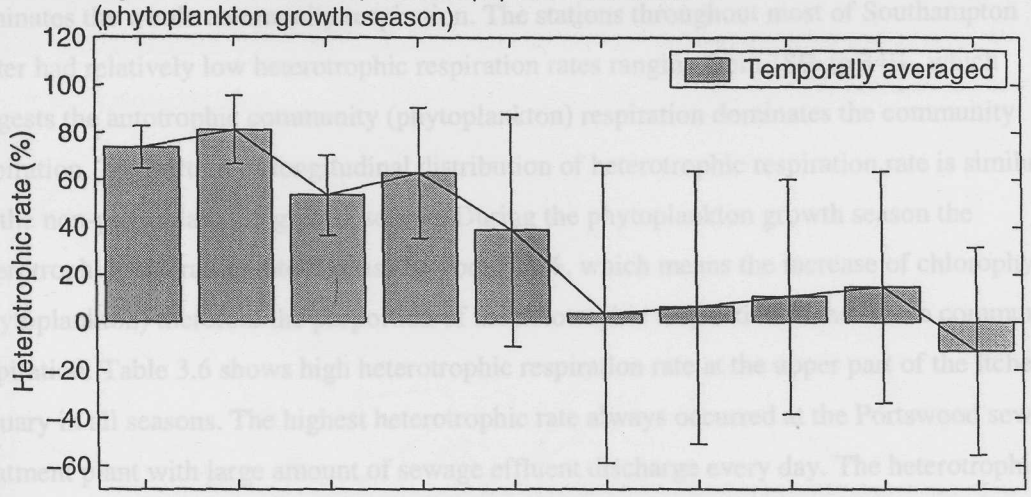

Figure 3.16c Heterotrophic rate (%) at 10 DO stations (all season)

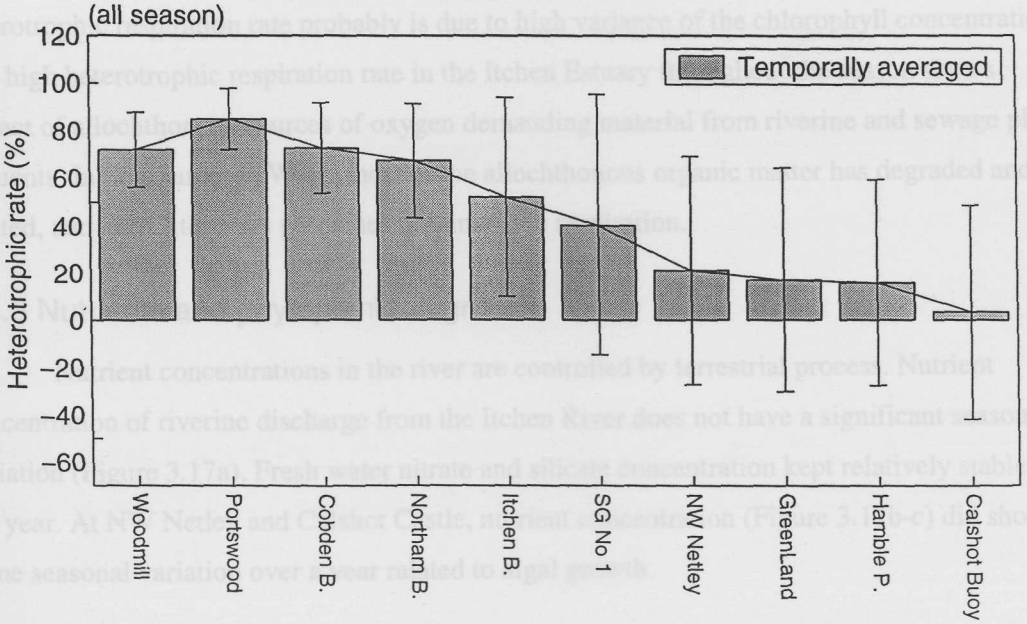

Table 3.6 R_{hetero} (heterotrophic rate) at 10 stations in the Itchen Estuary and Southampton Water

	Non-phytoplankton growth season		Phytoplankton growth season		Whole season	
	Average	Standard deviation	Average	Standard deviation	Average	Standard deviation
Woodmill	70%	0.20	74%	0.09	72%	0.16
Portswood WTW	92%	0.10	81%	0.14	85%	0.13
Cobden Bridge	84%	0.09	54%	0.17	73%	0.19
Northam Bridge	72%	0.19	63%	0.28	67%	0.24
Itchen Bridge	65%	0.18	39%	0.49	52%	0.42
SG No 1	72%	0.10	4%	0.62	40%	0.55
NW Netley	34%	0.34	6%	0.57	21%	0.48
Greenland	23%	0.44	11%	0.49	17%	0.47
Hamble Point	18%	0.34	15%	0.49	16%	0.44
Calshot Buoy	19%	0.42	-12%	0.43	3%	0.45

Figure 3.16 shows the estimated heterotrophic respiration rate is high in the Itchen Estuary as well as at DockHead (SG No 1) in the non-phytoplankton growth season with a percentage from 65% to 92%, which suggests the heterotrophic community respiration dominates the whole community respiration. The stations throughout most of Southampton Water had relatively low heterotrophic respiration rates ranging from 18% to 34%, which suggests the autotrophic community (phytoplankton) respiration dominates the community respiration. The pattern of longitudinal distribution of heterotrophic respiration rate is similar for the non-phytoplankton growth season. During the phytoplankton growth season the heterotrophic respiration rate decease by about 18%, which means the increase of chlorophyll a (phytoplankton) therefore the proportion of the autotrophic respiration in the whole community respiration. Table 3.6 shows high heterotrophic respiration rate at the upper part of the Itchen Estuary in all seasons. The highest heterotrophic rate always occurred at the Portswood sewage treatment plant with large amount of sewage effluent discharge every day. The heterotrophic respiration rate decreases gradually (meanwhile the increase of the proportion of the autotrophic respiration rate) down stream to Calshot Buoy. The high standard deviation of the estuarine heterotrophic respiration rate probably is due to high variance of the chlorophyll concentration. The high heterotrophic respiration rate in the Itchen Estuary throughout the season shows impact of allochthonous sources of oxygen demanding material from riverine and sewage plant effluents. In Southampton Water most of the allochthonous organic matter has degraded and diluted, and autochthonous processes dominate the respiration.

3.4.3 Nutrients and phytoplankton growth

Nutrient concentrations in the river are controlled by terrestrial process. Nutrient concentration of riverine discharge from the Itchen River does not have a significant seasonal variation (Figure 3.17a). Fresh water nitrate and silicate concentration kept relatively stable over the year. At NW Netley and Calshot Castle, nutrient concentration (Figure 3.17b-c) did show some seasonal variation over a year related to algal growth.

Figure 3.17 Seasonal variation of nutrient (nitrate, silicate and phosphate) and chlorophyll a concentration: a, estimated (by linear regression) nutrient concentration of riverine fresh water discharge from River Itchen; b, seasonal variation of nutrient concentration at NW Netley; c, seasonal variation of nutrient concentration at Calshot Buoy

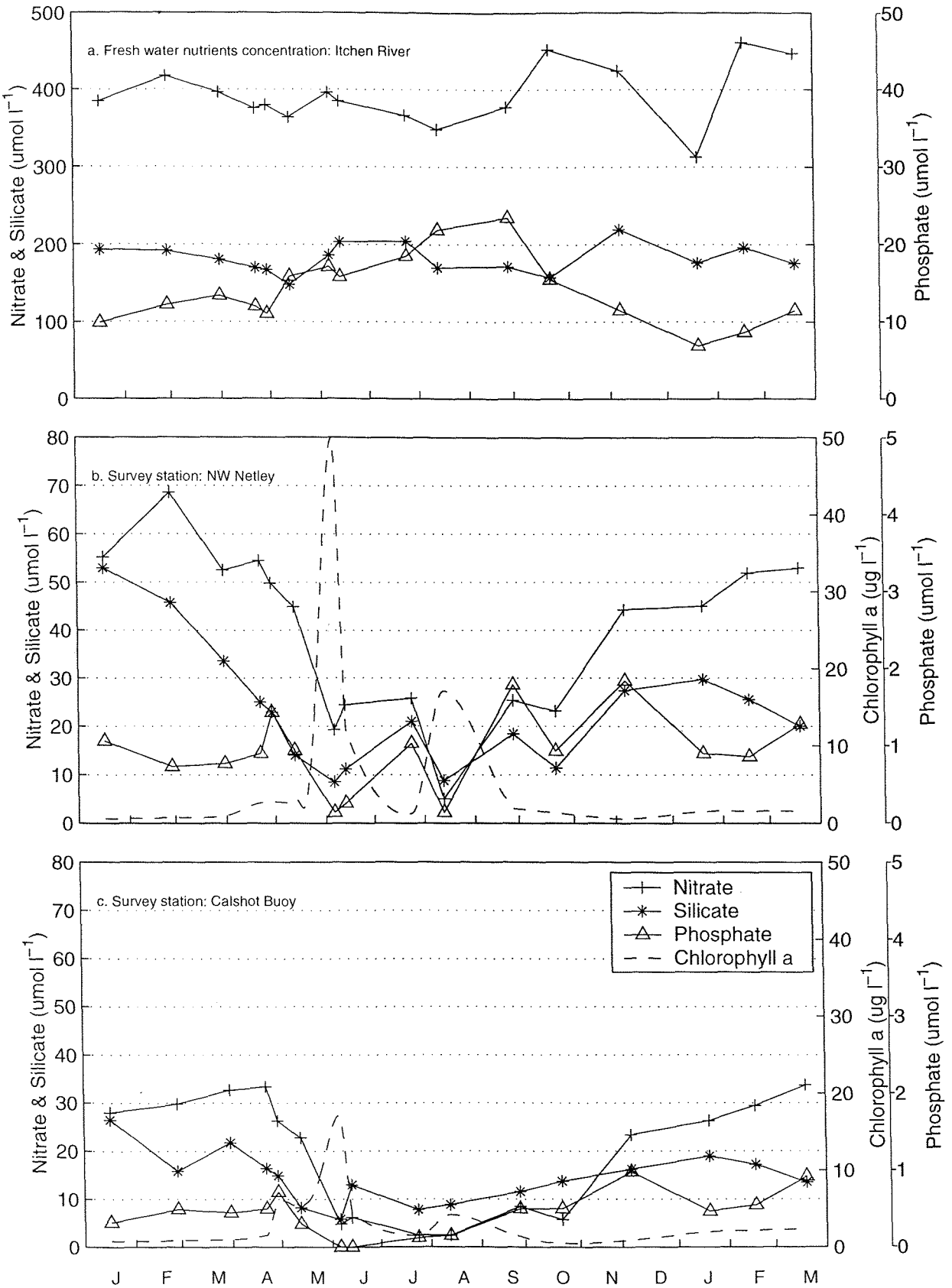

Figure 3.18a Nitrate distribution & removal of nitrate from water cloumn (results from transect survey on 12/08/98)

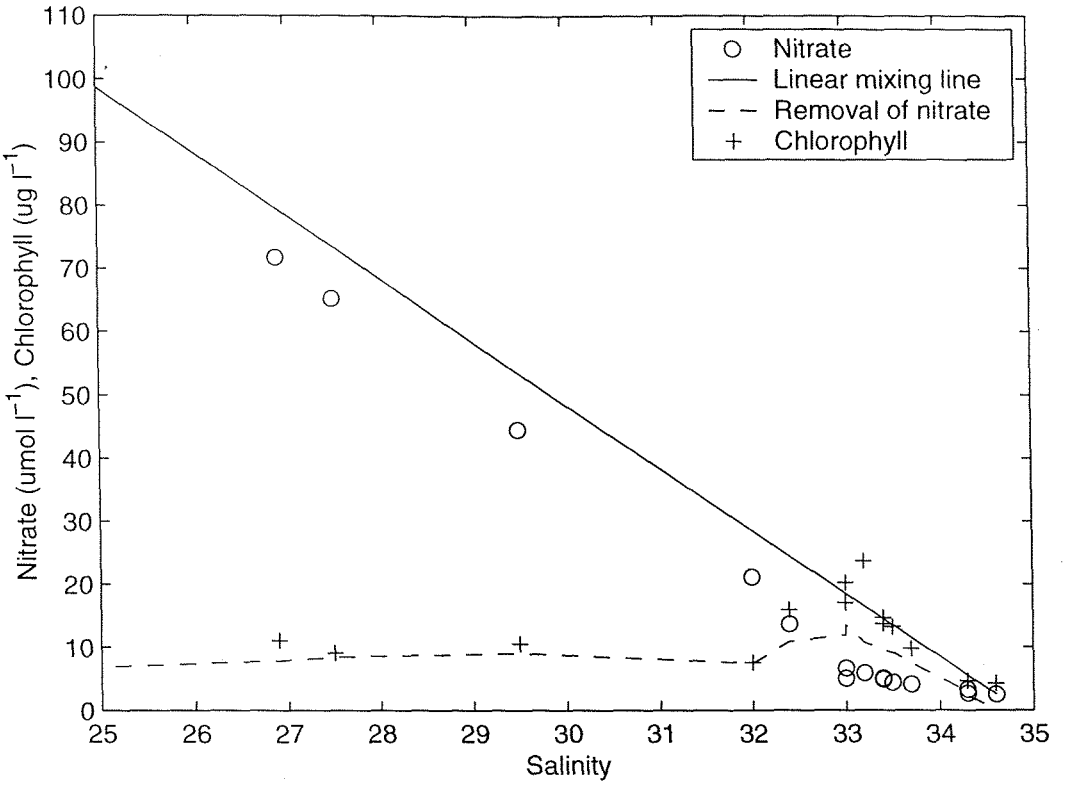

Figure 3.18b Relationship between chlorophyll and removal of nitrate (results from transect survey on 12/08/98)

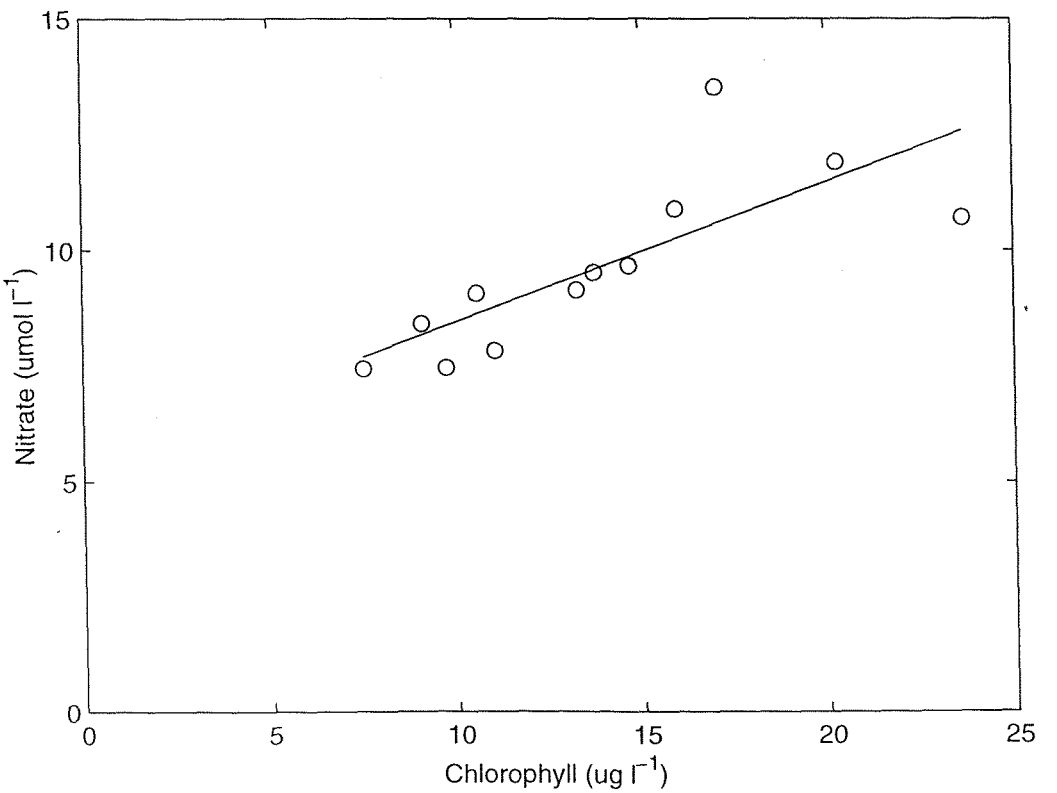

Nitrate concentration is more than 50 μmol l^{-1} at NW Netley from January 1998 to April 1998. From early May 1998, nitrate concentrations drop gradually initially then a rapid drop to 19.3 μmol l^{-1} on 05/06/89 during the diatom bloom. A slight recovery afterwards to 25.8 μmol l^{-1} and further decrease during the second (*Mesodinium*) bloom to an annual minimum value of 5.0 μmol l^{-1} coincident with the annual minimum in silicate concentration 8.8 μmol l^{-1} and phosphate 0.1 μmol l^{-1}. From September the nutrient concentrations increased, and by late winter and early spring 1999 nutrient levels had fully recovered before the next algal growth season.

The seasonal pattern of nutrient concentration at Calshot Buoy is quite similar to NW Netley with the main difference being the back ground concentration is much smaller than at NW Netley. The nutrients depletion during the algal bloom at Calshot Buoy is much more severe than at NW Netley. The concentration of depleted phosphate is below the detectable level during the first bloom on 05/06/98.

Nutrient concentration at NW Netley remained above a detectable level during algal bloom. There is no indication of nutrient limitation to algal growth at NW Netley, in contract to Calshot Buoy. The phosphate concentrations are below the detectable level and nitrate are 2.4 μmol l^{-1} and silicate concentrate 0.1 μmol l^{-1} during the algal bloom. Probably due to nutrient availability the magnitude of the algal bloom at Calshot Buoy is much lower than that at NW Netley as previously reported by Kifle and Purdie (1993).

Removal of nutrients can be estimated by the difference between the theoretical linear mixing line and survey data. During 12/08/98 survey, there was a *Mesodinium rubrum* bloom in Southampton Water and linear regression (Figure 3.18) between the chlorophyll and nitrate removal revealed a strong positive correlation with a correlation coefficient of 0.91. The data from 06/05/98 during the diatom bloom shows similar relationship.

3.4.4 Respiration rate measurement in similar estuaries

There are relatively few systemic measurements of community respiration rate and DO concentration reported in Southampton Water. In 1981, de Souza Lima & Williams (1978) carried out measurement of planktonic DO consumption in the Test Estuary and Southampton Water for about eight months. All samples were concentrated 4-7 fold by a filter with a mean pore size of 0.45 μm. Rees & Williams (1982) conducted a series of surveys including DO and community respiration in 1981 in Test Estuary to provide parameters for water quality model (Soulsby et al., 1984) of Southampton Water.

There are many similar studies in coastal waters and estuaries (Table 3.7). Sand-Jensen et al. (1990) and Jensen (1990) used a 1 μm filter to separate the bacteria community from other planktonic community in a shallow Danish bay. Results showed that size-fractionated (<1 μm)

Table 3.7 Water column respiration rate (μmol O_2 l^{-1} d^{-1}) in a variety of marine environments (adapted from Dortch, 1994)

Environment	Location	Rate (mmol O_2 m^{-3} d^{-1})	Reference
Estuarine	Chesapeake Bay-surface	0.00-45.31	Kemp et al., 1992
	Chesapeake Bay-	1.56-31.25	Kemp et al., 1992
	Chesapeake Bay-	6.56-65.63	Kemp & Boynton, 1980
	Chesapeake Bay-	25.00-53.13	Taft et al., 1980
	Core Sound, North Carolina, USA	11.50	Williams, 1966
	Doboy Sound, Georgia, USA	19.38	Ragotzkie, 1959
	Huizache-Caimanero Lagoon, Mexico	232.50	Edwards, 1978
	Loch Ewe, UK	3.13-7.81	Williams, 1981
	Narragansett Bay, Rhode Island, USA	14.28	Smayda, 1957
	Port Hacking Estuary, Australia	2.50	Bulleid, 1983
	Roskilde Fjord, Denmark	16.88-44.66	Jensen et al., 1990; Sand-Jensen et al., 1990
	Southampton Water, UK	4.44-11.16	de Souza Lima & Williams, 1978
	Test Estuary	0.60-177.00	Rees & Williams, 1981
	Southampton Water (non-phytoplankton growth season)	0.00-7.21	This study
	Southampton Water (phytoplankton growth season)	5.53-43.31	This study
	Itchen Estuary (non-phytoplankton growth season)	0.09-11.8	This study
	Itchen Estuary (phytoplankton growth season)	2.69-62.35	This study
	Wassau Sound, Georgia, USA	13.75	Turner, 1978
Coastal	English Channel-stratified	0.31-4.69	Holligan et al., 1994
	English Channel-frontal	1.34-53.69	Holligan et al., 1984
	English Channel-mixed	1.91-4.53	Holligan et al., 1984
	Georgia Bight, USA	1.19	Turner, 1978
	Georgia Bight, USA	22.28	Hopkinson, 1985
	Georgia Bight, USA	6.53	Westernhagen et al., 1986
	Long Island Sound, USA	7.56	Riley, 1941
	Louisiana shelf, USA 1976 Nov. & July, bottom	0.08-6.00	Yurner and Allen, 1982
	LS, 1990 July & Aug., surface	1.44-19.69	Benner et al., 1992
	LS, 1991 Feb., surface	2.41-13.44	Benner et al., 1992
	LS, 1991 Feb., surface	1.47-19.69	Chin-Leo and Benner, 1992
	LS, 1991 May-Cot, all depth	0.01-9.94	Dortch et al., 1994
	New York Bight, USA	2.81	Garside and Malone, 1978
	Dabob Bay, Washington, USA	0.66	Christensen and Packard, 1976
	Peru upwelling (eutrophic), 1969	4.41	Packard, 1969
	Peru upwelling (eutrophic), 1969	1.06	Sethell and Peckard, 1978, 1979

respiration was about 35% to 44% of total community respiration in the bay. The same size filter was used by Pomeroy et al. (1995) in The Gulf of Mexico to investigate microbial community respiration in the upper mixed layer of the with a respiration range of 0.13 μmol O_2 l^{-1} h^{-1} in the January to 1.4 μmol O_2 l^{-1} h^{-1} in June. Sampou and Kemp (1994) reported respiration rates from Chesapeake Bay where the picoplankton (<3 μm size fraction) accounted

for about 23%-89% of total planktonic community respiration rate. The DO depletion in the water column depends on the DO consumption in the water column by the planktonic community, DO supply though the surface re-aeration, and physical processes in the water column. Dortch et al. (1994) had conducted a monthly survey of water column respiration (estimated from enzymatic respiratory electron-transport-system activity) in Louisiana shelf in 1991, aiming to determine the spatial and temporal variability of respiration rates and some of the factors that influence them, to assess the role of water column respiration in the development of bottom water hypoxia. The results suggested the possibility that the formation of the hypoxia in bottom waters on the Louisiana shelf might be more dependent on the unique hydrography of the region rather than the water column respiration rates.

The respiration rates measured in Southampton Water are high compared with other estuarine and coastal waters. While many estuaries suffer from hypoxia and even anoxia, Southampton Water is still a relatively healthy estuary in term of oxygen saturation, despite a heavy load of oxygen demanding material from effluents and high autochthonous production of organic matter (primary production) in the algal growth season. The flushing time of Southampton Water is quite short in the order of days, and it is partially-mixed estuary with surface waters flowing out of the estuary and the oxygenated bottom water moving upstream to the head of the estuary. It is possible that the existence of strong estuary circulation and short flushing times cause replacement of oxygen depleted bottom water keeping the estuary healthy. In Southampton Water there is no physical obstacle preventing the full scale circulation such as is found in a fjord or if a sill exists at the mouth of an estuary, the deep dredge channel also possibly aids the development of the circulation.

3.5 Conclusion

The salinity distribution in Southampton Water suggests that the upper part of the Itchen Estuary is highly stratified, while the rest of the estuary is partially-stratified. Flushing times have been calculated using the salinity distribution, and the relative short flushing indicate passive tracers may move out of estuary quickly. The rapid flushing in the upper Itchen Estuary suggests high phytoplankton growth is prevented in this region. Water temperature had a clear seasonal variation, with a 26 days lag phase behind the solar elevation. Spatial variations in temperature are minor throughout the estuary.

The seasonal cycle of phytoplankton growth was dominated by two algal blooms in 1998: the first on 05/06/89 with maximum chlorophyll concentration of 50 $\mu g\ l^{-1}$, the second on 12/08/98 with maximum chlorophyll concentration of 20 $\mu g\ l^{-1}$. During the non algal growth season, chlorophyll concentration is below 2.0 $\mu g\ l^{-1}$, with average of about 1.00 $\mu g\ l^{-1}$.

Prior to the algal bloom, there were always a periods of good weather, rapid increase of water temperature and low SPM concentration therefore a high penetration of light in the water

column. This agreed with the findings of pervious research conducted in Southampton Water (Rees and Williams, 1982; Kifle & Purdie, 1993; Crawford et al., 1997) suggesting a combination of these factors trigger algal blooms. Rees & Williams (1982) emphasised the importance of the flushing by suggesting that the bloom only occurs when phytoplankton growth exceeds the loss of phytoplankton due to the flushing.

The reason for the collapse of the algal blooms is not very clear. Since there was continuous nutrient supply from riverine discharge and sewage effluents, nutrients were apparently not the limiting factor. Probably a combination of estuarine flushing, weakening of vertical stratification, increase in SPM concentration stirred by strong tidal current, reduced light or zooplankton grazing influence bloom collapse.

Community respiration rate had a clear longitudinal distribution in Southampton Water during the non-phytoplankton growth season. It decreased gradually from the head of Itchen Estuary, where the Itchen River discharges a large amount of oxygen demanding matter, downstream to the Calshot Buoy, where Southampton Water joins the Solent. In the upper part of Itchen Estuary, where bacterial oxidisation of organic matter dominated the DO consumption, the substantial level of the community respiration was maintained all year round.

This kind of pattern of distribution was interrupted by the algal growth period. During algal bloom events, community respiration increased with chlorophyll a with a maximum value on 05/06/98 during the diatom bloom of 62.35 $\mu mol\ O_2\ l^{-1}\ d^{-1}$. There is a strong linear relationship between chlorophyll concentration and community respiration, when the chlorophyll is greater than 5 $\mu g\ l^{-1}$ with a specific respiration rate of 1.266 $\mu mol\ O_2\ d^{-1}\ (\mu g\ chl)^{-1}$.

A persistent DO sag is observed in the upper parts of Itchen Estuary throughout the year, due to the high concentration of oxygen demanding matter from external inputs. In the lower Itchen Estuary and Southampton Water, the impact of organic matter load from the external sources is diluted, and the DO is usually saturated or near saturation during the non-phytoplankton growth season. Occasionally the algal growth causes the surface and bottom DO supersaturation during algal growth season. Extreme oxygen depletion after the collapse of the algal bloom was not observed. The relatively high DO saturation suggest that the Southampton Water is a relative healthy estuary. But in the upper part of Itchen Estuary, DO depletion may worsen during the summer season and under condition of low river discharge.

Chapter 4 Physical model structure

4.1 Introduction

Southampton Water is a partially-mixed estuary and has a typical vertical structure which is caused by riverine fresh water discharge. In addition lateral variation across the estuary is quite significant, and cannot be neglected (Southampton Water has a mean width of 2 km). Another reason for the development of a 3-D model is that in modelling the whole Solent estuarine system, you can not just single out the Southampton Water from the Solent and English Channel where a vertical 2-D model will be obviously inappropriate. Therefore ideally a 3-D model should be used to simulate tidal currents and estuarine circulation in Southampton Water. A 3-D finite element hydrodynamic model, based on the pioneering work of Wu (1986) and Shi (1996), has been developed. This a 3-D finite element baroclinic hydrodynamic model for estuaries and coastal seas with complex bathymetry and extensive tidal flats.

4.2 Dynamic and thermodynamic equations

The hydrodynamic equations which govern the movement of water mass consist of a continuity equation, momentum equations, temperature and salinity conservative equations and a state equation. Two simplifications have been made: first, it is assumed that the weight of the fluid identically balances the pressure (hydrostatic assumption), and second, density differences are neglected unless the differences are multiplied by gravity (Boussinesq approximation).

A left-hand Cartesian co-ordinate has been used with x increasing eastward, y increasing northward, and z increasing vertically downwards. The free surface is at $z=-\zeta(x,y,t)$ and the bottom is at $z=H(x,y)$. The equations are given by

$$\frac{\partial u}{\partial x}+\frac{\partial v}{\partial y}+\frac{\partial w}{\partial z}=0 \tag{4.1}$$

$$\frac{\partial u}{\partial t}+u\frac{\partial u}{\partial x}+v\frac{\partial u}{\partial y}+w\frac{\partial u}{\partial z}-fv=-\frac{1}{\rho_0}\frac{\partial P}{\partial x}+\frac{\partial}{\partial z}(\nu\frac{\partial u}{\partial z})+\varepsilon(\frac{\partial^2 u}{\partial x^2}+\frac{\partial^2 u}{\partial y^2}) \tag{4.2}$$

$$\frac{\partial v}{\partial t}+u\frac{\partial v}{\partial x}+v\frac{\partial v}{\partial y}+w\frac{\partial v}{\partial z}+fu=-\frac{1}{\rho_0}\frac{\partial P}{\partial y}+\frac{\partial}{\partial z}(\nu\frac{\partial v}{\partial z})+\varepsilon(\frac{\partial^2 v}{\partial x^2}+\frac{\partial^2 v}{\partial y^2}) \tag{4.3}$$

$$0=-\frac{1}{\rho}\frac{\partial P}{\partial z}+g \tag{4.4}$$

$$\frac{\partial T}{\partial t}+u\frac{\partial T}{\partial x}+v\frac{\partial T}{\partial y}+w\frac{\partial T}{\partial z}=\frac{\partial}{\partial z}(\kappa_z\frac{\partial T}{\partial z})+\frac{\partial}{\partial x}(\kappa_x\frac{\partial T}{\partial x})+\frac{\partial}{\partial y}(\kappa_y\frac{\partial T}{\partial y})+F_T \tag{4.5}$$

$$\frac{\partial S}{\partial t}+u\frac{\partial S}{\partial x}+v\frac{\partial S}{\partial y}+w\frac{\partial S}{\partial z}=\frac{\partial}{\partial z}(\kappa_z\frac{\partial S}{\partial z})+\frac{\partial}{\partial x}(\kappa_x\frac{\partial S}{\partial x})+\frac{\partial}{\partial y}(\kappa_y\frac{\partial S}{\partial y})+F_S \tag{4.6}$$

$$\rho=\rho(T,S) \tag{4.7}$$

$$w(z)=\frac{\partial}{\partial x}\int_z^h udz+\frac{\partial}{\partial y}\int_z^h vdz \tag{4.8}$$

Boundary condition at sea surface (z = -ζ):

$$w|_{z=-\varsigma}=-(\frac{\partial \varsigma}{\partial t}+u\frac{\partial \varsigma}{\partial x}+v\frac{\partial \varsigma}{\partial y}) \tag{4.9}$$

$$-\rho(\nu\frac{\partial u}{\partial z})_{-\varsigma}=\tau_{sx},\ -\rho(\nu\frac{\partial v}{\partial z})_{-\varsigma}=\tau_{sy} \tag{4.10}$$

$$P_{-\varsigma}=P_a \tag{4.11}$$

$$-(\kappa_z\frac{\partial T}{\partial z})_{-\varsigma}=Q_T,\ -(\kappa_z\frac{\partial S}{\partial z})_{-\varsigma}=Q_S \tag{4.12}$$

here τ_{sx}, τ_{sy} is the air-sea interface wind stress in x, y direction respectively, P_a is the atmospheric pressure at the sea surface, Q_T, Q_S is the temperature, and salinity flux at the sea surface.

Boundary condition at sea bottom (z = h):

$$w|_{z=h}=u\frac{\partial h}{\partial x}+v\frac{\partial h}{\partial y} \tag{4.13}$$

$$-\rho(\nu\frac{\partial u}{\partial z})_h=\tau_{bx},\ -\rho(\nu\frac{\partial v}{\partial z})_h=\tau_{by} \tag{4.14}$$

$$-(\kappa_z\frac{\partial T}{\partial z})_h=0,\ -(\kappa_z\frac{\partial S}{\partial z})_h=0 \tag{4.15}$$

where τ_{bx}, τ_{by} is the sea-bed friction stress. A slip condition is applied at the sea-bed, and slip and impermeable boundary condition at the coastal line:

$$\frac{\partial(u,v)}{\partial n}=0,\ (u,v)\cdot\vec{n}=0 \tag{4.16}$$

$$\kappa_x\frac{\partial T}{\partial x}n_x+\kappa_y\frac{\partial T}{\partial x}n_y=\kappa_x\frac{\partial S}{\partial x}n_x+\kappa_y\frac{\partial S}{\partial x}n_y=0 \tag{4.17}$$

here $\vec{n}=(n_x,n_y)$ is the vector perpendicular to the boundary line.

Boundary condition at water boundary:

$$\varsigma = \varsigma^* \tag{4.18}$$

$$\kappa_x \frac{\partial T}{\partial x} n_x + \kappa_y \frac{\partial T}{\partial x} n_y = \kappa_x \frac{\partial S}{\partial x} n_x + \kappa_y \frac{\partial S}{\partial x} n_y = 0 \tag{4.19}$$

here ζ^* is the observed water level or predicted water level at the water boundary.

Integrating the continuity equation (4.1) and the using boundary conditions (4.9), (4.10):

$$\frac{\partial \varsigma}{\partial t} + \frac{\partial}{\partial x}\int_{-\varsigma}^{h} u dz + \frac{\partial}{\partial y}\int_{-\varsigma}^{h} v dz = 0 \tag{4.20}$$

vertical integrate (4.4) and using (4.11):

$$P = P_a + g\int_{-\varsigma}^{z} \rho dz \tag{4.21}$$

4.3 Turbulence enclosure

There are different approaches for turbulence closure (Launder & Spalding, 1974; Mellor & Yamada, 1974; Mellor & Yamada, 1982; Luyten et al., 1996; Xing & Davies, 1996). Here a level 2.5 two equation Mellor-Yamada q^2-$q^2 l$ turbulence closure model (Mellor & Yamada, 1974; Mellor & Yamada, 1982) has been chosen. The model is the quasi-equilibrium version. Deleersnijder & Luyten (1994) had demonstrated the practical advantages of the quasi-equilibrium version of the Mellor-Yamada level 2.5 turbulence closure which has been modified by Galperin et al. (1988). The governing equations contain parameterized Reynolds stress and flux terms which account for the turbulent diffusion of momentum, heat, and salt. The equations for turbulence energy, q^2, and mixing length, l, take the form,

$$\frac{\partial q^2}{\partial t} + u\frac{\partial q^2}{\partial x} + v\frac{\partial q^2}{\partial y} + w\frac{\partial q^2}{\partial z} =$$

$$\frac{\partial}{\partial z}(k_q \frac{\partial q^2}{\partial z}) + 2\nu[(\frac{\partial u}{\partial z})^2 + (\frac{\partial v}{\partial z})^2] - \frac{2gk_z}{\rho_0}\frac{\partial \rho}{\partial z} - \frac{2q^3}{B_1 l} + F_Q \tag{4.22}$$

$$\frac{\partial q^2 l}{\partial t} + u\frac{\partial q^2 l}{\partial x} + v\frac{\partial q^2 l}{\partial y} + w\frac{\partial q^2 l}{\partial z} =$$

$$\frac{\partial}{\partial z}(k_q \frac{\partial q^2 l}{\partial z}) + lE_1\nu[(\frac{\partial u}{\partial z})^2 + (\frac{\partial v}{\partial z})^2] - \frac{lE_1 gk_z}{\rho_0}\frac{\partial \rho}{\partial z} - \frac{q^3}{B_1}\tilde{W} + F_l \tag{4.23}$$

where a wall proximity function is defined as:

$$\tilde{W} \equiv 1 + E_2(\frac{l}{kL})^2 \tag{4.24}$$

and where:

$$(L)^{-1} = (\varsigma + z)^{-1} + (h - z)^{-1} = \frac{1}{H}[\sigma^{-1} + (1-\sigma)^{-1}] \tag{4.25}$$

The terms F_q and F_l in equations are the horizontal mixing and are parameterized analogously to the horizontal mixing terms in temperature and salinity equations.

ν, k_z, and k_q are given as the following expressions,

$$\nu = lqS_M \tag{4.26a}$$

$$k_z = lqS_H \tag{4.26b}$$

$$k_q = lqS_q \tag{4.26c}$$

The stability functions, S_M, S_H and S_q are analytically derived, algebraic relations functionally dependent upon $\frac{\partial u}{\partial z}$, $\frac{\partial v}{\partial z}$, $g\rho_0^{-1}$, $\frac{\partial \rho}{\partial z}$, q, l. These relations derive from closure hypotheses described by Mellor (1973) and summarised by Mellor and Yamada (1982). The stability functions S_M, S_H and S_q are dimensionless functions of G_M and G_H, which are defined as

$$G_M \equiv \frac{l^2}{q^2}[(\frac{\partial u}{\partial z})^2 + (\frac{\partial v}{\partial z})^2] = \frac{l^2}{q^2 H^2}[(\frac{\partial u}{\partial \sigma})^2 + (\frac{\partial v}{\partial \sigma})^2] \tag{4.27a}$$

$$G_H \equiv \frac{l^2 g}{q^2 \rho_0}\frac{\partial \rho}{\partial z} = \frac{l^2 g}{q^2 \rho_0 H}\frac{\partial \rho}{\partial \sigma} \tag{4.27b}$$

then the stability functions become

$$S_M[6A_1A_2G_M] + S_H[1 - 3A_2B_2G_M - 12A_1A_2G_H] = A_2 \tag{4.28a}$$

$$S_M[1 + 6A_1^2G_M - 9A_1A_2G_H] - S_H[12A_1^2G_H + 9A_1A_2G_H] = A_1(1 - 3C_1) \tag{4.28b}$$

$$S_q = 0.20 \tag{4.28c}$$

which are readily solved for S_M, S_H are functions of G_M, G_H by applying to laboratory data [Mellor and Yamada, 1982], the empirical constants were assigned the values

here $(A_1, A_2, B_1, B_2, C_1) = (0.92, 0.74, 16.6, 10.1, 0.08)$

and

$(E_1, E_2) = (1.8, 1.33)$ (4.29)

Boundary condition of the 1-D model in σ-coordinates. The boundary will be:

at sea surface ($\sigma = 0$):

$$q^2 = B_1^{2/3}U_{ts}^2 \tag{4.30a}$$

$$q^2 l = 0 \tag{4.30b}$$

at sea bottom ($\sigma = 1$):

$$q^2 = B_1^{2/3} U_{tb}^2 \tag{4.31a}$$

$$q^2 l = 0 \tag{4.31b}$$

where U_{ts}, U_{tb} is surface and bed friction velocity computed from the surface and sea bed stress respectively.

4.4 The σ coordinate transformation

The σ co-ordinate was first introduced by Phillips (1957) for meteorological weather forecasting. Now it is popular with a broad application in modelling of the ocean system (e.g. Blumberg & Mellor, 1987; Blumberg, 1992; Song & Haidvogel, 1994; Lynch & Werner, 1991).

Using σ co-ordinate transformation,

$$\sigma = \frac{z+\varsigma}{H} \qquad (\text{here } H = h+\varsigma\ ) \tag{4.32}$$

Equation (4.1), (4.2), (4.3), (4.4) and (4.5) may now be written as

$$\frac{\partial \varsigma}{\partial t} + \frac{\partial}{\partial x}[H\int_0^1 u d\sigma] + \frac{\partial}{\partial y}[H\int_0^1 v d\sigma] = 0 \tag{4.33}$$

$$\frac{\partial uH}{\partial t} + \frac{\partial u^2 H}{\partial x} + \frac{\partial uvH}{\partial y} + \frac{\partial uw^*}{\partial \sigma} - fvH =$$

$$-gH\frac{\partial \varsigma}{\partial x} - \frac{gH^2}{\rho_0}\frac{\partial}{\partial x}(\int_0^\sigma \rho d\sigma) + \frac{gH}{\rho_0}\frac{\partial H}{\partial x}\int_0^\sigma \sigma\frac{\partial \rho}{\partial \sigma}d\sigma + \frac{\partial}{\partial \sigma}(\frac{\nu}{H}\frac{\partial u}{\partial \sigma}) + \varepsilon H(\frac{\partial^2 u}{\partial x^2} + \frac{\partial^2 u}{\partial y^2}) + \varepsilon_x \tag{4.34}$$

$$\frac{\partial uH}{\partial t} + \frac{\partial uvH}{\partial x} + \frac{\partial v^2 H}{\partial y} + \frac{\partial vw^*}{\partial \sigma} + fuH =$$

$$-gH\frac{\partial \varsigma}{\partial y} - \frac{gH^2}{\rho_0}\frac{\partial}{\partial y}(\int_0^\sigma \rho d\sigma) + \frac{gH}{\rho_0}\frac{\partial H}{\partial y}\int_0^\sigma \sigma\frac{\partial \rho}{\partial \sigma}d\sigma + \frac{\partial}{\partial \sigma}(\frac{\nu}{H}\frac{\partial v}{\partial \sigma}) + \varepsilon H(\frac{\partial^2 v}{\partial x^2} + \frac{\partial^2 v}{\partial y^2}) + \varepsilon_y \tag{4.35}$$

$$\frac{\partial TH}{\partial t} + \frac{\partial TuH}{\partial x} + \frac{\partial TvH}{\partial y} + \frac{\partial Tw^*}{\partial \sigma} = \frac{\partial}{\partial \sigma}(\frac{K_z}{H}\frac{\partial T}{\partial \sigma}) + \frac{\partial}{\partial x}(HK_x\frac{\partial T}{\partial x}) + \frac{\partial}{\partial y}(HK_y\frac{\partial T}{\partial y}) + HF_T + \varepsilon_T \tag{4.36}$$

$$\frac{\partial SH}{\partial t} + \frac{\partial SuH}{\partial x} + \frac{\partial SvH}{\partial y} + \frac{\partial Sw^*}{\partial \sigma} = \frac{\partial}{\partial \sigma}(\frac{K_z}{H}\frac{\partial S}{\partial \sigma}) + \frac{\partial}{\partial x}(HK_x\frac{\partial S}{\partial x}) + \frac{\partial}{\partial y}(HK_y\frac{\partial S}{\partial y}) + HF_S + \varepsilon_S$$

(4.37)

$$\rho = \rho(T,S) \tag{4.38}$$

$$w^* = \frac{1}{H}[\frac{\partial \zeta}{\partial t}(1-\sigma)] + \frac{\partial}{\partial x}[H\int_\sigma^1 u d\sigma] + \frac{\partial}{\partial y}[H\int_\sigma^1 v d\sigma] \tag{4.39}$$

$$\frac{\partial q^2 H}{\partial t} + \frac{\partial q^2 uH}{\partial x} + \frac{\partial q^2 vH}{\partial y} + \frac{\partial q^2 w^*}{\partial \sigma} =$$

$$\frac{\partial}{\partial \sigma}(\frac{k_q}{H}\frac{\partial q^2}{\partial \sigma}) + \frac{2\nu}{H}[(\frac{\partial u}{\partial \sigma})^2 + (\frac{\partial v}{\partial \sigma})^2] - \frac{2gk_z}{\rho_0}\frac{\partial \rho}{\partial \sigma} - \frac{2q^3 H}{B_1 l} + F_Q + \varepsilon_Q \tag{4.40}$$

$$\frac{\partial q^2 lH}{\partial t} + \frac{\partial q^2 luH}{\partial x} + \frac{\partial q^2 lvH}{\partial y} + \frac{\partial q^2 lw^*}{\partial \sigma} =$$

$$\frac{\partial}{\partial z}(\frac{k_q}{H}\frac{\partial q^2 l}{\partial \sigma}) + \frac{lE_1\nu}{H}[(\frac{\partial u}{\partial \sigma})^2 + (\frac{\partial v}{\partial \sigma})^2] - \frac{lE_1 gk_z}{\rho_0}\frac{\partial \rho}{\partial \sigma} - \frac{q^3 H}{B_1}\tilde{W} + F_l + \varepsilon_l \tag{4.41}$$

here ε_x, ε_y, ε_T, ε_S, ε_Q, ε_l are the negligible terms at σ transformation.

Boundary condition at surface (σ = 0),

$$-\rho(\nu\frac{\partial u}{\partial \sigma})_0 = H\tau_{sx},\ -\rho(\nu\frac{\partial v}{\partial \sigma})_0 = H\tau_{sy} \tag{4.42a}$$

$$-(K_z\frac{\partial T}{\partial \sigma})_0 = HQ_T,\ -(K_z\frac{\partial S}{\partial \sigma})_0 = HQ_S \tag{4.42b}$$

$$(q^2)_0 = B_1^{2/3}U_{ts}^2,\ (q^2 l)_0 = 0 \tag{4.42c}$$

and at sea bottom (σ = 1),

$$-\rho(\nu\frac{\partial u}{\partial \sigma})_1 = H\tau_{bx},\ -\rho(\nu\frac{\partial v}{\partial \sigma})_1 = H\tau_{by} \tag{4.43a}$$

$$-(K_z\frac{\partial T}{\partial \sigma})_1 = 0,\ -(K_z\frac{\partial S}{\partial \sigma})_1 = 0 \tag{4.43b}$$

$$(q^2)_1 = B_1^{2/3}U_{ts}^2,\ (q^2 l)_1 = 0 \tag{4.43c}$$

here, u, v, w^* is the velocity of x, y, σ co-ordinate respectively.

4.5 Numerical methods

A mode split method has been used in the time integration, at time interval Δt, $n\Delta t < t \leq (n+1)\Delta t$, there are three steps. A mass conservation scheme, which is crucial to the success of

the further development of the water quality model, had been developed by Shi (1996). The upstream mass conservative scheme had replaced a modified characteristic line method. A detailed description of the numerical discrete scheme is not given here (see e.g. Shi, 1996; Shi & Xi, 1995; Wu, 1986).

First step $n\Delta t < t \leq (n+1/3)\,\Delta t$, using the vertical momentum and mass conservative upstream scheme,

$$\frac{1}{3}\frac{\partial u^{(1)}H}{\partial t}+\frac{\partial u^{(1)}w^{*}}{\partial \sigma}=0 \tag{4.44a}$$

$$\frac{1}{3}\frac{\partial v^{(1)}H}{\partial t}+\frac{\partial v^{(1)}w^{*}}{\partial \sigma}=0 \tag{4.44b}$$

$$\frac{1}{3}\frac{\partial T^{(1)}H}{\partial t}+\frac{\partial T^{(1)}w^{*}}{\partial \sigma}=0 \tag{4.44c}$$

$$\frac{1}{3}\frac{\partial S^{(1)}H}{\partial t}+\frac{\partial S^{(1)}w^{*}}{\partial \sigma}=0 \tag{4.44d}$$

$$\frac{1}{3}\frac{\partial q^{2(1)}H}{\partial t}+\frac{\partial q^{2(1)}w^{*}}{\partial \sigma}=0 \tag{4.44e}$$

$$\frac{1}{3}\frac{\partial q^{2}l^{(1)}H}{\partial t}+\frac{\partial q^{2}l^{(1)}w^{*}}{\partial \sigma}=0 \tag{4.44f}$$

Second step $(n+1/3)\Delta t < t \leq (n+2/3)\,\Delta t$, using the horizontal momentum and mass conservative upstream scheme,

$$\frac{1}{3}\frac{\partial u^{(2)}H}{\partial t}+\frac{\partial (u^{(2)})^{2}H}{\partial x}+\frac{\partial u^{(2)}v^{(2)}H}{\partial y}=0 \tag{4.45a}$$

$$\frac{1}{3}\frac{\partial v^{(2)}H}{\partial t}+\frac{\partial u^{(2)}v^{(2)}H}{\partial x}+\frac{\partial (v^{(2)})^{2}H}{\partial y}=0 \tag{4.45b}$$

$$\frac{1}{3}\frac{\partial T^{(2)}H}{\partial t}+\frac{\partial T^{(2)}u^{(2)}H}{\partial x}+\frac{\partial T^{(2)}v^{(2)}H}{\partial y}=0 \tag{4.45c}$$

$$\frac{1}{3}\frac{\partial T^{(2)}S}{\partial t}+\frac{\partial S^{(2)}u^{(2)}H}{\partial x}+\frac{\partial S^{(2)}v^{(2)}H}{\partial y}=0 \tag{4.45d}$$

$$\frac{1}{3}\frac{\partial q^{2(2)}H}{\partial t}+\frac{\partial q^{2(2)}u^{(2)}}{\partial x}+\frac{\partial q^{2(2)}v^{(2)}}{\partial y}=0 \tag{4.45e}$$

$$\frac{1}{3}\frac{\partial q^2 l^{(2)} H}{\partial t}+\frac{\partial q^2 l^{(2)} u^{(2)}}{\partial x}+\frac{\partial q^2 l^{(2)} v^{(2)}}{\partial y}=0 \qquad (4.45f)$$

Third step $(n+2/3)\Delta t < t \le (n+1)\,\Delta t$, using the Galerkin finite element method,

$$\frac{1}{3}\frac{\partial u^{(3)} H}{\partial t}-fv^{(3)}H=$$

$$-gH\frac{\partial \varsigma}{\partial x}-\frac{gH^2}{\rho_0}\frac{\partial}{\partial x}(\int_0^\sigma \rho d\sigma)+\frac{gH}{\rho_0}\frac{\partial H}{\partial x}\int_0^\sigma \sigma\frac{\partial \rho}{\partial \sigma}d\sigma+\frac{\partial}{\partial \sigma}(\frac{\nu}{H}\frac{\partial u^{(3)}}{\partial \sigma})+\varepsilon H(\frac{\partial^2 u^{(3)}}{\partial x^2}+\frac{\partial^2 u^{(3)}}{\partial y^2})$$

(4.46a)

$$\frac{1}{3}\frac{\partial v^{(3)} H}{\partial t}+fu^{(3)}H=$$

$$-gH\frac{\partial \varsigma}{\partial y}-\frac{gH^2}{\rho_0}\frac{\partial}{\partial y}(\int_0^\sigma \rho d\sigma)+\frac{gH}{\rho_0}\frac{\partial H}{\partial y}\int_0^\sigma \sigma\frac{\partial \rho}{\partial \sigma}d\sigma+\frac{\partial}{\partial \sigma}(\frac{\nu}{H}\frac{\partial v^{(3)}}{\partial \sigma})+\varepsilon H(\frac{\partial^2 v^{(3)}}{\partial x^2}+\frac{\partial^2 v^{(3)}}{\partial y^2})$$

(4.46b)

$$\frac{1}{3}\frac{\partial T^{(3)} H}{\partial t}=\frac{\partial}{\partial \sigma}(\frac{K_z}{H}\frac{\partial T^{(3)}}{\partial \sigma})+\frac{\partial}{\partial x}(HK_x\frac{\partial T^{(3)}}{\partial x})+\frac{\partial}{\partial y}(HK_y\frac{\partial T^{(3)}}{\partial y})+HF_T \qquad (4.46c)$$

$$\frac{1}{3}\frac{\partial S^{(3)} H}{\partial t}=\frac{\partial}{\partial \sigma}(\frac{K_z}{H}\frac{\partial S^{(3)}}{\partial \sigma})+\frac{\partial}{\partial x}(HK_x\frac{\partial S^{(3)}}{\partial x})+\frac{\partial}{\partial y}(HK_y\frac{\partial S^{(3)}}{\partial y})+HF_S \qquad (4.46d)$$

$$\frac{1}{3}\frac{\partial q^{2(3)} H}{\partial t}=\frac{\partial}{\partial \sigma}(\frac{k_q}{H}\frac{\partial q^{2(3)}}{\partial \sigma})+\frac{2\nu}{H}[(\frac{\partial u}{\partial \sigma})^2+(\frac{\partial v}{\partial \sigma})^2]-\frac{2gk_z}{\rho_0}\frac{\partial \rho}{\partial \sigma}-\frac{2q^3 H}{B_1 l}+F_Q^{(3)}$$

(4.46e)

$$\frac{1}{3}\frac{\partial q^2 l^{(3)} H}{\partial t}=\frac{\partial}{\partial z}(\frac{k_q}{H}\frac{\partial q^2 l^{(3)}}{\partial \sigma})+\frac{lE_1\nu}{H}[(\frac{\partial u}{\partial \sigma})^2+(\frac{\partial v}{\partial \sigma})^2]-\frac{lE_1 gk_z}{\rho_0}\frac{\partial \rho}{\partial \sigma}-\frac{q^3 H}{B_1}\tilde{W}+F_l^{(3)}$$

(4.46f)

Figure 4.1 shows the finite element grid.

(a) (b)

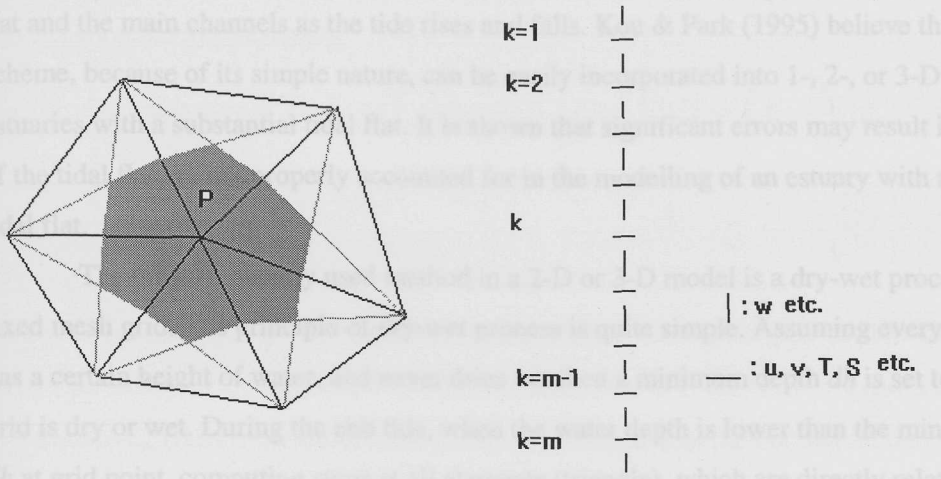

Figure 4.1 Horizontal (a) and vertical (b) relative positions of grids points
(shaded area represents the mass concentration area)

For continuity equation, the time integration will carry out in one time step using conservative mass scheme.

$$\overline{u} = \int_0^1 u d\sigma \, , \overline{v} = \int_0^1 v d\sigma \tag{4.47}$$

$$\frac{\varsigma_i^{n+2/3} - \varsigma_i^{n-1/3}}{\Delta t} A_i = \frac{H_i^{n+2/3} - H_i^{n-1/3}}{\Delta t} A_i = \oint_{\Gamma_i} H^{n-1/3} (\overline{u}, \overline{v})^{n-1/3} \cdot (n_x, n_y) d\Gamma \tag{4.48}$$

the vertical velocity w is computed in a similar way to the tidal elevation ζ

4.6 Tidal flat

In Southampton Water, the proportion of the tidal prism over the tidal flat is about 20% at spring tide, and 15% at average tide, and about 10% at neap tide.

Although it is quite difficult and costly to deal with a tidal flat, including the tidal flat in the model is very important to accurately predict the tidal prism. Thus tidal currents are more accurate in some areas (e. g. Southampton Water) where the tidal flat extends over a significant proportion of the whole area. Also the tidal flat is important for the exchange of matter (e.g. oxygen, nitrogen, phosphorus) at the water-sediment interface.

There are different methods to deal with a tidal flat. One method (Shi, 1996) is to change the mesh grid in a certain time interval to fit the land-water boundary, but this is at the cost in time and accuracy of the model. Kou & Park(1995) gave a simple scheme to account for

the influence of tidal flat in a vertical-longitude 2-D model. The scheme, which treats the tidal flat as a temporary storage area, accounts for the water and material exchanges between the tidal flat and the main channels as the tide rises and falls. Kou & Park (1995) believe that the scheme, because of its simple nature, can be easily incorporated into 1-, 2-, or 3-D models of estuaries with a substantial tidal flat. It is shown that significant errors may result if the effects of the tidal flat are not properly accounted for in the modelling of an estuary with an extensive tidal flat.

The most frequently used method in a 2-D or 3-D model is a dry-wet process with a fixed mesh grid. The principle of dry-wet process is quite simple. Assuming every grid point has a certain height of water, and never dries out then a minimum depth *dh* is set to judge if the grid is dry or wet. During the ebb tide, when the water depth is lower than the minimum depth *dh* at grid point, computing stops at all elements (triangle), which are directly related to this grid point. During the flood tide, when the water level rises to a point that water level at two grid points of an element is higher than that of third grid with a minimum water depth *dh*, then computing of the element is restarted. This principle has been used in this 3-D model.

4.7 Box model

Box models are simple but robust and easy to use. They have numerous applications in the marine environment: for example, Dyer & Taylor (1973), and Dyer (1973) gave a modified version of a prism model; Munekage (1990, 1992, 1995) applied a two-layer box model to tidal exchange and DO budget in Uranouchi Bay, Japan; Bierman, Jr. et al. (1994) used a 3-D box model to determine the mass (primary production, DO) balance in the Mississippi River plume region; Roson et al. (1997) used a non-stationary box model to determine residual fluxes in a partially mixed estuary.

The principle of a box model is the conservation of matter. The flux of water mass between different boxes will be determined by advection and mixing which comes from observation or model results. Salinity, as conservative matter, is normally used to calibrate the box model, by the determination of the water mass exchange between different boxes. A detailed description of box models is given by Wells (1996).

Initially a box model with a simple 3-D structure was the proposed approach to couple the water quality model (DO model) with the hydrodynamic model in Southampton Water. Since a momentum and mass conservative scheme has been successfully used in the 3-D hydrodynamic model, and 3-D advection-dispersion model, it was decided not to pursue the application of a box model.

4.8 Mass conservative scheme

The principle of mass conservative in an aquatic medium can be described by the mass conservation integral equation:

$$\frac{\partial}{\partial t}\iiint_{\Omega} C dx dy dz = -\sum Sinks + \sum Sources + \int_{\Gamma} C(\vec{n}\cdot\vec{V})d\Gamma + \int_{\Gamma} K\cdot\frac{\partial C}{\partial n}d\Gamma \qquad (4.49)$$

(1) (2) (3) (4) (5)

where C represents the mass (e.g. salinity, dissolved oxygen, nutrient), and C could be 1 when the water volume is concerned; term (1) on the left side is the local time difference of the total mass over domain Ω; term (2) on the right side of equation is the total sink (rate) term within the domain Ω, while term (3) is the source (rate) terms within the domain Ω; term (4) on the right side of the equation is the mass flux rate due to advection across the boundary Γ of domain Ω; term (5) on the right side is the mass exchange due to the eddy dispersion and mixing across the boundary Γ of domain Ω.

If the boundary Γ of the domain Ω is divided into four boundaries; Γ_1, land-water boundary; Γ_2, open water boundary; Γ_3, air-water boundary and Γ_4, water-sediment boundary, then the term (3) and term (4) in equation (4.49) can be rewriten respectively as following,

$$\int_{\Gamma} C(\vec{n}\cdot\vec{V})d\Gamma = \int_{\Gamma_1} C(\vec{n}\cdot\vec{V})d\Gamma + \int_{\Gamma_2} C(\vec{n}\cdot\vec{V})d\Gamma + \int_{\Gamma_3} C(\vec{n}\cdot\vec{V})d\Gamma + \int_{\Gamma_4} C(\vec{n}\cdot\vec{V})d\Gamma \qquad (4.50)$$

$$\int_{\Gamma} K\cdot\frac{\partial C}{\partial n}d\Gamma = \int_{\Gamma_1} K\cdot\frac{\partial C}{\partial n}d\Gamma + \int_{\Gamma_2} K\cdot\frac{\partial C}{\partial n}d\Gamma + \int_{\Gamma_3} K\cdot\frac{\partial C}{\partial n}d\Gamma + \int_{\Gamma_4} K\cdot\frac{\partial C}{\partial n}d\Gamma \qquad (4.51)$$

According to equation (4.49), numerical experiments have been conducted in Southampton Water to examine the numerical behaviour of the mass conservative scheme. The water mass and salinity as tracers were chosen to test the model. Since the conservative behaviour of the water mass and salinity, there are no sink and source terms within the domain. It is assumed that there are no advective flux and mixing flux across the air-water interface Γ_3 and water-sediment interface Γ_4, and no mixing flux across the land-water boundary Γ_1. Equation (4.49) is then simplified,

$$\frac{\partial}{\partial t}\iiint_{\Omega} C dx dy dz = \int_{\Gamma_1} C(\vec{n}\cdot\vec{V})d\Gamma + \int_{\Gamma_2} C(\vec{n}\cdot\vec{V})d\Gamma + \int_{\Gamma_2} K\cdot\frac{\partial C}{\partial n}d\Gamma \qquad (4.51)$$

Equation (4.50) can be expressed alternatively,

$$\int_{\Gamma_1} C(\vec{n}\cdot\vec{V})d\Gamma = \frac{\partial}{\partial t}\iiint_{\Omega} C dx dy dz - \int_{\Gamma_2} C(\vec{n}\cdot\vec{V})d\Gamma - \int_{\Gamma_2} K\cdot\frac{\partial C}{\partial n}d\Gamma \qquad (4.52)$$

(1) (2) (3) (4)

where term (1) on the left side of the equation (4.52) is the point sources on the land-water boundary Γ_1 (e.g. riverine discharge, industrial and domestic sewage effluents) into the estuary; term (2) on the right side is the local time difference of the total mass over domain Ω; term (3) on the right side is the advective flux across the open water boundary Γ_2 of domain Ω; term (4) on the right side is the mixing flux across the boundary Γ_2 of domain Ω.

Integrating equation (4.52) over a time interval [t, t+t_0]. Then we have the equation

$$\int_t^{t+t_0}\int_{\Gamma_1} C(\vec{n}\cdot\vec{V})d\Gamma dt = \iiint_{\Omega} C dx dy dz\Big|_{t=t}^{t=t+t_0} - \int_t^{t+t_0}\int_{\Gamma_2} C(\vec{n}\cdot\vec{V})d\Gamma dt - \int_t^{t+t_0}\int_{\Gamma_2} K\cdot\frac{\partial C}{\partial n}d\Gamma dt \qquad (4.53)$$

Equation (4.53) means the point sources of tracer C, into domain Ω from land-water boundary Γ_1, can be estimated by monitoring the advective and mixing flux across the open water boundary Γ_2 and by monitoring the change of total amount of tracer C over time interval [t, t+t_0] within the domain Ω. In the fact the data of the point source have been set in the model, so comparing the data set in the model with the magnitude of the point sources estimated from the equation (4.53) can be used to quantify the accuracy of the mass conservative scheme of the model.

There are 4 different control boundaries to look at the conservation in the four domains limited by the boundary: control boundary 1, a open boundary across Dockhead controlling the Itchen Estuary; control boundary 2, a open boundary across Dockhead controlling the Test Estuary; control boundary 3, a open boundary across Calshot Castle controlling the whole Southampton Water; control boundary 4, a open boundary set at the open boundary including all model domain.

The time of the numerical experiment begins randomly from 00:00 on 14/06/99 for a 15 day run. The only input at the land-water boundary, fresh water (salinity is 0.0) sources are the River Itchen, River Test and River Hamble, with fresh water river flow rate of 7 $m^3 s^{-1}$, 15 $m^3 s^{-1}$ and 2 $m^3 s^{-1}$ respectively. The calculated fresh water discharge, by monitoring the flux across the control open boundary 1 and 2, is 14.9932 $m^3 s^{-1}$ for the River Test, and 6.9951 $m^3 s^{-1}$ for the River Itchen. The calculated freshwater discharge from whole Southampton Water area (controlled open boundary 3) is about 23.9714 $m^3 s^{-1}$, while the real total discharge is 24 $m^3 s^{-1}$. The estimated freshwater discharge (Figure 4.2) from whole model domain is about 23.9208 $m^3 s^{-1}$, and the relative magnitude of the estimated figure, 23.9208 $m^3 s^{-1}$ comparing with model input of 24 $m^3 s^{-1}$ is 0.9967.

From the Itchen Estuary control area, model result shows the Itchen Estuary is a source of salt. Comparing with the fresh water flux, and it is equivalent to that the fresh water discharged from Itchen River have a salinity of about 0.1012. While the error from the Test Estuary means that in Test Estuary area there is a source of salt, which is equivalent to the fresh

Figure 4.2 Total riverine fresh water discharge for 15 days period, comparison between the result estimated by monitoring the boundary 4 controlling whole model domain with real model input

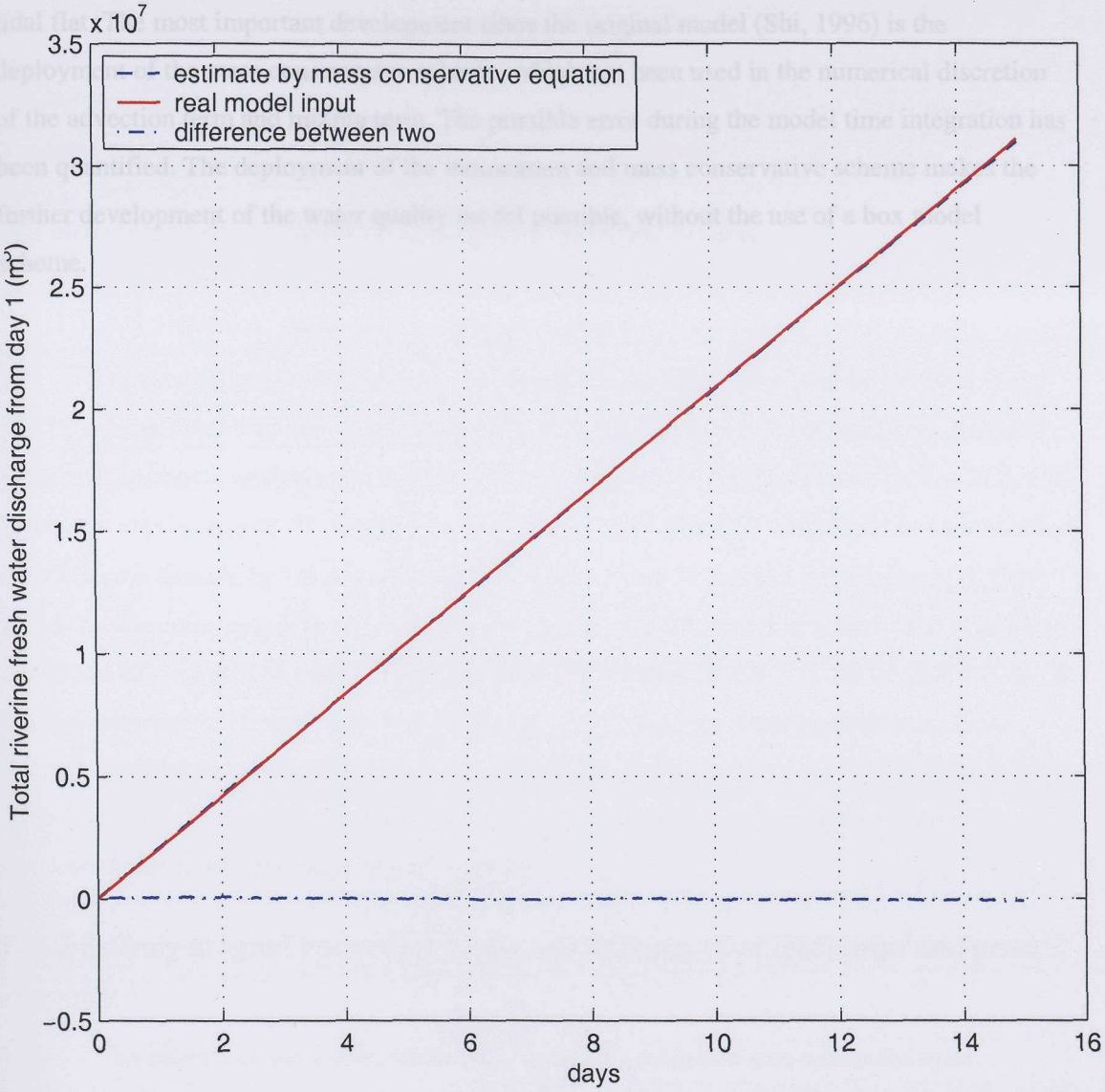

water discharged from the River Test with a salinity of 0.1240. The result from Southampton Water means the fresh water discharged from River Test, River Itchen, and River Hamble has a salinity of 0.1873. The result estimated from whole domain means that the fresh water discharged from three rivers has a salinity of 0.3057.

4.9 Conclusion

A level 2.5 two equation Mellor-Yamada q^2-q^2l turbulence closure model has been used in this 3-D baroclinic hydrodynamic model, and a dry-wet process also used to cope with the tidal flat. The most important development since the original model (Shi, 1996) is the deployment of the mass conservative scheme, which has been used in the numerical discretion of the advection term and mixing term. The possible error during the model time integration has been quantified. The deployment of the momentum and mass conservative scheme makes the further development of the water quality model possible, without the use of a box model scheme.

Chapter 5 Application of 3-D baroclinic hydrodynamic model in Southampton Water

5.1 Introduction

A 3-D baroclinic finite element hydrodynamic model has been developed, and applied to Southampton Water and the Solent estuarine system to examine the tidal elevation, currents, estuarine circulation, salinity distribution, tidal induced water mass transportation and water exchange. Figure 5.1 shows the model area and finite element grid which covers about 3,150 km^2. The model consists of 1417 nodes and 2,674 triangles. The largest grid area is about 8 km^2, and the smallest is only 0.02 km^2. The flexible triangle grid is well suited to the complex boundary and bathymetry of Southampton Water and the Solent.

5.2 Boundary conditions of the hydrodynamic model

5.2.1 Tidal elevation data at the open boundary

The tidal elevation data at the open boundary were kindly provided by Dr. Neil Wells and Proudman Oceanographic Laboratory (POL). 26 tidal harmonic constituents are provided from tidal harmonic analysis of the POL's Continental Shelf (CS3) model results. The POL CS3 model covers the area 48:07'N-62:53'N, 11:50'W-12:50E. The CS3 model grid has a resolution of 1/9 degree latitude by 1/6 degree longitude (approximate 12 km ×12 km, Figure 5.2). This grid is coarse compared with the finite element model grid (about 2-3 km, near open boundary) of the Solent system. The total 26 tidal harmonic constituents (Table 5.1) can be grouped into 5 diurnal constituent, 10 semi-diurnal constituents, and 11 shallow water constituents. Tidal current and tidal elevation within the model domain are driven by the tidal elevation from the open boundary. No attempt has been made to improve the result by tuning the boundary conditions due to the limitation of data sources.

5.2.2 Salinity at open boundary, water temperature, river discharge and point sources

The salinity of sea water, when it flows into the modelled area across the open boundary, is fixed at 34.5. Water temperature in the estuary is not implicitly modelled, and it regarded as an external force given by observation data from monthly surveys. The daily variation of the water temperature will be ignored. Daily fresh water discharge data from the River Test, River Itchen and River Hamble (Figure 2.8) were provided by the Environment Agency. Sewage discharge from point sources follows the data given in HR Wallingford report EX 3253 (1995).

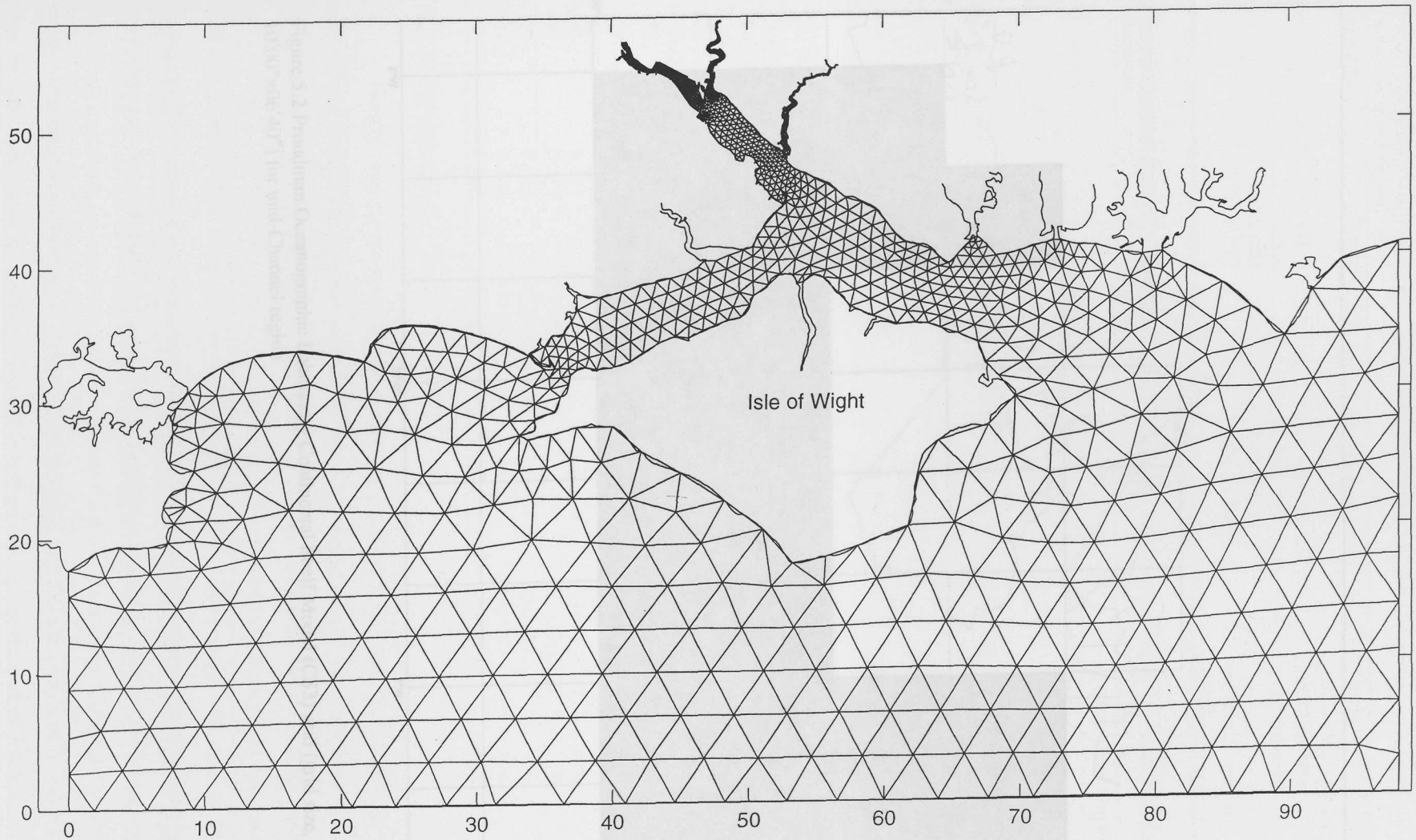

Figure 5.1 Model area and finite element grid of the Solent estuarine system (km)

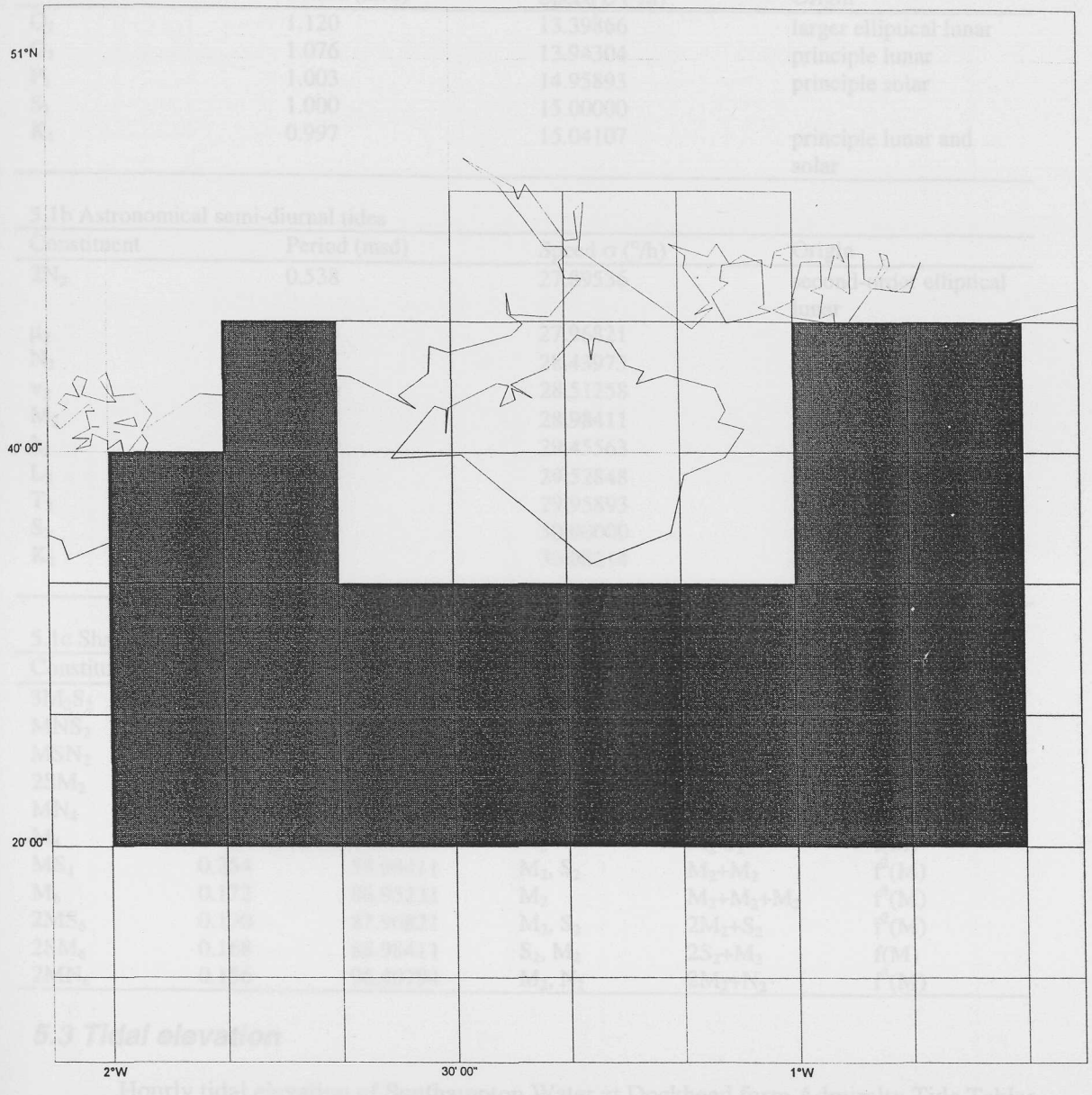

Figure 5.2 Proudman Oceanographic Laboratory Continental Shelf Model (CS3) grid (grid size, 10′00″×06′40″) for mid-Channel region

Table 5.1 Harmonic tidal constituents for boundary condition

5.1a Astronomical diurnal tides

Constituent	Period (msd)	Speed σ (°/h)	Origin
Q_1	1.120	13.39866	larger elliptical lunar
O_1	1.076	13.94304	principle lunar
P_1	1.003	14.95893	principle solar
S_1	1.000	15.00000	
K_1	0.997	15.04107	principle lunar and solar

5.1b Astronomical semi-diurnal tides

Constituent	Period (msd)	Speed σ (°/h)	Origin
$2N_2$	0.538	27.89536	second-order elliptical lunar
μ_2	0.536	27.96821	variational
N_2	0.527	28.43973	larger ellipitical lunar
ν_2	0.526	28.51258	larger evectional
M_2	0.518	28.98411	principle lunar
λ_2	0.509	29.45563	smaller evectional
L_2	0.508	29.52848	smaller ellipitical lunar
T_2	0.501	29.95893	larger ellipitical solar
S_2	0.500	30.00000	principle solar
K_2	0.499	30.08214	declinational lunar & declinational solar

5.1c Shallow-water harmonic constituents

Constituent	Period (msd)	Speed σ (°/h)	Generated by	Angular speeds	Nodal factor
$3M_2S_2$	0.557	26.95231	M_2, S_2	$3M_2$-$2S_2$	$f^3(M)$
MNS_2	0.540	27.42383	M_2, N_2, S_2	M_2+N_2-S_2	$f^2(M)$
MSN_2	0.490	30.54437	M_2, S_2, N_2	M_2+S_2-N2	$f^2(M)$
$2SM_2$	0.483	31.01590	S_2, M_2	$2S_2$-M_2	f(M)
MN_4	0.261	57.45563	M_2, N_2	M_2+N_2	$f^2(M)$
M_4	0.258	57.96821	M_2	M_2-S_2	f(M)
MS_4	0.254	58.98411	M_2, S_2	M_2+M_2	$f^2(M)$
M_6	0.172	86.95231	M_2	M_2+M_2+M_2	$f^3(M)$
$2MS_6$	0.170	87.96821	M_2, S_2	$2M_2$+S_2	$f^2(M)$
$2SM_6$	0.168	88.98411	S_2, M_2	$2S_2$+M_2	f(M)
$2MN_6$	0.156	96.40794	M_2, N_2	$2M_2$+N_2	$f^3(M)$

5.3 Tidal elevation

Hourly tidal elevation of Southampton Water at Dockhead form Admiralty Tide Tables (ATT) has been used to compare with the 2-D and 3-D model results. Figure 5.3 is a direct comparison of the tidal elevation between the 2-D model, 3-D model and one decimal hourly predicted tide (ATT) from 1 June to 20 June 1998. The model output shows that tidal elevation in Southampton Water has been extremely distorted by the shallow water components, which is caused by the limited water depth, bottom friction and local topography. The distortion has take the form of a 'double high water', and 'young flood stand'. During spring tides (Figure 5.3b1), following low water the water level rises, but then there is a slackening of the tidal stream and a water level stand for a further two hours before the final rapid rise to high water, over the next three hours. This slackening effect is known locally as the 'young flood stand'. The flood and double high water last approximately nine hours, leaving only 3 hours for the ebb, which has

Figure 5.3a1 Comparison of predicted tidal elevation with computed tidal elevation from 3–D model and 2–D model, Dockhead

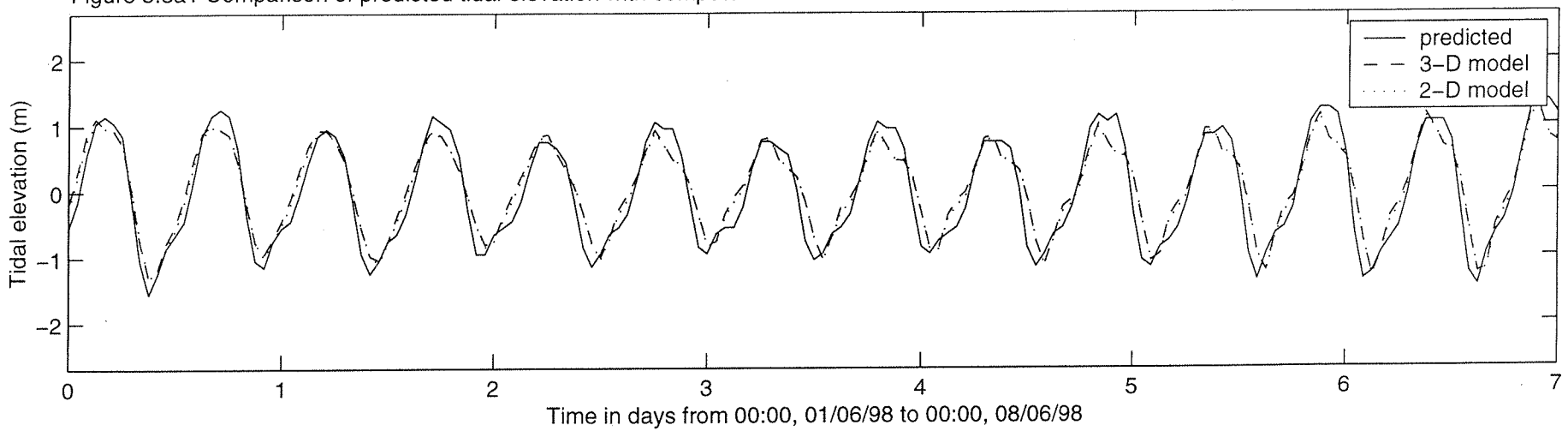

Figure 5.3a2 Error of computed tidal elevation from 3–D model and 2–D model, Dockhead

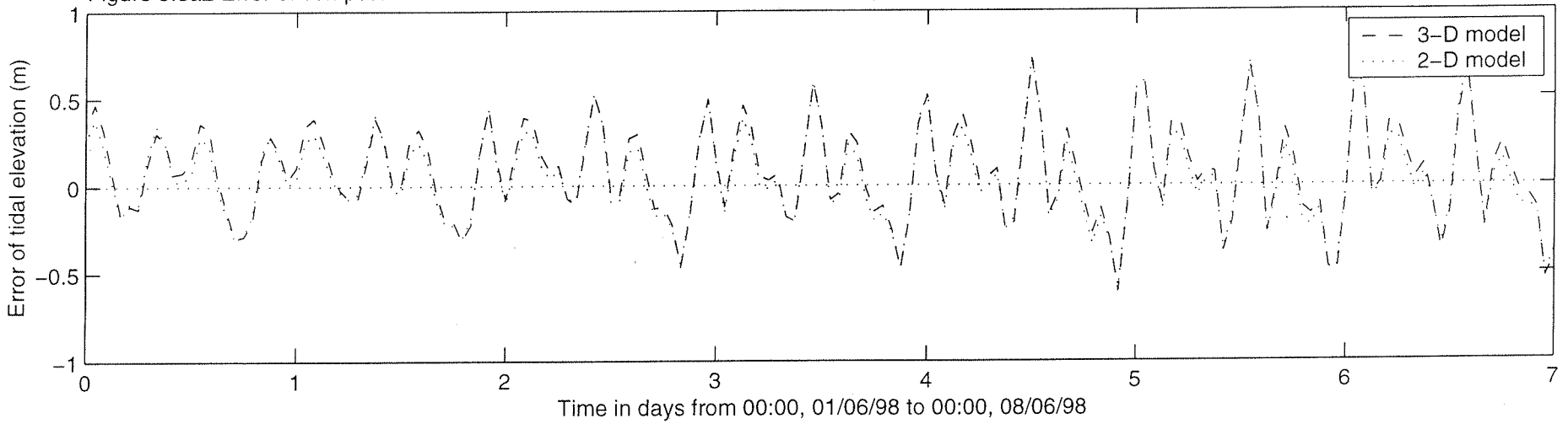

Figure 5.3b1 Comparison of predicted tidal elevation with computed tidal elevation from 3–D model and 2–D model, Dockhead

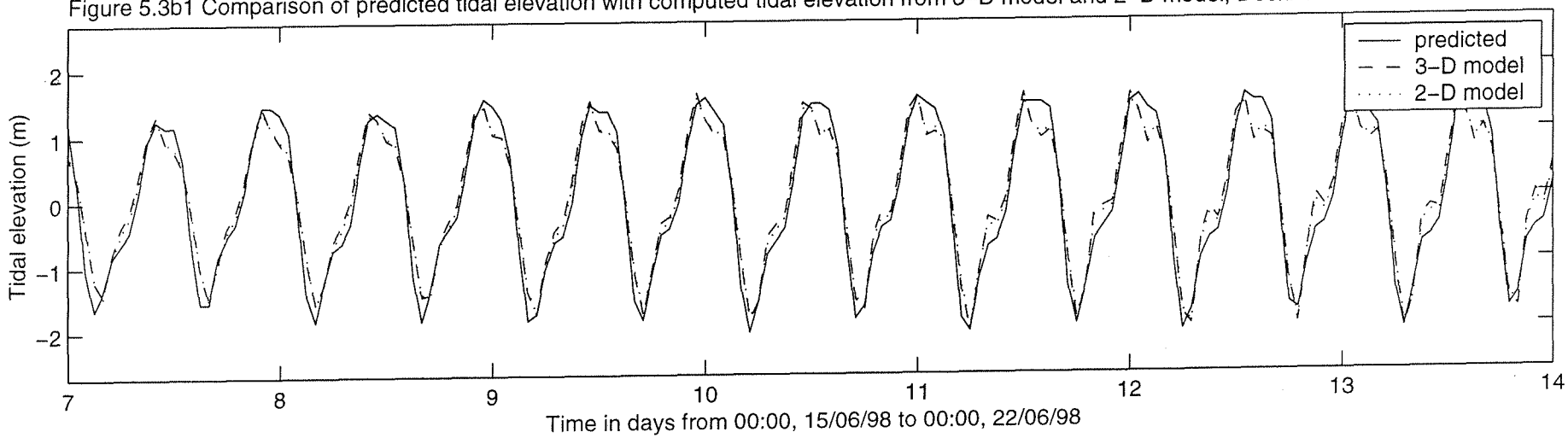

Figure 5.3b2 Error of computed tidal elevation from 3–D model and 2–D model, Dockhead

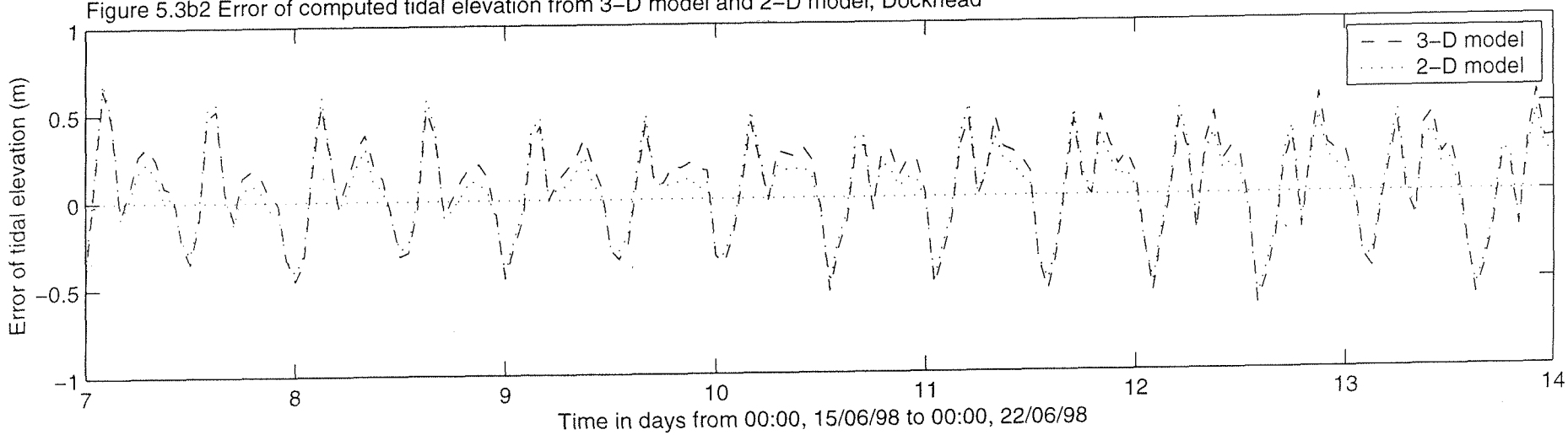

Figure 5.3c1 Comparison of predicted tidal elevation with computed tidal elevation from 3–D model and 2–D model, Dockhead

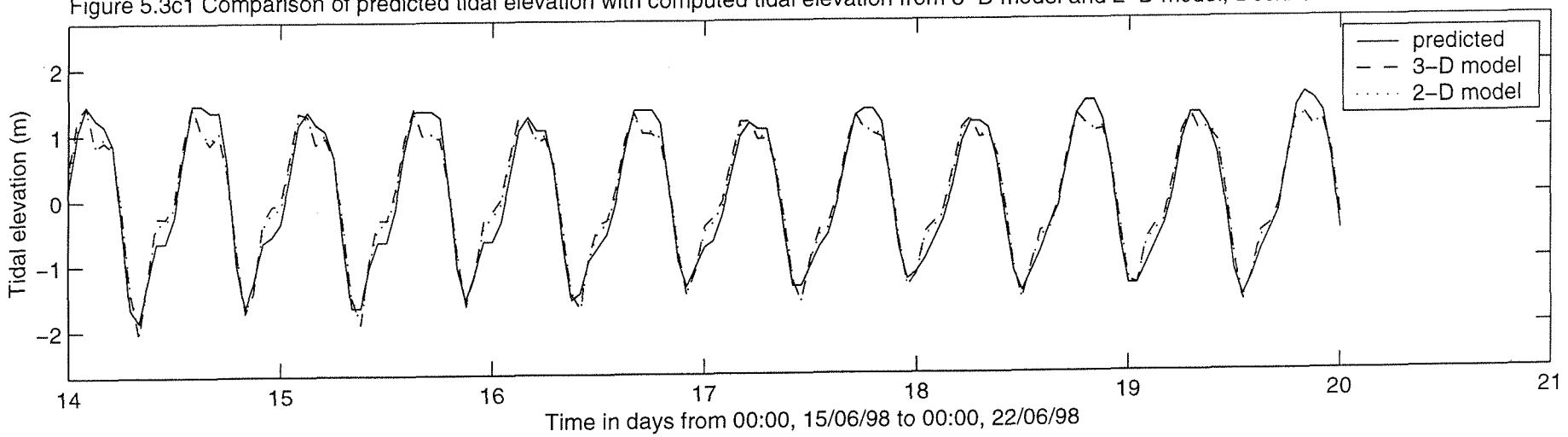

Figure 5.3c2 Error of computed tidal elevation from 3–D model and 2–D model, Dockhead

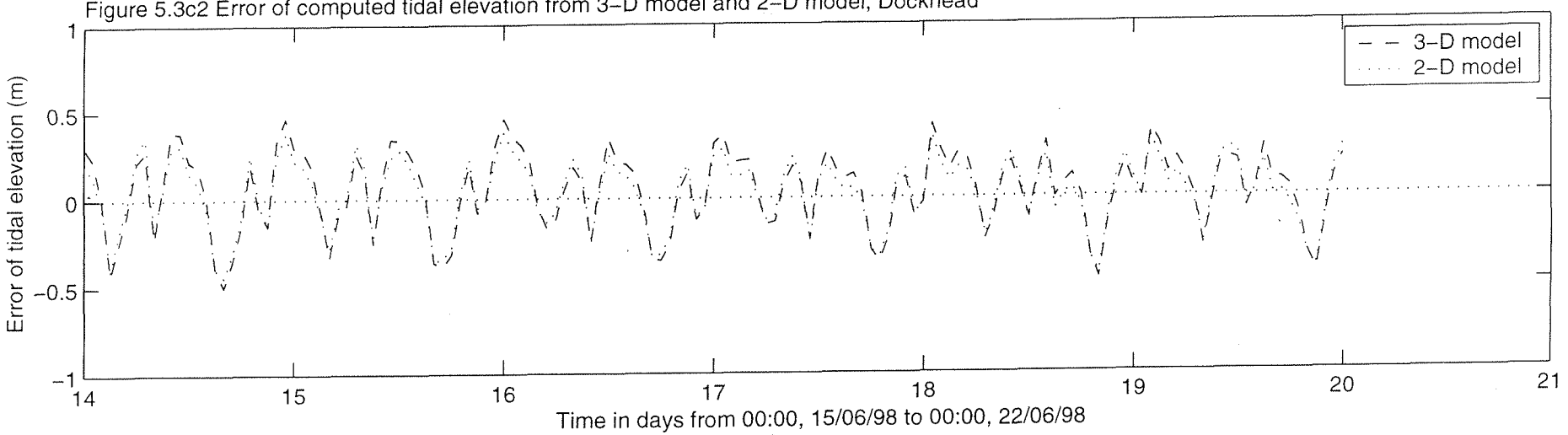

therefore very strong tidal currents. During the modelled period, the tidal range at neaps is about 250 cm, about half of the tidal range at spring tide, 430 cm. Presuming the hourly one decimal ATT tide prediction is accurate without any meteorological factors acting on it, the standard deviation of the errors between the 2-D model results and ATT predicted tide is 26.42 cm, standard deviation of errors between the 3-D model results and ATT predicted tide is 28.66 cm. The maximum tidal range during this period is 430 cm, so the ratio of standard deviation of errors for 2-D and 3-D model to tidal range is 0.0614 and 0.0667 respectively.

The main differences between the model results and predicted tide are:

1) the model tidal range is smaller than the ATT predicted.
2) young flood stand in the model is over pronounced.
3) rising of the water level at first stage of the flood tide is quicker than the ATT predicted (this means the rate of water level rising at the second stage of flood tide will be smaller than the ATT predicted, therefore smaller magnitude of flood tidal currents at the second flood stage).
4) the second high water is smaller than the first one, while the first high water is well modelled.

It is not exactly known which factors cause the error between the modelled tidal elevation and ATT predicted one, but it is believed that the open boundary condition is poor with a coarse resolution of 12 km. There are two possible steps to improve the model results:

1. providing a finer tidal boundary condition from a higher resolution tidal hydrodynamic model
2. having harmonic analysis of model results, compared with the tidal harmonic constant from a tide gauge station within the model area, and tuning the main astronomical tidal constituents individually.

Both steps should make it possible to look at the unique tidal features and non linear interaction of tidal dynamics of the Southampton Water and the Solent area in future work

The difference between the 2-D model and 3-D model for tidal elevation is small, and the standard deviation of the errors form the 2-D model (26.42 cm) is smaller that that of 3-D model (28.66 cm). The duration of flood tide in the 2-D model result is slightly longer than that in the 3-D model, which gives more time for the ebb tide in 3-D model than that in the 2-D model. One apparent explanation is that the bottom friction is stronger in 2-D model than that in 3-D model. The stronger bottom friction results in a longer flood time and shorter ebb time (therefore stronger ebb currents).

5.4 Tidal currents

Figure 5.4a-d shows the depth-averaged tidal currents from the 3-D model in the Solent estuarine system at different phases of a tidal cycle with a medium tidal range. The tidal

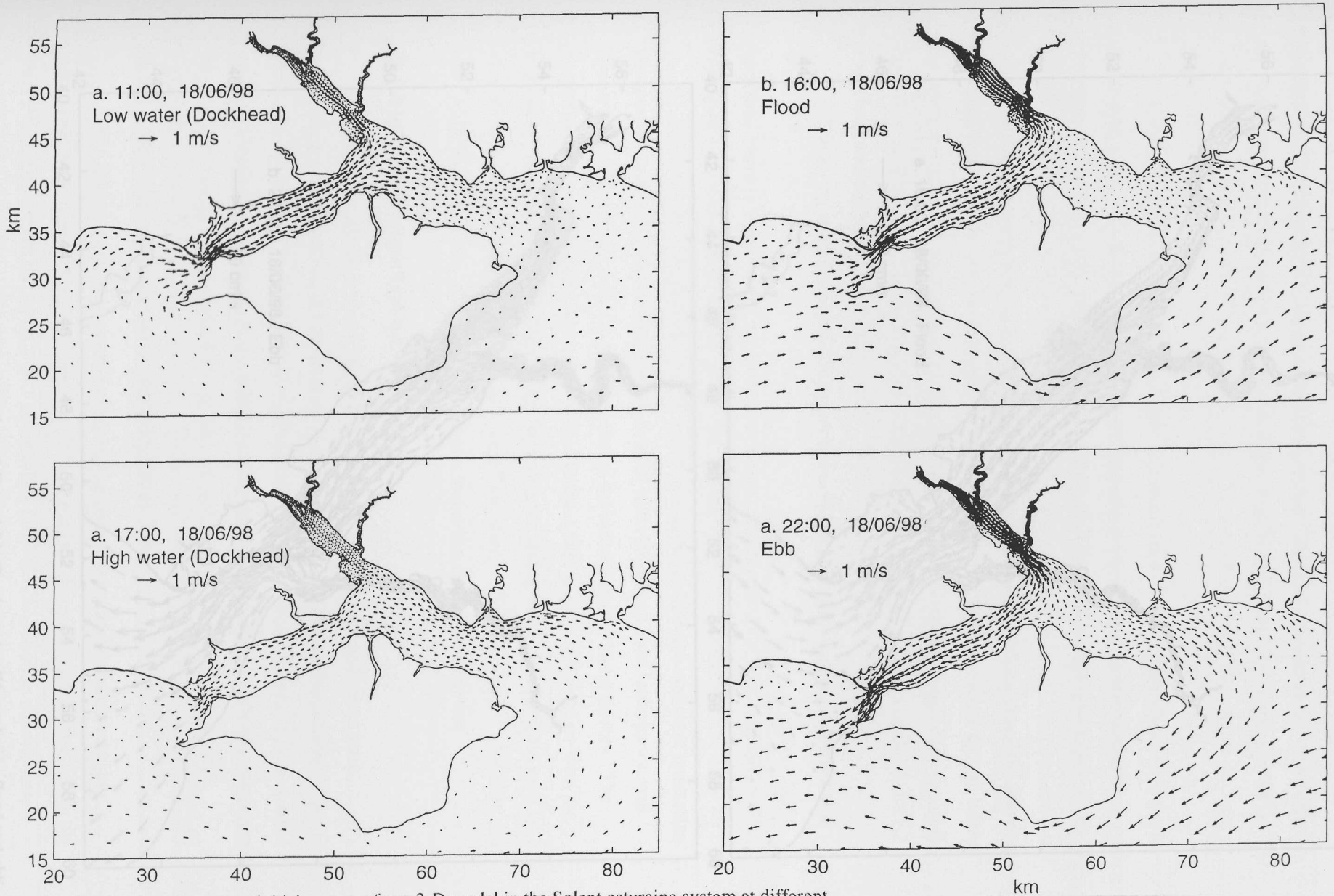

Figure 5.4 Depth-averaged tidal currents from 3-D model in the Solent esturaine system at different phases of a tidal cycle

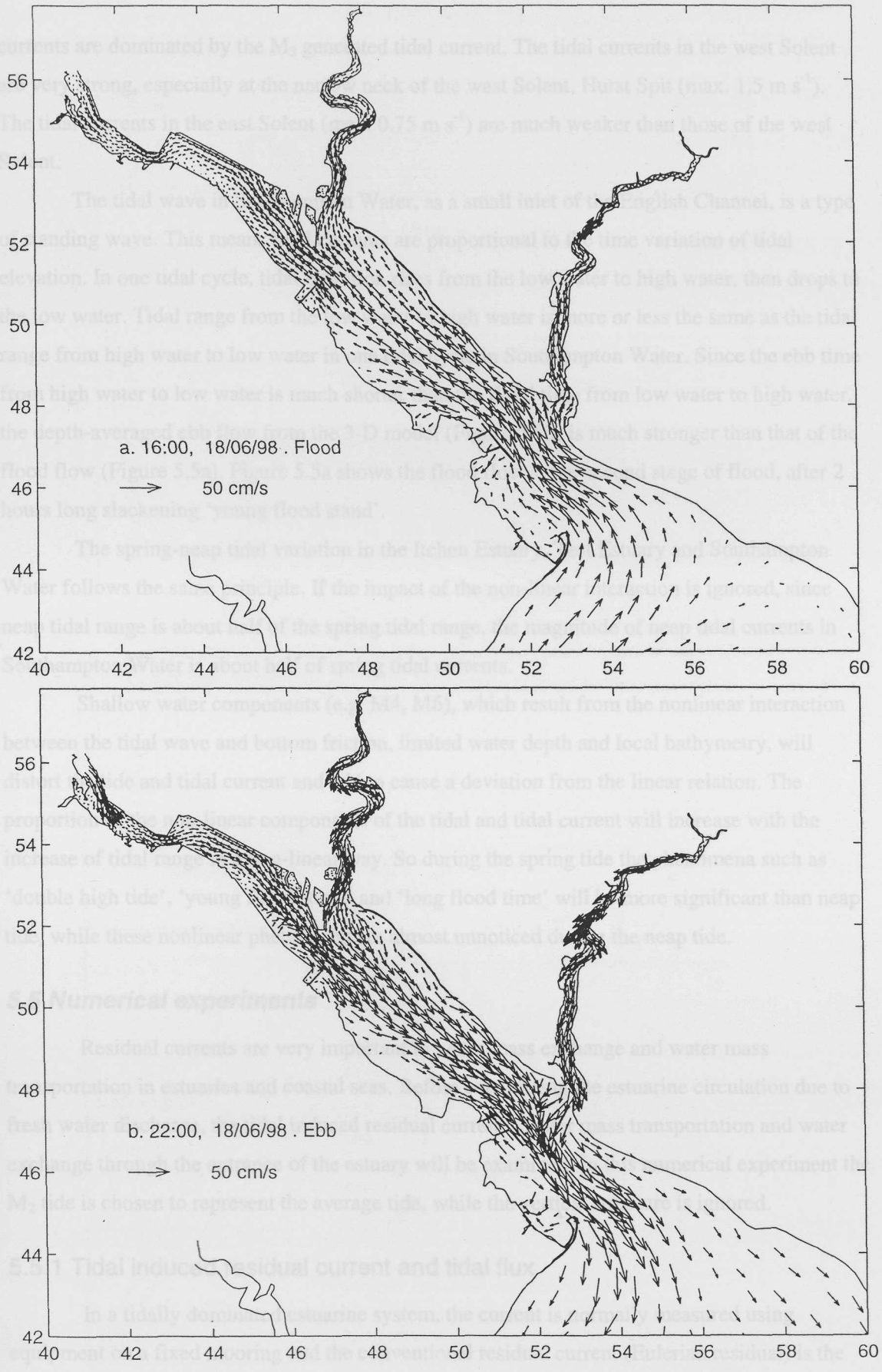

Figure 5.5 Depth-averaged tidal currents from 3-D model in Southampton Water during flood and ebb of a tidal cycle

currents are dominated by the M_2 generated tidal current. The tidal currents in the west Solent are very strong, especially at the narrow neck of the west Solent, Hurst Spit (max. 1.5 m s^{-1}). The tidal currents in the east Solent (max. 0.75 m s^{-1}) are much weaker than those of the west Solent.

The tidal wave in Southampton Water, as a small inlet of the English Channel, is a type of standing wave. This means tidal currents are proportional to the time variation of tidal elevation. In one tidal cycle, tidal elevation rises from the low water to high water, then drops to the low water. Tidal range from the low water to high water is more or less the same as the tidal range from high water to low water in one tidal cycle in Southampton Water. Since the ebb time from high water to low water is much shorter than the flood time from low water to high water, the depth-averaged ebb flow from the 3-D model (Figure 5.5b) is much stronger than that of the flood flow (Figure 5.5a). Figure 5.5a shows the flood flow at the second stage of flood, after 2 hours long slackening 'young flood stand'.

The spring-neap tidal variation in the Itchen Estuary, Test Estuary and Southampton Water follows the same principle. If the impact of the non-linear interaction is ignored, since neap tidal range is about half of the spring tidal range, the magnitude of neap tidal currents in Southampton Water is about half of spring tidal currents.

Shallow water components (e.g. M4, M6), which result from the nonlinear interaction between the tidal wave and bottom friction, limited water depth and local bathymetry, will distort the tide and tidal current and add to cause a deviation from the linear relation. The proportion of the non-linear components of the tidal and tidal current will increase with the increase of tidal range in a non-linear way. So during the spring tide the phenomena such as 'double high tide', 'young flood stand' and 'long flood time' will be more significant than neap tide, while these nonlinear phenomena are almost unnoticed during the neap tide.

5.5 Numerical experiments

Residual currents are very important in water mass exchange and water mass transportation in estuaries and coastal seas. Before considering the estuarine circulation due to fresh water discharge, the tidal induced residual currents, water mass transportation and water exchange through the entrance of the estuary will be examined. In this numerical experiment the M_2 tide is chosen to represent the average tide, while the vertical structure is ignored.

5.5.1 Tidal induced residual current and tidal flux

In a tidally dominated estuarine system, the current is normally measured using equipment on a fixed mooring and the conventional residual current (Eulerian residual) is the time average of current measured over a certain time interval. The Eulerian residual may represent the water mass transport in the open sea but is not suitable for an estuarine system

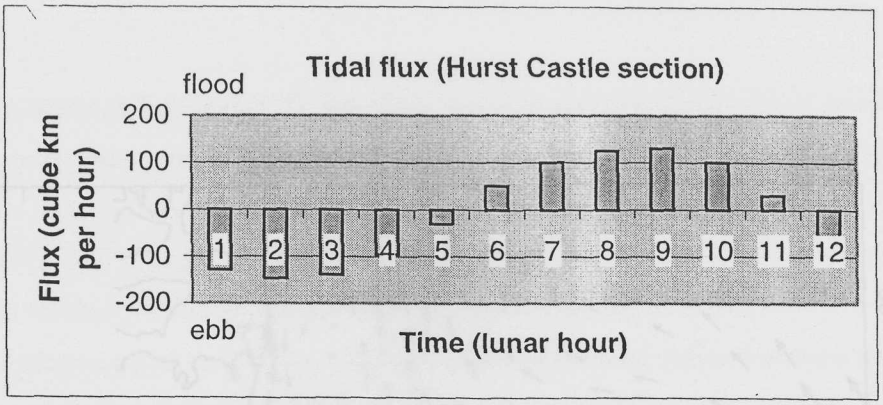

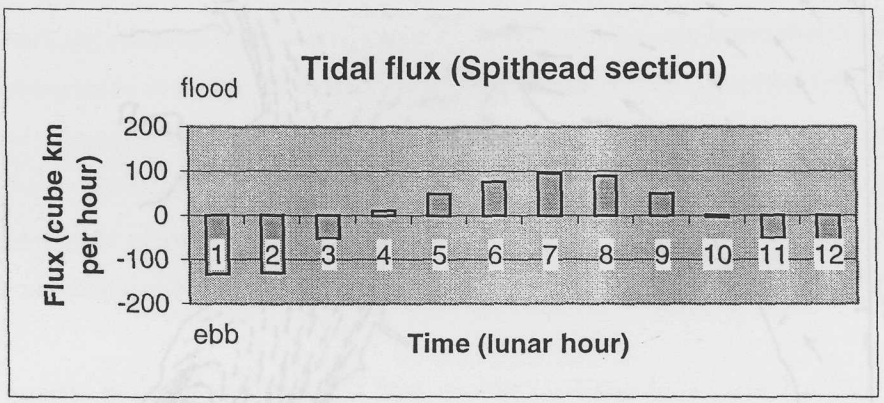

Figure 5.8 Tidal flux through sections across the west Solent at Hurst Castle and east Solent at Spithead

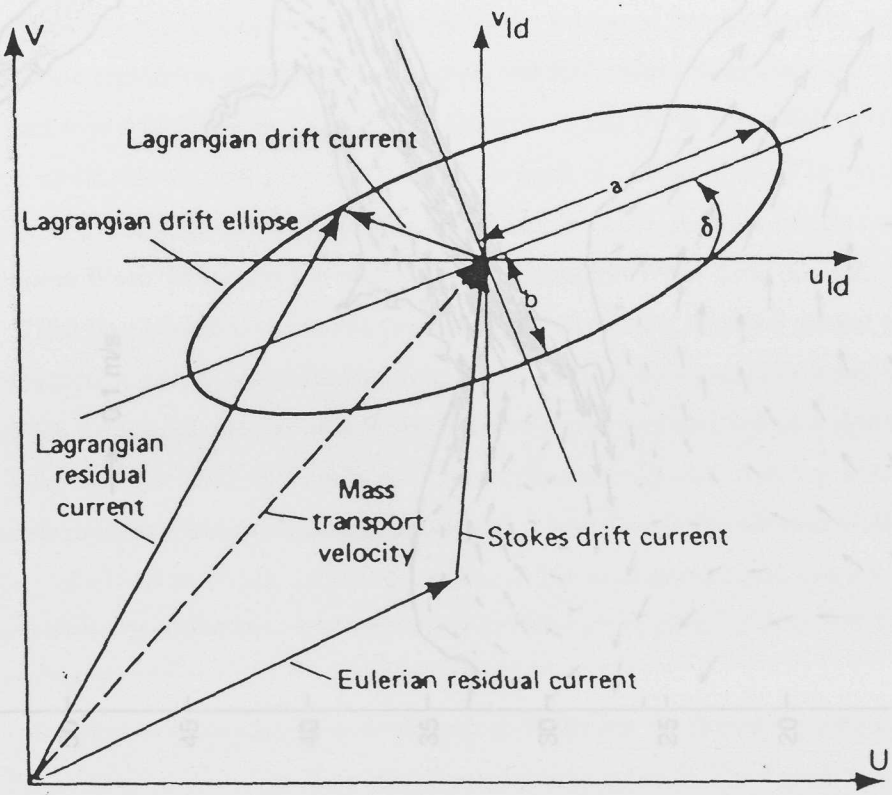

Figure 5.6 The Schematic diagram of the interrelation between the Eulerian residual current, the Stokes drift, the mass transport velocity (mean Lagrangian residual), the Lagrangian drift, and the Lagrangian residual current (from Chen et al., 1986)

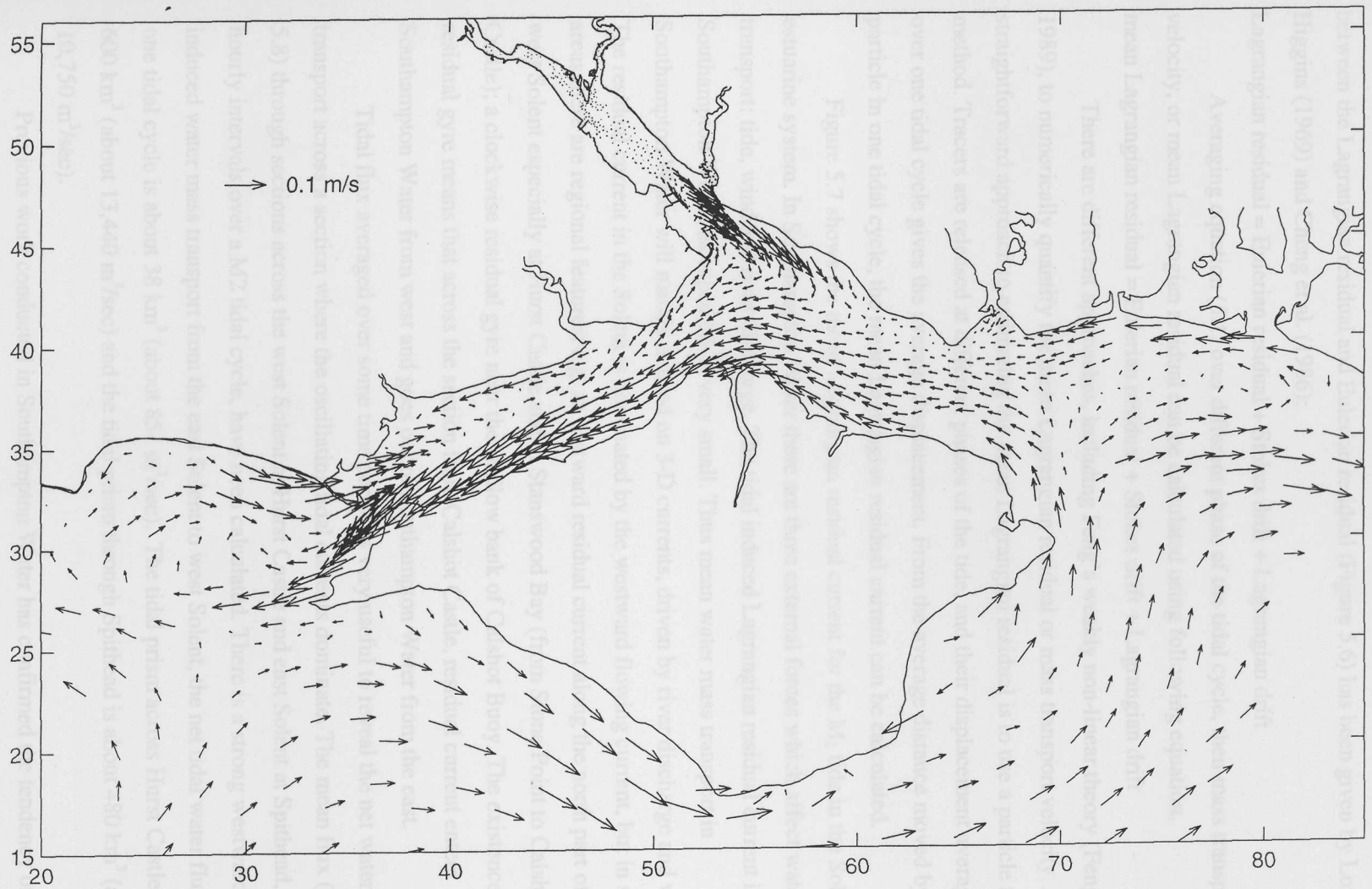

Figure 5.7 M_2 tidal induced mean Lagrangian residual current in the Solent estuarine system

which has a complex bathymetry. To determine actual water mass transport it is necessary to follow the water mass over a complete tidal cycle (Lagrangian residual). The relationship between the Lagrangian residual and Eulerian residual (Figure 5.6) has been given by Longuet-Higgins (1969) and Cheng et al. (1986):

Lagrangian residual = Eulerian residual + Stokes drift + Lagrangian drift (5.1)

Averaging equation (5.1) over different phase of the tidal cycle, then mass transport velocity, or mean Lagrangian residual can be calculated using following equation,

mean Lagrangian residual = Eulerian residual + Stokes drift + Lagrangian drift (5.2)

There are different approaches, including Feng's weakly non-linear theory (Feng, 1989), to numerically quantify the mean Lagrangian residual or mass transport velocity. A straightforward approach to estimating the mean Lagrangian residual is to use a particle tracking method. Tracers are released at different phases of the tide, and their displacement averaged over one tidal cycle gives the average displacement. From the average distance moved by a particle in one tidal cycle, the mean Lagrangian residual current can be calculated.

Figure 5.7 shows the mean Lagrangian residual current for the M_2 tide in the Solent estuarine system. In Southampton Water there are three external forces which affect water mass transport: tide, wind and river discharge. The tidal induced Lagrangian residual current in Southampton Water, as expected, is very small. Thus mean water mass transport in Southampton Water will mainly depend on 3-D currents, driven by river discharge and wind. The residual current in the Solent is dominated by the westward flowing current, but in some areas there are regional features; e.g. an eastward residual current along the north part of the west Solent especially at Hurst Castle and in Stanswood Bay (from Stone Point to Calshot Castle); a clockwise residual gyre near the shallow bank of Calshot Buoy. The existence of this residual gyre means that across the section from Calshot Castle, residual current enters Southampton Water from west and goes out of Southampton Water from the east.

Tidal flux averaged over some time period is very useful to reveal the net water transport across a section where the oscillating tidal currents dominate. The mean flux (Figure 5.8) through sections across the west Solent at Hurst Castle and east Solent at Spithead, at hourly intervals over a M2 tidal cycle, have been calculated. There is a strong westward tidal induced water mass transport from the east Solent to west Solent, the net tidal water flux over one tidal cycle is about 38 km^3 (about 851 m^3/sec). The tidal prism across Hurst Castle is about 600 km^3 (about 13,440 m^3/sec) and the tidal prism through Spithead is about 480 km^3 (about 10,750 m^3/sec).

Previous work conducted in Southampton Water has confirmed the tendency of net water mass transport, although there are differences in magnitude. Flow conditions in the west Solent have been investigated by Dyer and King (1975), and Blain (1980). Dyer and King (1975) confirm that there is a tendency of east to west residual flow in the west Solent. Blain

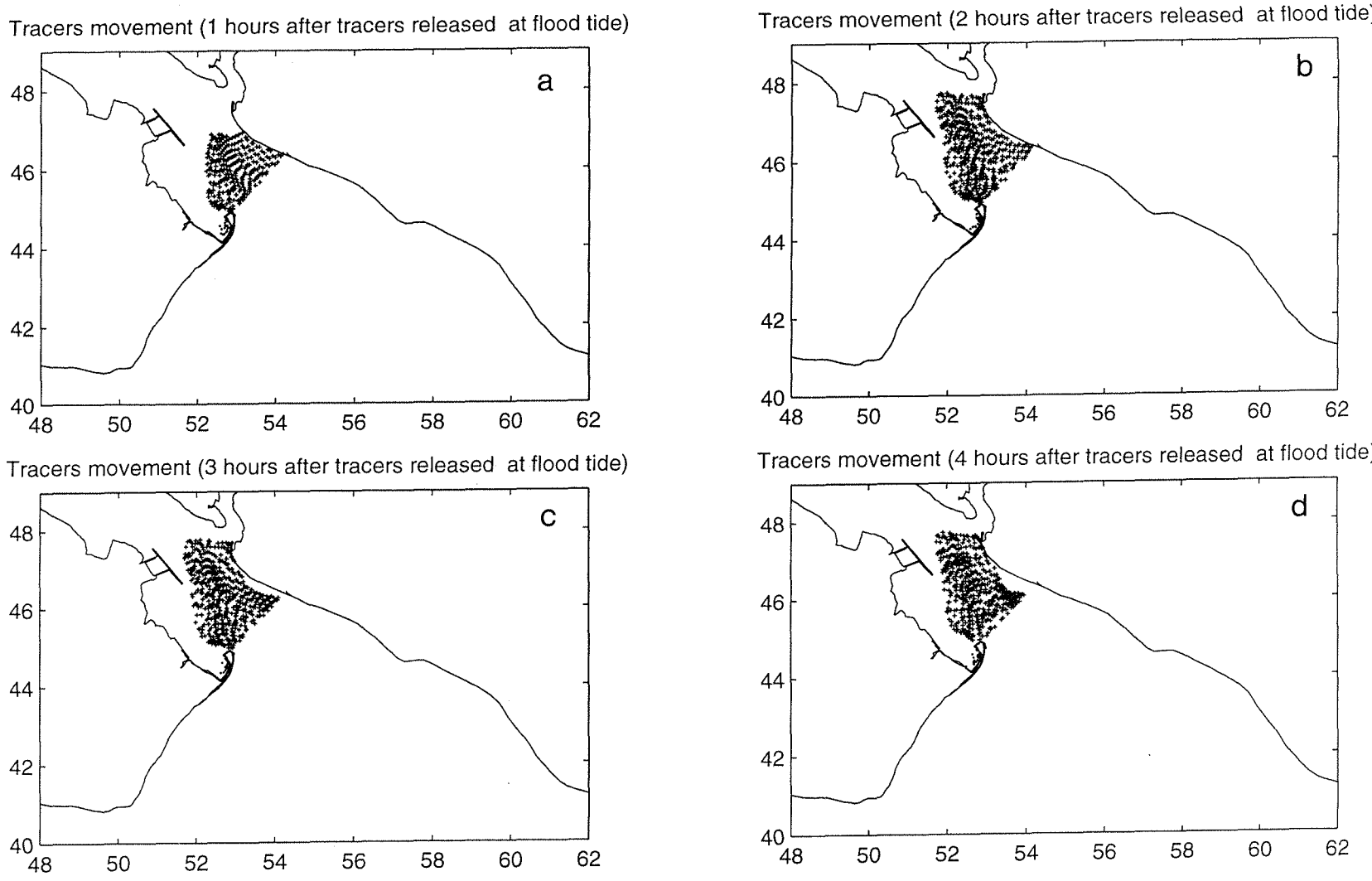

Figure 5.9 Water exchange between Southampton Water and the Solent through a section across the estuary at Calshot castle. All tracers are released at mid-flood tide; + represents the water mass from the Solent entering Southampton Water; • shows the water mass originated from Southampton Water entering the Solent

Tracers movement (5 hours after tracers released at flood tide)

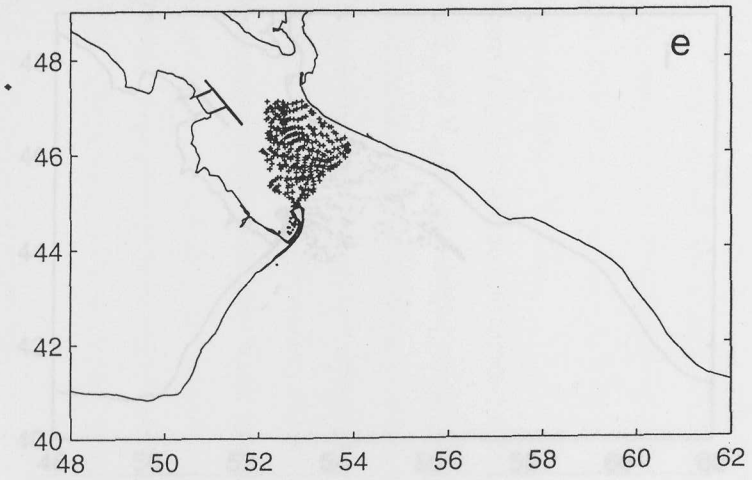

Tracers movement (6 hours after tracers released at flood tide)

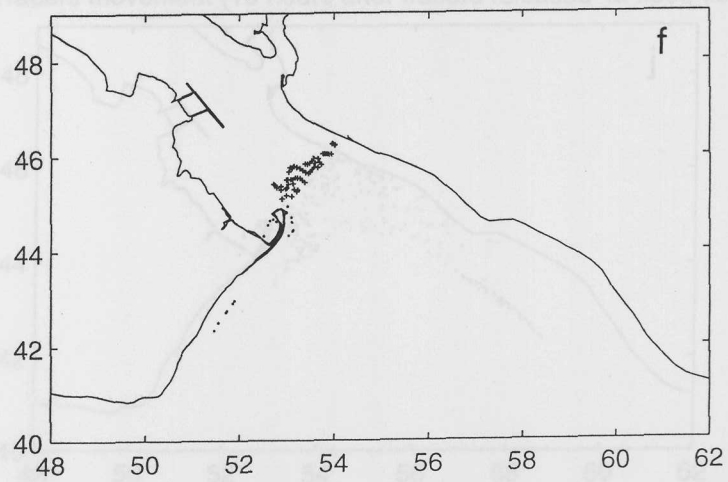

Tracers movement (7 hours after tracers released at flood tide)

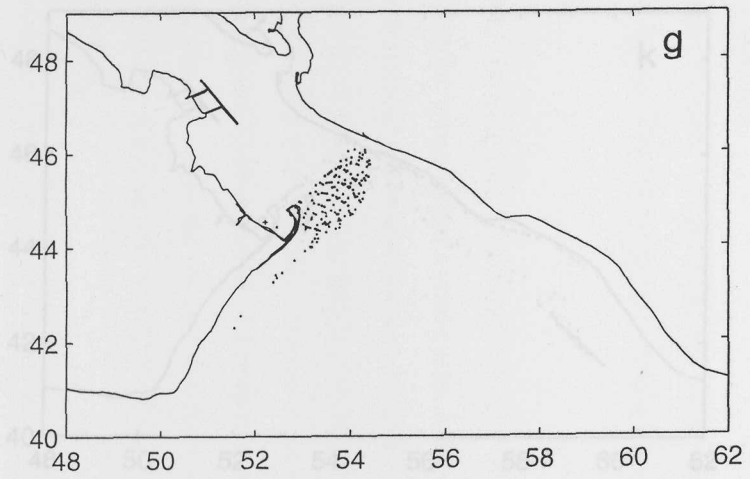

Tracers movement (8 hours after tracers released at flood tide)

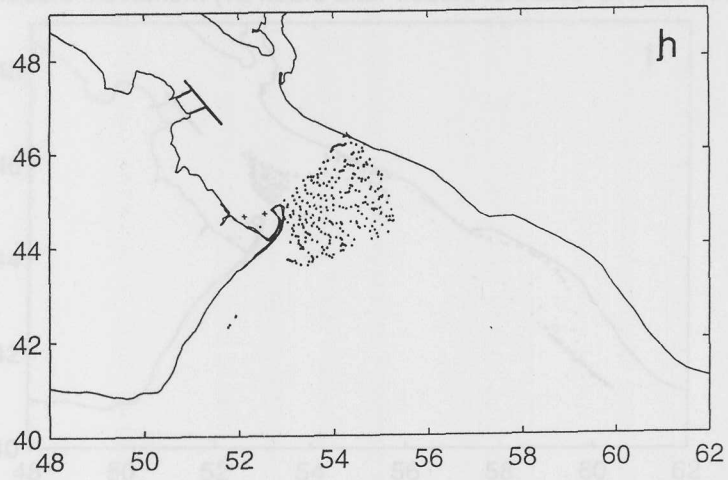

Tracers movement (9 hours after tracers released at flood tide)

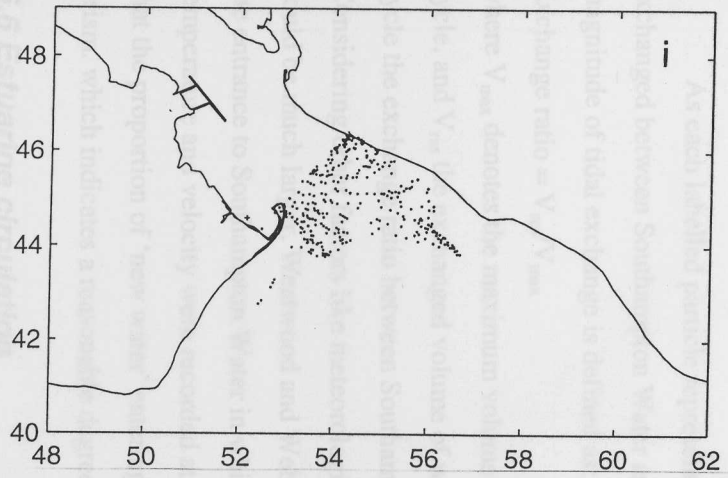

Tracers movement (10 hours after tracers released at flood tide)

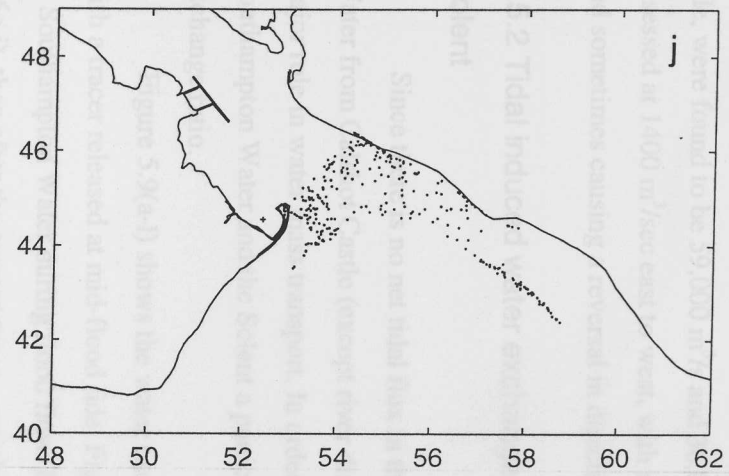

Tracers movement (11 hours after tracers released at flood tide)

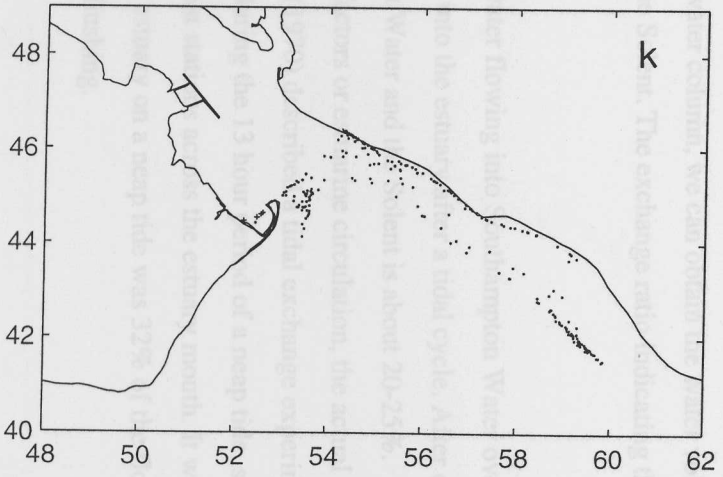

Tracers movement (12 hours after tracers released at flood tide)

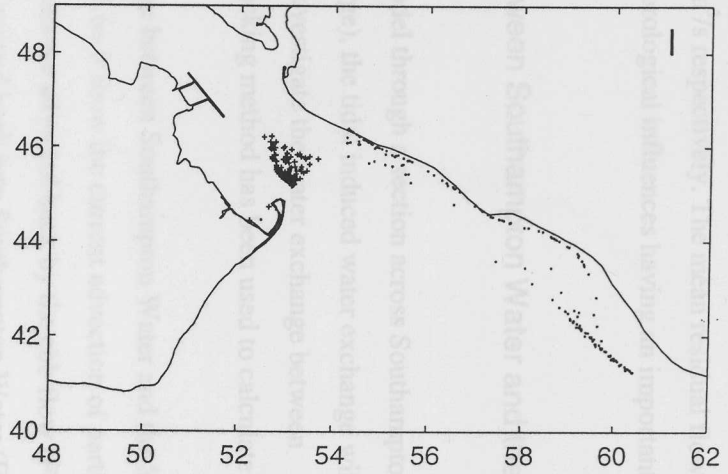

(1980) has recorded the tidal levels at six stations between Calshot and Totland for a minimum period of one year. The maximum ebb and flood flows at Hurst Narrows, during a typical spring tide, were found to be 59,000 m^3/s and 36,000 m^3/s respectively. The mean residual flow was assessed at 1400 m^3/sec east to west, with meteorological influences having an important effect and sometimes causing a reversal in direction.

5.5.2 Tidal induced water exchange between Southampton Water and the Solent

Since there is no net tidal flux in the model through a section across Southampton Water from Calshot Castle (except river discharge), the tidal induced water exchange will play a major role in water mass transport. In order to investigate the water exchange between Southampton Water and the Solent a particle tracking method has been used to calculate the exchange ratio.

Figure 5.9(a-l) shows the water exchange between Southampton Water and the Solent with a tracer released at mid-flood tide. Figure 5.6a-b show the current advection of particles in to Southampton Water during flood flow. Particles are advected back by the ebb flow (Figure 5.6c-i), then after the current turns, particles are moved back into Southampton Water (Figure 5.6j-k). Following one tidal cycle (Figure 5.6l), some water mass is advected out of Southampton Water by the Lagrangian residual current along the north coast and some water mass intrudes into Southampton Water along Calshot Spit.

As each labelled particle represents a water column, we can obtain the water volume exchanged between Southampton Water and the Solent. The exchange ratio indicating the magnitude of tidal exchange is defined as:

$$\text{Exchange ratio} = V_{res}/V_{max} \qquad (5.3)$$

where V_{max} denotes the maximum volume of water flowing into Southampton Water over a tidal cycle, and V_{res} the exchanged volume of water into the estuary after a tidal cycle. After one tidal cycle the exchange ratio between Southampton Water and the Solent is about 20-25%. Considering other factors like meteorological factors or estuarine circulation, the actual figure could be much larger. Westwood and Webber (1970) described a tidal exchange experiment at the entrance to Southampton Water in which, during the 13 hour period of a neap tide, salinity, temperature and velocity were recorded at 6 boat stations across the estuary mouth. It was found that the proportion of 'new water' entering the estuary on a neap tide was 32% of the flood tidal prism. which indicates a reasonable degree of flushing.

5.6 Estuarine circulation

From the above analysis there is no apparent M_2 tidal (representing the mean tide) induced residual current in Southampton Water. The main water mass transport and water mass

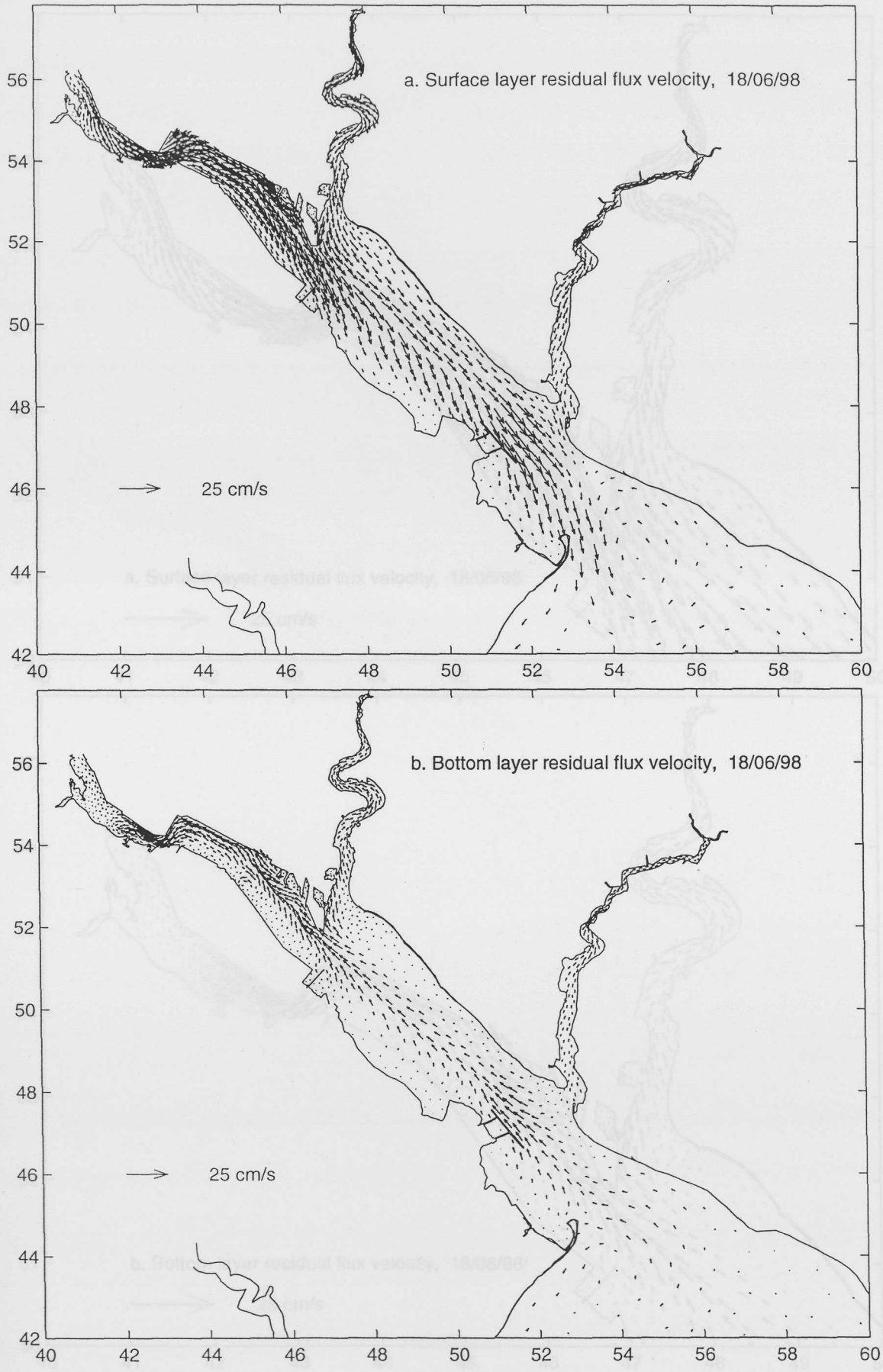

Figure 5.10 Surface and bottom layer residual flux velocity from 3-D model in Southampton Water, 18/06/98

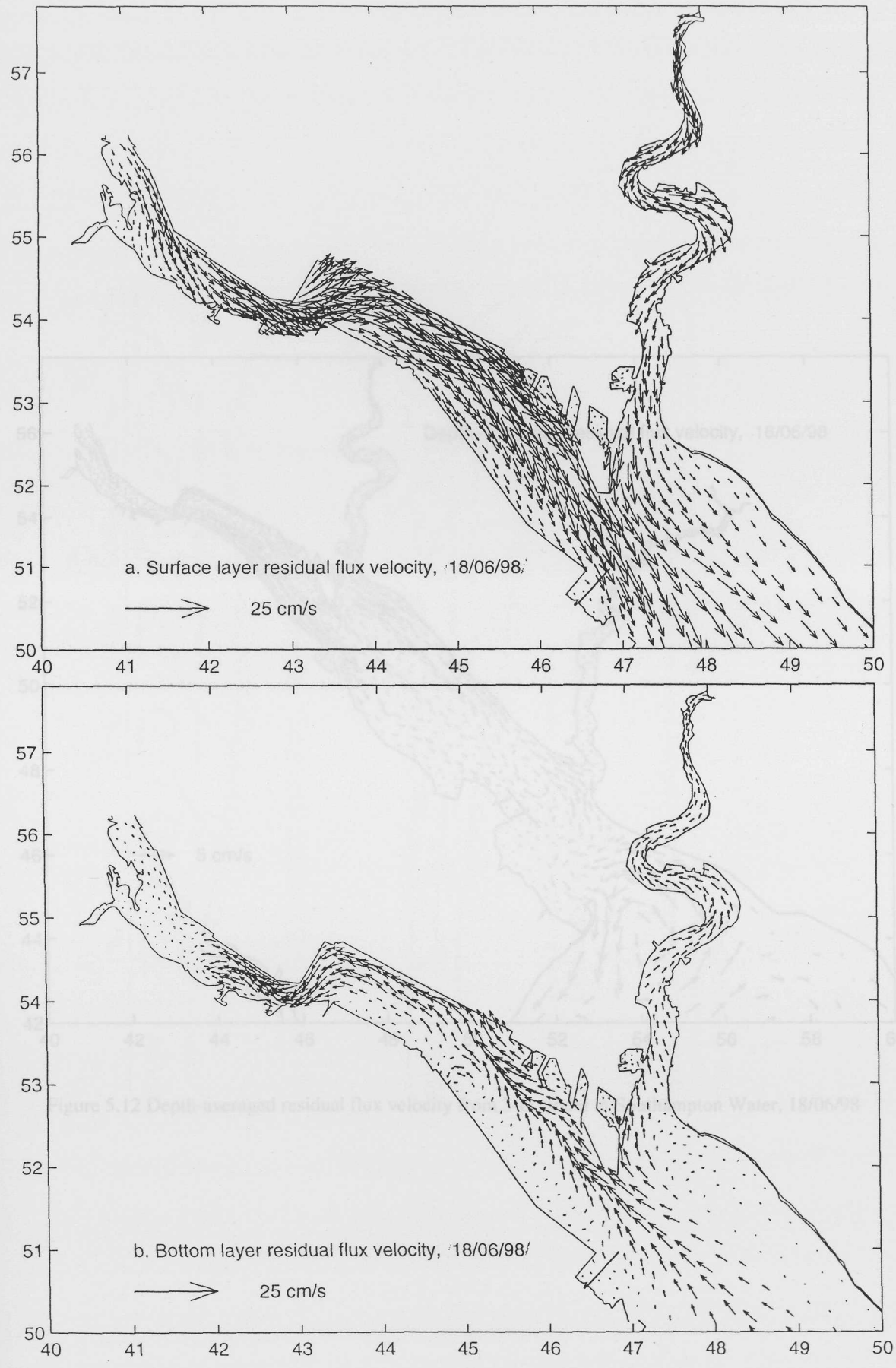

Figure 5.11 Surface and bottom layer residual flux velocity from 3-D model in the Test Estuary and the Itchen Estuary. 18/06/98

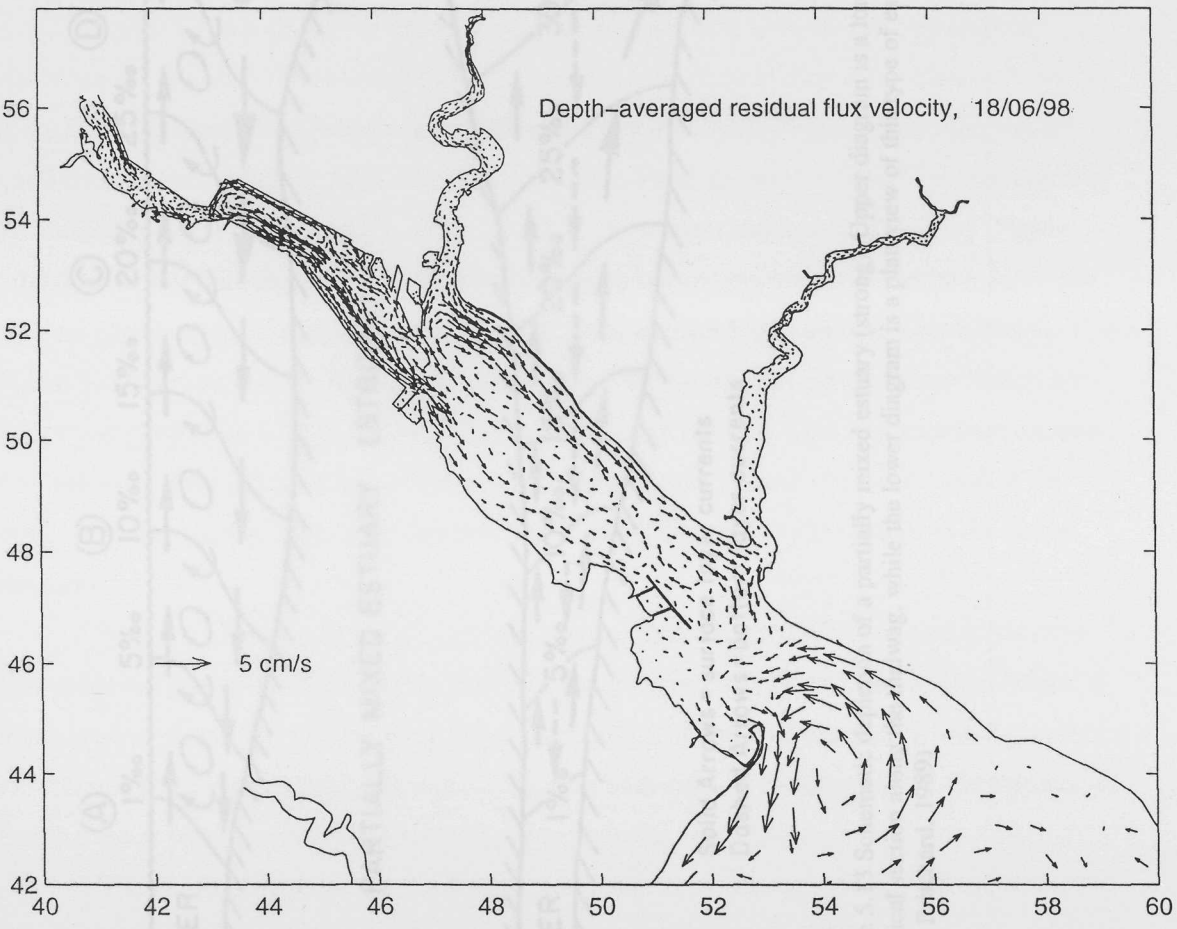

Figure 5.12 Depth-averaged residual flux velocity from 3-D model in Southampton Water, 18/06/98

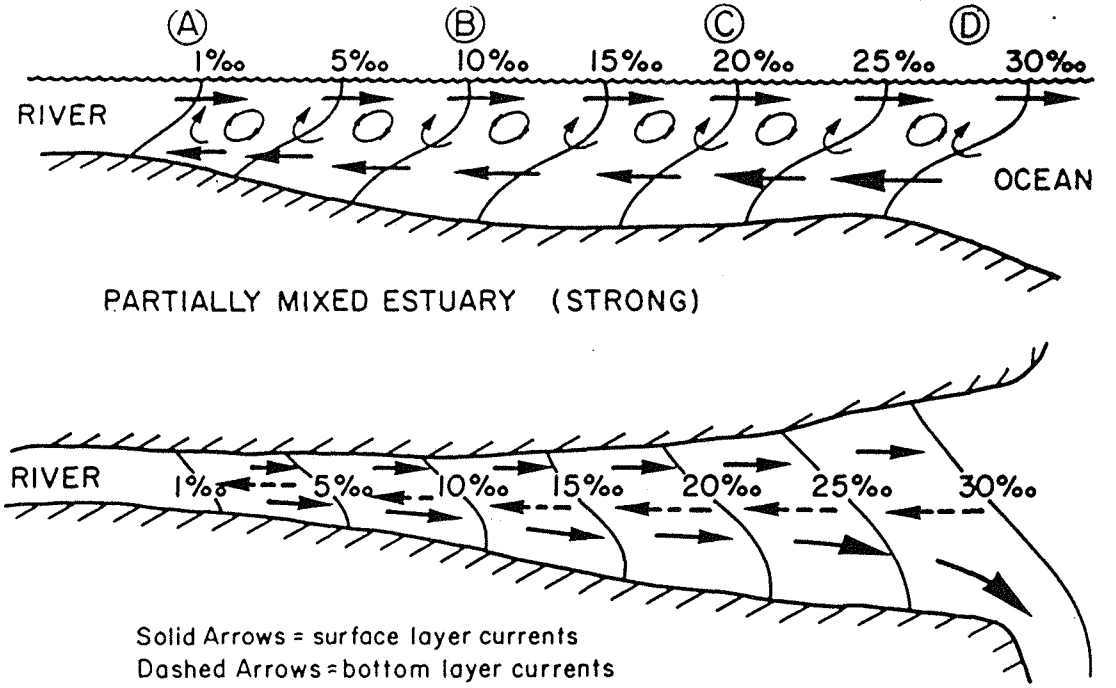

Figure 5.13 Schematic depiction of a partially mixed estuary (strong). Upper diagram is a longitudinal – vertical section along the thalwag, while the lower diagram is a plan view of this type of estuary (from Pritchard, 1989)

exchange in Southampton Water therefore will rely on estuarine circulation, driven by the surface slope of the fresh water discharge and the baroclinic effect of the density gradient. To define the residual flux velocity V_{rfv}:

defining operator: $<*>= \int_{t}^{t+t_0} *dt$ represents a time average over time period $[t, t+t_0]$.

$$V_{rfv}=\frac{<H(u_k, v_k)>}{<H>}, \tag{5.4}$$

where H is the water depth, and (u_k, v_k) is the velocity of layer k.

Figure 5.10a-b shows the modelled surface residual flux velocity in Southampton Water, on 18-19, June 1998 averaged over 25 hours. The surface fresher water clearly flows out of the Itchen Estuary, Test Estuary and Hamble Estuary into Southampton Water, the surface water then meets the Solent, with a tendency to drift towards the west Solent. The magnitude of the surface residual flux velocity is about 10 cm/s. The bottom residual flux velocity (Figure 5.10b) is smaller than the surface, with its direction upstream opposite to the surface flow. The residual current is mainly in the deep channel of Southampton Water and the Test Estuary. Figure 5.10b shows that on the shallow bank of the Test Estuary and Southampton Water, no saltier water intrusion occurs. Figure 5.11a-b gives a more detailed view of the surface residual flux velocity in the Itchen and Test Estuary. The bottom saltier water stops at the end of the dredged channel in the upper Test Estuary. The residual flux velocity is smaller in the Itchen Estuary.

Figure 5.12 shows the depth averaged residual flux velocity. There is a constant river flow from the end of the River Itchen, River Test and River Hamble. In Southampton Water, a depth-averaged residual flux flows up stream from the deep dredged channel, while the water flow is out of the estuary from the shallow bank on both sides of the channel. At the entrance to Southampton Water, residual flows are likely to go to the west Solent.

The characteristics of the residual in Southampton Water agree well with the schematic depiction of a partially mixed estuary (Figure 5.13) from Pritchard (1989).

5.7 Comparison of currents measurement and model results

A 25 hours survey was conducted at Hound Buoy, Southampton Water on 18-19/06/98. The current and salinity data have been kindly provided by Dr Jonathan Sharples. Figure 5.14a is the comparison of ATT tidal prediction (solid line) and modelled tidal elevation (dash line) at Dockhead over this time period. The standard deviation of the error (dot dash line) is 18.76 cm, providing the tidal range of 2.7831 m, the ratio of standard variation to tidal range is 0.0674.

Figure 5.14b is the observed tidal elevation, analysed tidal elevation and modelled tidal elevation at Hound Buoy on 18-19 June 1998. The measured tidal elevation has a strong

Figure 5.14a Comparison of predicted tidal elevation with computed tidal elevation (3D 9–layer model output) at Dockhead

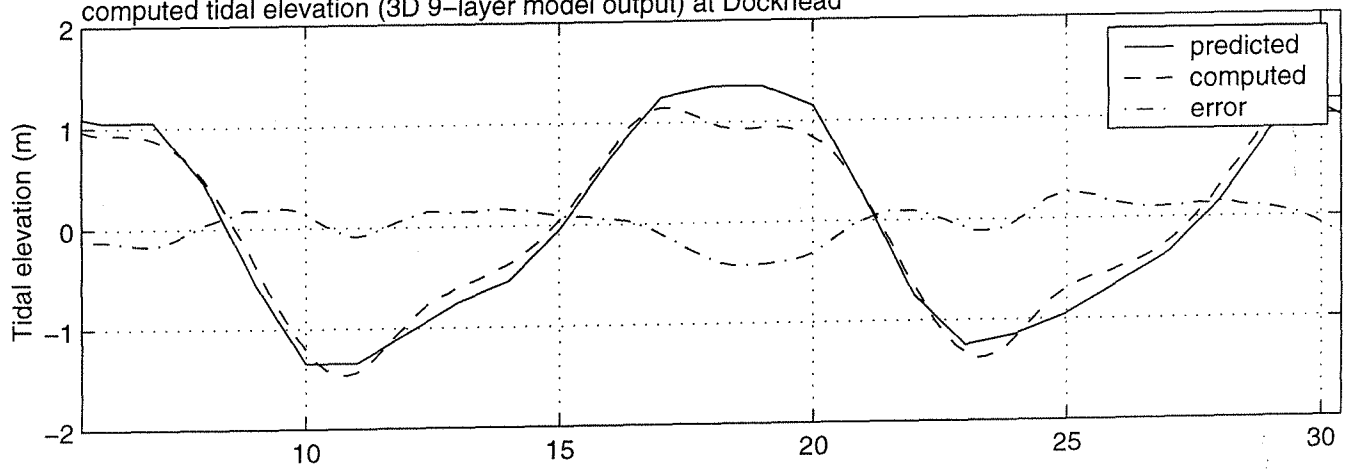

Figure 5.14b Comparison of ADCP observed tidal elevation with analysed, computed tidal elevation (3D 9–layer model output) at Hound Buoy

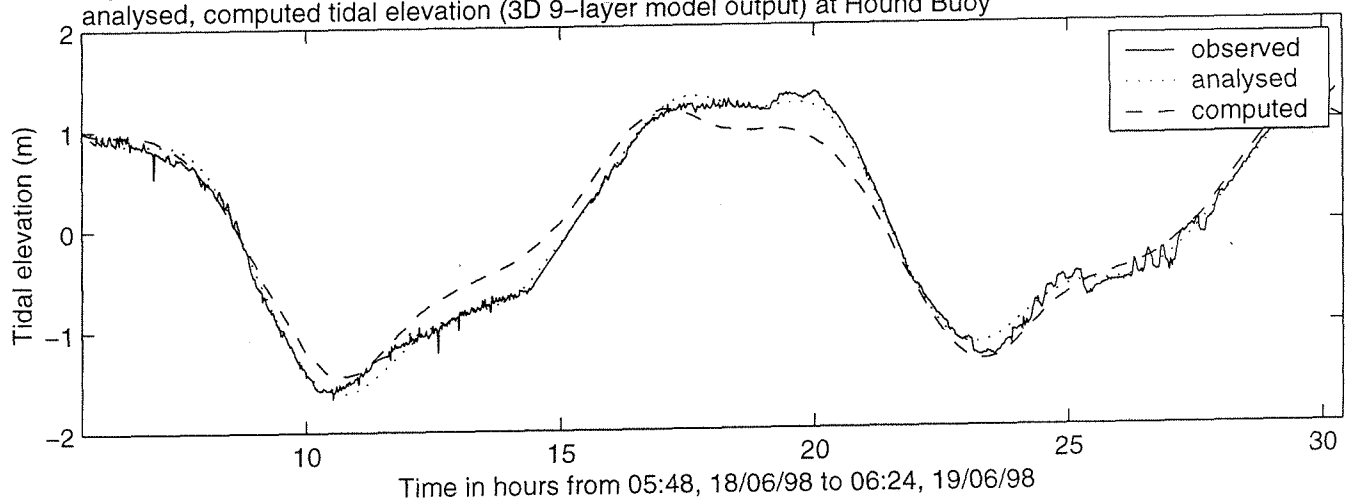

Figure 5.15a Depth–averaged longitudinal tidal current (observed) at Hound Buoy

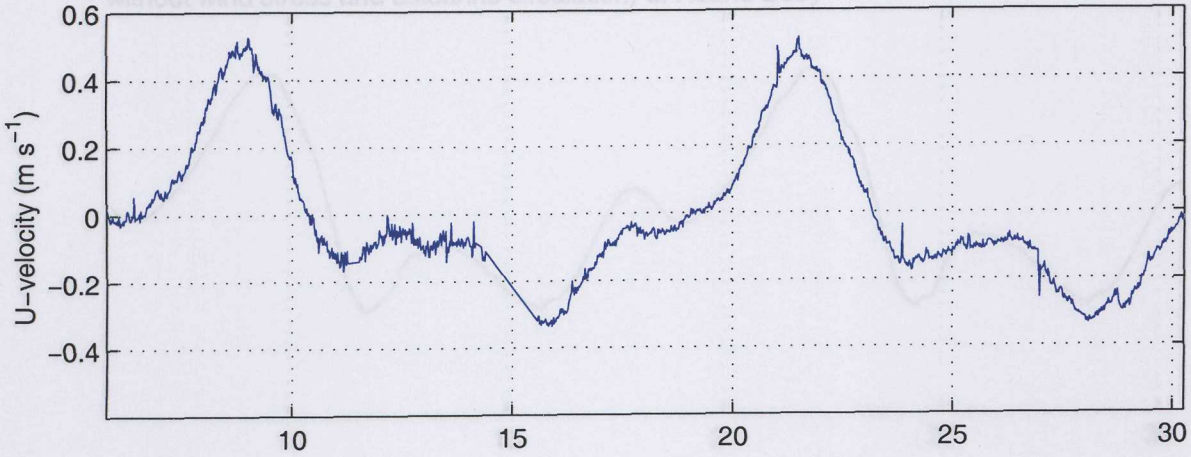

Figure 5.15b Longitudinal tidal current (observed) at Hound Buoy

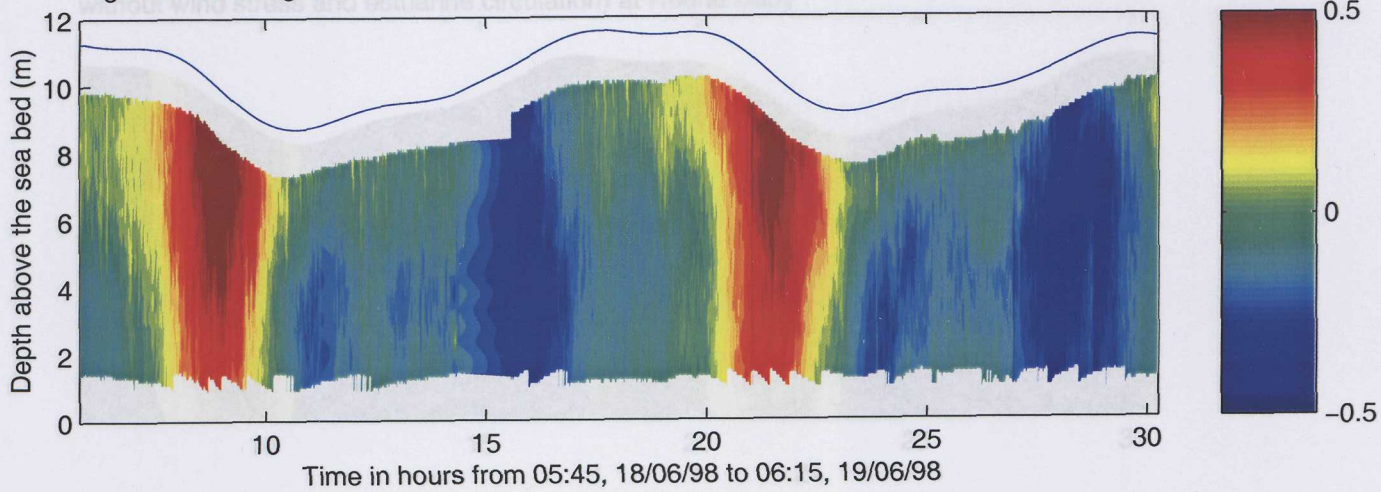

Figure 5.16a Depth–averaged longitudinal tidal current (9–layer model output, without wind stress and estuarine circulation) at Hound Buoy

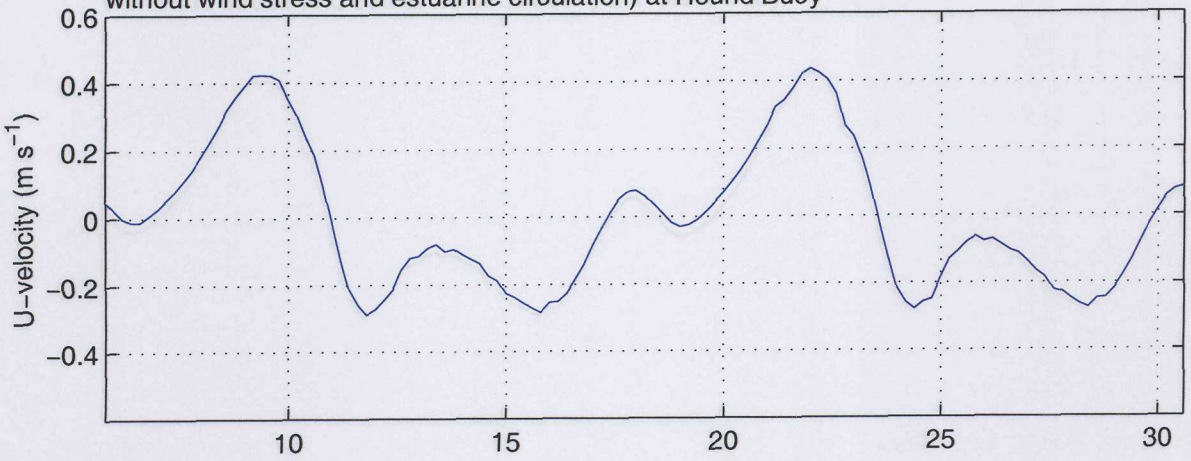

Figure 5.16b Longitudinal tidal current (9–layer model output, without wind stress and estuarine circulation) at Hound Buoy

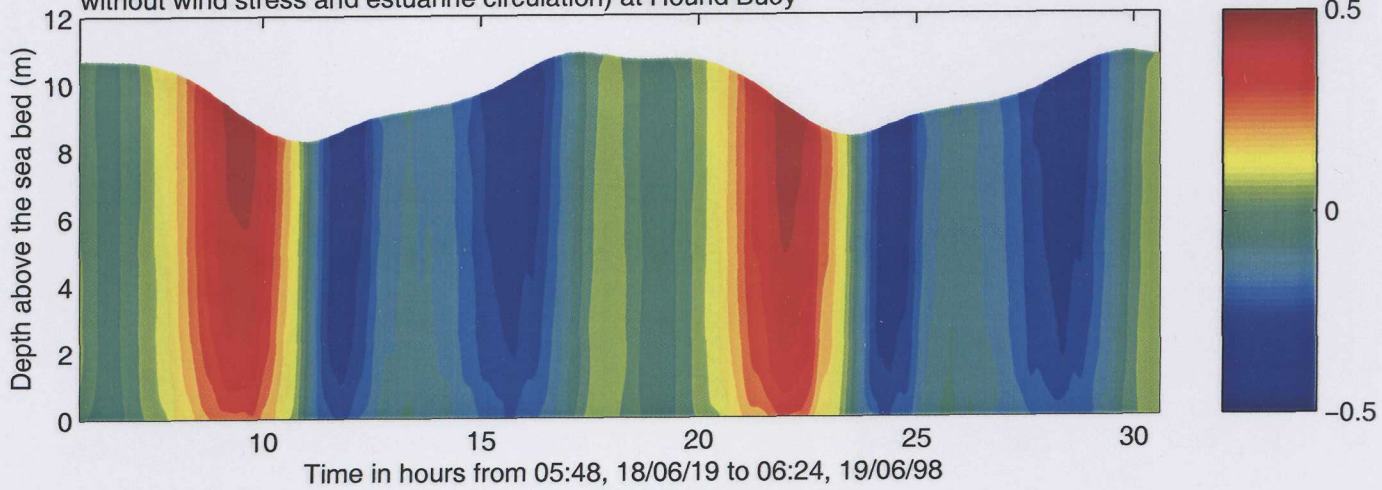

Figure 5.17a Depth–averaged longitudinal tidal current (9–layer model output, with wind stress and estuarine circulation) at Hound Buoy

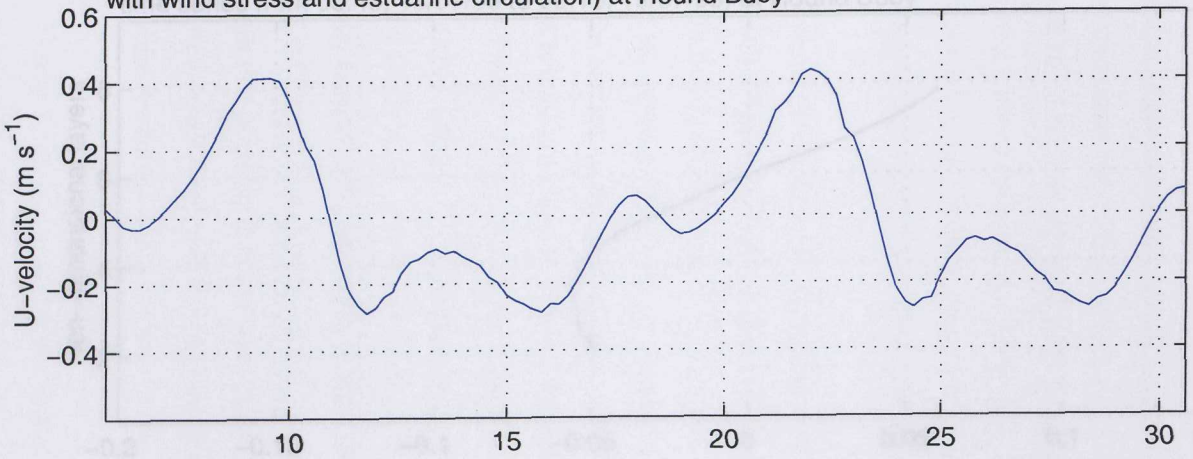

Figure 5.17b Longitudinal tidal current (9–layer model output, with wind stress and estuarine circulation) at Hound Buoy

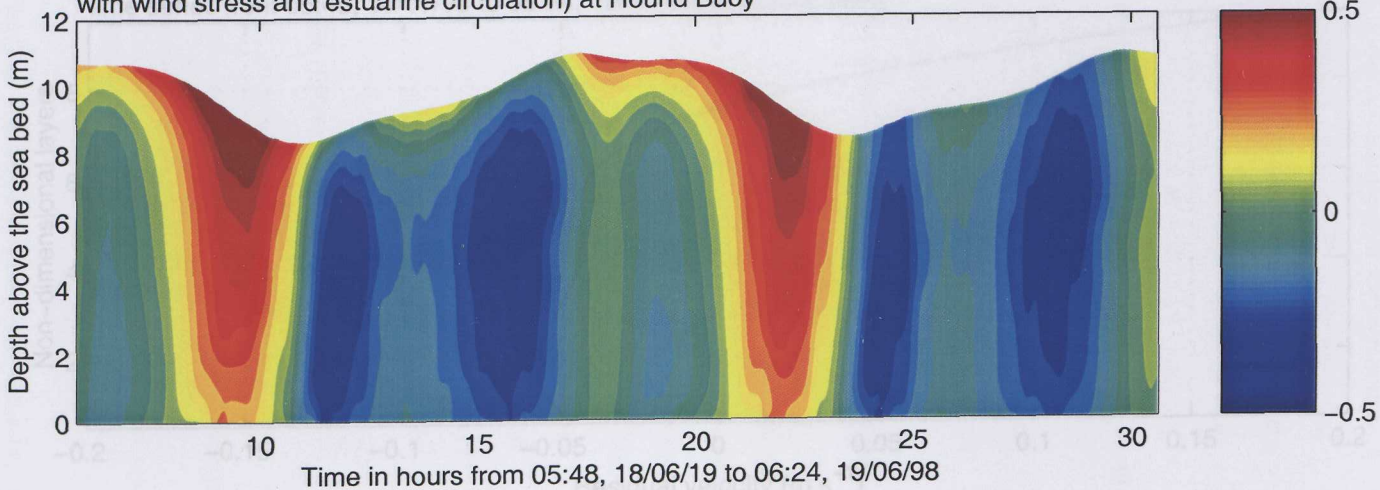

Figure 5.18a Vertical profile of longitudinal residual flux velocity (observed, time series from 05:45, 18/07/98 to 06:15, 19/07/98) at Hound Buoy

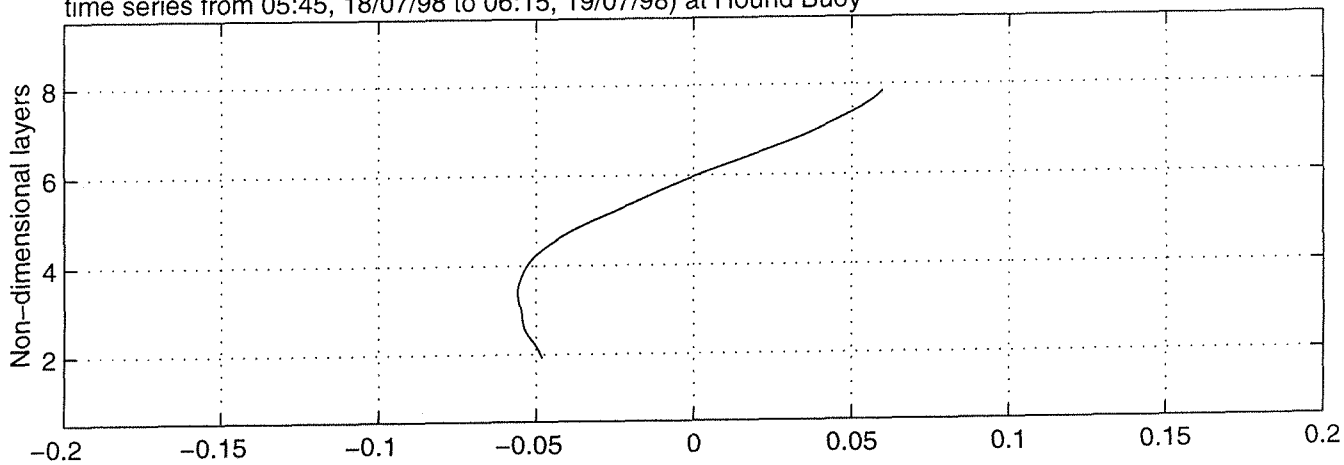

Figure 5.18b Vertical profile of longitudinal residual flux velocity (9–layer model output, time series from 05:48, 18/07/98 to 06:24, 19/07/98) at Hound Buoy

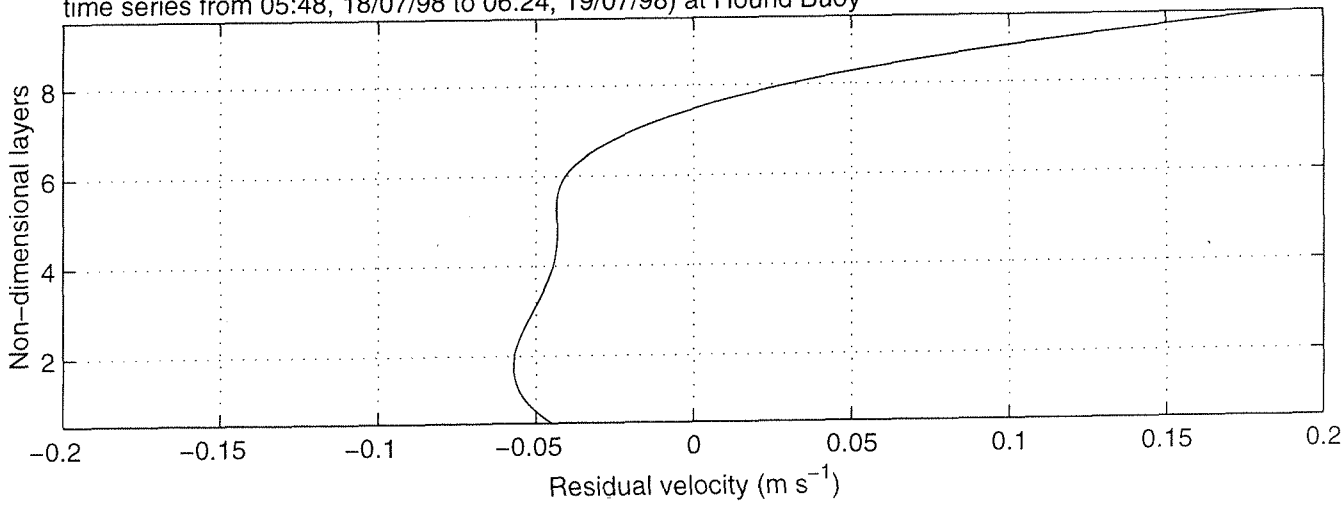

irregular noise. The tidal analysis uses three constituents M2, M4 and M6, because the tides are dominated by the semi-diurnal tide (mainly M2) and characterised by the shallow water component (represented by M4 and M6). The modelled tidal elevation over pronounces the 'young flood stand' during the flood, and the second high tide is smaller than the observed result. To look at the detail of the vertical profile of the currents, Figure 5.15 is the observed longitude currents (from ADCP) along the direction of the main channel. The flood tide lasts longer than the ebb tide, so the magnitude of the flood tide (30 cm s^{-1}, in depth average, and maximum is 40 cm s^{-1}) is smaller than the ebb tide (43 cm s^{-1} average and 60 cm s^{-1} maximum). The position of the maximum velocity is different within the water column during the flood and ebb. The maximum ebb current occurred at the surface of the water column, while the maximum flood current occurred in the middle of water column. Figure 5.16 is the modelled tidal current without the estuarine circulation. From the vertical current profile, the maximum velocity always occurs at the surface, with some shear stress throughout the water column. There is no surface wind stress, only stress caused by bottom friction of the tidal currents, and acting in a direction opposite to that of the tidal currents. When the effect of surface slope and the baroclinic effect of the density gradient due to fresh water discharge is take into account, the model result (Figure 5.17) reveals the main features of the current in a partially-mixed estuary. Maximum flood current occurs in the middle of the water column and the maximum ebb current occurs at the surface. The depth averaged current agrees quite well with the observed one. The time of the maximum flood however is different, as previously mentioned, the first stage of flood tide is over pronounced, leaving the maximum flood to occur at the first stage of flood, while the longer lasting second flood stage has a weaker current. Both modelled (Figure 5.17) and observed (Figure 5.15) currents experienced different stage of one tidal cycle, from ebb-low water-first stage flood-'young flood stand'-second stage flood-'double high water'-ebb to next tidal cycle, although the magnitude of the currents may be different.

One feature is interesting but difficult to observe, occurs during the relatively long stable high tide period before the rapid drop of the ebb tide, when vertical momentum exchange coefficient is small. The pressure gradient allows the bottom denser salty water to move up stream while the fresher surface water moves down stream although the water level change is small.

Figure 5.18a-b is the modelled and observed vertical profile of residual flux velocity. The vertical profile of the residual flux velocity from field survey (Figure 5.18a) is quite similar to the analytic results from Prandle's (1986) and Wilson's (1988) work. The main difference between the modelled and observed is that the turning point of seaward residual and landward residual of the modelled is shallower than that of the observed residual flux velocity.

Figure 5.19 Tidal elevation (solid line) and tidal range (dash line) at Dockhead. Six different time periods when salinity distributions shown,
wet season: 1, neap tide; 2, mean tide; 3, spring tide,
dry season: 4, neap tide; 5, mean tide; 6, spring tide.

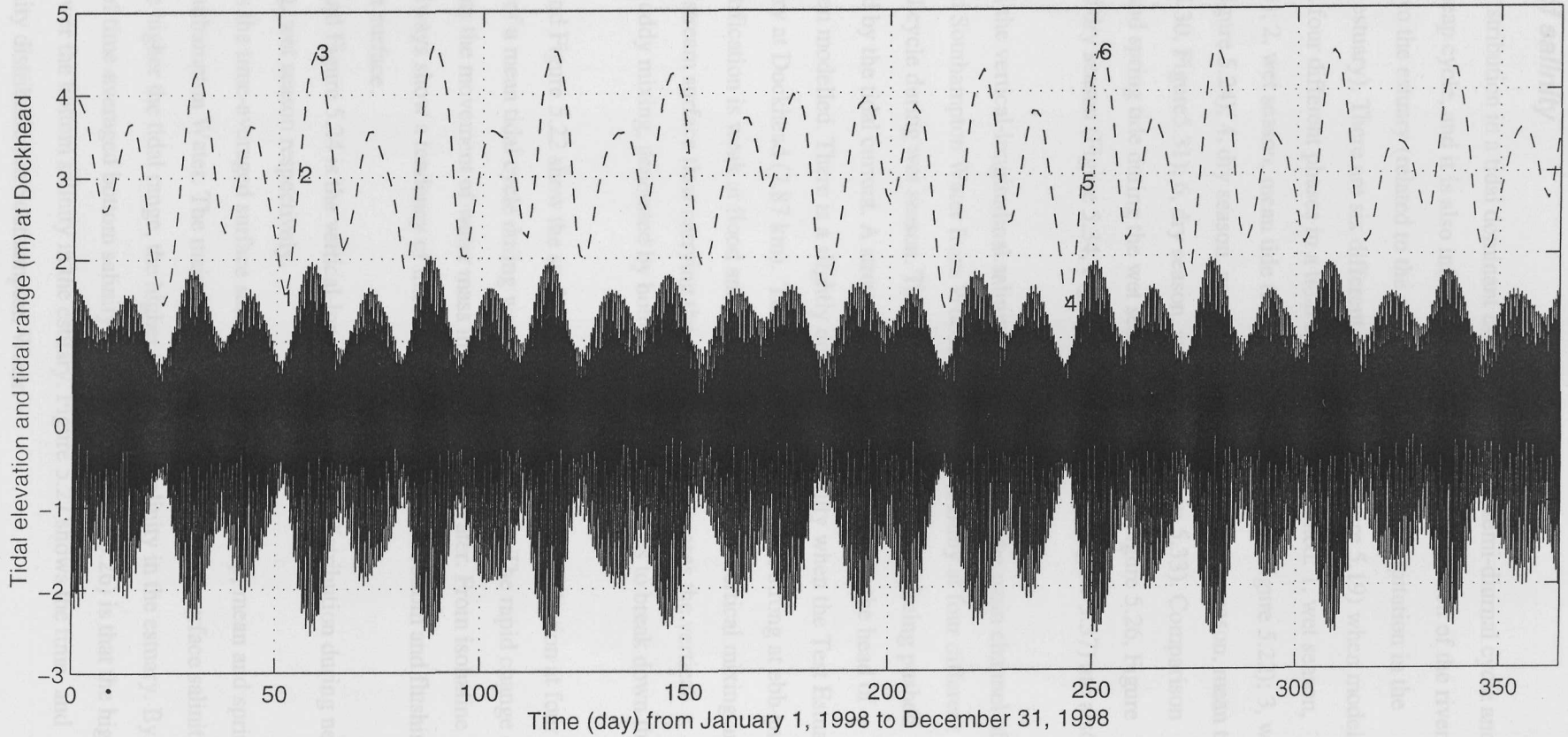

5.8 Distribution of salinity

The salinity distribution in a tidal dominant estuary has a clear semi-diurnal cycle and half-monthly spring-neap cycle, and it is also influenced by the seasonal variation of the riverine fresh water discharge to the estuary (related to the seasonal variation of precipitation in the catchment area of the estuary). There are six different time periods (Figure 5.19) when modelled salinity distribution at four different phases in a tidal cycle will be presented: 1, wet season, neap tide (Figure 5.23); 2, wet season, mean tide (Figure 5.20, Figure 5.21, Figure 5.22); 3, wet season, spring tide (Figure 5.24); 4, dry season, neap tide (Figure 5.32); 5, dry season, mean tide (Figure 5.29, Figure 5.30, Figure5.31); 6, dry season, spring tide (Figure 5.33). Comparison between neap, mean and spring tide during the wet season (Figure 5.25, Figure 5.26, Figure 5.27, Figure 5.28) and dry season (Figure 5.34, Figure 5.35, Figure 5.36, Figure 5.37) are also made.

Figure 5.20 is the vertical-longitudinal salinity distribution along the main channel of the Itchen Estuary and Southampton Water from Woodmill to Calshot Buoy at four different phases of a mean tidal cycle during wet season. The results show the isohaline being pushed forward and backward by the tidal current. A strong vertical stratification near the head of Itchen Estuary has been modelled. There is a slightly decrease of salinity when the Test Estuary joins the Itchen Estuary at Dockhead (7.87 km). The vertical stratification is strong at ebb and at low water, and stratification is weak at flood and at high water due to the vertical mixing and advection. The down stream surface flow carrying the fresher water increases the vertical gradient, and vertical eddy mixing, generated by bottom friction stress, tries to break down the vertical stratification.

Figure 5.21 and Figure 5.22 show the surface and bottom salinity distribution at four different tidal phases of a mean tidal cycle during wet season respectively. The rapid change of the isohaline represents the movement of water mass in Southampton Water. From isohaline distribution, results always show a tendency of intrusion of saltier water at bottom and flushing out of fresher water at surface.

Figure 5.23 and Figure 5.24 is the vertical-longitudinal salinity distribution during neap, wet season and spring, wet season respectively.

Figure 5.25 is the time-averaged surface salinity distribution for neap, mean and spring tidal conditions in Southampton Water. The main pattern of the time-averaged surface salinity distribution is that the higher the tidal range, the higher the surface salinity in the estuary. By contrast, the pattern of time-averaged bottom salinity distribution (Figure 5.26) is that the higher the tidal range, the lower the bottom salinity in the estuary. Figure 5.27 shows the time- and depth- averaged salinity distribution in Southampton Water.

Figure 5.20 Longitudinal salinity distribution along main channel of the Itchen Estuary and Southampton Water form Woodmill to Calshot Buoy during wet season

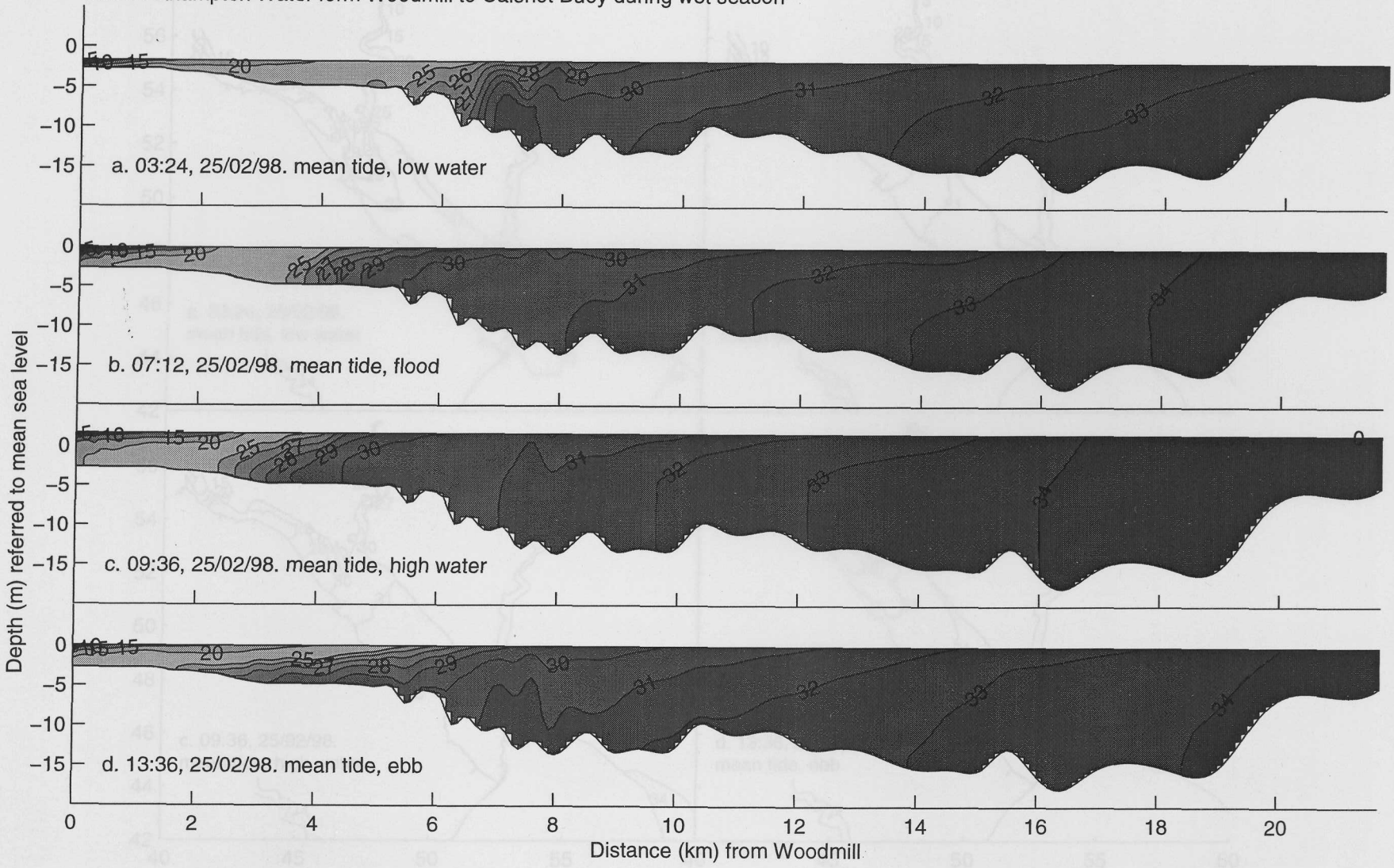

Figure 5.21 Surface salinity distribution (9–layer model output) in Southampton Water during wet season

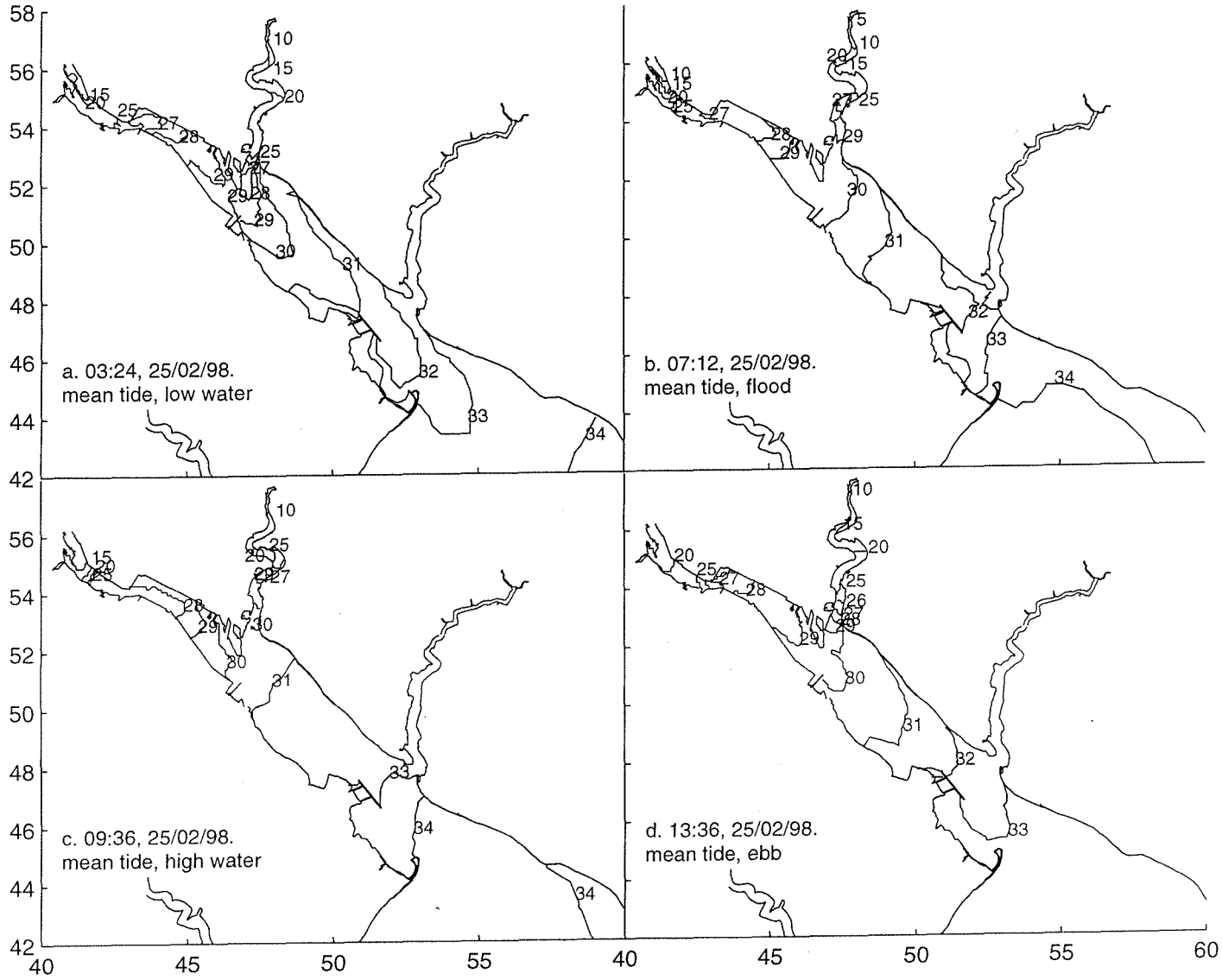

Figure 5.22 Bottom salinity distribution (9–layer model output) in Southampton Water during wet season

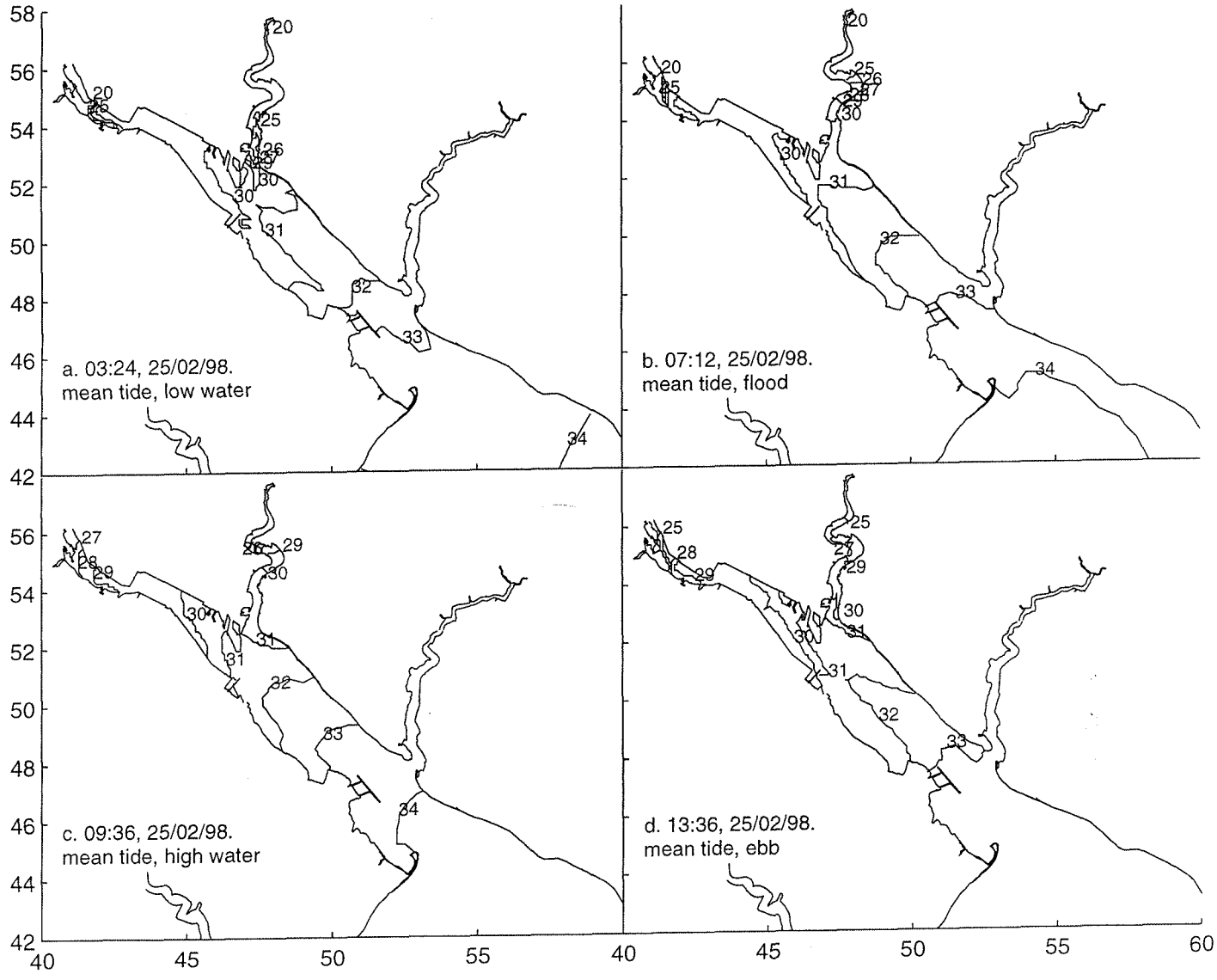

Figure 5.23 Longitudinal salinity distribution along main channel of the Itchen Estuary and Southampton Water form Woodmill to Calshot Buoy during wet season

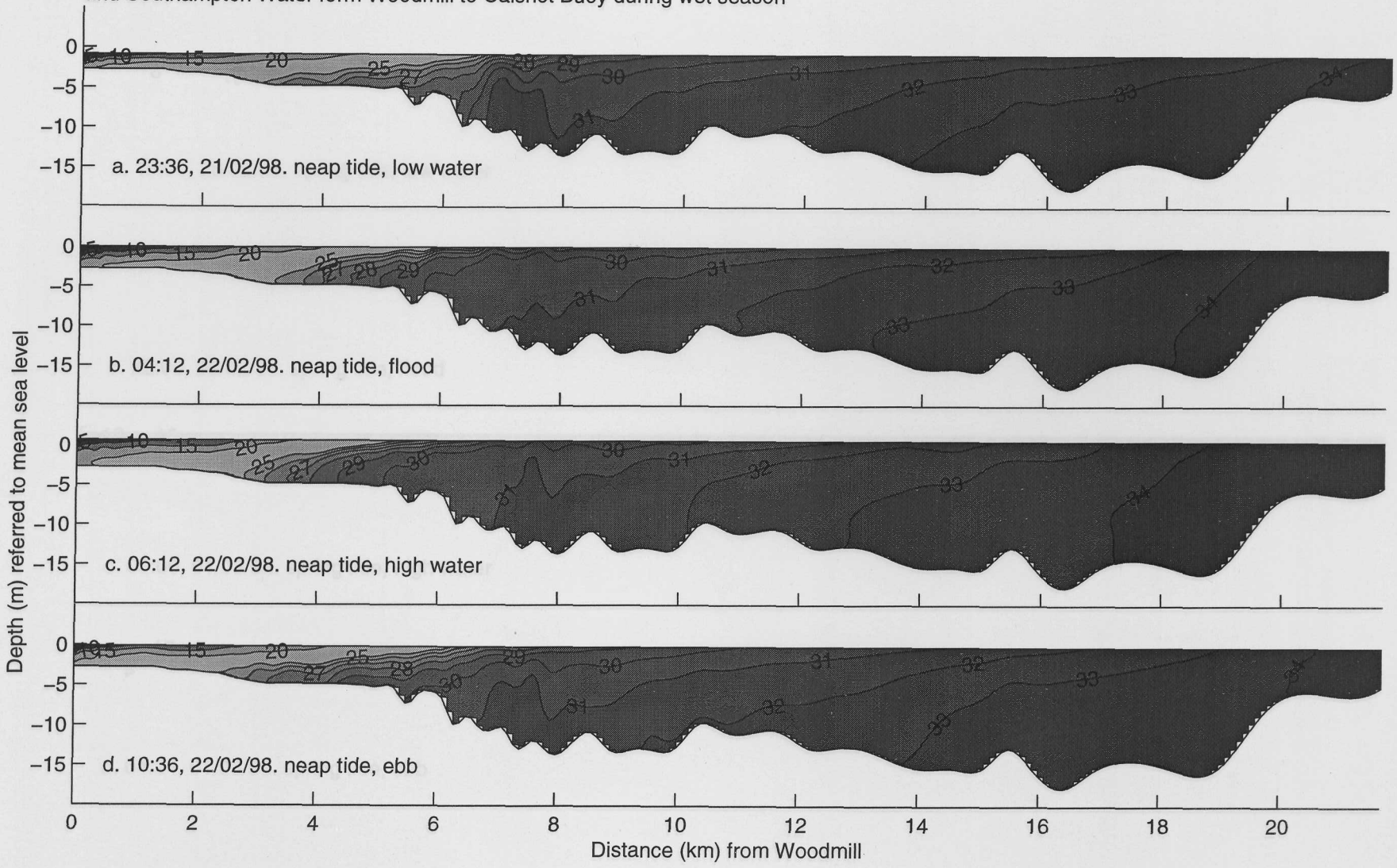

Figure 5.24 Longitudinal salinity distribution along main channel of the Itchen Estuary and Southampton Water form Woodmill to Calshot Buoy during wet season

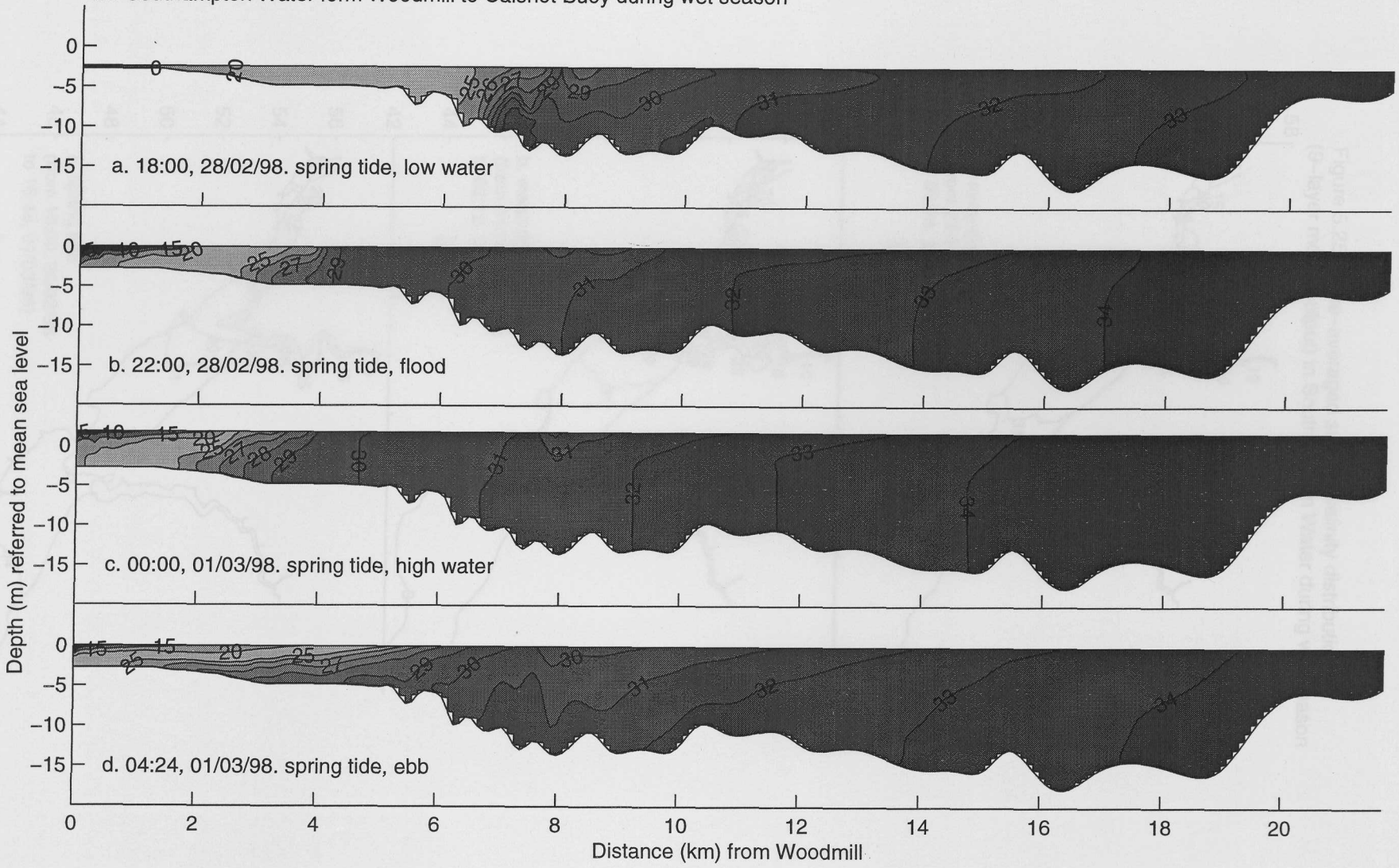

Figure 5.25 Time–averaged surface salinity distribution (9–layer model output) in Southampton Water during wet season

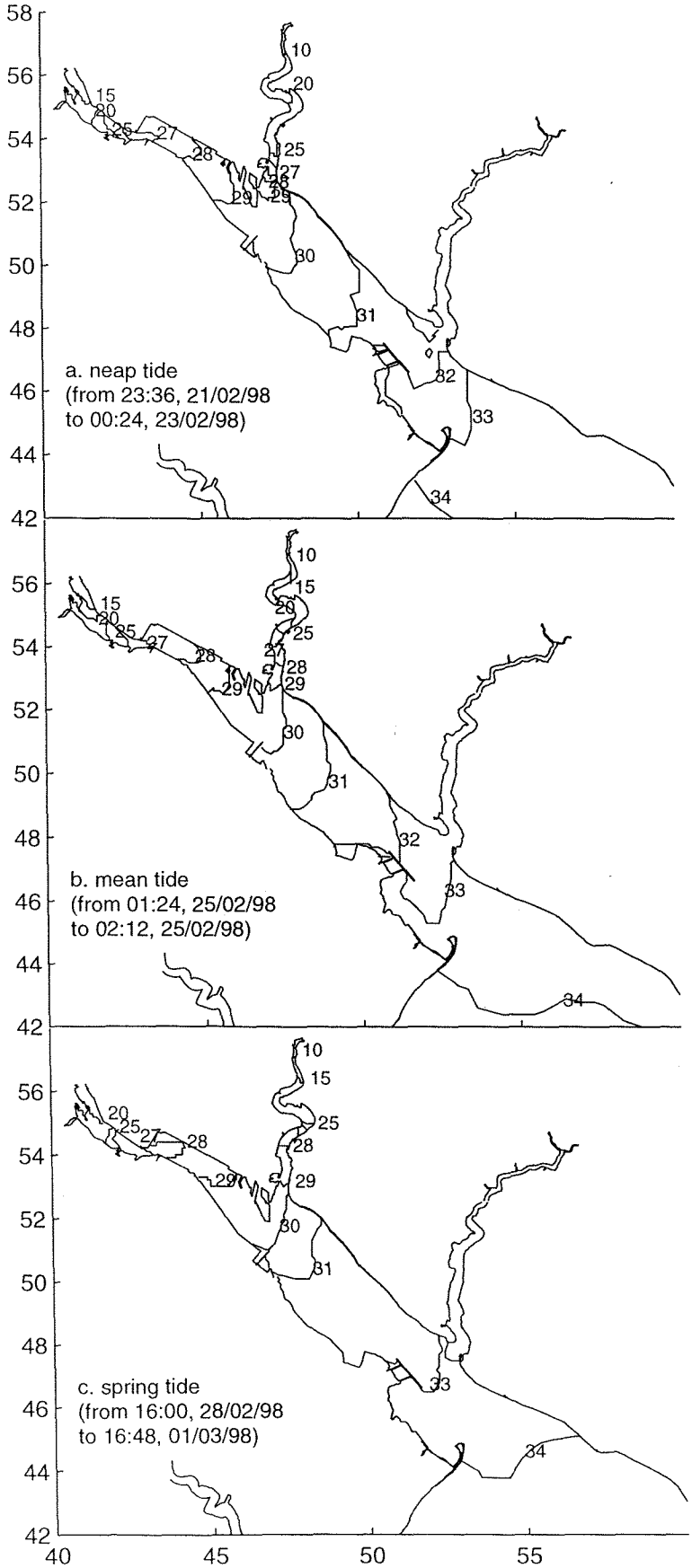

Figure 5.26 Time-averaged bottom salinity distribution (9-layer model output) in Southampton Water during wet season

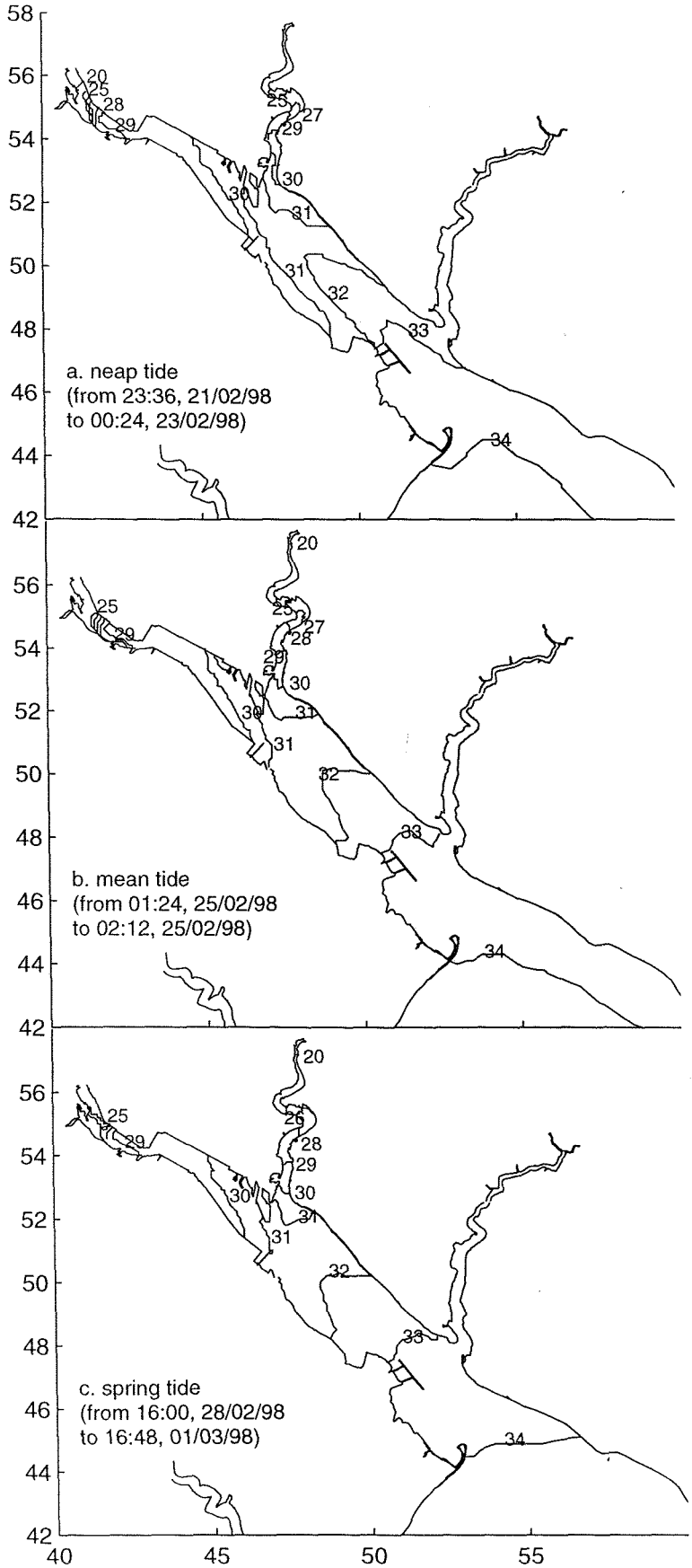

Figure 5.27 Time– and depth–averaged salinity distribution (9–layer model output) in Southampton Water during wet season

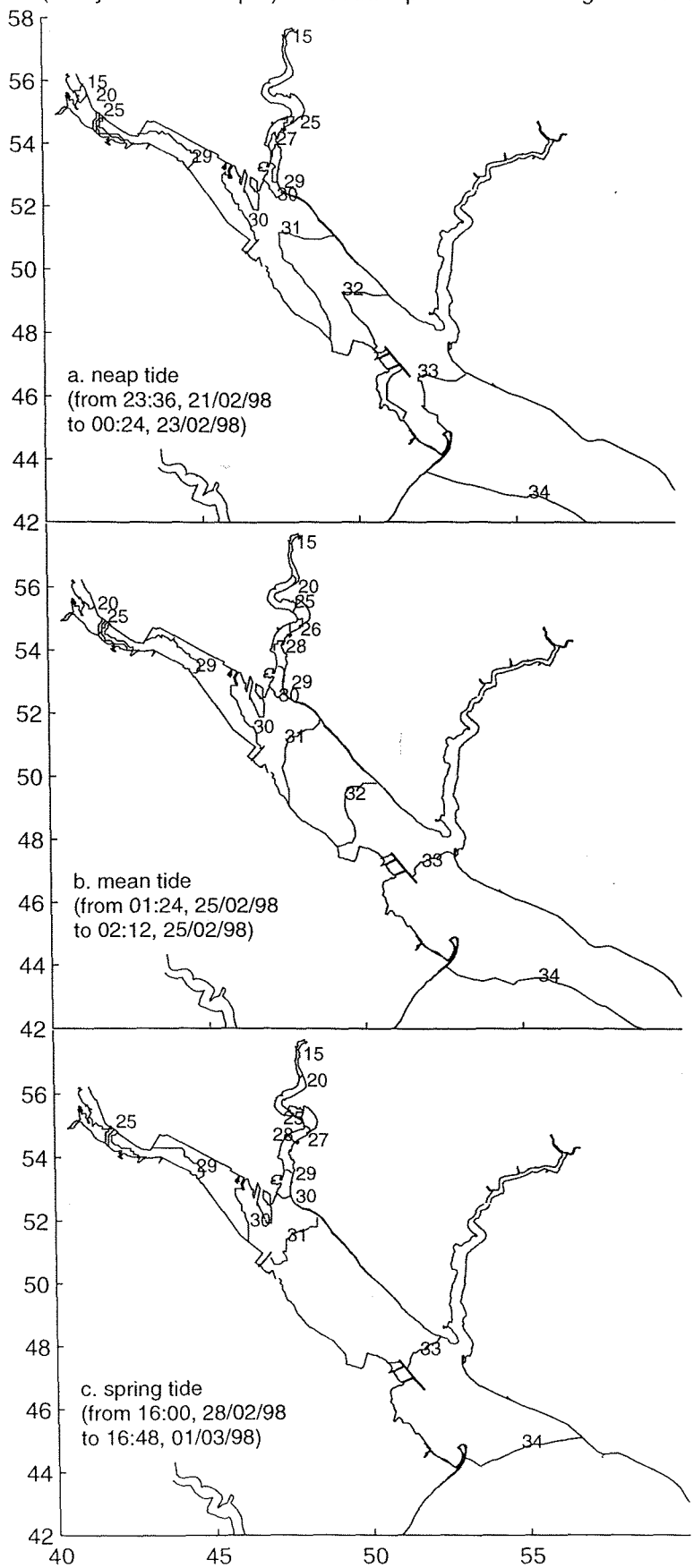

Figure 5.28 Longitudinal time–averaged salinity distribution along main channel of the Itchen Estuary and Southampton Water form Woodmill to Calshot Buoy during wet season

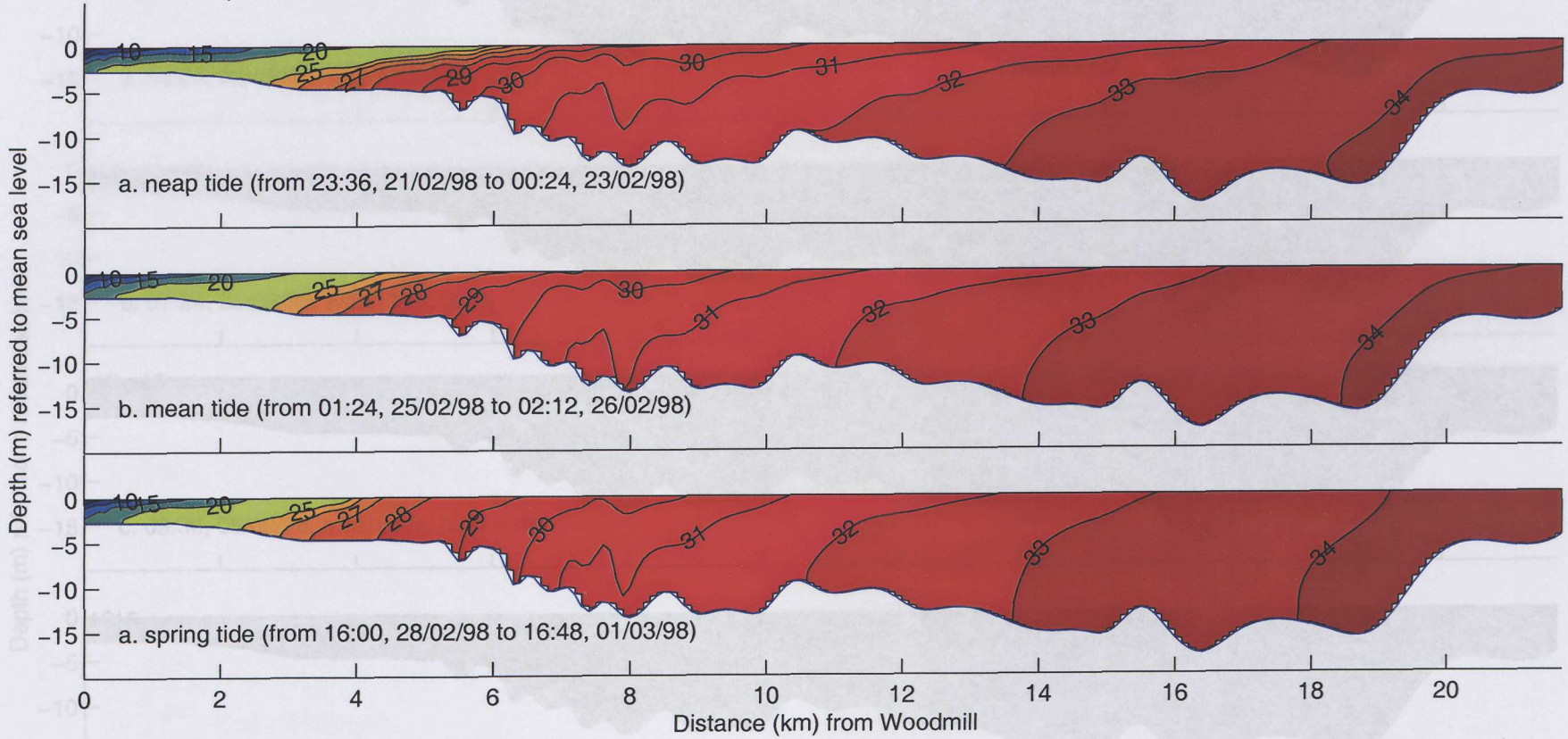

Figure 5.29 Longitudinal salinity distribution along main channel of the Itchen Estuary and Southampton Water form Woodmill to Calshot Buoy during dry season

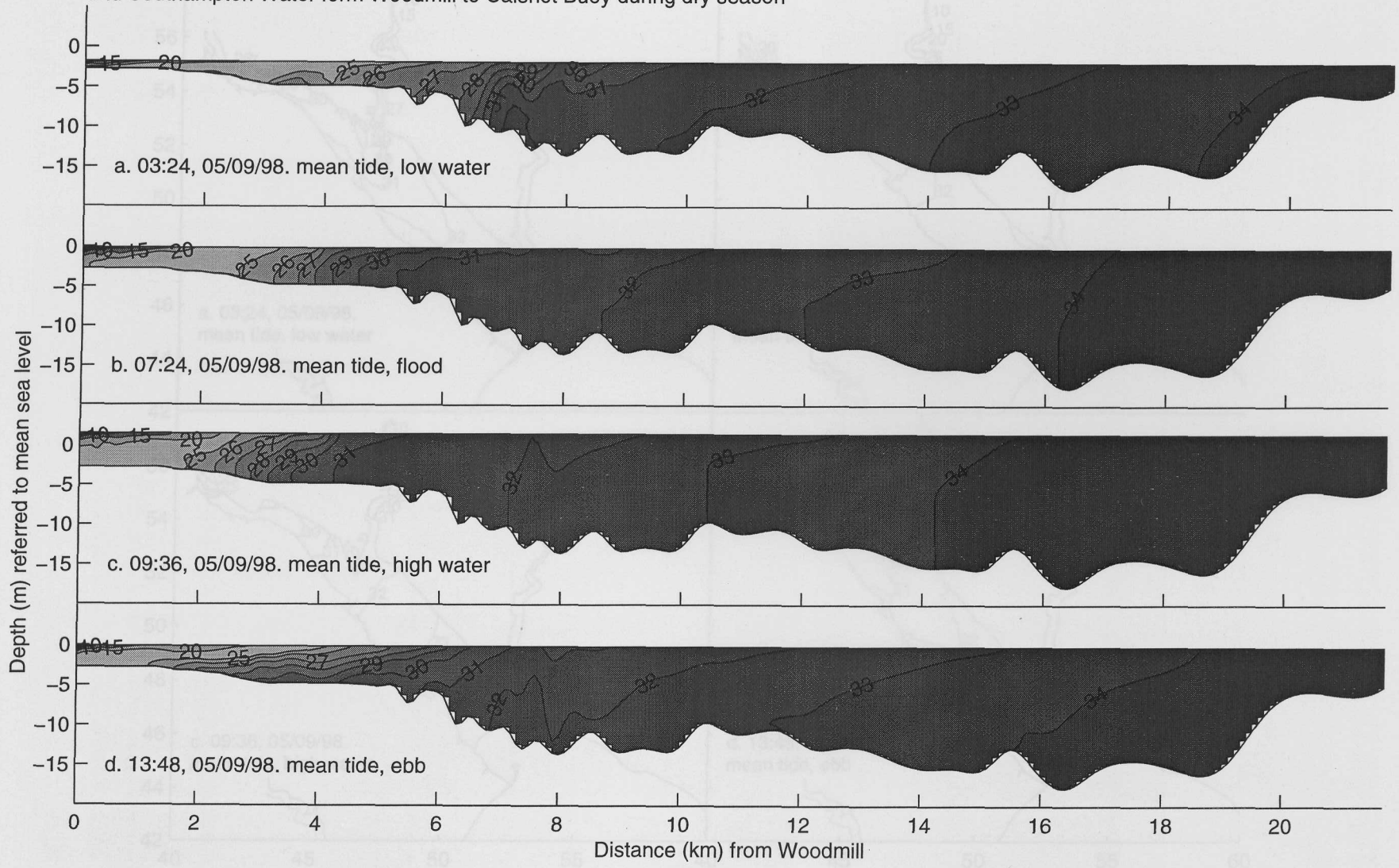

Figure 5.30 Surface salinity distribution (9–layer model output) in Southampton Water during dry season

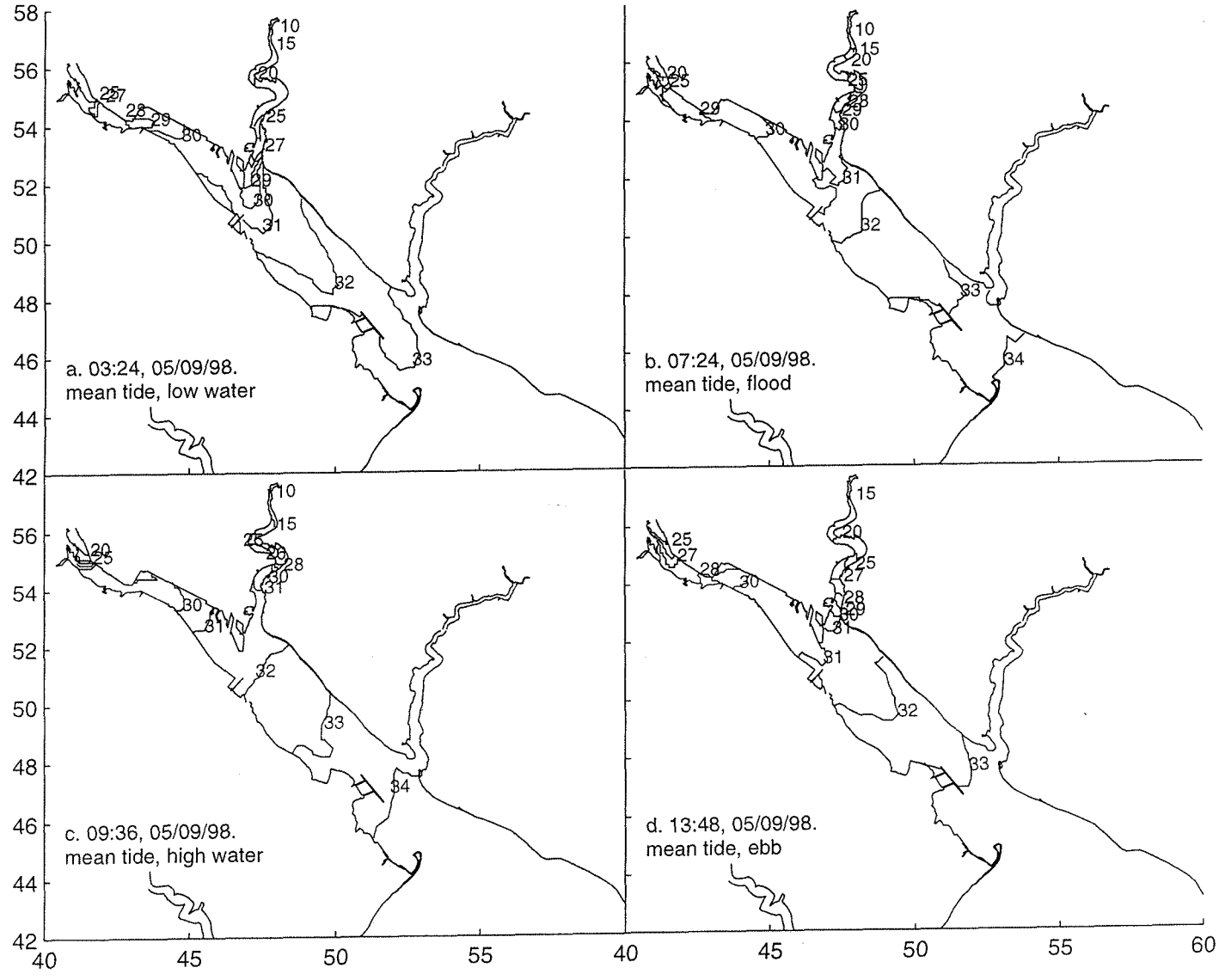

Figure 5.31 Bottom salinity distribution (9–layer model output) in Southampton Water during dry season

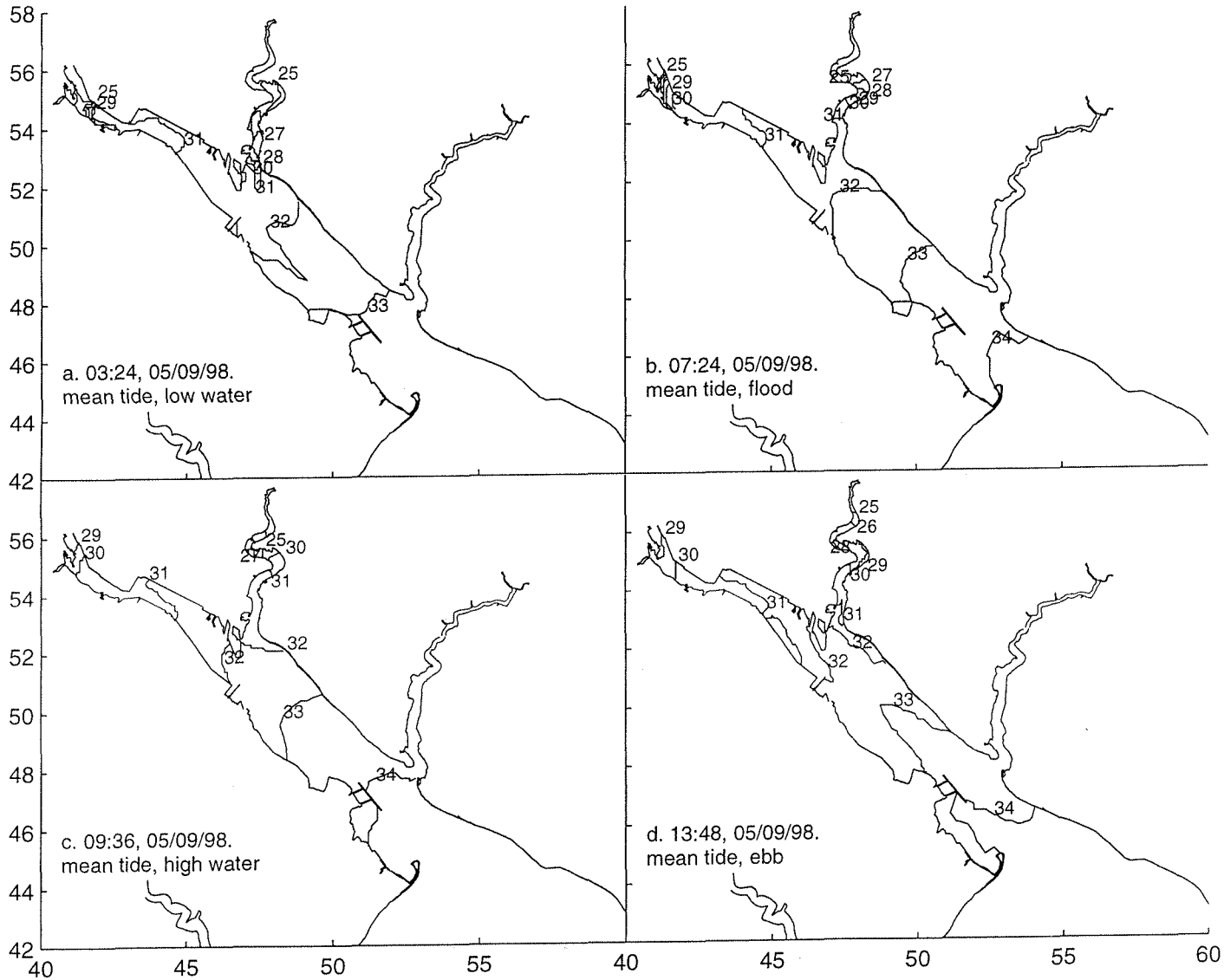

Figure 5.32 Longitudinal salinity distribution along main channel of the Itchen Estuary and Southampton Water form Woodmill to Calshot Buoy during dry season

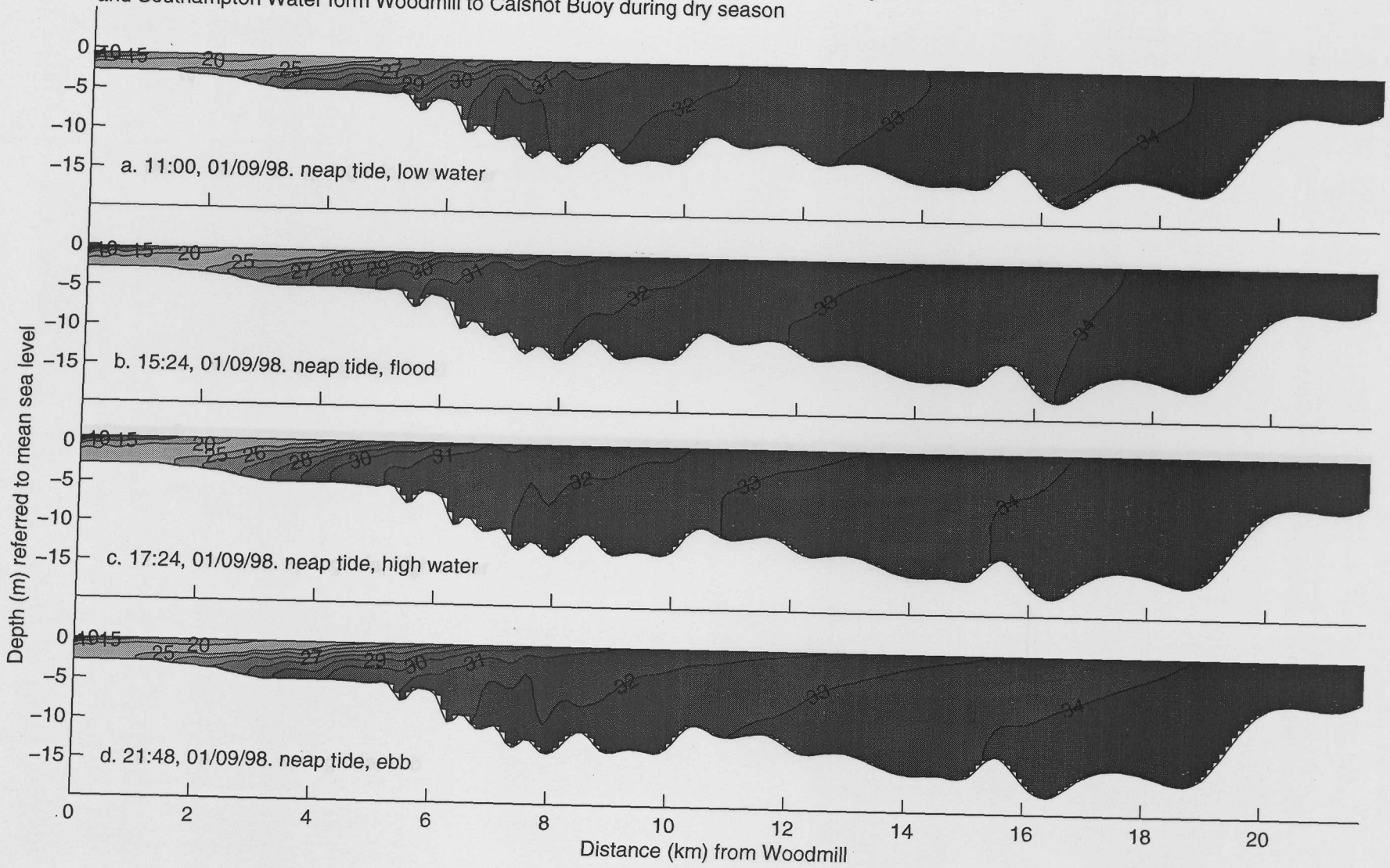

Figure 5.33 Longitudinal salinity distribution along main channel of the Itchen Estuary and Southampton Water form Woodmill to Calshot Buoy during dry season

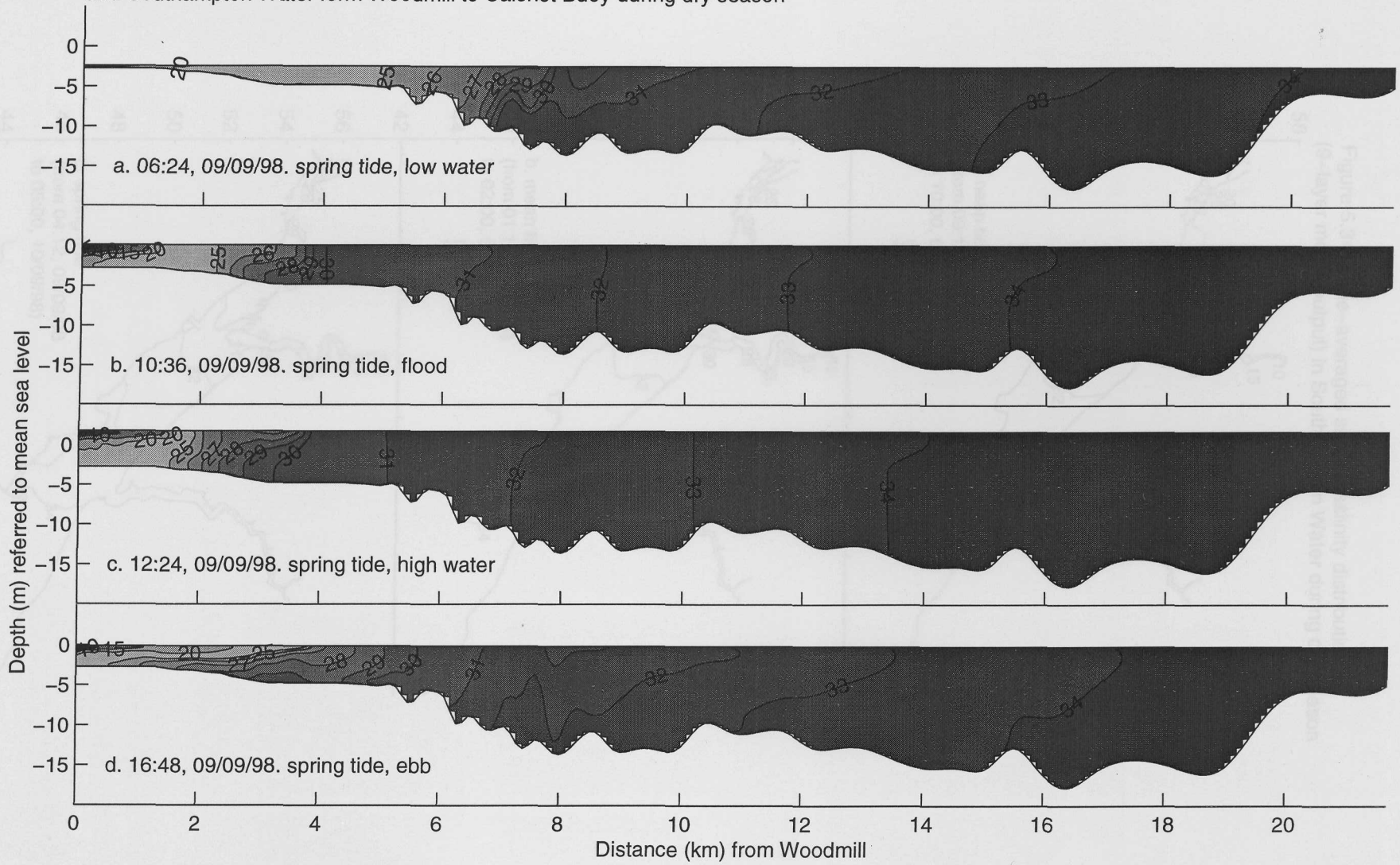

Figure 5.34 Time-averaged surface salinity distribution (9-layer model output) in Southampton Water during dry season

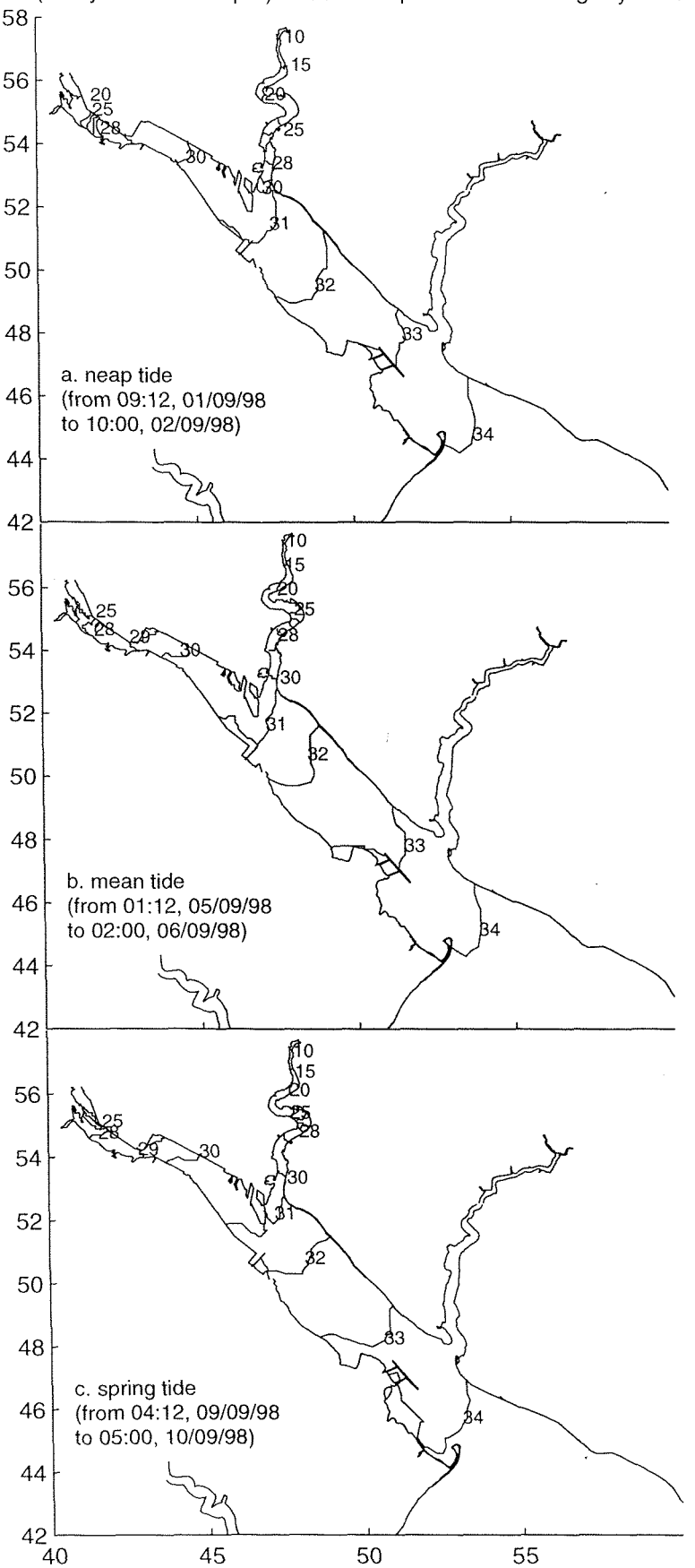

Figure 5.35 Time-averaged bottom salinity distribution (9-layer model output) in Southampton Water during dry season

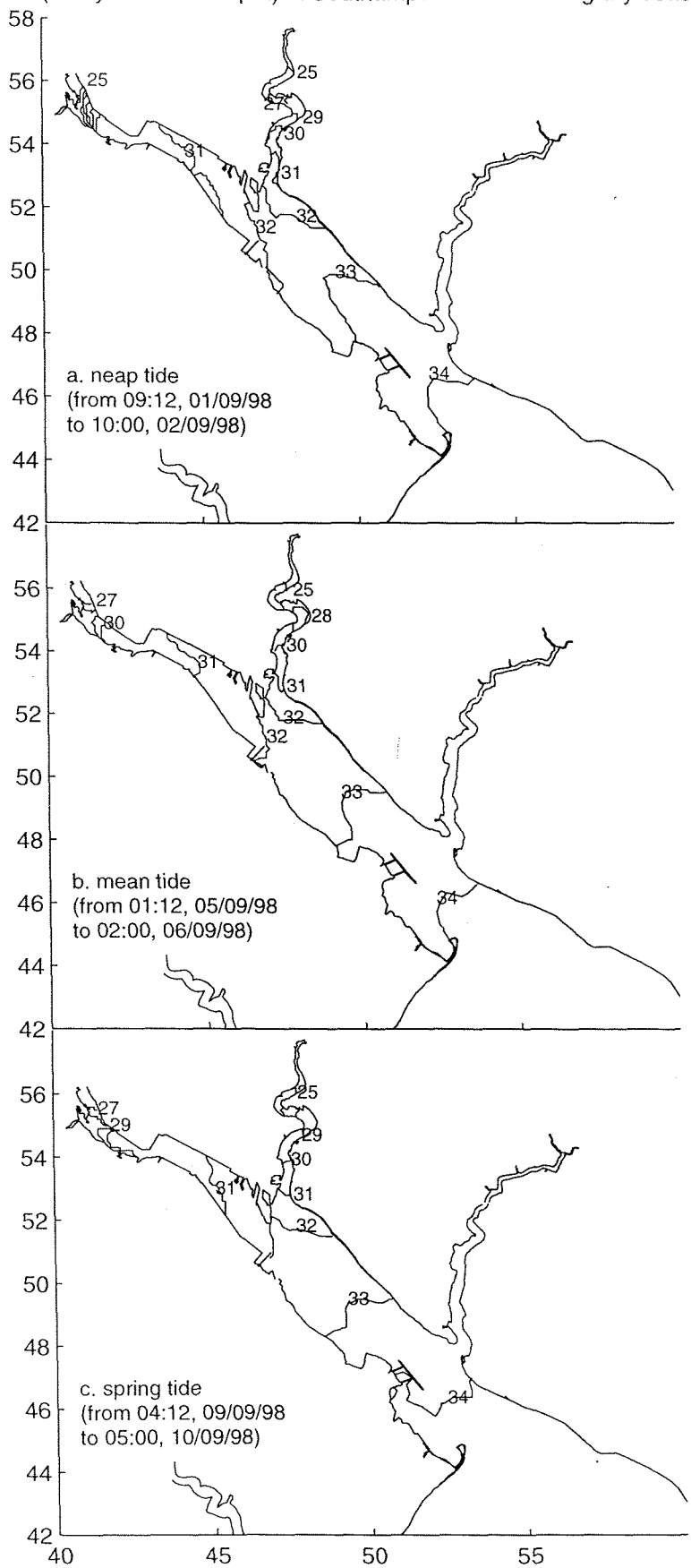

Figure 5.36 Time– and depth–averaged salinity distribution (9–layer model output) in Southampton Water during dry season

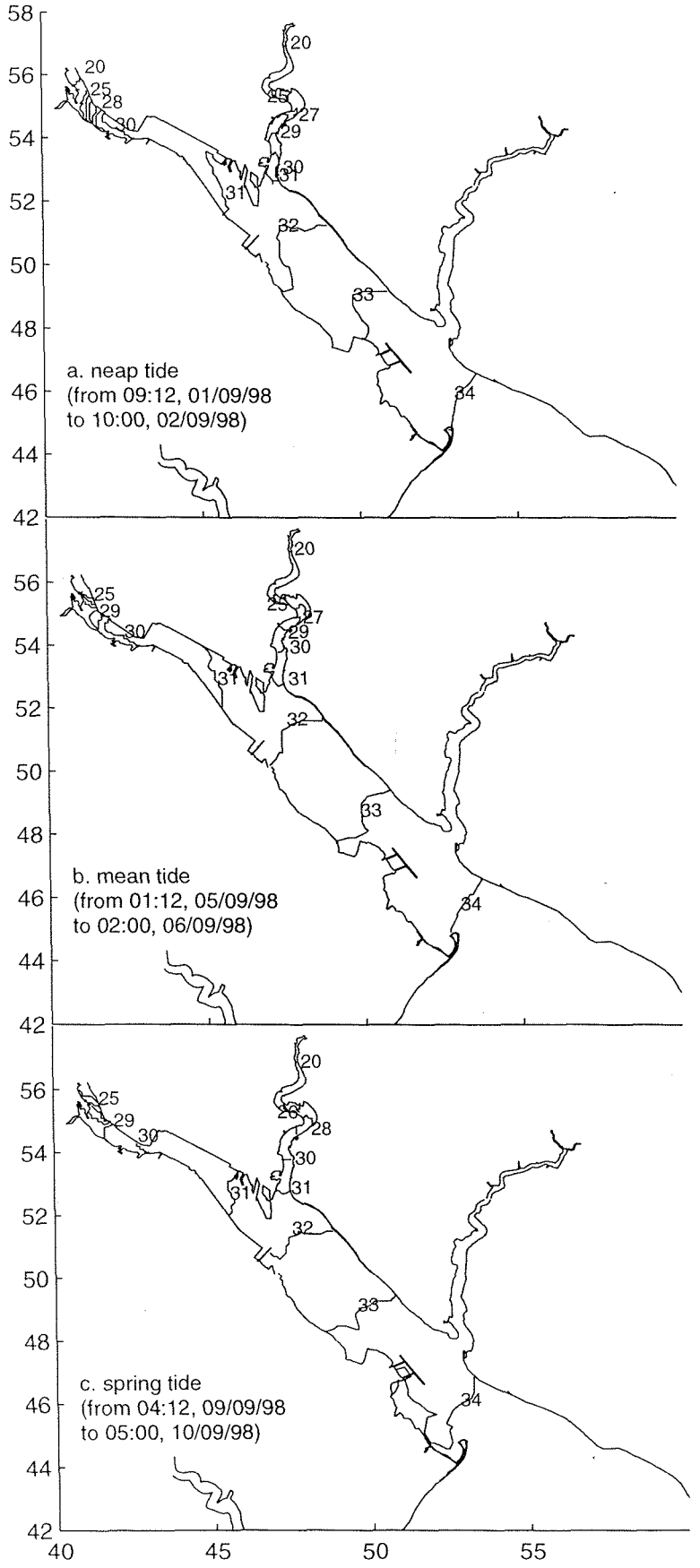

Figure 5.37 Longitudinal time–averaged salinity distribution along main channel of the Itchen Estuary and Southampton Water form Woodmill to Calshot Buoy during dry season

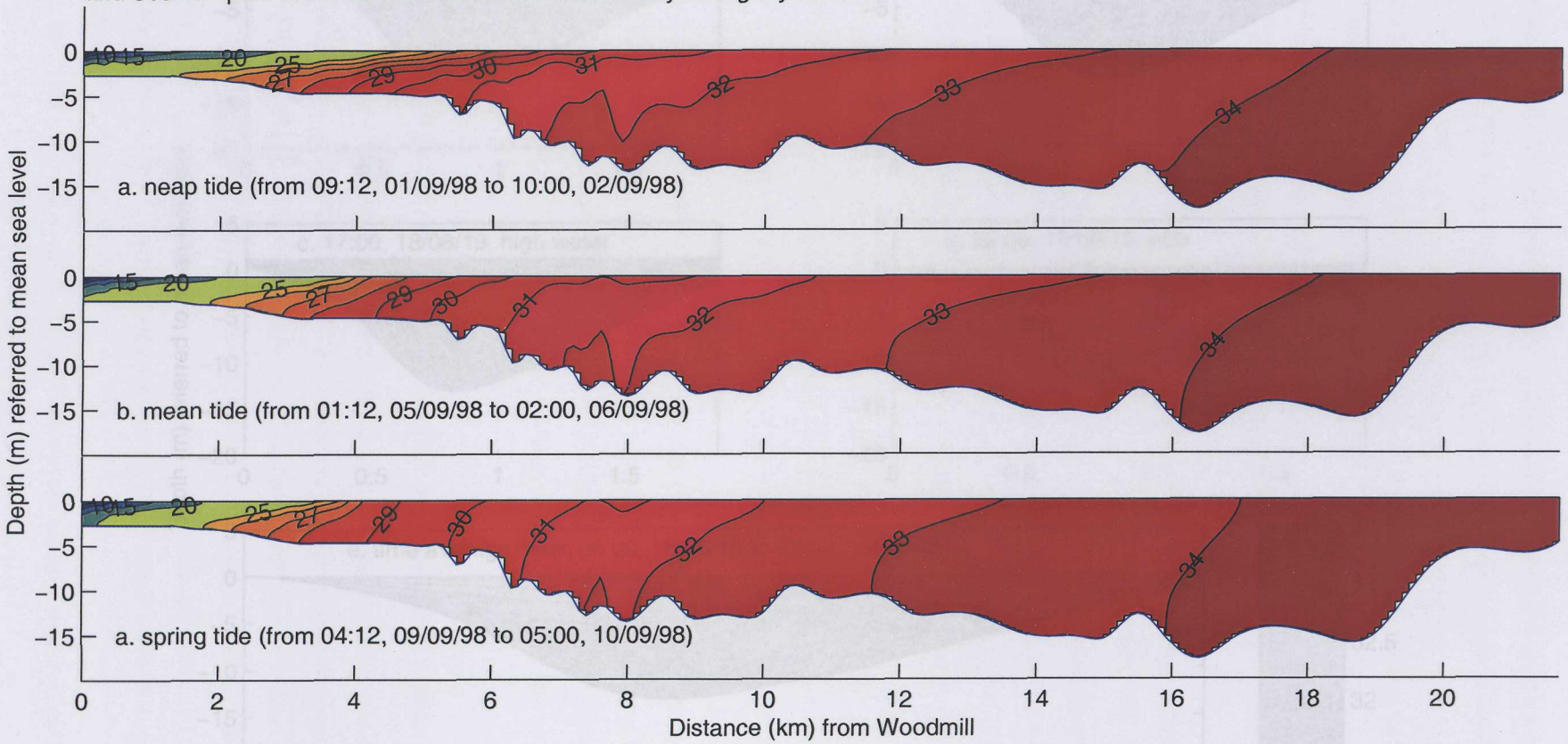

Figure 5.38 Lateral salinity distribution at the section across Southampton Water at Hound Buoy

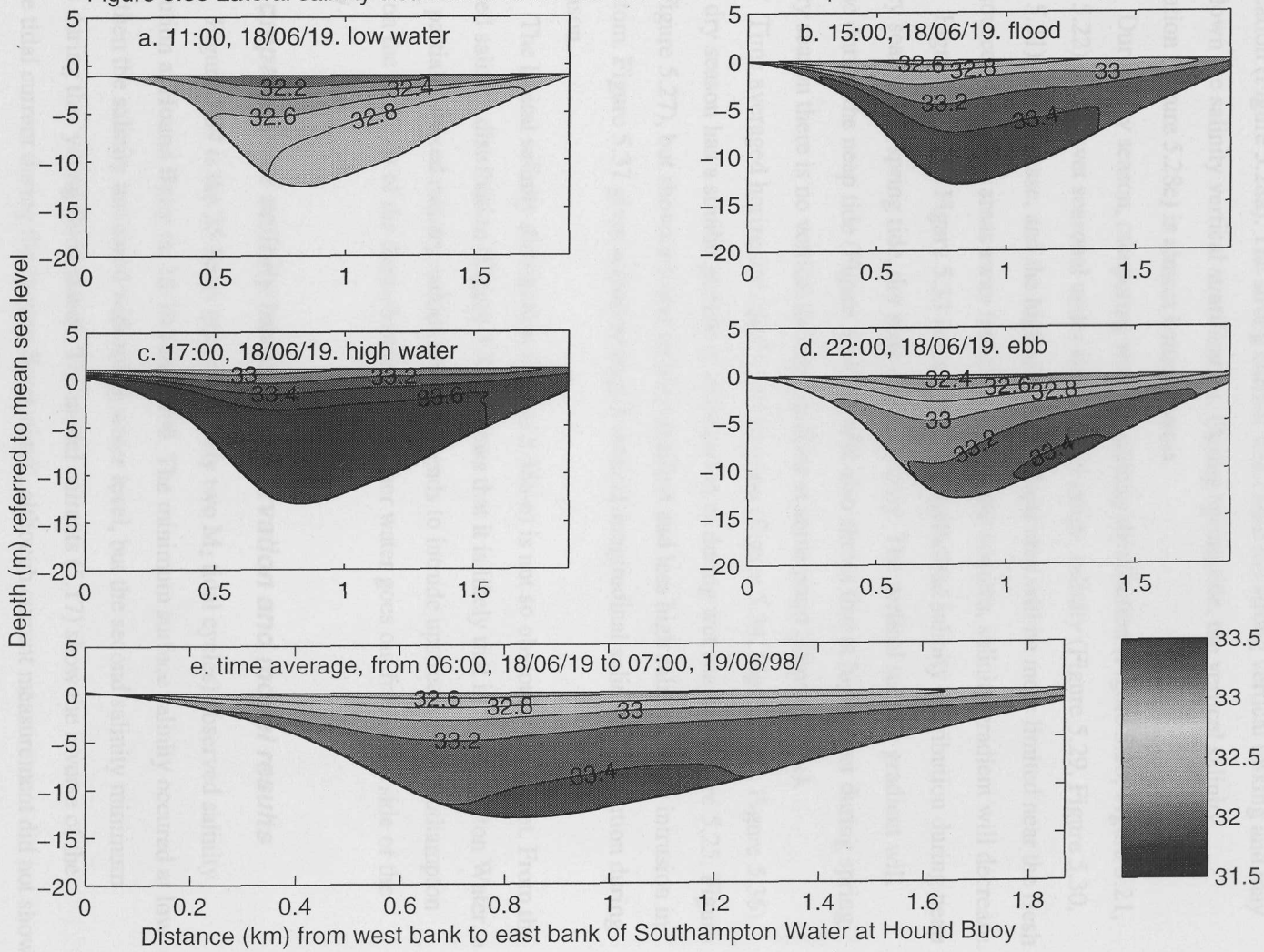

Time averaged vertical-longitudinal salinity distribution (Figure 5.28) shows a clear neap-spring variation. The vertical stratification will increase when tidal range decreases. During neap tide, weak current causes weak vertical eddy mixing, hence strong vertical salinity stratification (Figure 5.28a). The strong current will cause the strong vertical mixing and may break down the salinity vertical stratification. During spring tide, the vertical salinity distribution (Figure 5.28c) is almost homogeneous.

During dry season, comparing with the salinity distribution (Figure 5.20, Figure 5.21, Figure 5.22) during wet seasonal under similar tidal range, salinity (Figure 5.29, Figure 5.30, Figure 5.31) will increase, and the high salinity gradient area will be more limited near the fresh water sources. For most areas away from the fresh water sources, salinity gradient will decrease.

Figure 5.32 and Figure 5.33 is the vertical-longitudinal salinity distribution during neap tide, dry season and spring tide, dry season respectively. The vertical salinity gradient will increase during the neap tide (Figure 5.32). Model also shows that at high water during spring tide, dry season there is no vertical salinity gradient at some point (Figure 5.33c).

Time averaged horizontal salinity distribution (Figure 5.34, Figure 5.35, Figure 5.36) during dry season has a similar pattern of distribution as during wet season (Figure 5.25, Figure 5.26, Figure 5.27), but shows a lower salinity gradient and less high salinity water intrusion in the bottom. Figure 5.37 gives a time-averaged vertical-longitudinal salinity distribution during dry season.

The lateral salinity distribution (Figure 5.38a-e) is not so obvious to interpret. From the averaged salinity distribution (Figure 5.38e) shows that it is likely that in Southampton Water, a typical partially-mixed estuary, saltier sea water tends to intrude upstream into Southampton Water on the east side of the deep channel, the fresher water goes out from west side of the estuary.

5.9 Comparison of salinity between observation and model results

Figure 5.39 is the 25 hours (approximately two M_2 tidal cycles) observed salinity distribution at Hound Buoy on 18-19 June 1998. The minimum surface salinity occured at low water, then the salinity increased with rising water level, but the second salinity minimum occurs during the 'young flood stand'. The model currents (5.17) show the reverse of the surface tidal current during the 'young flood stand', although current measurement did not show the surface current. The decrease of salinity during the 'young flood stand' strongly suggests that the currents reversed at the surface.

A further interesting feature is the decrease of the surface salinity after the first high water, and increase of the salinity in bottom water, which is probably due to the decrease of vertical eddy mixing at the stable stage of double high water. The weak vertical eddy mixing makes the longitudinal density gradient overcome the shear stress between the surface and

Figure 5.39a Depth–averaged salinity (observed) at Hound Buoy

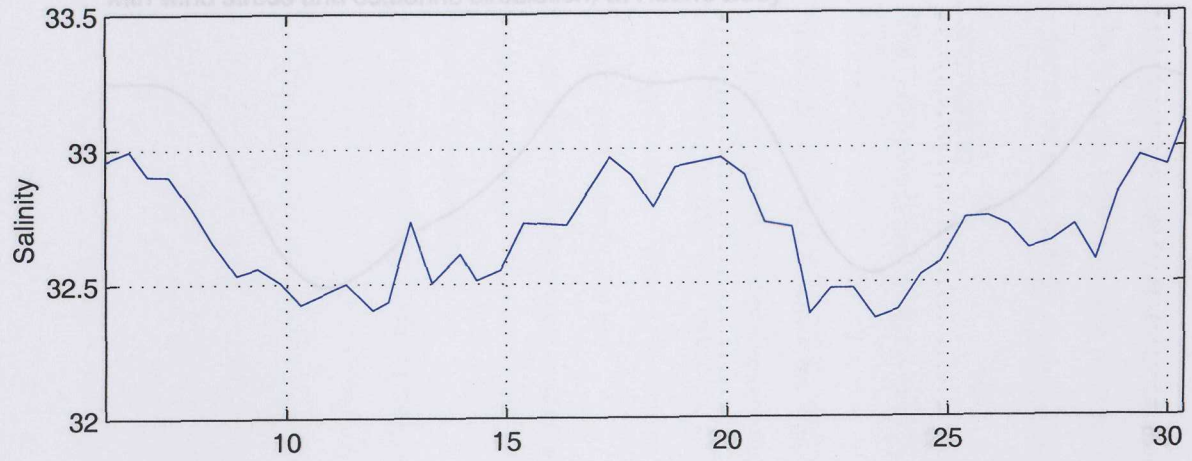

Figure 5.39b Salinity in water column (observed) at Hound Buoy

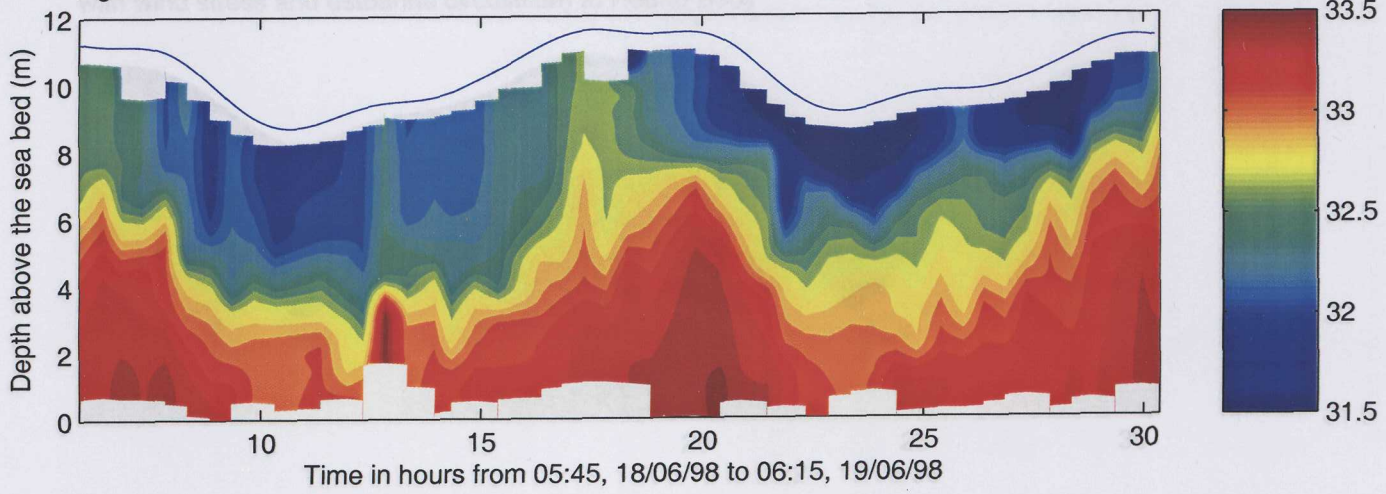

Figure 5.40a Depth–averaged salinity (9–layer model output, with wind stress and estuarine circulation) at Hound Buoy

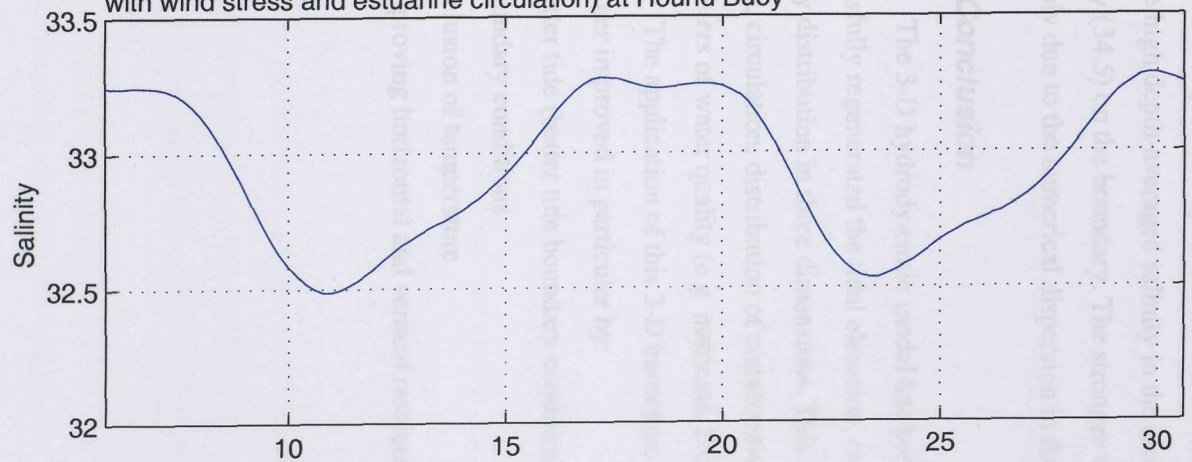

Figure 5.40b Salinity in water column (9–layer model output, with wind stress and estuarine circulation) at Hound Buoy

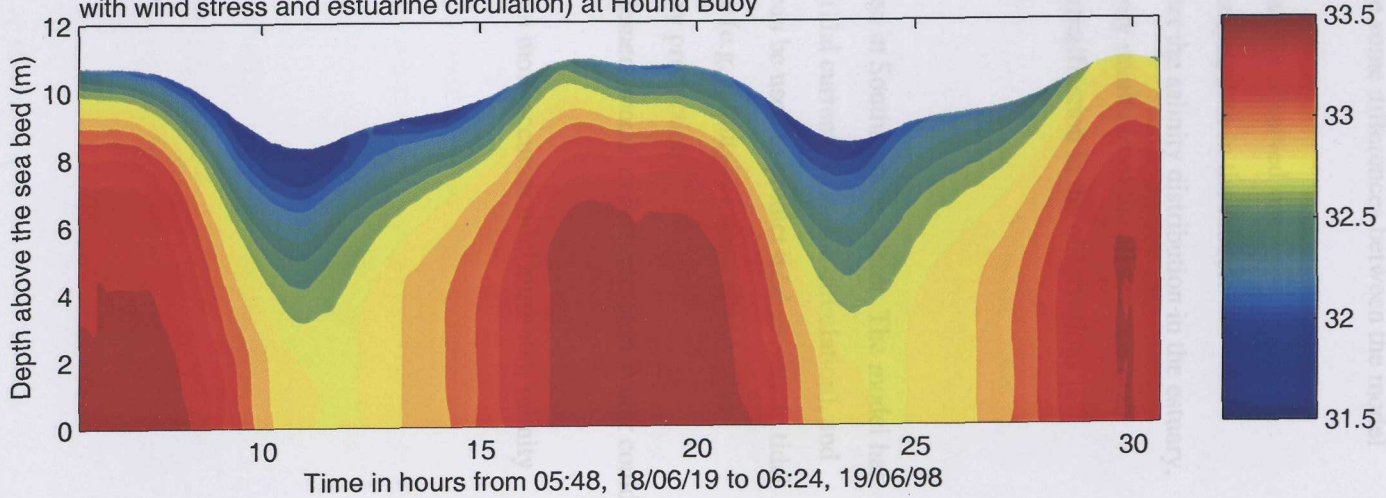

bottom layer. Both are related to the unique 'young flood stand' and 'double high water' in Southampton Water.

The model results (Figure 5.40) successfully regenerate these phenomena, with the same pattern of salinity distribution. However there are some differences between the model result and the observed salinity distribution:

1. The modelled depth-averaged salinity is higher than the observed one.
2. The vertical stratification is stronger in the observations than in the model.

Salinity boundary condition will certainly affect the salinity distribution in the estuary, and the high depth-averaged salinity in the model mainly results from the all seasons high salinity (34.5) on the boundary. The stronger vertical stratification in the observations is probably due to the numerical dispersion in the model.

5.10 Conclusion

The 3-D hydrodynamic model has been applied in Southampton Water. The model has successfully regenerated the tidal elevation, currents (tidal current, estuarine circulation), and salinity distribution in three dimensions. This model can be used to predict tidal elevation, tidal current, circulation, distribution of conservative matter (e.g. salinity) or non-conservative parameters of water quality (e.g. nutrients, DO, primary production).

The application of this 3-D baroclinic finite element model in Southampton Water could be further improved in particular by:

1. Better tide (better tide boundary condition therefore more accurate tidal currents), salinity boundary conditions
2. Inclusion of temperature
3. Improving horizontal and vertical resolution

Chapter 6 DO model structure

6.1 Introduction

A simple approach to modelling dissolved oxygen in an aquatic environment (e.g. Streeter & Phelps, 1925; O'Connor, 1960) is to simulate DO consumption by the bacterial degradation of organic matter, which is discharged from external sources (e.g. sewage, industrial effluents and riverine discharge). Like terrestrial plants, aquatic plants (mainly algae) release free oxygen during photosynthesis and produce new organic matter. As a consequence of algal photosynthesis, the release of the oxygen may cause DO supersaturation, whereas algal respiration and the degradation of detritus will decrease the DO concentration. When the DO consumption rate reaches a certain magnitude that the atmospheric re-aeration of oxygen is unable to compensate, the water may become hypoxic and even anoxic. In some natural aquatic systems, hypoxia or anoxia may occur even when there is no direct human impact. Over past decades, man's extensive activities in coastal regions and river catchments have resulted in an increase of direct inorganic nutrient discharge and indirect nutrient (organic matter) discharge. This nutrient enrichment may stimulate the growth of aquatic plants, and result in undesirable consequences. Under these circumstances, a more sophisticated approach to water quality modelling is needed to take account of the impact of local plant growth on DO concentration.

A model has been established consisting of two components:

1. External model; this models the DO consumption due to oxidisation of organic matter discharged into the estuary from external sources (e.g. domestic sewage, industrial effluents and riverine inputs), and also nutrient distribution in waters without algal growth.
2. Internal model: this models the impact of algal photosynthesis on the estuarine water quality (internal means the oxygen demanding organic matter is generated locally, not from the external sources).

In the following sections of Chapter 6, firstly an advection-dispersion equation is introduced to give some idea about how the water quality model will be integrated with the hydrodynamic model; then a detailed description of the external model and internal model is presented.

6.2 Advection-dispersion equation of a contaminant

Considering sources and sinks, the mass conservative equation governing all the contaminant C in the aquatic medium can be written as:

$$\frac{dC}{dt} = \frac{\partial}{\partial z}(K_z \frac{\partial C}{\partial z}) + \frac{\partial}{\partial x}(K_x \frac{\partial C}{\partial x}) + \frac{\partial}{\partial y}(K_y \frac{\partial C}{\partial y}) + \sum Sources - \sum Sinks \qquad (6.1)$$

where $\frac{dC}{dt} = \frac{\partial C}{\partial t} + u\frac{\partial C}{\partial x} + v\frac{\partial C}{\partial y} + w\frac{\partial C}{\partial z}$ (6.2)

Using equation (6.2) and rearranging equation (6.1) in an alternative way, we have,

$$\frac{\partial C}{\partial t} = \left[u\frac{\partial C}{\partial x} + v\frac{\partial C}{\partial y} + w\frac{\partial C}{\partial z}\right] - \left[\frac{\partial}{\partial z}(K_z\frac{\partial C}{\partial z}) + \frac{\partial}{\partial x}(K_x\frac{\partial C}{\partial x}) + \frac{\partial}{\partial y}(K_y\frac{\partial C}{\partial y})\right]$$

(1) (2) (3)

$$+\sum Sources - \sum Sinks \qquad (6.3)$$

(4) (5)

where term (1) is the temporal rate of change of concentration C; term (2) on the right side of equation (6.3) is the advection term, representing the passive transport of contaminant by the water; term (3) is the mixing term, i.e. mixing of the contaminant due to turbulence; term (4) and term (5) are the source and sink terms.

Since the contaminants are assumed to be passive particles driven by the water movement and turbulence, the following description of the DO model will focus on the source and sink terms due to the chemical and biological processes. The physical processes have been dealt with in Chapter 4 i.e. physical model structure. The simplified equation is thus given by,

$$\frac{\partial C}{\partial t} = \sum Sources - \sum Sinks \qquad (6.4)$$

6.3 External model (DO-BOD) structure

6.3.1 State variables and model equations

The external model simulates the DO consumption due to oxidation of organic matter discharged from external sources (e.g. domestic sewage, industrial effluents and riverine inputs), and also the nutrient distribution in waters without algal growth. There are 10 state variables (Table 6.1) in the external model. These state variables are chosen to make full use of the data available from Southampton Water, and to make the model applicable to a range of real aquatic environment problems.

Table 6.1 State variables of the external model

Symbol	Description	Unit
CES	Slow dissolved carbonaceous biological oxygen demand	μmol O_2 l^{-1}
CEF	Fast dissolved carbonaceous biological oxygen demand	μmol O_2 l^{-1}
CEPS	Slow particulate carbonaceous biological oxygen demand	μmol O_2 l^{-1}
CEPF	Fast particulate carbonaceous biological oxygen demand	μmol O_2 l^{-1}
NE	Organic nitrogen	μmol N l^{-1}
NA	Ammonium	μmol N l^{-1}
NN	Nitrate+nitrite	μmol N l^{-1}
PH	Dissolved inorganic phosphate	μmol P l^{-1}
DO	Dissolved oxygen	μmol O_2 l^{-1}

The model equations are as following:

$$\frac{\partial CES}{\partial t} = -k_{cs} CES \tag{6.5}$$

$$\frac{\partial CEF}{\partial t} = -k_{cf} CEF \tag{6.6}$$

$$\frac{\partial CEPS}{\partial t} = -k_{cs} CEPS \tag{6.7}$$

$$\frac{\partial CEPF}{\partial t} = -k_{cf} CEPF \tag{6.8}$$

$$\frac{\partial NE}{\partial t} = -k_{ne} NE \tag{6.9}$$

$$\frac{\partial NA}{\partial t} = k_{ne} NE - NITRIFI \tag{6.10}$$

$$\frac{\partial NN}{\partial t} = NITRIFI \tag{6.11}$$

$$\frac{\partial PH}{\partial t} = 0 \tag{6.12}$$

$$\frac{\partial DO}{\partial t} = -k_{cs} CES - k_{cs} CES - k_{cs} CES - k_{cs} CES - 2 \cdot NITRIFI + REAERA \tag{6.13}$$

where k_{cs} is the oxidisation rate of CES and CEPS; k_{cf} is the oxidisation rate of CEF and CEPF; k_{ne} is the decomposition rate of the organic nitrogen; NITRIFI is the nitrification of ammonia to nitrite; REAERA is the rate of re-aeration of the free oxygen in the water from the atmosphere.

The right side of the phosphate equation (6.12) is zero, which means that phosphate is conservative in the external model.

6.3.2 Oxygen-demanding matter (BOD and COD)

Oxygen-demanding matter is mainly organic in nature and subject to bacterial decay. Bacterial degradation results in the oxidation of organic molecules to stable inorganic compounds (e.g. CO_2, ammonia, nitrate and phosphate).

The chemical composition of organic matter in the sea is extremely complex and different constituents require different amounts of oxygen to achieve complete oxidation. It is impracticable to analyse sea water to discover its exact contents, so, the overall oxygen demand for complete oxidation is measured directly. There are two methods usually adopted for direct measurement of oxygen demand of sea water.

Chemical oxygen demand (COD) is measured by adding an oxidant ($KMnO_4$ in sea water, $K_2Cr_2O_4$ in fresh water), with sulphuric acid (H_2SO_4), to a water sample. The sample is

titrated after a standard interval to determine the amount of oxidant remaining. From this, the total amount of oxidizable material can be calculated.

Biological oxygen demand (BOD) is the usual method of measuring the oxygen demand of organic matter. The DO concentration in a water sample is measured before and after bacterial digestion for a standard time (for example three or five days, recorded as BOD_3 or BOD_5, respectively). This gives a direct measure of the amount of oxygen used in the bacterial degradation of the sample.

The measurement of COD is simpler and easier to handle than the measurement of BOD, and is much more extensively used to indicate sewage effluent load. For a particular water sample, the COD:BOD ratio can be measured, and an empirical ratio (about 2.0-5.0) can be estimated by analysis of different samples. The problem is that the interpretation of COD is more ambiguous than that of BOD and it is better to use BOD, as far as aerobic bacterial degradation is concerned. Details of COD and BOD methods are given by HMSO (1983).

There are four components of BOD and one component of organic nitrogen in the external model. The use of four components of carbonaceous BOD is based on studies which have shown that the rate of oxidation of organic matter in sea water is best represented by a composite exponential. It is assumed that the oxygen demanding matter consisted of several components which are oxidised independently at different rates. Studies by Water Research Centre (WRc) at Stevenage indicated that the oxidisation of a wide range of organic wastes can be adequately represented by the use of two rate constants, one being one fifth the value of the other, so that:

$$k_{cs}=0.2k_{cf} \tag{6.14}$$

The fast rate constant k_{cf} for carbonaceous material at 20 °C is usually taken to be 0.23 per day. The hydrolysis rate of the organic nitrogen is 0.26 d^{-1} (HR Wallingford, 1995).

6.3.3 Atmosphere re-aeration

Diffusion of free oxygen across the air-sea interface is often considered to be a Fickian process driven by the concentration gradient at the boundary. The diffusion coefficient D_a can be simplistically described as follows:

$$D_a = \lambda \frac{(O_{sat} - O)}{O_{sat}} \tag{6.15}$$

where O_{sat} is the saturation concentration of DO as a function of temperature, salinity and pressure; λ is the gas exchange coefficient, expressed in units of g m^{-2} h^{-1} at 100% saturation deficit (this coefficient varies with time as a function of air and water turbulence). The relation between dynamic physical variables and gas exchange coefficient have been much discussed (Liss, 1973; Wanninkhof, 1992) and λ can be estimated using field data. D'Avanzo and Kremer

(1994) gave a simplified equation, which neglects the water surface condition, to estimate the gas exchange coefficient λ:

$$\lambda = 0.117exp(0.15W_{10}) \quad (6.16)$$

where W_{10} is the wind speed (m/s) measured on site and converted to a standard height of 10 m with a logarithmic correction (Hartman & Hammond, 1985). The empirical DO saturation equation in sea water is given by Weiss (1970),

$$O_{sat}=-173.4292+249.6339*(T_a/100)+143.3483*log(T_a/100)-21.8492*T_a/100+S*(-0.033096+0.014259*(T_a/100)-0.001700*(T_a/100)2) \quad (6.17)$$

where T_a is absolute temperature at the sea surface and S is salinity.

6.3.4 Nitrification

The nitrification of ammonia to nitrate is as follows:

$$NH_3+2O_2=HNO_3+H_2O. \quad (6.18)$$

Thus, 2 mols of O_2 are needed to oxidise 1 mol NH_3 and produce 1 mol of nitrate.

$$NITRIFI=k_{nf}NA \quad (6.19)$$

where k_{nf} is the nitrification rate.

6.4 Internal model (phytoplankton growth model) structure

6.4.1 State variables and model equations

A model is used to examine the impact of phytoplankton growth on DO saturation in the estuary. The total number (Table 6.2) of state variables in the internal model is 9. The state variables have been chosen to represent basic functional compartments of an aquatic ecosystem.

Table 6.2 State variables of the internal model

Symbol	Description	Unit
I	Solar irradiance	μmol quanta m^{-2} s^{-1}
CAR	Algal carbon	μmol C l^{-1}
CHL	Chlorophyll	μg chl l^{-1}
Z	Zooplankton carbon	μmol C l^{-1}
D	Detrital carbon	μmol C l^{-1}
NA	Ammonium	μmol N l^{-1}
NN	Nitrate+nitrite	μmol N l^{-1}
PH	Dissolved inorganic phosphate	μmol P l^{-1}
DO	Dissolved oxygen	μmol O_2 l^{-1}

Model equations:

$$\frac{dI}{dz} = k_0 I \quad (6.20)$$

$$\frac{\partial CAR}{\partial t} = PHOTO - RESP - MORTP - GRAZ1 \quad (6.21)$$

$$\frac{\partial CHL}{\partial t} = CHPRP - \frac{CHL}{CAR}(MORTP + GRAZ1) \tag{6.22}$$

$$\frac{\partial Z}{\partial t} = (1 - c_{zg1} - c_{zd1})GRAZ1 + (1 - c_{zg2} - c_{zd2})GRAZ2 - MORTZ \tag{6.23}$$

$$\frac{\partial D}{\partial t} = MORTP + MORTZ + c_{zd1}GRAZ1 - (1 - c_{zd2})GRAZ2 - k_d D \tag{6.24}$$

$$\frac{\partial NA}{\partial t} = \frac{N}{CAR}(c_{zg1}GRAZ1 + c_{zg2}GRAZ2 + k_d D - r_{na}PHOTO + RESP) - NITRIFI \tag{6.25}$$

$$\frac{\partial NN}{\partial t} = NITRIFI - \frac{N}{CAR}(1 - r_{na})PHOTO \tag{6.26}$$

$$\frac{\partial PH}{\partial t} = \frac{PH}{CAR}(c_{zg1}GRAZ1 + c_{zg2}GRAZ2 + k_d D - PHOTO + RESP) \tag{6.27}$$

$$\frac{\partial DO}{\partial t} = r_{na}PHOTO + (1 - r_{na})r_{nn}PHOTO - RESP$$

$$- k_d D - c_{zg1}GRAZ1 - c_{zg2}GRAZ2 - 2NITRIFI + REAERA \tag{6.28}$$

where k_0 is the light attenuation coefficient; *PHOTO* is the phytoplankton photosynthesis; *RESP* is phytoplankton respiration; *MORTP* is the phytoplankton mortality; *CHPRP* is reproduction of the photosynthetic pigment term; *CHL/CAR* is the current phytoplankton chlorophyll:carbon ratio; *N/CAR* is the phytoplankton nitrogen:carbon ratio; *PH/CAR* is the phytoplankton phosphorus:carbon ratio; *GRAZ1* is the zooplankton grazing of phytoplankton; *GRAZ2* is the zooplankton grazing of detritus; c_{zg1} is the proportion of excretion by zooplankton grazing of phytoplankton; c_{zd1} is the proportion of digestion by zooplankton grazing of phytoplankton; c_{zg2} is the proportion of excretion by zooplankton grazing of detritus; c_{zd2} is the proportion of digestion by zooplankton grazing of detritus; *MORTZ* is the zooplankton mortality; k_d is the decomposition rate of detritus; k_{na} is the proportion of the ammonium nitrogen in all nitrogen utilised by phytoplankton photosynthesis; r_{nn} is the ratio of oxygen released when ammonium was used and oxygen released when nitrate was used by the phytoplankton.

The processes involved in the internal model are mainly those which can be simply parameterised from the survey data collected or from the previous work carried out in Southampton Water. Many assumptions to simplify the processes have been made to derive the equations of the internal model. One of these assumptions is that the photosynthetic quotient and respiratory quotient is 1, if ammonium is taken up during photosynthesis and is the end product during respiration. The carbon:nitrogen:phosphorous:oxygen ratio has been fixed during the organic matter cycling in the internal model using the Redfield ratio (C:N:P:O_2 ratio is 106:16:1:106, when the ammonia nitrogen is the final product) (Redfield, 1934; Alvarez-Borrego et al., 1975; Nixon et al., 1976, 1980; Nixon, 1981).

The heterotrophic bacterioplankton are not explicitly represented in the internal model. Consideration of bacterial decay of organic matter would make the water quality model more complicated. There are some marine ecosystem models (e.g. Fasham et al., 1990; Kuhn & Radach, 1997) that include a bacterial compartment. Since the live cycle of bacteria is much shorter that of phytoplankton, to some extent the absence of heterotrophic bacterioplankton in the model may be compensated by parameterizing the detritus compartment degradation rate.

A more detailed discussion is given to these processes which have not been explicitly quantified.

6.4.2 Solar radiation beneath sea surface

Solar radiation not only influences the physical process by heating, but also is the energy source for aquatic photosynthesis, therefore understanding and modelling the distribution of solar irradiance throughout the water column is very important to provide accurate parameterization of phytoplankton growth.

6.4.2.1 Light attenuation in sea water

Modelling the attenuation of monochromatic light I with depth is given by the following differential equation:

$$dI=-kIdz \tag{6.29}$$

where k (m^{-1}) is the light attenuation coefficient. If the surface irradiance is I_0, integrating the equation from surface to depth z gives:

$$I(z) = I_0 exp(-kz) \tag{6.30}$$

This means monochromatic light reduces exponentially with depth. The light-attenuating properties of water can be conveniently described by a mean k value for Photosynthetically Available Radiation (PAR, 400-700 nm) rather than a series of k values for different wavelengths (Kirk, 1994).

The light attenuation will be effected by the sea water background attenuation, soluble yellow substance (SYS), particulate suspended matter and phytoplankton.

The total light attenuation coefficient k_0 is the sum of sea water background attenuation k_1, attenuation coefficient k_2 of soluble substances, attenuation coefficient k_3 of particulate suspended matter (SPM, including inert particulate matter and particulate organic matter) and attenuation coefficient k_4 of phytoplankton,

$$k_0=k_1+k_2+k_3+k_4. \tag{6.31}$$

Considering attenuation coefficient k_2 of SYS is the product of SYS concentration SY and the SYS-specific attenuation coefficient α_2; attenuation coefficient k_3 of SPM is the product of SPM concentration SP and the SPM-specific attenuation coefficient α_3; attenuation

coefficient k_4 of phytoplankton is the product of chlorophyll *a* concentration *CHL* and the chlorophyll specific attenuation coefficient α_4:

$$k_0 = k_1 + \alpha_2 \cdot SY + \alpha_3 \cdot SP + \alpha_4 \cdot CHL. \tag{6.32}$$

In sea water the SYS concentration is much lower than that of the fresh water, and in most parts of the estuarine and coastal waters, the SYS consists of the SYS originating from fresh water discharge and local SYS from the coastal sea. Assuming the linear conservative dilution of the SYS from the fresh water source with the same SYS concentration, then

$$SY = SY_s + (\frac{S_b - S}{S_b})(SY_f - SY_s), \tag{6.33}$$

where SY_f is the *SYS* concentration of the fresh water; SY_s is the *SYS* concentration of the sea water; S_b is the salinity of the sea water and S is the salinity.

Similarly *SP* consist of the inert particulate matter SP_i and particulate organic matter SP_o,

$$SP = SP_i + SP_o. \tag{6.34}$$

Rearranging the equation (6.33), then the new equation is,

$$k_0 = (k_1 + \alpha_2 SY_s + \alpha_3 SP_i) + \alpha_2 (\frac{S_b - S}{S_b})(SY_f - SY_s) + \alpha_3 SP_o + \alpha_4 CHL. \tag{6.35}$$

Let,

$$k_1' = k_1 + \alpha_2 SY_s + \alpha_3 SP_i \tag{6.36}$$

$$k_2' = \alpha_2 (\frac{S_b - S}{S_b})(SY_f - SY_s) \tag{6.37}$$

$$k_3' = \alpha_3 SP_o \tag{6.38}$$

$$k_4' = \alpha_4 CHL \tag{6.39}$$

The new expression for light attenuation coefficient will be the same in appearance as the equation (6.32),

$$k_0 = k_1 + k_2 + k_3 + k_4, \tag{6.40}$$

where the k_2 is the light attenuation due to soluble yellowish substance from the fresh water discharge; k_3 is the light attenuation due to the particulate organic matter; k_4 is the light attenuation due to the phytoplankton. Equation (6.40) means when light penetrate vertically a short distance of Δz in the water, a proportion of k_4/k_0 of all light absorbed in the water are absorbed by the phytoplankton.

The term photic depth (Z_{eu}) is intuitively easier to understand than the total light attenuation k_0. For convenience, the photic depth is defined as a depth where light intensity decreases to 1% of the surface irradiance incident, i.e. $Z_{eu} = log(100/1)/k_0 = 4.6/k_0$. The photic zone is the zone above the photic depth. In oceanic waters photic depth is about 100 m (which

means $k_0 \cong 0.05$), in coastal water it is of the order of 15 m and in estuarine water it is seldom as much as 3 m.

Another depth is the compensation depth (Z_{comp}) for phytoplankton where the photosynthesis is the same as the phytoplankton respiration. Above this depth phytoplankton can growth, while beneath this depth phytoplankton can not sustain their growth. Day (1979) suggested that it is generally accepted that the compensation depth Z_{comp} and photic depth Z_{eu} can be regarded as the same.

Another depth related to the PAR irradiance is the critical depth above which the total photosynthesis and respiration is in balance providing the whole water column is well mixed. This is quite important if modelling the phytoplankton growth in the ocean where the phytoplankton are trapped in a well mixed surface layer from the sea surface to the depth of thermocline. If the critical depth is above the thermocline then PAR irradiance is unable to sustain phytoplankton growth in the water column.

The surface irradiance in the internal model uses hourly data provided by the UK Meteorological Office. The solar irradiance data, mean hourly data with unit of W s^{-1}, are mainly from a Met station on Thorny Island. Since some data are missing for some short periods, the data from Met station at Lymington are used during these time periods.

6.4.2.2 Parameterisation of the light attenuation coefficient in the Itchen Estuary and Southampton Water

A set of light attenuation coefficient data as well as the salinity and SPM from a previous study (Smith, 1997) have been used to parameterise the background light attenuation coefficient in the Itchen Estuary and Southampton Water. A multiple linear regression was used in an attempt to establish a linear relation between light attenuation k (m^{-1}), salinity S and SPM (mg l^{-1}) concentration. The multiple linear regression equation from the data is given,

$$k=1.1193-0.0016S+0.0494SPM \tag{6.41}$$

The light attenuation is relatively higher at the head of the estuary where fresh water discharges, if the SPM concentration is the same, but the impact of salinity (due to dissolved yellowish substances) on light attenuation is quite limited. Over the maximum range of salinity (0-35), the maximum difference is only 0.056 m^{-1}. This is probably because the River Itchen flows through a chalk valley, so water does not contain much humic substances.

The total light attenuation coefficient (k_0) is,

$$k_0=k_1+k_2+k_3+k_4 \tag{6.42}$$

here the background light attenuation coefficient $k_1=1.1193-0.0016S_b+0.0494SPM$; the light attenuation coefficient due to yellow substances from fresh water discharge $k_2=-0.0016\ (S-S_b)$.

6.4.2.3 Modelling solar irradiance in the internal model

The energy conservation principle has been used to derive how many quanta are absorbed in a water column with an area of Δs and thickness of Δz in time of Δt,

Assuming the Light intensity in the layer surface of depth z is I_0, then the total light flux penetrating the surface area of Δs in Δt time interval is $\Delta s \Delta t I_0$; at depth of the $z+\Delta z$ the light flux is $\Delta s \Delta t I_0 \exp(-k_0 \Delta z)$, so the total light which has been absorbed in a volume of $\Delta s \Delta z$ in a time of Δt is:

$$E = \Delta s \Delta t I_0 (1 - e^{-k_0 \Delta z}) \tag{6.43}$$

The total quanta absorb by phytoplankton is:

$$E_{CHL} = \frac{k_4}{k_0} \Delta s \Delta t I_0 (1 - e^{-k_0 \Delta z}) = \Delta s \Delta t I_0 (1 - e^{-k_0 \Delta z}) \frac{\alpha_4}{k_0} CHL . \tag{6.44}$$

In a water layer with thickness of Δz the average light intensity is:

$$I_e = \frac{1}{\Delta z} \int_z^{z+\Delta z} I_0 e^{-k_0 z} dz = \frac{I_0}{k_0 \Delta z} (1 - e^{-k_0 \Delta z}) = I_0 \frac{(1 - e^{-k_0 \Delta z})}{k_0 \Delta z}, \tag{6.45}$$

and apparently $0 < I_e \leq I_0$.

6.4.3 Phytoplankton photosynthesis and growth

6.4.3.1 Photosynthesis as a function of irradiance

Ryther (1956) used experimental data to describe the photosynthesis of phytoplankton as a function of irradiance. His generalised model was used to develop a method for estimating primary production in the ocean from the chlorophyll content of the water, incident solar radiation, and the extinction coefficient of visible light in the water column (Ryther & Yentsch, 1957). Since then, numerous studies have been conducted to derive a general model of photosynthesis for aquatic phytoplankton (Platt, 1980; Platt, 1981; Platt, 1983; Falkowski, 1981; Harrison et al., 1985; Sakshaug et al., 1989; Cullen, 1990).

Platt (1981) proposed a model relating irradiance to photosynthesis rate (P_I) where

$$P_I = P_m \tanh(\alpha I / P_m) \tag{6.46}$$

here P_m (μmol C (μg Chl)$^{-1}$ s^{-1}) is the maximum photosynthesis rate and α is the initial gradient of the curve. Platt et al. (1980) included a photoinhibitation term:

$$P_1 = P_m (1 - e^{-\alpha I / P_m}) e^{-\beta I / P_m} \tag{6.47}$$

where β is a photoinhabitation coefficient.

The equation used in the Fasham et al. (1990) model is in a different form,

$$P_1 = \frac{P_m \alpha I}{(P_m^{\,2} + \alpha^2 I^2)^{1/2}} \tag{6.48}$$

Whereas Kawamiya (1994) gives the following equation that includes the photoinhabitation,

$$P_I = I/I_{opt}\, exp(1-I/I_{opt})P_m \tag{6.49}$$

A similar equation to (6.49) has been used to describe the phytoplankton photosynthesis in the internal model.

6.4.3.2 Derivation of a phytoplankton photosynthesis model under principle of energy conservation

From 6.4.2.4, in an area of Δs with depth of Δz in Δt time interval the total quanta absorbed by phytoplankton E_{CHL} (μmol quanta) is given by,

$$E_{CHL} = \Delta s \Delta t I_0 (1 - e^{-k_0 \Delta z}) \frac{\alpha_4}{k_0} CHL. \tag{6.50}$$

Assuming ϕ_{max} is the maximum quantum yield of the phytoplankton, then the maximum possible yield Y_{CHL} ((μmol C) from E_{CHL} is,

$$Y_{CHL} = \Delta s \Delta t I_0 (1 - e^{-k_0 \Delta z}) \frac{\alpha_4}{k_0} \phi_{\max} CHL. \tag{6.51}$$

The fact is that not all the energy will be converted by photosynthetic pigment into chemical energy in form of algal carbon. The efficiency of the photosynthesis depends on the irradiance I_e (6.46):

$$\text{The efficiency of the photosynthesis} = \frac{(1 - e^{-\beta I_e})}{\beta I}, \tag{6.52}$$

where $\beta = 1/I_s$; I_s is the saturation onset parameter. The actual yield Y_{CHL} in term of algal carbon will be,

$$Y_{CHL} = \Delta s \Delta t I_0 (1 - e^{-k_0 \Delta z}) \frac{\alpha_4}{k_0} \phi_{\max} CHL \frac{(1 - e^{-\beta I_e})}{\beta I_e}, \tag{6.53}$$

or alternatively

$$Y_{CHL} = (\Delta s \Delta z \Delta t) I_0 \alpha_4 \phi_{\max} \frac{(1 - e^{-k_0 \Delta z})}{k_0 \Delta z} \frac{(1 - e^{-\beta I_e})}{\beta I_e} CHL. \tag{6.54}$$

Using (6.46) to eliminate I_e, then,

$$Y_{CHL} = (\Delta s \Delta z \Delta t) \alpha_4 \phi_{\max} \frac{(1 - e^{-\beta I_e})}{\beta} CHL. \tag{6.55}$$

The equation (6.56) will be used in the internal model. The (6.56) means that in a $\Delta s \Delta z$ volume water in a Δt time interval the averaged photosynthesis rate P_I (μmol C (μg chl)$^{-1}$ s^{-1}) is given by,

$$P_1 = \alpha_4 \phi_{\max} \frac{(1 - e^{-\beta I_e})}{\beta} \tag{6.56}$$

We can rewrite equation (6.56),

$$P_1 = P_m (1 - e^{-\beta I_e}) \tag{6.57}$$

where $P_m = \frac{\alpha_4 \phi_{\max}}{\beta}$. Thus is the same form of equation of Platt (1980)'s (6.48), if photoinhibatation is ignored.

6.4.3.3 Threshold limitation approach

Plant nutrients are the essential elements for phytoplankton growth. In the aquatic environment, the most likely nutrients limiting phytoplankton growth are nitrogen and phosphorous. There are many different approaches to modelling nutrient limitation of phytoplankton growth.

The supply of nutrients to photosynthesis is represented by a factor Q. For a single nutrient

$Q=C/(C+K)$ and new $P = Q \cdot P_1$

where C is the nutrient concentration; K is the half-saturation concentration.

In the case of nitrogen, both nitrate and ammonia can be used for photosynthesis. Phytoplankton may favour ammonia, and this can be represented by a different formula.

Fasham (1990) and Kuhn (1996) use the following formula,

$$Q_n = \frac{NA/h_{na} + NN/h_{nn}}{1 + NA/h_{na} + NN/h_{nn}}, \tag{6.58}$$

where N_n is the concentration of nitrate; Nr is the concentration of ammonia; K_1 is the half-saturation of nitrate; K_2 is the half-saturation of ammonia.

Kawamiya (1994) introduce the ammonium inhibition coefficient ψ,

$$Q_n = \frac{NN/h_{nn}}{1 + NN/h_{nn}} e^{-\psi NA} + \frac{NA/h_{na}}{1 + NA/h_{na}}, \tag{6.59}$$

For two nutrients $Q=Q_1 \cdot Q_2$, or $Q=min(Q_1, Q_2)$.

Here a threshold limitation approach is used to model the factor which limits phytoplankton photosynthesis, either by nutrients or by solar irradiance.

If the U_N (μmol N (μg chl)$^{-1}$ s^{-1}) is the maximum uptake rate of inorganic nitrogen, then the nitrogen limited growth rate P_2 is

$$P_2 = \frac{CAR}{N} \cdot \frac{NA/h_{na} + NN/h_{nn}}{1 + NA/h_{na} + NN/h_{nn}} U_N, \tag{6.60}$$

where h_{na} is the half-saturation concentration of ammonium which allows the half maximum nitrogen uptake rate of phytoplankton (when the nitrate concentration is zero); h_{nn} is the half-

saturation concentration of nitrate which allows the half maximum nitrogen uptake rate of phytoplankton (when the ammonium concentration is zero); *CAR/N* is the carbon:nitrogen ratio.

Similarly the phosphate limited growth rate P_3 is,

$$P_3 = \frac{CAR}{P} \cdot \frac{PH / h_{ph}}{1 + PH / h_{ph}} U_P, \tag{6.61}$$

where U_p is the maximum phosphate uptake rate; the h_{ph} is the half-saturation concentration which allows the half growth rate; *CAR/P* is the carbon phosphate ratio.

The growth rate of the phytoplankton is subjected to the inorganic nitrogen, phosphate and solar irradiance. The phytoplankton growth rate

$$P=min(P_1, P_2, P_3). \tag{6.62}$$

Under this condition the photosynthesis term of (6.22) will be,

$$PHOTO=P \cdot CHL \tag{6.63}$$

here the photosynthesis term is the net photosynthesis.

6.4.3.4 Reproduction of the photosynthesis pigment

In the external model, phytoplankton biomass is represent by the algal carbon. We have set an optimal carbon to chlorophyll ratio r_{cchl} =50 μg C (μg chl)$^{-1}$=4.17 μmol C (μg chl)$^{-1}$. If the carbon chlorophyll ratio becomes more than r_{cchl} then chlorophyll reproduction begins, if the value of the ratio is less than r_{cchl} then no reproduction of the chlorophyll pigment occurs. The loss of chlorophyll is proportional to the mortality of phytoplankton biomass and zooplankton grazing.

$$CHPRP = c_{chl}\, max(0, \frac{CAR}{CHL} r_{cchl} - 1) CHL \tag{6.64}$$

here the c_{chl} is the specific chlorophyll reproduction rate.

6.4.4 Phytoplankton respiration and mortality

The phytoplankton light respiration rate and dark respiration is different. Light respiration rate is higher than the dark respiration rate due to phytoplankton photosynthetic activity. Part of photorespiration which exceeds the dark respiration rate is assumed to be proportional to the photosynthesis rate, and has been deducted from the photosynthesis rate. The phytoplankton respiration rate here is the dark respiration rate.

The form of the phytoplankton dark respiration is simple,

$$RESP=c_{res}CHL \tag{6.65}$$

where c_{res} is the specific respiration rate, which has been measured in Southampton Water.

$$MORTP= c_{pmor} \frac{CAR}{h_{pmor} + CAR} CAR \tag{6.66}$$

where c_{pmor} is the phytoplankton specific mortality rate; h_{pmor} is the half-saturation constant for phytoplankton mortality.

Phytoplankton respiration itself does not cause the loss of chlorophyll. The loss of chlorophyll due to phytoplankton mortality is proportional to the mortality of phytoplankton biomass.

6.4.5 Zooplankton grazing and mortality

The zooplankton mortality term uses the similar formula to phytoplankton mortality,

$$MORTZ = c_{zmor} \frac{Z}{h_{zmor} + Z} Z \tag{6.67}$$

where c_{zmor} is the zooplankton specific mortality rate; h_{zmor} is the half-saturation constant for zooplankton mortality. The zooplankton mortality term includes all losses due to natural zooplankton mortality, respiration, and grazing pressure from higher levels of the aquatic food chain.

The zooplankton is assumed to graze on phytoplankton and detritus. The expression for zooplankton grazing on phytoplankton is,

$$GRAZ1 = c_{zg} \frac{p_1 CAR^2}{h_{zg}(p_1 CAR + p_2 D) + p_1 CAR^2 + p_2 D^2} Z \tag{6.68}$$

Where c_{zg} is the specific zooplankton grazing rate; h_{zg} is the half-saturation constant for zooplankton grazing; p1, p2 are respectively measures of the zooplankton preferences for phytoplankton, and detritus when their concentrations are equal.

Only a proportion (about $1-c_{zg1}-c_{zd1}$) of the total zooplankton grazing on phytoplankton will turn into zooplankton growth. Proportion of c_{zg1} will lose due to excretion by zooplankton, and proportion of c_{zd1} will turn into detritus.

A similar expressions of the zooplankton grazing on detritus are given by,

$$GRAZ2 = c_{zg} \frac{p_1 D^2}{h_{zg}(p_1 CAR + p_2 D) + p_1 CAR^2 + p_2 D^2} Z . \tag{6.69}$$

6.4.6 Detritus (particulate organic matter)

The sources of detritus in the internal model come from the phytoplankton mortality, zooplankton mortality, and part of zooplankton grazing, which has not been assimilated. Zooplankton graze on phytoplankton as well as detritus. The decomposition of detrital carbon reminerlizes the organic nutrient at a rate of k_d. The possible intermediate procedure of degradation of particulate organic matter has been ignored, in order to simplify the model.

6.4.7 Nutrients in the internal modal

Inorganic plant nutrients modelled in the internal model are ammonium, nitrate, and phosphate. As mentioned before, the ratio between carbon, nitrogen, phosphorus and oxygen have been fixed during the cycling of organic matter. The main sink for inorganic nutrients in the model is phytoplankton photosynthesis. All other sinks, e.g. denitrification and particle absorption, of nutrients have been ignored. The first product remineralization of inorganic nutrient, nitrogen, is ammonia. Ammonia is nitrified (oxidised) to nitrate. The formula of nitrification is

$$NITRIFI=k_{nf}NA, \tag{6.70}$$

where k_{nf} is the specific nitrification rate.

6.4.8 DO in the internal model

The sources of free oxygen in waters are phytoplankton photosynthesis and atmosphere re-aeration. The amount of free oxygen released from photosynthesis will depend on the uptake of ammonia or nitrate. Respiration and all organic matter decomposition processes (decomposition of detritus, excretion of zooplankton, community respiration) will consume the DO.

6.5 Temperature dependence of the processes

The rate of the processes involved in the external and internal models may depend on the water temperature. The decomposition rate of the organic matter, hydrolysis rate of the organic nitrogen, and nitrification rate in the external model, phytoplankton growth rate, phytoplankton respiration rate, and detrital carbon decomposition rate in the internal model are assumed to depend on the water temperature. The rates are multiplied by a factor in form of

$$e^{c_T(T-T_0)} \tag{6.71}$$

where c_T is the temperature coefficient; T is the water temperature; T_0 is the temperature that the rate set. For different processes the temperature coefficient c_T and T_0 is different.

6.6 Sedimentation of suspended particulate organic matter

The suspended particulate organic matter is subject to sinking, and the sedimentation processes of the particulate matter have been take account in the water quality model. The suspended particulate matter (SPM) is assumed totally passive in the water, which means it will not affect the currents. The vertical profile of the SPM is decided by the balance between downward sink term, which SPM descend in speed of v_{SPM} (SPM settling velocity) and mixing term which bring up the SPM to the surface by the vertical turbulence mixing. Using the split mode method, from (6.4), for any particulate matter which is subject to gravity, an additional equation is needed.

$$\frac{\partial C}{\partial t} = v_{SPM} \frac{\partial C}{\partial z} \tag{6.72}$$

where C represents any suspended particulate matter; v_{SPM} is the SPM settling velocity in the water column. The v_{SPM} usually is a function of size, shape and particle as well as density of sea water, but in the model, a fixed particle settling velocity (1.0 m h^{-1}) is given.

The deposition processes is ignored, for all state variables in the model, therefore the bottom boundary condition is,

$$\left.\frac{\partial C}{\partial z}\right|_{z=h} = 0 \tag{6.73}$$

6.7 Link substances and integration of the external model and internal model

There are some common state variables between the external and internal models. These include ammonium, nitrate, phosphate and dissolved oxygen, and are called link substances between the external model and internal model. The total number of state variables of the integrated water quality model is 14 (Table 6.3). Figure 6.1 gives a schematic diagram of the integrated water quality (DO) model.

Table 6.3 state variables (symbol, description and unit) of external, internal model and the link substances

symbol	description	unit
External model		
CES	Slow dissolved carbonaceous biological oxygen demand	μmol O_2 l^{-1}
CEF	Fast dissolved carbonaceous biological oxygen demand	μmol O_2 l^{-1}
CEPS	Slow particulate carbonaceous biological oxygen demand	μmol O_2 l^{-1}
CEPF	Fast particulate carbonaceous biological oxygen demand	μmol O_2 l^{-1}
NE	Organic nitrogen	μmol N l^{-1}
Internal model		
I	Solar irradiance	μmol quanta m^{-2} s^{-1}
CAR	Algal carbon	μmol C l^{-1}
CHL	Chlorophyll	μg chl l^{-1}
Z	Zooplankton carbon	μmol C l^{-1}
D	Detrital carbon	μmol C l^{-1}
Link substances		
NA	Ammonium	μmol N l^{-1}
NN	Nitrate+nitrite	μmol N l^{-1}
PH	Dissolved inorganic phosphate	μmol P l^{-1}
DO	Dissolved oxygen	μmol O_2 l^{-1}

The integration of the external model and internal model may require the rewriting of the equations of link substances (ammonium, nitrate, phosphate and dissolved oxygen). Practically, similar to the hydrodynamic model, a mode split method was used to solve the model equations, and the external model and internal model will be solved separately. Although it might increase the CPU time, the clear advantage of the split mode method is that the method

allows us to distinguish between the impact of the external load to the water quality and the impact of the internal algal growth to the water quality.

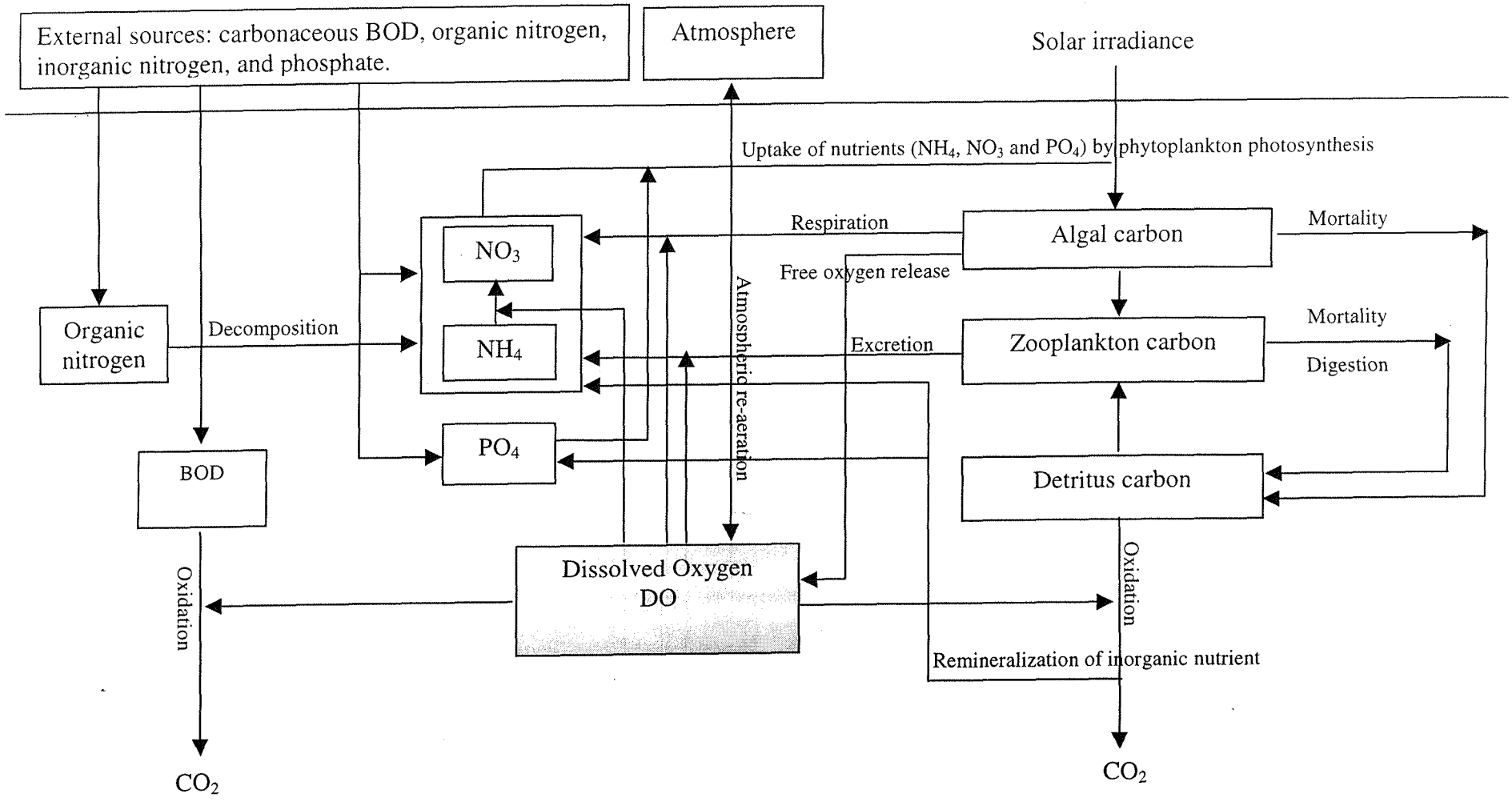

Figure 6.1 Schematic diagram of water quality (DO) model. Model integrates external (DO-BOD) model and internal model (phytoplankton growth model). The inorganic nutrients (NH_4, NO_3 and PO_4) and dissolved oxygen (DO) are the link substances between external model and internal model

Chapter 7 Application of water quality (DO) model in Southampton Water

The general-purpose water quality (DO) model described in Chapter 6 has been applied to the Southampton Water and the Solent estuarine system. Model results from the external model and the integrated water quality model are presented, and compared with the observed field data from the surveys. A brief discussion is given of the DO dynamics within the model and the model performance.

7.1 Model configuration

The coupled hydrodynamic model and water quality model was run for a one year period from January 1, 1998 to December 31, 1998 using a Pentium-II 450 computer. The time step Δt was 10 seconds. Ideally a vertical 9-layer model was to be used, but this would cost at least 1 week CPU time to run one year of the model, and during development of the model this would be extremely time consuming. Finally the vertical resolution of the water quality model was reduced to three layers, and the model then required about 2-3 days CPU time to simulate a one year period. The model results presented here are the output from the three-layer model, in which the water column was vertically divided into three layers: a surface layer, middle layer and bottom layer. All the parameters used in the water quality model are given in Appendix 1 and Appendix 2. The value of most of the parameters has been estimated from the literature to achieve a reasonable performance.

7.2 Initial condition and boundary condition

In Chapter 2 the loads of contaminants (e.g. BOD, nutrients) from sewage plants, industrial effluents and riverine discharge into Southampton Water, Test Estuary, Itchen Estuary and Hamble Estuary have been given. The loads of the inorganic nutrients (nitrate, phosphate) have been updated by the survey data. The daily river flow data from the three main rivers, Test, Itchen and Hamble, entering Southampton Water were provided by the Environment Agency. Hourly solar irradiance, wind speed and wind direction data were provided by the UK Meteorological Office. SPM concentration in the estuary is given by interpolation of the measured SPM concentration taken during the field sampling.

Setting of the open boundary condition is more difficult than the land-water boundary, since there are few data available in the area near the open boundary. Table 7.1 gives the settings of the open boundary conditions for the water quality model. The magnitude of these fall in the range of a previous measurements by Southern Water Authority 1981.

Table 7.1 Settings of the open boundary conditions in water quality model

State variable	Description	Value	unit
CES	Slow carboneous BOD	0	μmol O_2 l^{-1}
CEF	Fast carboneous BOD	0	μmol O_2 l^{-1}
CEPS	Slow particulate carbonaceous BOD	0	μmol O_2 l^{-1}
CEPF	Fast particulate carboneous BOD	0	μmol O_2 l^{-1}
NE	Organic nitrogen	0	μmol N l^{-1}
I	Solar irradiance		μmol quanta m^{-2} s^{-1}
CAR	Phytoplankton carbon	4.2	μmol C l^{-1}
CHL	Chlorophyll a	1	μg l^{-1}
Z	Zooplankton carbon	0.42	μmol C l^{-1}
D	Detritus	4.2	μmol C l^{-1}
NA	Ammonium	0.05	μmol N l^{-1}
NN	Nitrate	0.20	μmol N l^{-1}
PH	Phosphate	0.05	μmol P l^{-1}
DO	Dissolved oxygen	100	% saturation

Initial conditions of state variables were set assuming the conservative behaviour of all contaminants with salinity, then running the program for a period of time to minimise the impact of the initial settings. The model was initiated several days before January 1, 1998 but without any chemical and biological processes. After midnight of 31/12/97, all processes in the water quality model were switched on. Model results in early January 1998 show some impact of the initial conditions, but this were gradually eliminated within two weeks during the winter period when the phytoplankton are not so active.

7.3 Results from the external (DO-BOD) model

Firstly the water quality model is run to examine the direct impact of the external sources to the water quality in the Itchen Estuary and Southampton Water. The results will provide the baseline of water quality in the estuary. All the results from the water quality model will be daily averaged results, unless otherwise specified.

7.3.1 Salinity

Since all the state variables of the water quality model are passive, they will not influence the estuarine circulation and therefore the salinity distribution in the estuary. The only factor which may change the estuarine circulation and salinity distribution is the fresh water discharge from the River Test, Itchen and Hamble.

The annual variation of surface and bottom salinity distribution along the main channel of the Itchen Estuary and Southampton Water, from Woodmill to Calshot Buoy, are shown in Figure 7.1a-b. The main fresh water discharge in the Itchen Estuary is the Itchen River from Woodmill at the head of the estuary. The 1998 average river flow from Itchen River is about 5.98 m^3 s^{-1}. The baroclinic effect of fresh water discharge results in a well developed estuarine

Figure 7.1 Seasonal variation of a) surface and b) bottom salinity from 3-layer model in the Itchen Estuary and Southampton Water

a. Surface

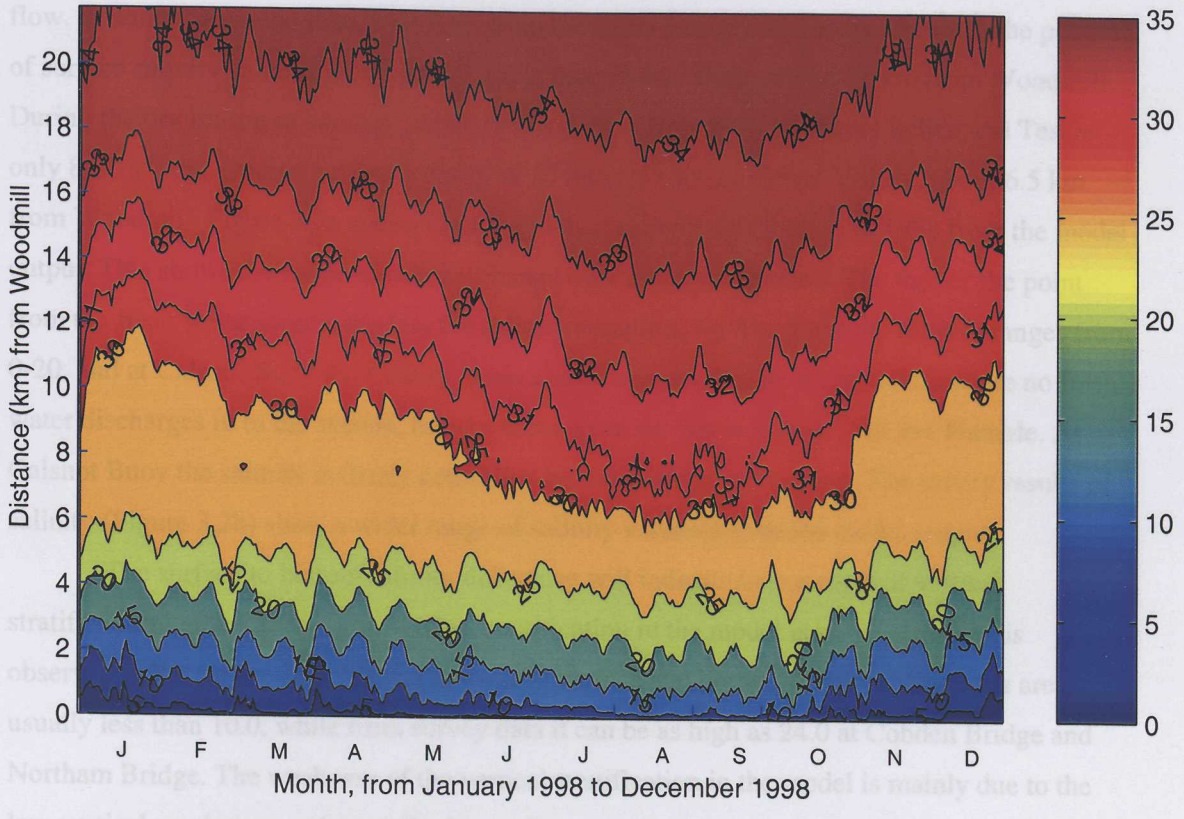

b. Bottom

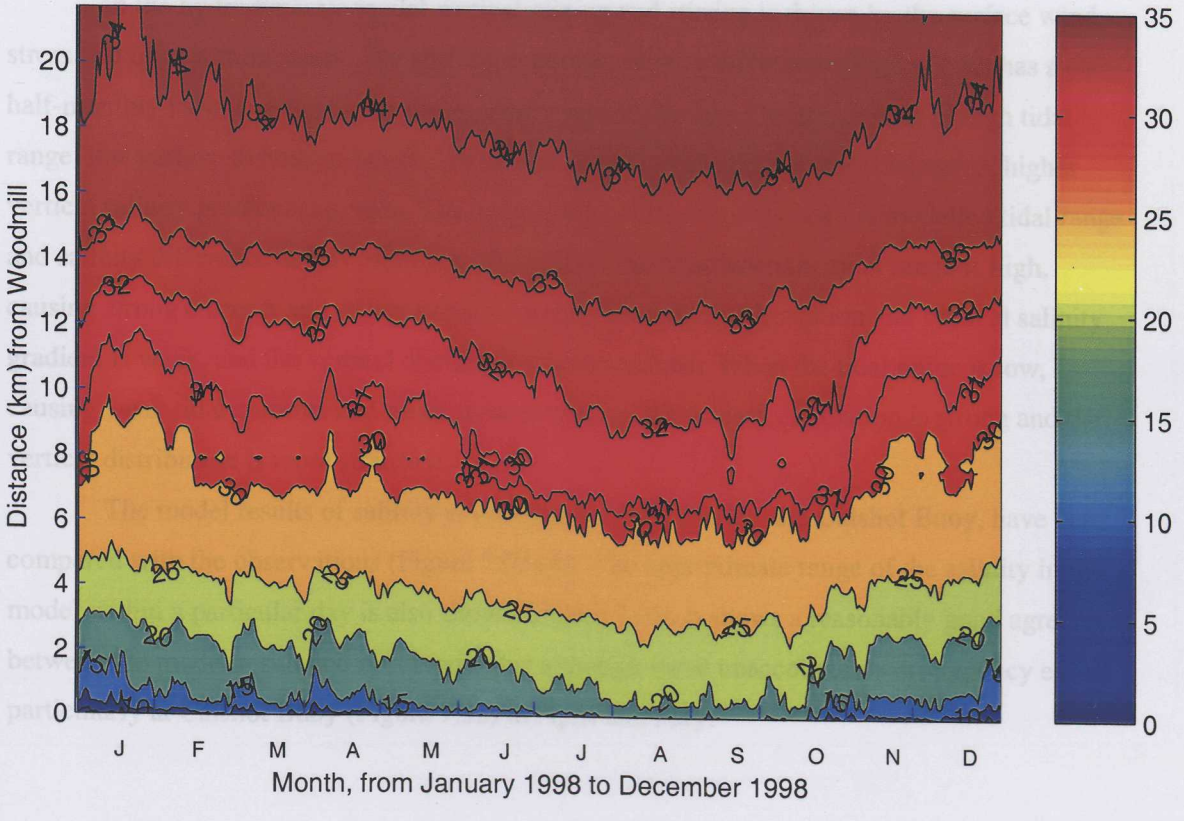

circulation, a fresher surface water flow out of the estuary and the saltier bottom water flow landward to compensate the seaward surface flow.

The seasonal variation of salinity (Figure 7.1a-b) results from the variation of river flow. In winter when the total river flow from the River Itchen and Test is 25 $m^3 s^{-1}$, the position of surface salinity value of 30 (Figure 7.1a) is near Hound Buoy, about 11 km from Woodmill. During the dry season in summer, when the total river flow from the rivers Itchen and Test is only 8 $m^3 s^{-1}$, the average surface salinity of 30 retreats back to Ocean Village, about 6.5 km from Woodmill. Figure 7.2a shows the longitudinal salinity distribution in 1998 from the model output. This shows the range of salinity change over a one year period. The farther the point from the fresh water source, the less the salinity variation. At Woodmill the salinity ranges from 0-20, and at Calshot Buoy the salinity rarely shows any change. In the model there are no fresh water discharges in to the system, besides those from the River Itchen, Test and Hamble. At Calshot Buoy the salinity is firmly controlled by the boundary condition. The survey results of salinity (Figure 3.2b) show a wider range of salinity variation than the model output.

The surface to bottom salinity difference will indicate the strength of vertical stratification in the estuary. The vertical stratification in the model is not as strong as is observed in the survey data. The daily average surface and bottom salinity differences are usually less than 10.0, while from survey data it can be as high as 24.0 at Cobden Bridge and Northam Bridge. The weakness of the vertical stratification in the model is mainly due to the low vertical resolution, and partially due to the ever-existing numerical dispersion.

In the hydrodynamic model vertical mixing and stirring is driven by the surface wind stress and tidal bottom stress. The surface to bottom salinity difference (Figure 7.2c) has a clear half-monthly variation due to the spring-neap cycle of the tide. During periods of high tidal range, low surface to bottom salinity difference occurs, while during low tidal range, higher vertical salinity gradients are seen. The correlation coefficient between the modelled tidal range and salinity difference at NW Netley is –0.48. It is clear that when the tidal range is high, causing strong currents and strong vertical mixing, the estuary circulation and vertical salinity gradient is weak, and the vertical distribution more uniform. When the tidal range is low, causing weak tidal currents and weak vertical mixing, the estuary circulation is strong and the vertical distribution is more stratified.

The model results of salinity at two stations, NW Netley and Calshot Buoy, have been compared with the observations (Figure 7.03a-b). The approximate range of the salinity in the model within a particular day is also shown. Figure 7.03a-b shows a reasonably good agreement between the model result and observed value although some unaccountable discrepancy exists particularly at Calshot Buoy (Figure 7.3b) in April and May.

Figure 7.2a Longituidinal distribution of salinity from 3–layer model

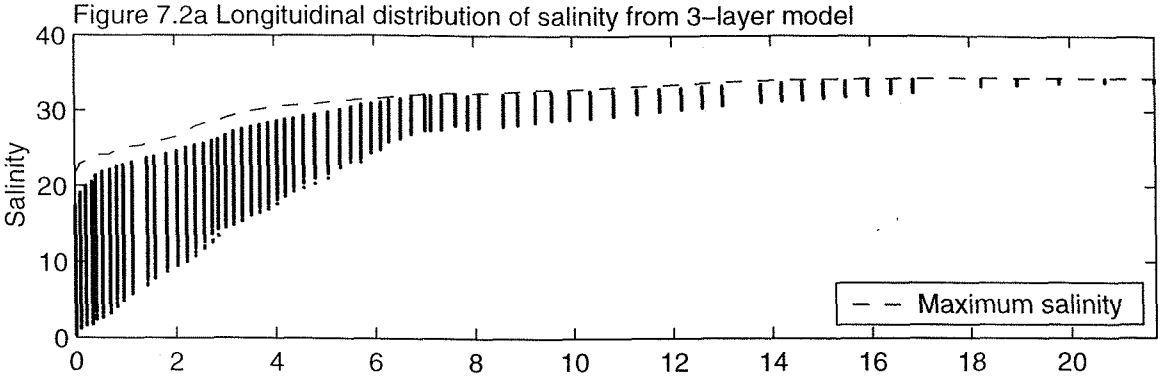

Figure 7.2b Longituidinal distribution of surface–bottom salinity differences from 3–layer model

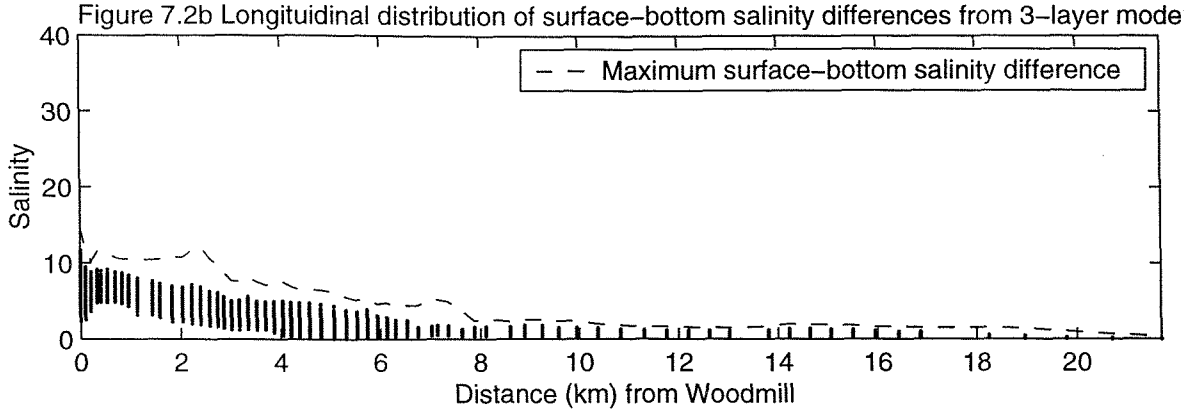

Figure 7.2c Comparison between the tidal range (dash–dot line) and surface–bottom salinity differences (solid line) at NW Netley

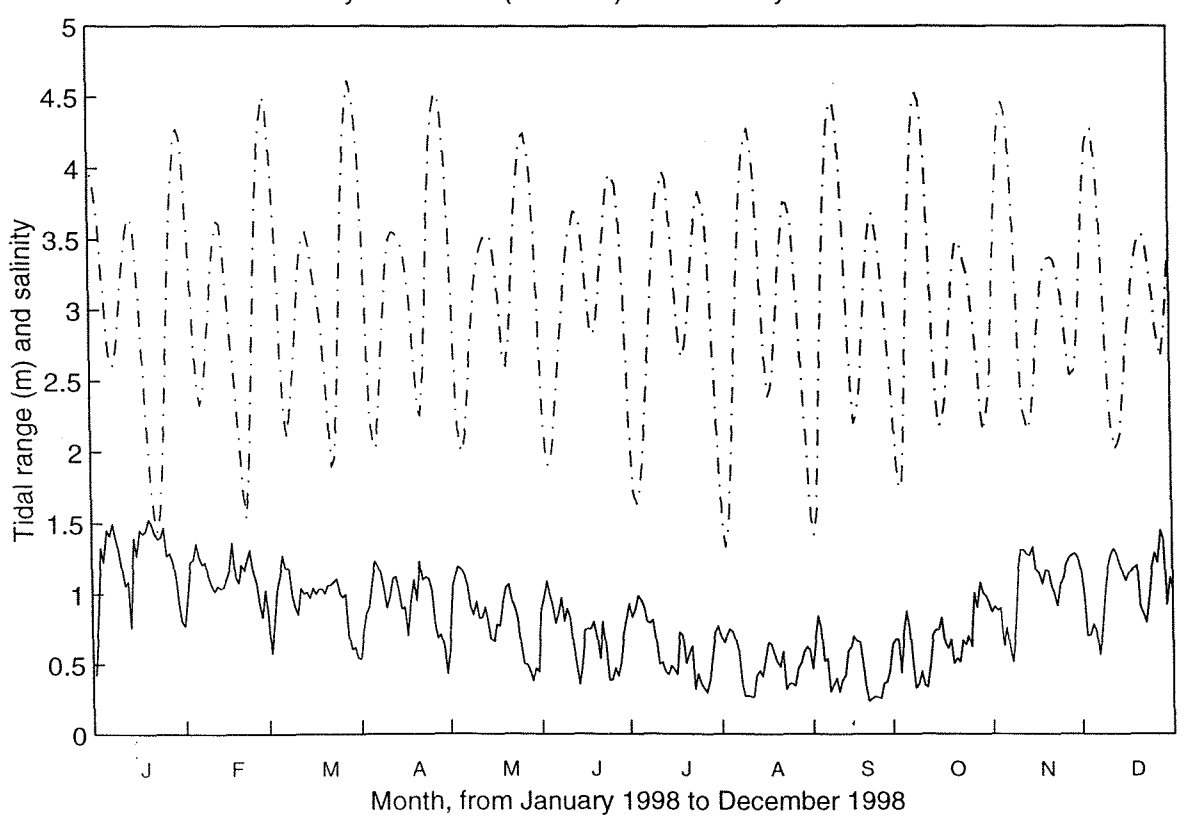

Figure 7.3 Annual variation of the surface salinity at a) NW Netley and b) Calshot Buoy: comparison between observations and model output

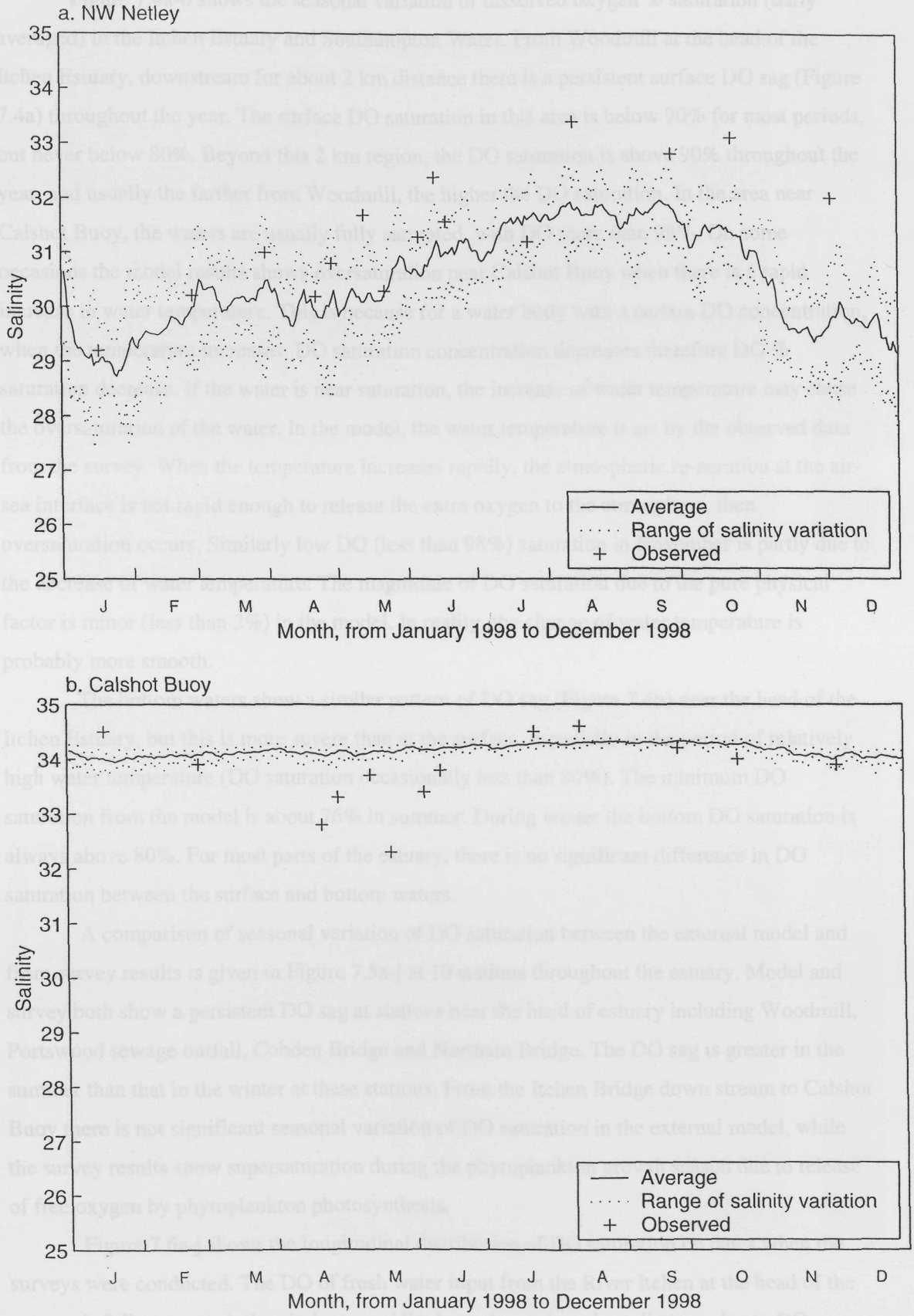

7.3.2 Dissolved oxygen

Figure 7.4a-b shows the seasonal variation of dissolved oxygen % saturation (daily averaged) in the Itchen Estuary and Southampton Water. From Woodmill at the head of the Itchen Estuary, downstream for about 2 km distance there is a persistent surface DO sag (Figure 7.4a) throughout the year. The surface DO saturation in this area is below 90% for most periods, but never below 80%. Beyond this 2 km region, the DO saturation is above 90% throughout the year, and usually the farther from Woodmill, the higher the DO saturation. In the area near Calshot Buoy, the waters are usually fully saturated, with DO more than 98%. On some occasions the model results shows oversaturation near Calshot Buoy when there is a rapid increase in water temperature. This is because for a water body with a certain DO concentration, when the temperature increases, DO saturation concentration decreases therefore DO % saturation decrease. If the water is near saturation, the increase of water temperature may cause the oversaturation of the water. In the model, the water temperature is set by the observed data from the survey. When the temperature increases rapidly, the atmospheric re-aeration at the air-sea interface is not rapid enough to release the extra oxygen to the atmosphere, then oversaturation occurs. Similarly low DO (less than 98%) saturation in November is partly due to the decrease of water temperature. The magnitude of DO saturation due to the pure physical factor is minor (less than 2%) in the model. In reality, the change of water temperature is probably more smooth.

The bottom waters show a similar pattern of DO sag (Figure 7.4b) near the head of the Itchen Estuary, but this is more severe than at the surface, especially in the period of relatively high water temperature (DO saturation occasionally less than 80%). The minimum DO saturation from the model is about 76% in summer. During winter the bottom DO saturation is always above 80%. For most parts of the estuary, there is no significant difference in DO saturation between the surface and bottom waters.

A comparison of seasonal variation of DO saturation between the external model and from survey results is given in Figure 7.5a-j at 10 stations throughout the estuary. Model and survey both show a persistent DO sag at stations near the head of estuary including Woodmill, Portswood sewage outfall, Cobden Bridge and Northam Bridge. The DO sag is greater in the summer than that in the winter at these stations. From the Itchen Bridge down stream to Calshot Buoy there is not significant seasonal variation of DO saturation in the external model, while the survey results show supersaturation during the phytoplankton growth season due to release of free oxygen by phytoplankton photosynthesis.

Figure 7.6a-j shows the longitudinal distribution of DO saturation on dates when the surveys were conducted. The DO of fresh water input from the River Itchen at the head of the estuary is fully saturated, then it drops rapidly downstream in a short distance due to DO

Figure 7.4 Seasonal variation of a) surface and b) bottom DO saturation (%) from external model in the Itchen Estuary and Southampton Water

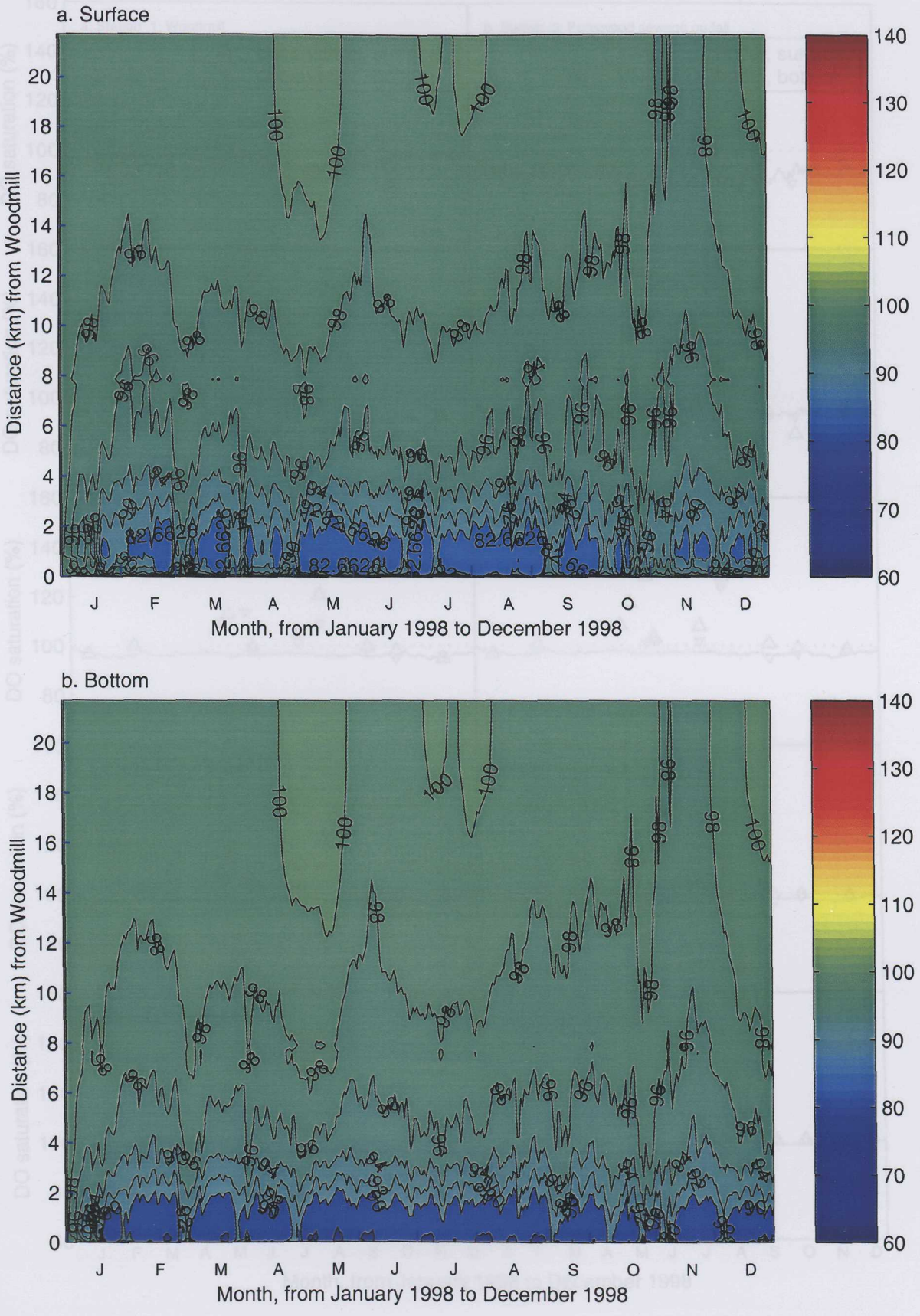

Figure 7.5a–j Seasonal variation of DO saturation (%), comparison between external model results and observations at 10 survey stations

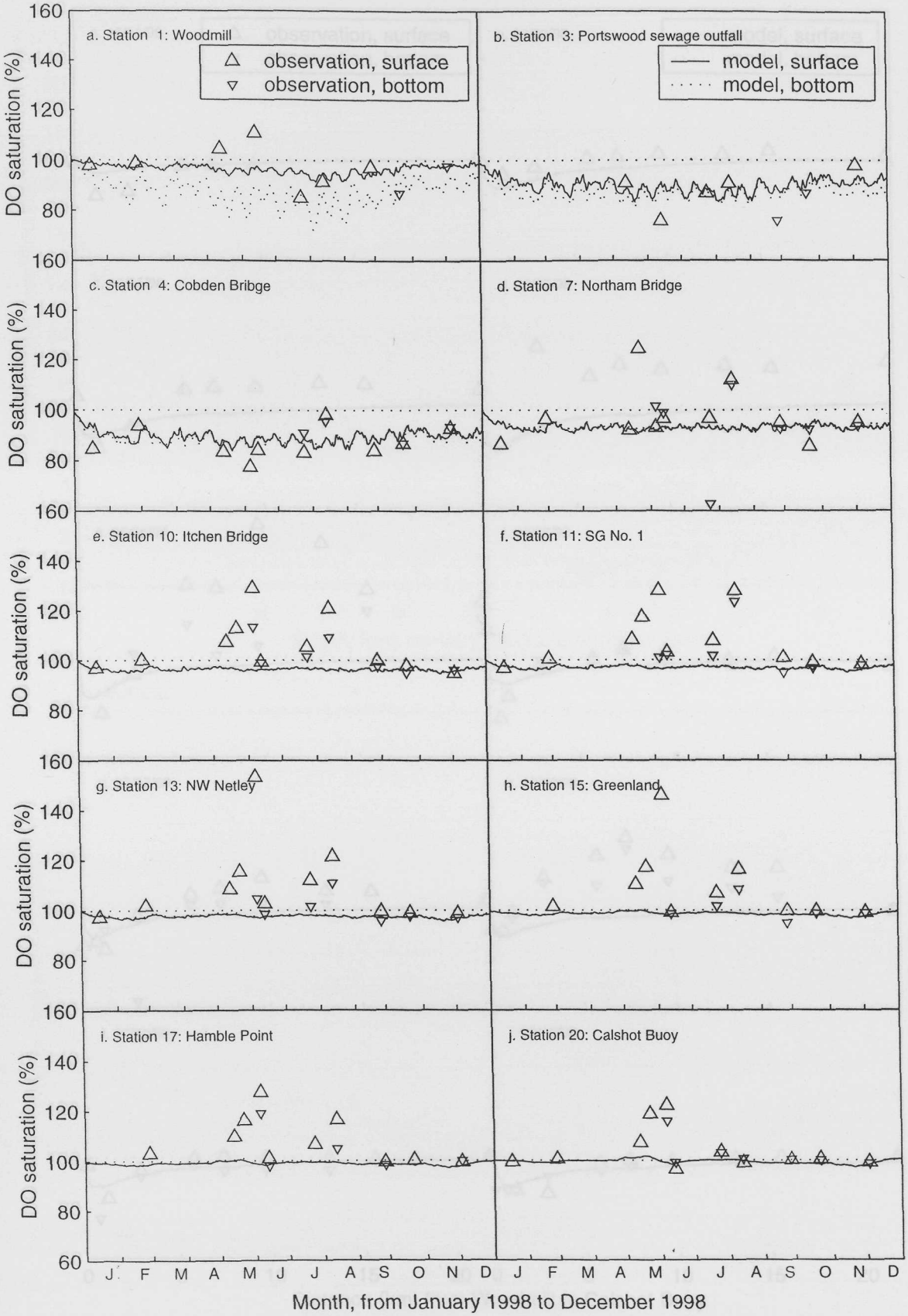

Figure 7.6a–j Longitudinal distribution of DO saturation (%), comparison between external model results and observations in 1998

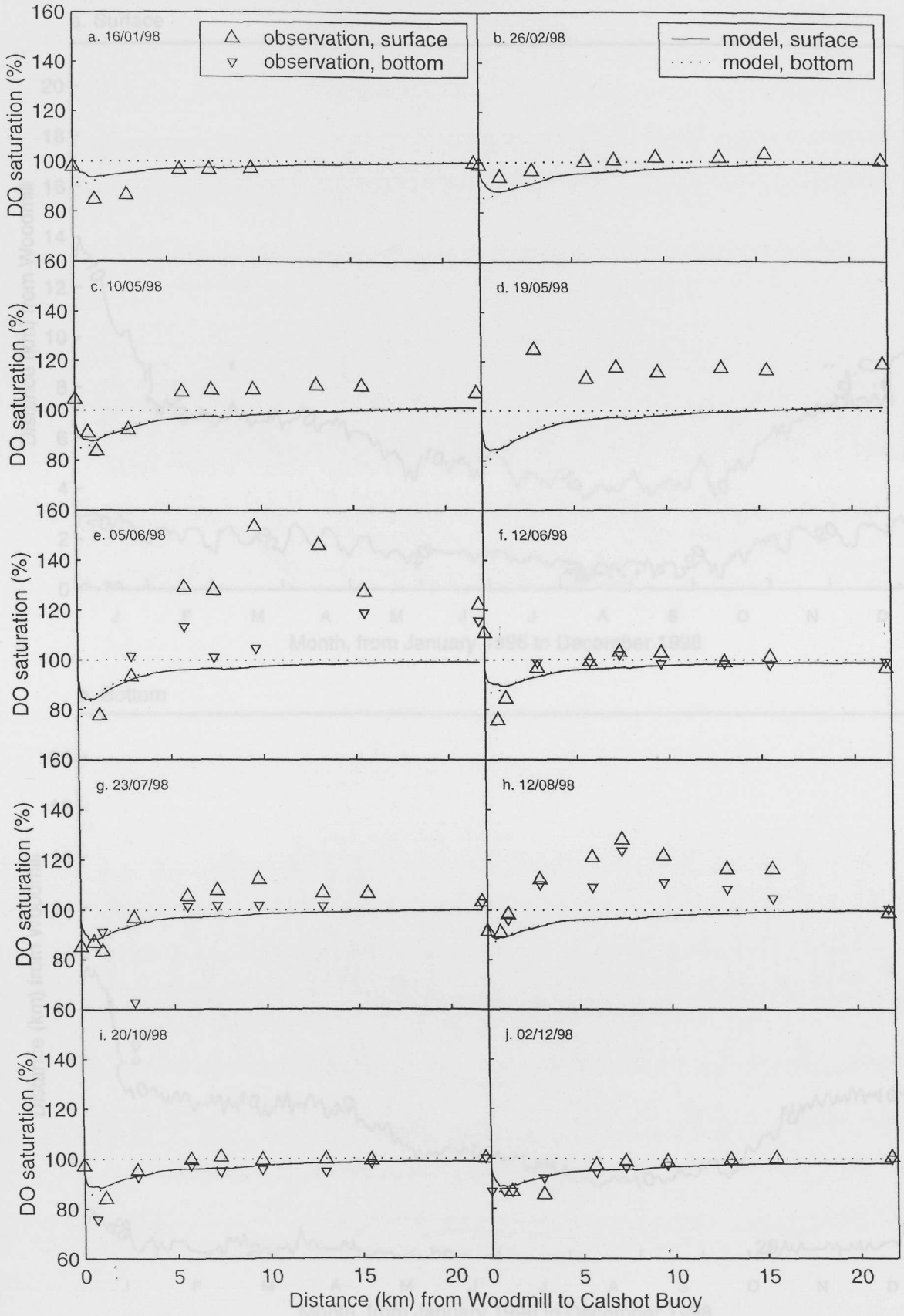

Figure 7.7 Seasonal variation of a) surface and b) bottom dissolved carbonaceous biochemical oxygen demand (umol O2 l^{-1}) in the Itchen Estuary and Southampton Water

a. Surface

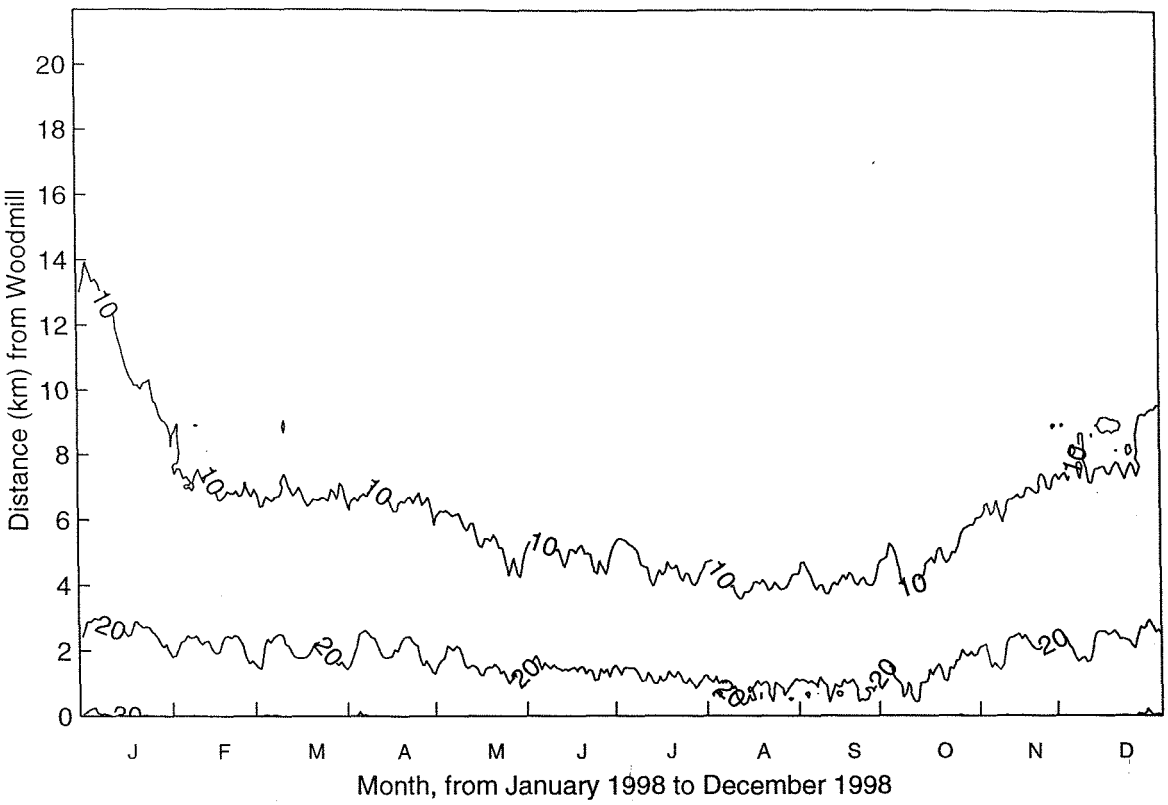

b. Bottom

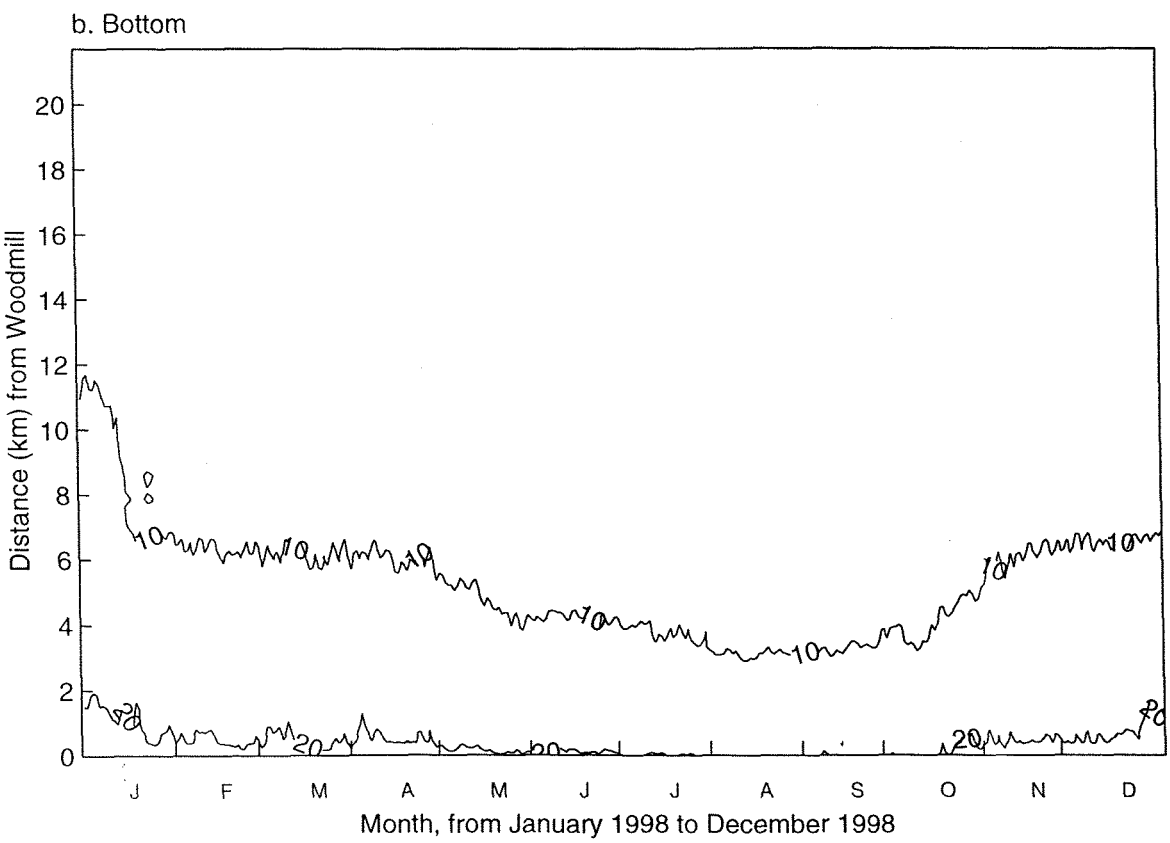

Figure 7.8 Seasonal variation of a) surface and b) bottom particulate carbonaceous biochemical oxygen demand (umol O2 l^{-1}) in the Itchen Estuary and Southampton Water

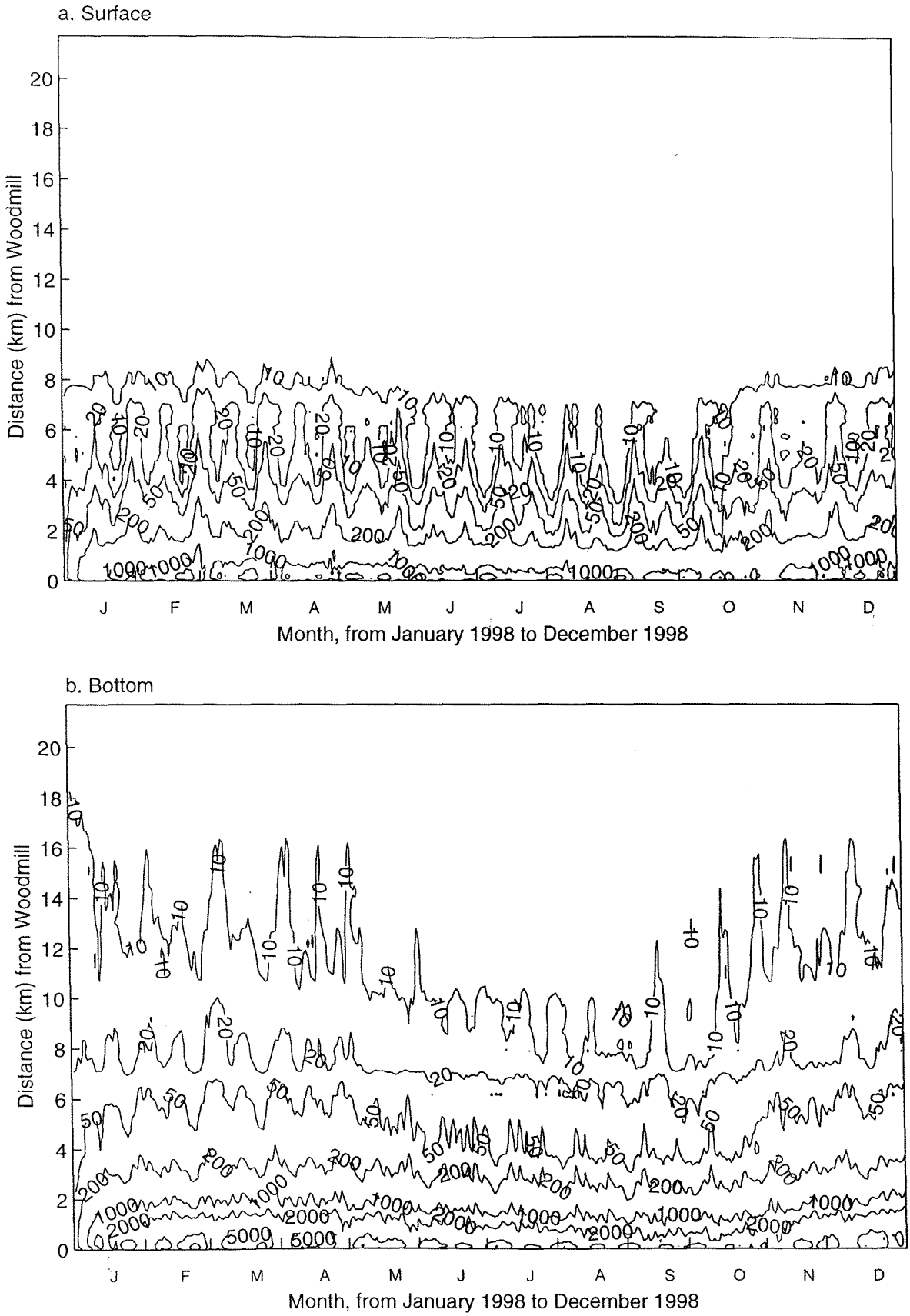

consumption by external BOD loads. The DO, after reaching a minimum value near Portswood sewage outfall (0.68 km) and Cobden Bridge (1.12 km) recovers downstream to a value approaching 100%. The model has successfully simulated the DO sag for all periods of the year, but the DO saturation values are relatively low downstream compared with the survey result during the phytoplankton growth season, when DO supersaturation was observed during the survey.

7.3.3 Oxygen demanding matter

There are only two processes which consume dissolved oxygen in the external model, one is oxidation of organic oxygen demanding matter, and the other is the nitrification of ammonia nitrogen. The BOD is the main sink of dissolved oxygen, and the impact of nitrification is minor to the DO concentration. The total year averaged BOD load into the Itchen Estuary is about 970 kg d^{-1}, of which about 780 kg d^{-1} comes from the Itchen River (HR Wallingford, 1995). Of the BOD load from the River Itchen, about 50% is dissolved carbonaceous biochemical oxygen demand, and half is particulate organic oxygen demanding matter.

The surface dissolved carbonaceous biochemical oxygen demand concentration (Figure 7.7a) range is between 5.0-30.0 μmol l^{-1}. The bottom concentration (Figure 7.7b) range between 3.0-23.0 which is lower than the surface concentration. The estuarine circulation contributes to this surface/bottom difference. In the summer the BOD load is lower than the winter due to the reduced river flow in the summer. The seasonal variation of the dissolved carbonaceous biochemical oxygen demand concentration (Figure 7.7a-b) reflects this factor.

The distribution of particulate organic oxygen demanding matter is quite different to the distribution of the dissolved organic oxygen demanding matter (Figure 7.8a-b). The maximum surface particulate organic matter concentration near the head of the estuary (Figure 7.8a) is about 1000-2000 μmol l^{-1}. The concentration decreases downstream to about 10 μmol l^{-1} near Dockhead (8 km from Woodmill), where the Itchen Estuary joins Southampton Water. The surface particulate organic matter shows a strong pattern of half-month oscillation, which is related to the spring neap cycle of tidal currents.

The bottom particulate organic matter concentrations (Figure 7.8b) are much higher than the surface concentration due the sedimentation of particulate matter. The concentration can be as high as 5000 μmol l^{-1}. There is apparent accumulation of particulate organic matter near the head of the estuary, where the landward bottom estuarine circulation ends.

7.3.4 Inorganic nutrients

The inorganic nutrients, including ammonium, nitrite and phosphate have been modelled in the external model.

Figure 7.9 Seasonal variation of a) surface and b) bottom ammonium concentration (umol l^{-1}) from external model in the Itchen Estuary and Southampton Water

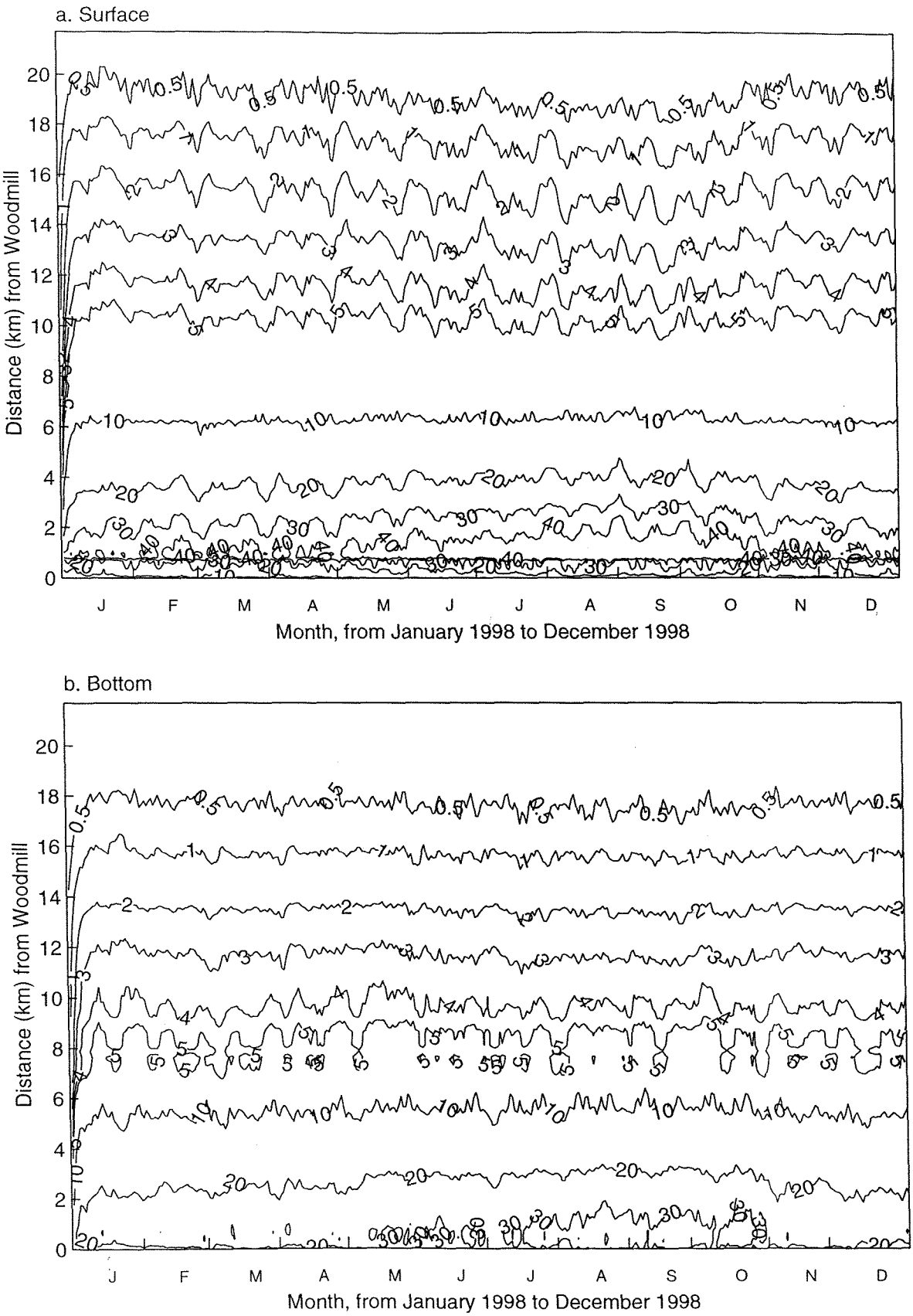

Figure 7.10 Seasonal variation of a) surface and b) bottom nitrate concentration (umol l^{-1}) from external model in the Itchen Estuary and Southampton Water

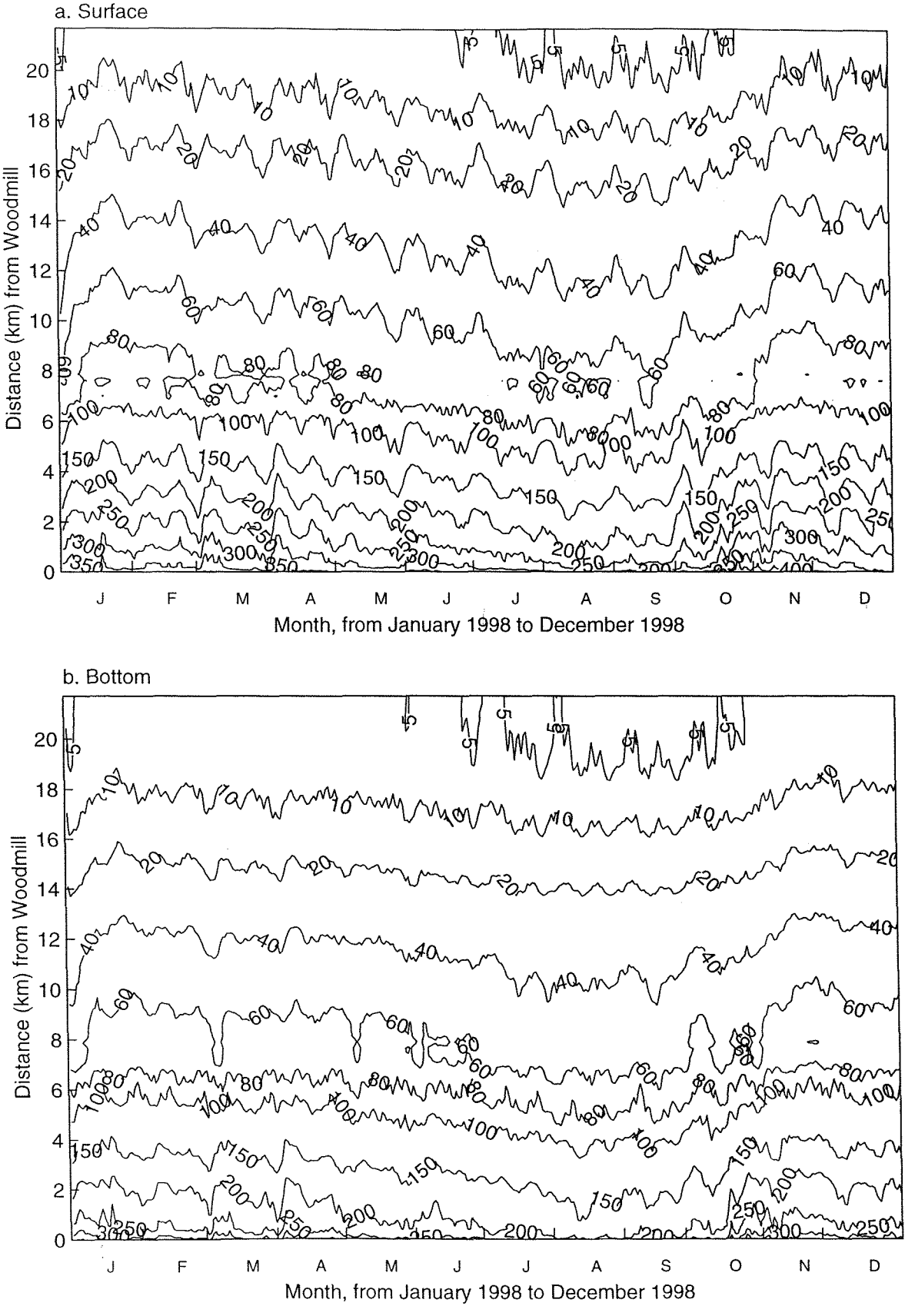

Figure 7.11 Annual variation of the surface nitrate, phosphate concentration at NW Netley and Calshot Buoy: comparison between observations and external model output

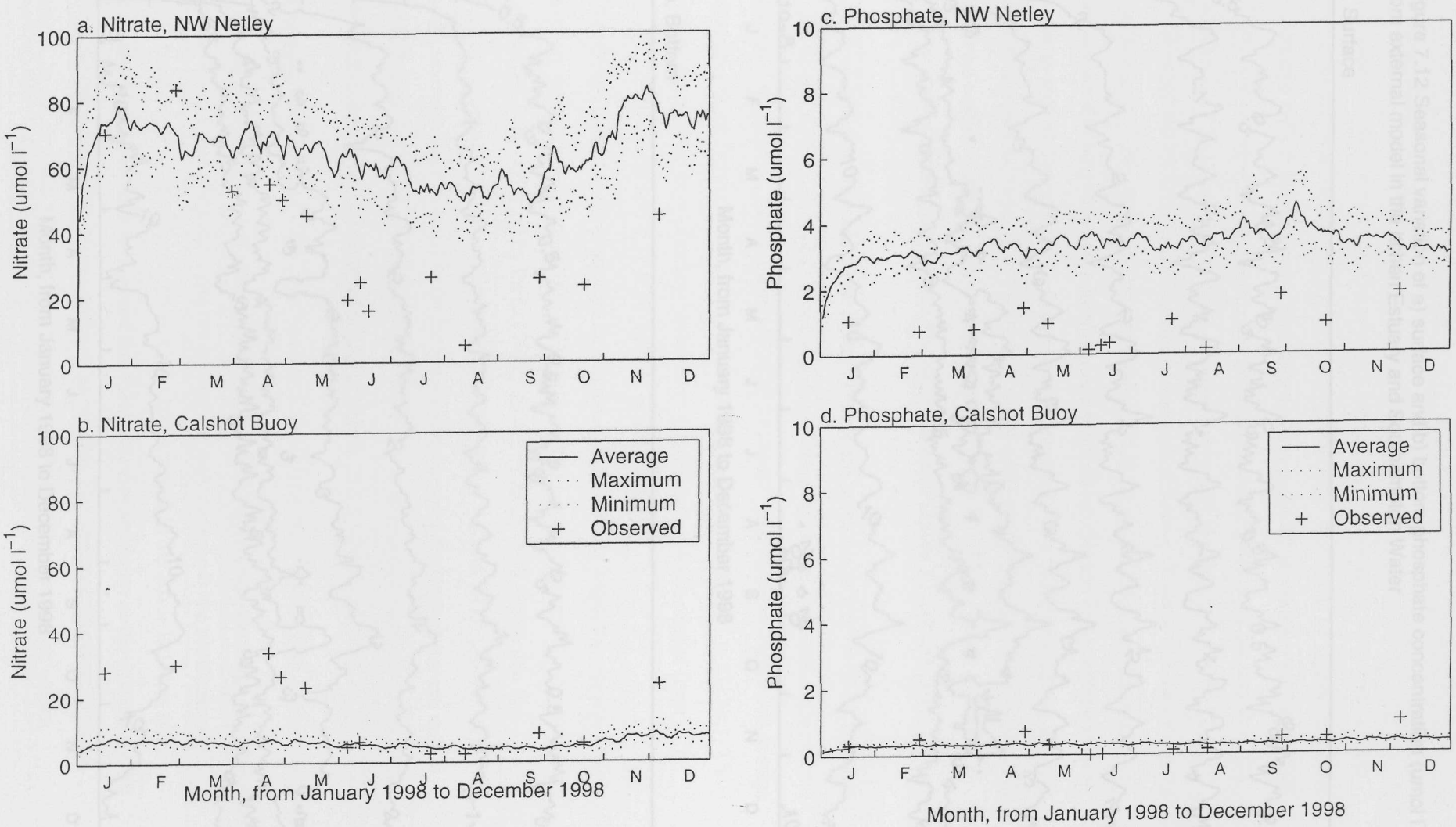

Figure 7.12 Seasonal variation of a) surface and b) bottom phosphate concentration (umol l^{-1}) from external model in the Itchen Estuary and Southampton Water

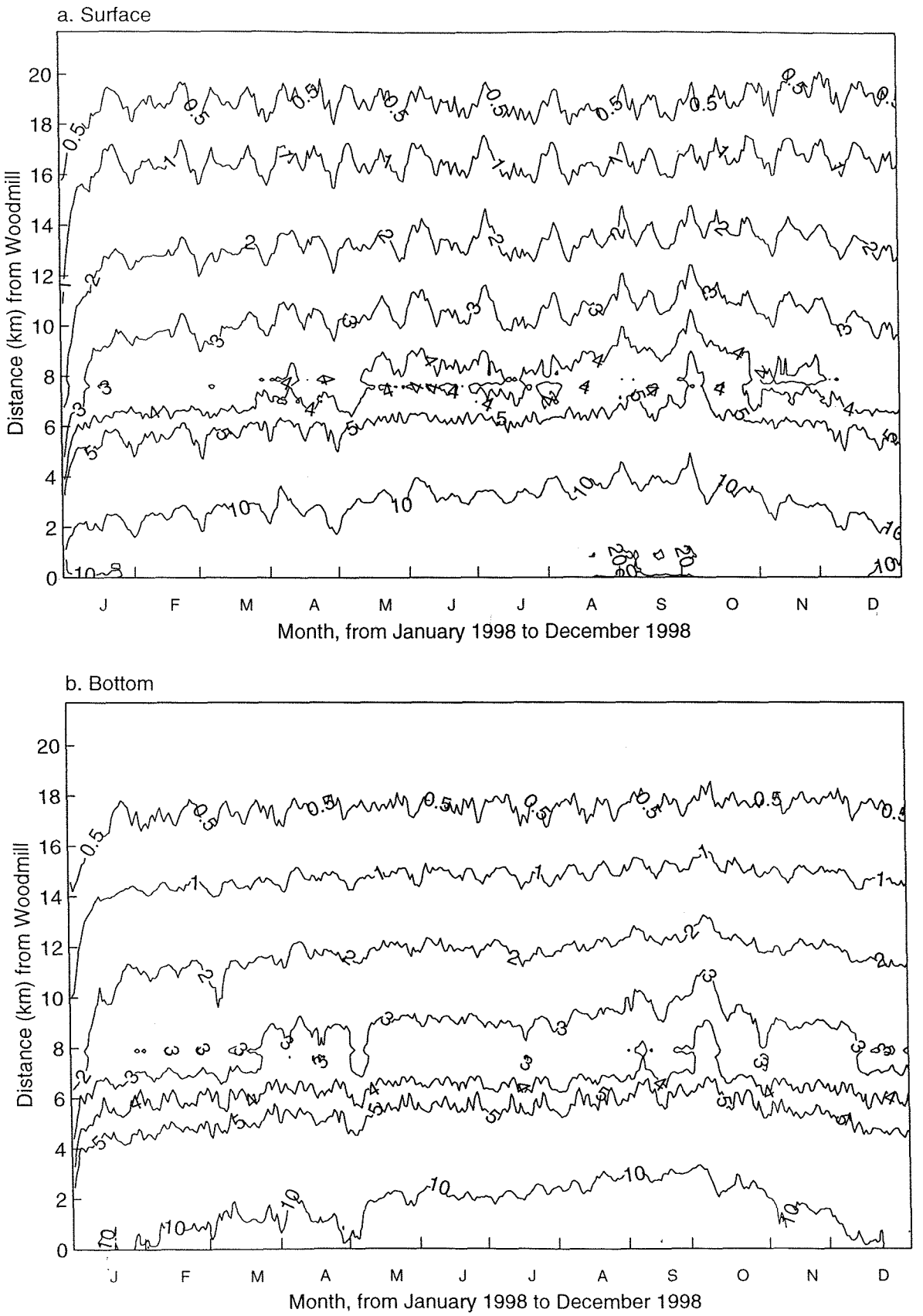

7.3.4.1 Ammoniacal nitrogen

The direct loads of ammonium in estuaries are mainly from point sources like sewage effluent rather than riverine discharge. Ammonium derived from hydrolysis of organic nitrogen is minor compared with direct discharge. The main sources in the Itchen Estuary are Portswood Sewage Plant, near the head of the estuary, and Woolston Sewage Plant, near the mouth of the estuary, with loads of 520 kg d^{-1} and 260 kg d^{-1} respectively (HR Wallingford, 1995). The impact of the direct discharge of ammonium from Portswood Sewage Plant is apparent from the model results (Figure 7.9a). At the Portswood Sewage Plant (about 700 m from Woodmill) where effluents are discharged, surface ammonium concentration (Figure 7.9a) shows a peak, which can be as high as 50 μmol l^{-1}. The ammonium concentration is stable throughout the year, without significant seasonal variation. The bottom water ammonium concentration (Figure 7.9b) is lower than the surface concentration.

Ammonium concentration was not routinely measured during all surveys. The observation made by Southern Water Authority during 1976-1980 suggested that the surface ammonium concentration observed in the Itchen Estuary are in the range from 8.07-12.14 μmol l^{-1} in the winter and 4.35-7.14 μmol l^{-1} in the summer. During the winter the value observed at Woodmill was 8.07 μmol l^{-1}, then it increased to 12.14 μmol l^{-1} just after the Portswood sewage outfall, then decreased further downstream to a concentration of 9.93 μmol l^{-1} at SG No1. The winter surface ammonium concentration observed in Southampton Water ranged from 5.78-15.12 μmol l^{-1} in the winter and 4.71-8.21 μmol l^{-1} in the summer.

In a more recent survey conducted by Southern Water in July 1994, the ammonium concentrations observed were from 0.00-14.28 μmol l^{-1} at Ocean Village to 14.28-71.42 μmol l^{-1} at Cobden Bridge. Data collected by Pietri (1998) during summer 1998 shown that the ammonium concentration of fresh water from the Itchen River is about 20.00 μmol l^{-1}. The ammonium concentration increased in the Itchen Estuary between Portswood sewage outfall and Cobden Bridge to a range of 40.00-110.00 μmol l^{-1}, then ammonium concentrations were diluted downstream to below 10.00 μmol l^{-1} at Dockhead.

7.3.4.2 Nitrate

The main direct sources of nitrate to the estuary are from riverine discharge (2,000 kg d^{-1} from Itchen River , year averaged), and the second but minor source is the nitrification of ammonium from the sewage effluent. The nitrate concentration in the River Itchen is quite stable throughout the year, so it is expected that the nitrate concentration in the external model will follow the same pattern of annual variation as salinity. The seasonal variation of nitrate concentration in the external model is shown in Figure 7.10a-b. The decrease of nitrate

concentration in July, August and September are directly the results of the decrease of riverine discharge during these months. The model overestimates the nitrate concentration at NW Netley (9.59 km) (Figure 7.11a) during the phytoplankton growth season, and underestimates it at Calshot Buoy (21.70 km) (Figure 7.11b).

7.3.4.3 Phosphate

The main sources of phosphate to the Itchen Estuary are the Itchen River (120 kg d^{-1} in average) and Portswood sewage outfall (130 kg d^{-1}). The phosphate concentration from the Itchen River (Table 3.4, Figure 3.17a) is almost double during the summer, although the total phosphate loads do not show much variation. Seasonal variation of phosphate concentration (Figure 7.12a-b) shows the tendency of this increase with an increase of surface and bottom phosphate concentration in the Itchen Estuary especially in the upper parts of the estuary during summer and autumn. In comparison to survey data, the model overestimates the phosphate concentration at NW Netley (Figure 7.11c), and generally shows the right range of phosphate at Calshot Buoy (Figure 7.11d).

7.3.4.4 Nutrients against salinity

The nutrient concentrations derived from the external model are plotted (Figure 7.13 – 7.15) against salinity to compare with data from three transect surveys. During the winter (02/12/98) the model output for nitrate and phosphate (Figure 7.13a, c) fits the observations quite well. Figure 7.13a shows a linear dilution of nitrate over its complete range of salinity (0-35). The divergence of the ammonium and phosphate from the linear dilution line (Figure 7.13b-c) in the low salinity region is due to the inputs from the Portswood sewage effluent. The surface ammonium concentration (Figure 7.13b) is about 7.00 μmol l^{-1} at low salinity and it increase sharply to about 40.00 μmol l^{-1} at a point with salinity of 12, where the sewage discharges in to the Itchen Estuary. Not far from the point where sewage is discharged, the surface and bottom ammonium and phosphate concentrations are close to the dilution line. Figure 7.13b-c indicates how significant the impact of the Portswood sewage outfall is on the water quality (ammonium and phosphate) in the estuary. In comparison, the contribution of Portswood sewage effluent towards nitrate concentration in the estuary is trivial.

During the first (diatom) bloom on 05/06/98, the nutrient concentrations from the external model (Figure 7. 14a, c) are mostly higher than the observed values. During the second (*Mesodinium*) bloom, similarly, the model results (Figure 7.15a, c) do not fit the observation, compared with the winter results (Figure 7.13a, c).

From Figure 7.13-7.15, the external model results show evidence of addition of nitrate and phosphate, i.e. model results above dilution line connecting highest salinity and lowest salinity data point, whereas the ammonium model output indicates removal due to nitrification.

Figure 7.13 Nutrients (daily averaged output (external model), observations) plotted against salinity in the Itchen Estuary and Southampton Water, 02/12/98

Figure 7.13a Nitrate against salinity

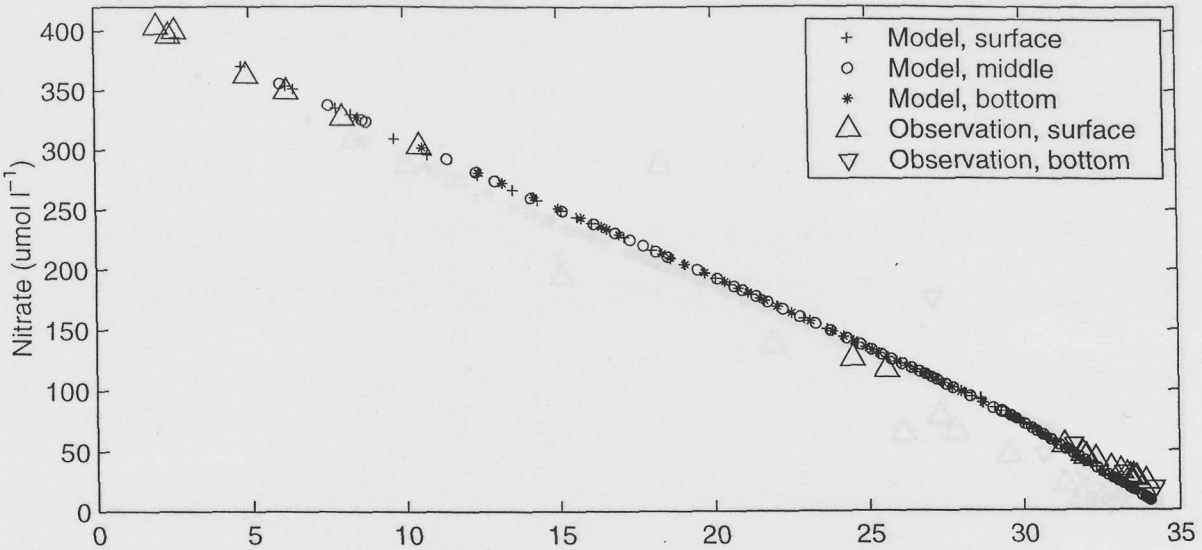

Figure 7.13b Ammonium against salinity

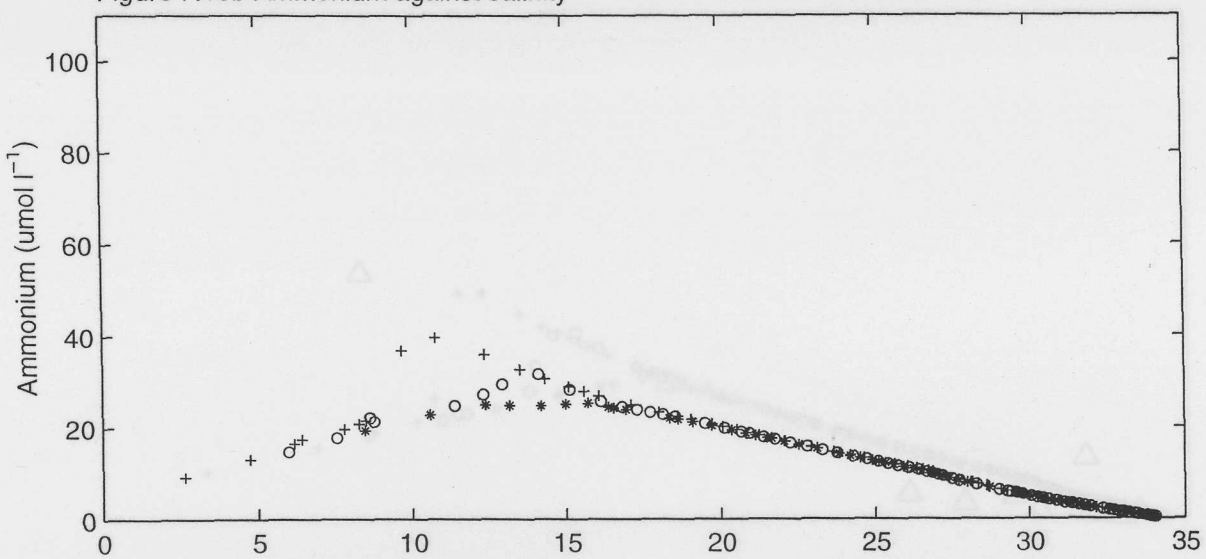

Figure 7.13c Phosphate against salinity

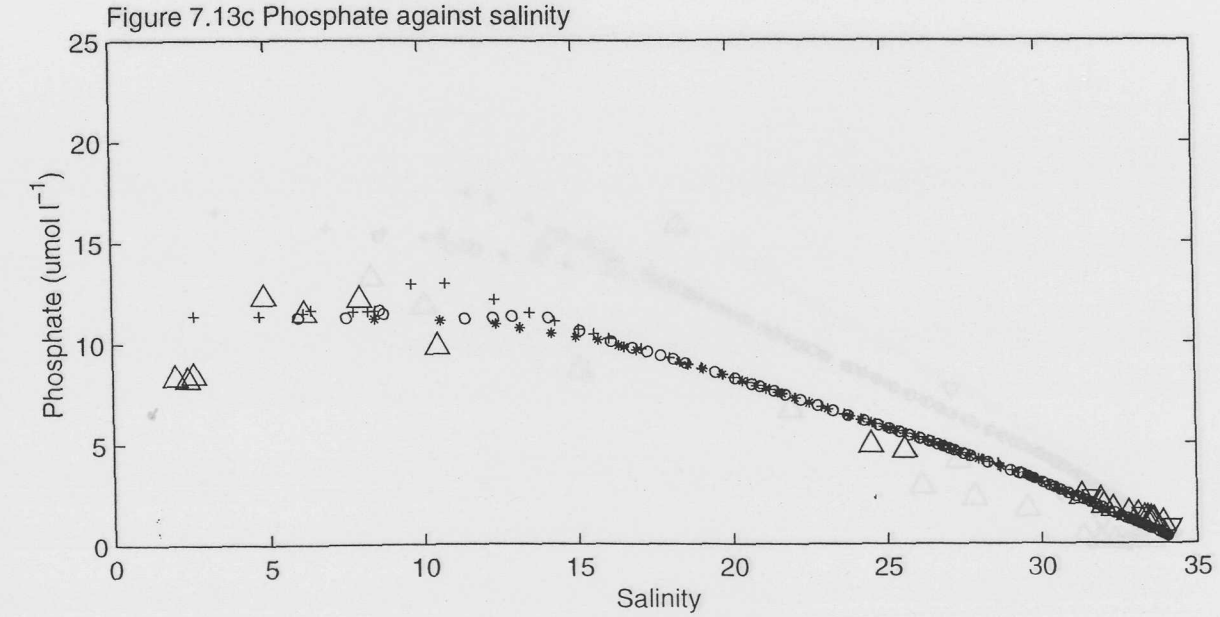

Figure 7.14 Nutrients (daily averaged output (external model), observations) plotted against salinity in the Itchen Estuary and Southampton Water, 05/06/98

Figure 7.14a Nitrate against salinity

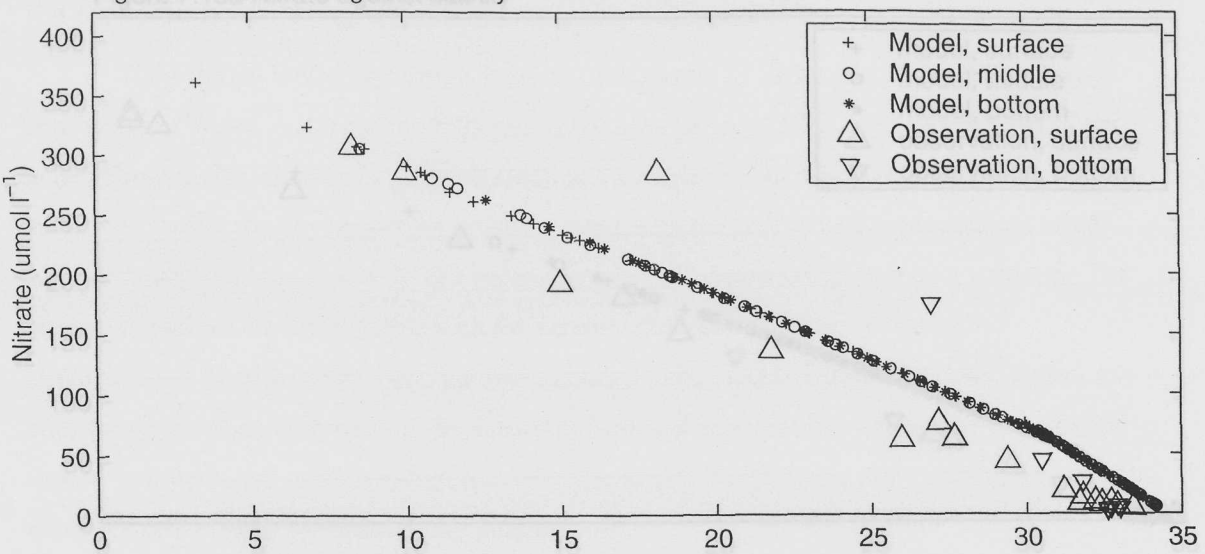

Figure 7.14b Ammonium against salinity

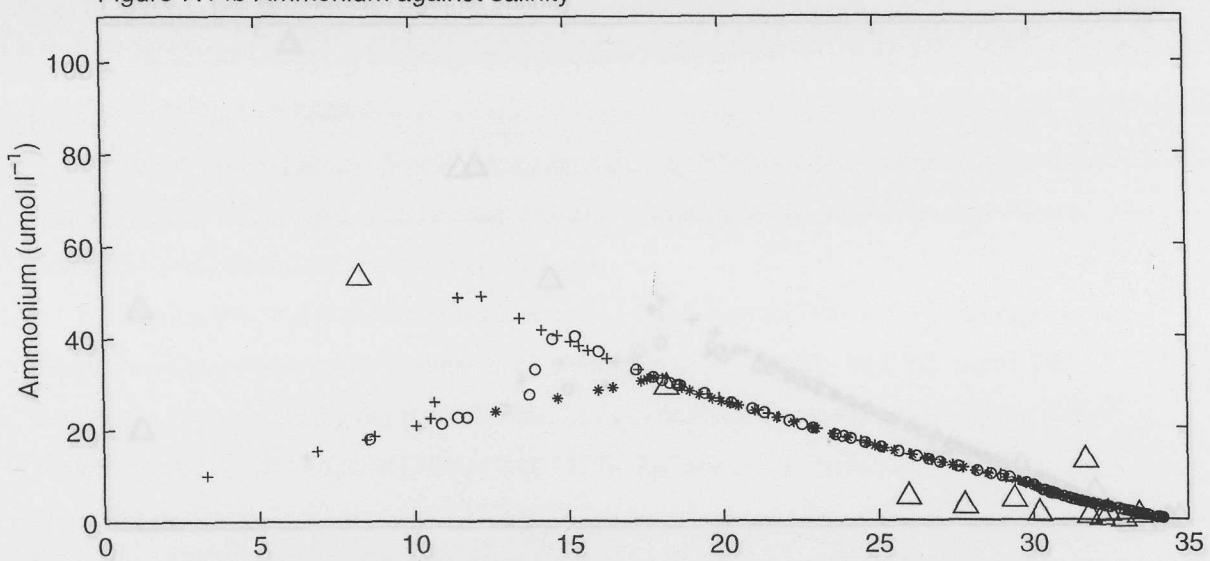

Figure 7.14c Phosphate against salinity

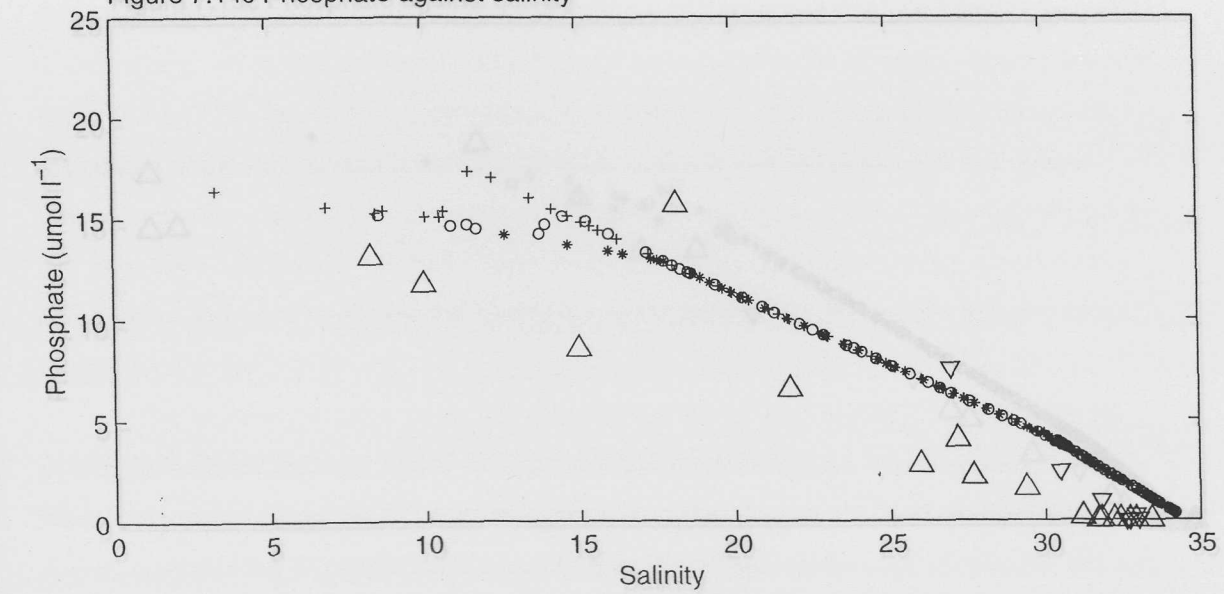

Figure 7.15 Nutrients (daily averaged output (external model), observations) plotted against salinity in the Itchen Estuary and Southampton Water, 12/08/98

Figure 7.15a Nitrate against salinity

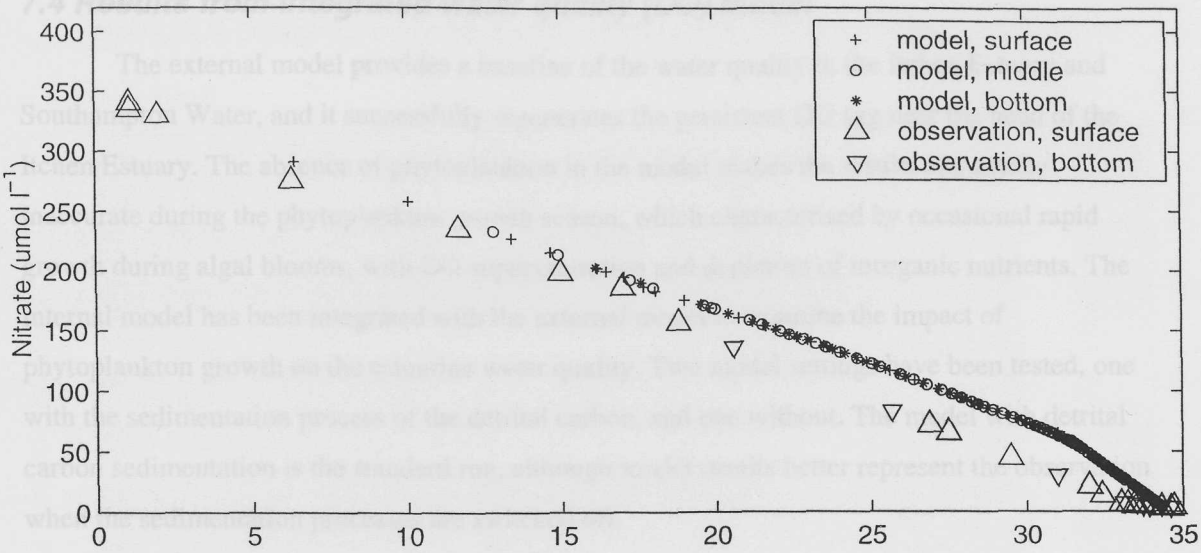

Figure 7.15b Ammonium against salinity

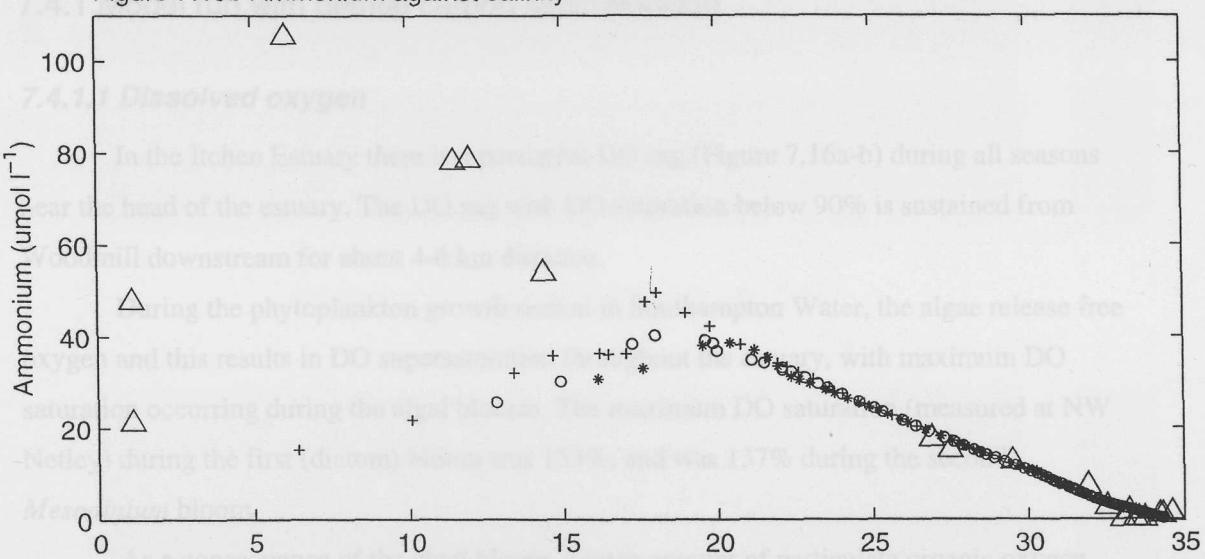

Figure 7.15c Phosphate against salinity

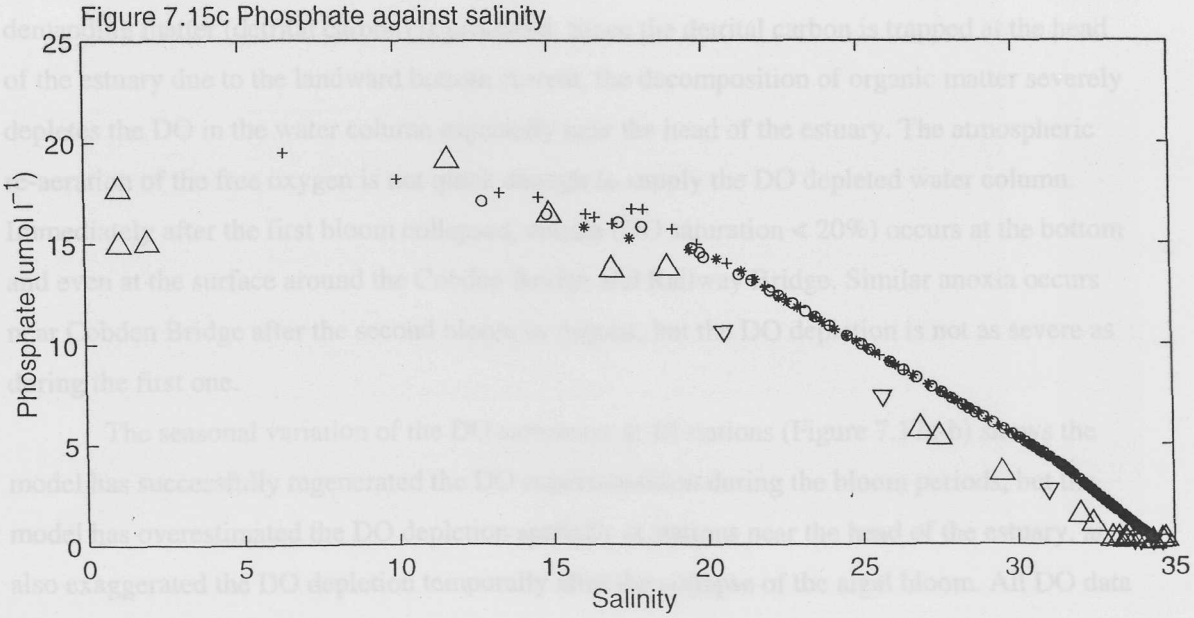

7.4 Results from integrated water quality (DO) model

The external model provides a baseline of the water quality in the Itchen Estuary and Southampton Water, and it successfully regenerates the persistent DO sag near the head of the Itchen Estuary. The absence of phytoplankton in the model makes the results apparently inaccurate during the phytoplankton growth season, which characterised by occasional rapid growth during algal blooms, with DO supersaturation and depletion of inorganic nutrients. The internal model has been integrated with the external model to examine the impact of phytoplankton growth on the estuarine water quality. Two model settings have been tested, one with the sedimentation process of the detrital carbon, and one without. The model with detrital carbon sedimentation is the standard run, although model results better represent the observation when the sedimentation processes are switched off.

7.4.1 Model run with detrital carbon sedimentation

7.4.1.1 Dissolved oxygen

In the Itchen Estuary there is a persistent DO sag (Figure 7.16a-b) during all seasons near the head of the estuary. The DO sag with DO saturation below 90% is sustained from Woodmill downstream for about 4-6 km distance.

During the phytoplankton growth season in Southampton Water, the algae release free oxygen and this results in DO supersaturation throughout the estuary, with maximum DO saturation occurring during the algal blooms. The maximum DO saturation (measured at NW Netley) during the first (diatom) bloom was 153%, and was 137% during the second *Mesodinium* bloom.

As a consequence of the algal bloom, a large amount of particulate organic oxygen demanding matter (detrital carbon) is produced. Since the detrital carbon is trapped at the head of the estuary due to the landward bottom current, the decomposition of organic matter severely depletes the DO in the water column especially near the head of the estuary. The atmospheric re-aeration of the free oxygen is not quick enough to supply the DO depleted water column. Immediately after the first bloom collapsed, anoxia (DO saturation < 20%) occurs at the bottom and even at the surface around the Cobden Bridge and Railway Bridge. Similar anoxia occurs near Cobden Bridge after the second bloom in August, but the DO depletion is not as severe as during the first one.

The seasonal variation of the DO saturation at 10 stations (Figure 7.17a-b) shows the model has successfully regenerated the DO supersaturation during the bloom periods, but the model has overestimated the DO depletion spatially at stations near the head of the estuary, and also exaggerated the DO depletion temporally after the collapse of the algal bloom. All DO data

Figure 7.16 Seasonal variation of a) surface and b) bottom DO saturation (%) from integrated model (with sedimentation) in the Itchen Estuary and Southampton Water

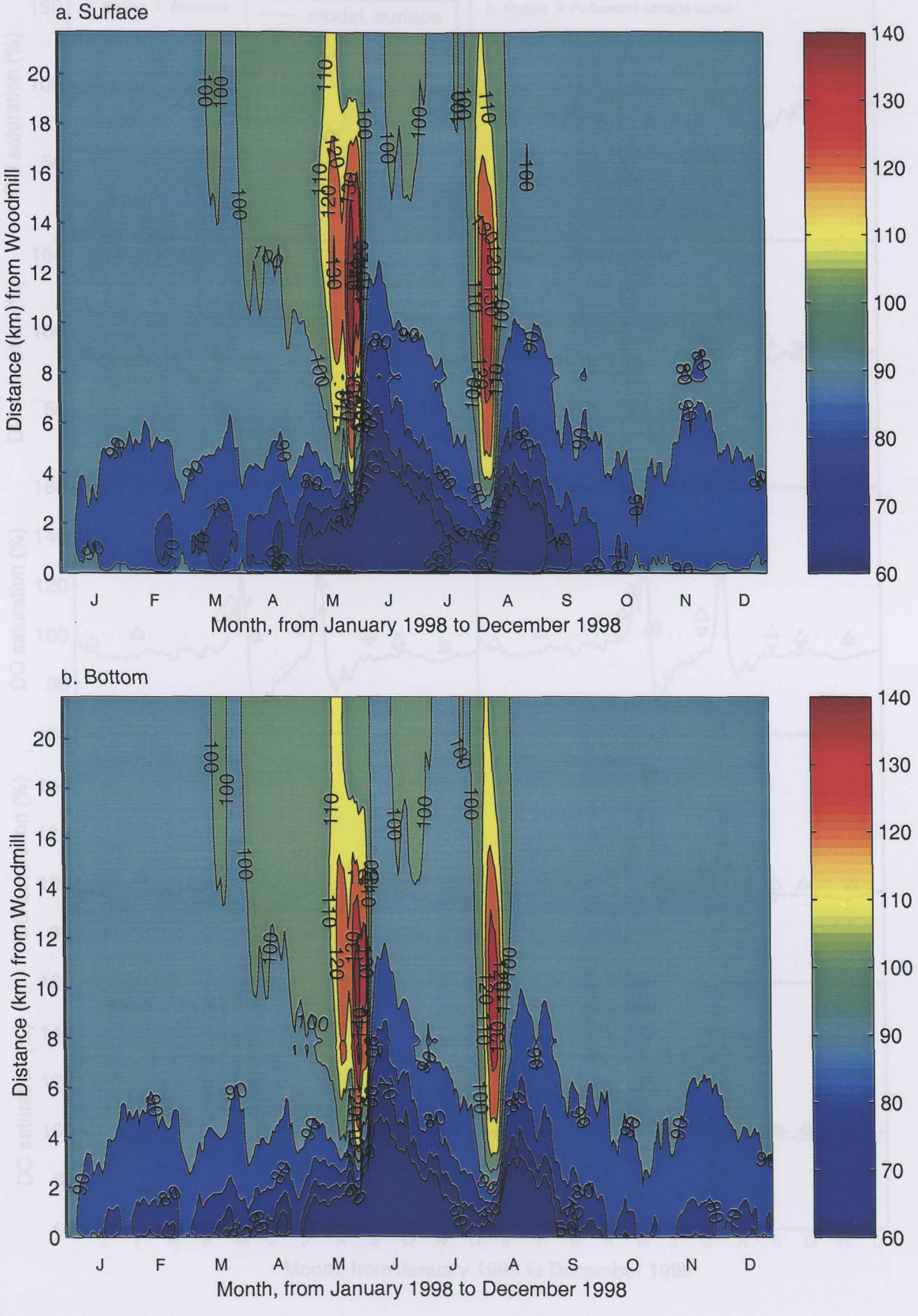

Figure 7.17a–j Seasonal variation of DO saturation (%), comparison between integrated model (with sedimentation) results and observations at 10 survey stations

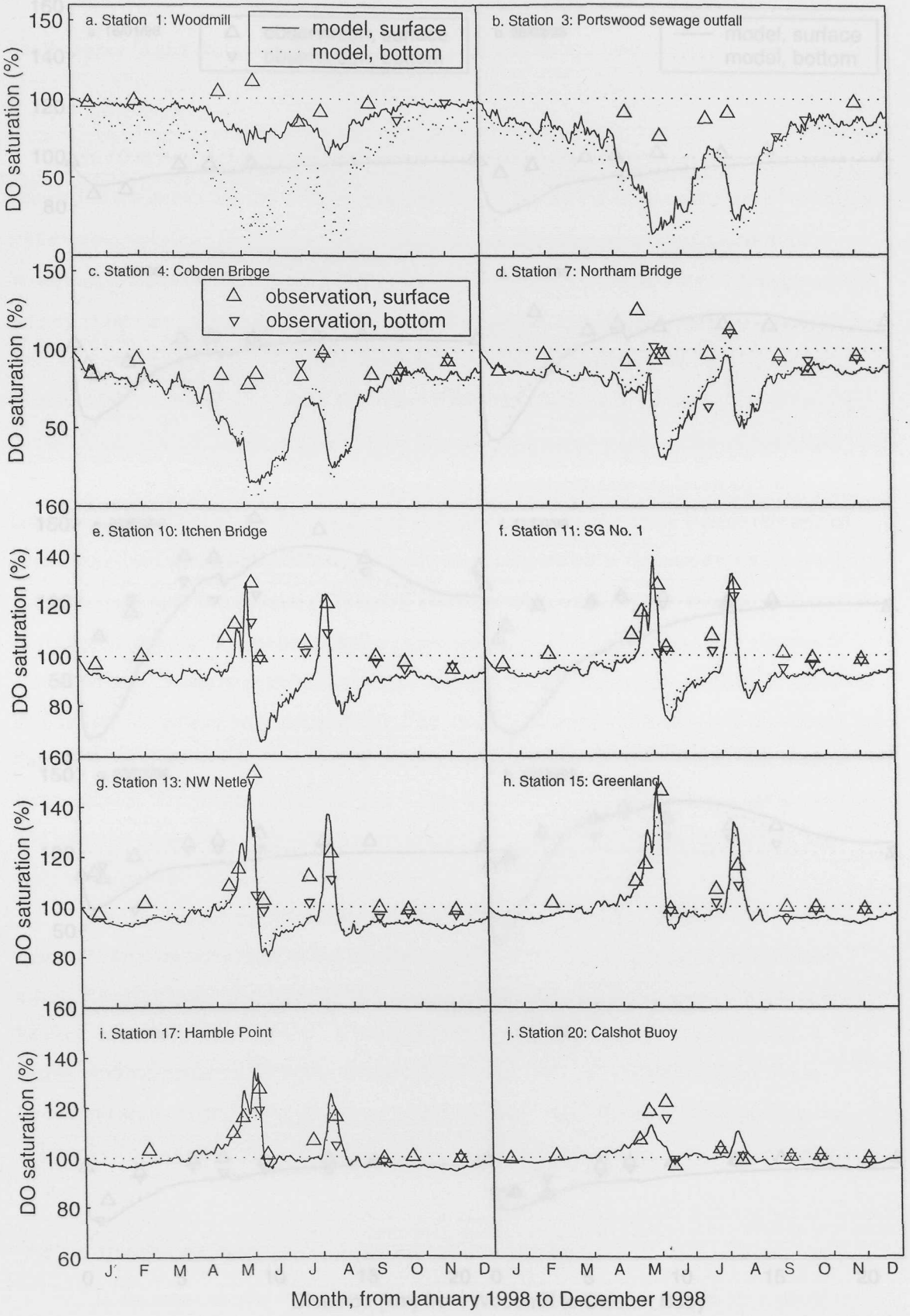

Figure 7.18a–j Longitudinal distribution of DO saturation (%), comparison between integrated model (with sedimentation) results and observations in 1998

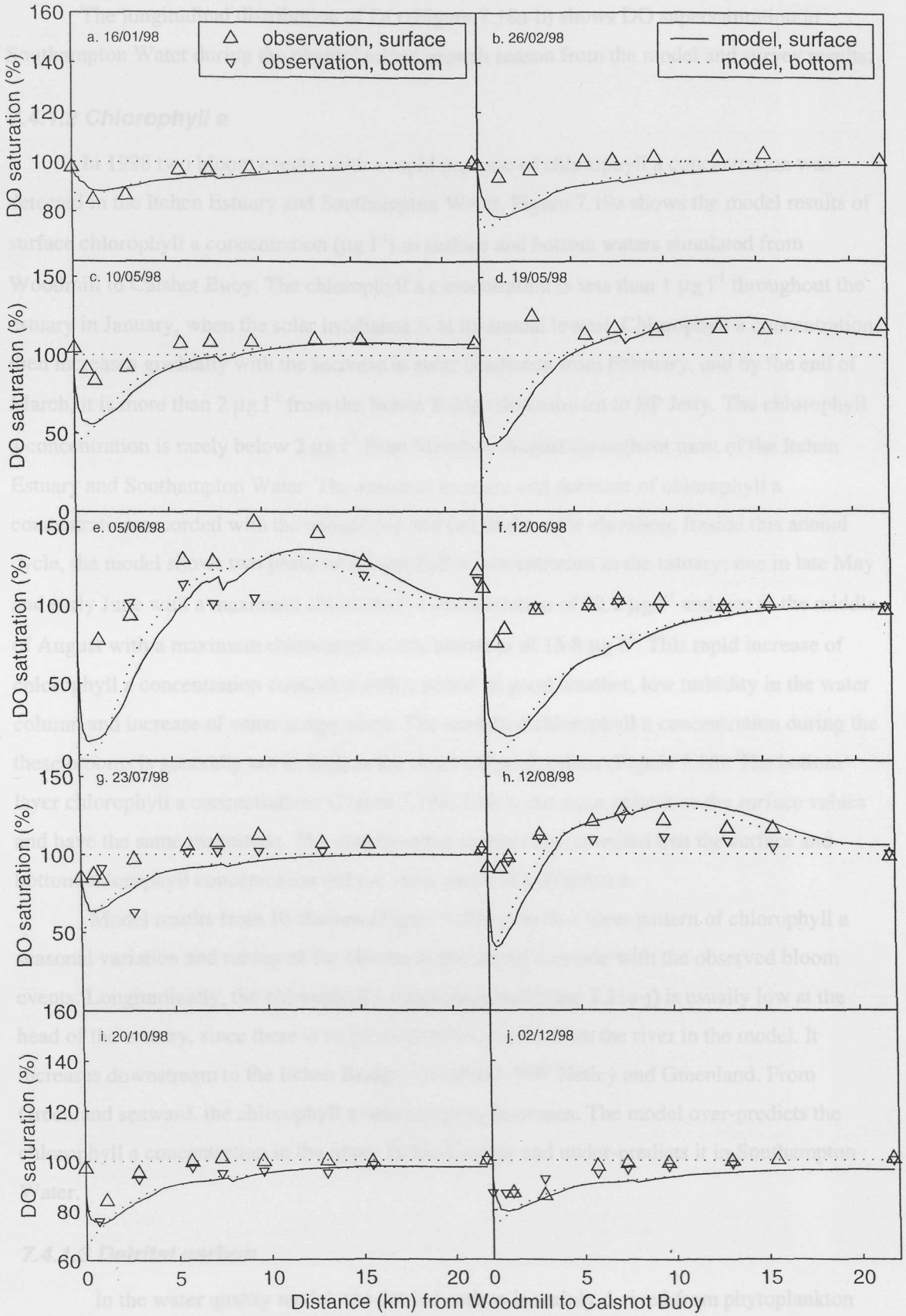

from the transect survey are above 64% saturation, while the model shows a value of below 10% saturation above Cobden Bridge.

The longitudinal distribution of DO (Figure 7.18a-b) shows DO supersaturation in Southampton Water during the phytoplankton growth season from the model and survey results.

7.4.1.2 Chlorophyll a

In 1998 two bloom events, with a rapid increase of chlorophyll a concentration was detected in the Itchen Estuary and Southampton Water. Figure 7.19a shows the model results of surface chlorophyll a concentration ($\mu g\ l^{-1}$) in surface and bottom waters simulated from Woodmill to Calshot Buoy. The chlorophyll a concentration is less than 1 $\mu g\ l^{-1}$ throughout the estuary in January, when the solar irradiance is at its annual lowest. Chlorophyll a concentration then increases gradually with the increase in solar irradiance from February, and by the end of March, it is more than 2 $\mu g\ l^{-1}$ from the Itchen Bridge downstream to BP Jetty. The chlorophyll a concentration is rarely below 2 $\mu g\ l^{-1}$ from March to August throughout most of the Itchen Estuary and Southampton Water. The seasonal increase and decrease of chlorophyll a concentration accorded with the annual rise and fall of the solar elevation. Beside this annual cycle, the model shows two peaks of chlorophyll a concentration in the estuary; one in late May and early June with a maximum chlorophyll a concentration of 22.1 $\mu g\ l^{-1}$ and one in the middle of August with a maximum chlorophyll a concentration of 15.8 $\mu g\ l^{-1}$. This rapid increase of chlorophyll a concentration coincided with a period of good weather, low turbidity in the water column and increase of water temperature. The modelled chlorophyll a concentration during the these blooms is generally not as high as the observed peak values (Figure 7.20). The bottom layer chlorophyll a concentrations (Figure 7.19b) follow the same pattern as the surface values and have the same magnitude. The data from the surveys also revealed that the surface and bottom chlorophyll concentration did not show much of a difference.

Model results from 10 stations (Figure 7.20a-j) show a clear pattern of chlorophyll a seasonal variation and timing of the blooms in the model coincide with the observed bloom events. Longitudinally, the chlorophyll a concentration (Figure 7.21a-j) is usually low at the head of the estuary, since there is no phytoplankton source from the river in the model. It increases downstream to the Itchen Bridge, Dockhead, NW Netley and Greenland. From Greenland seaward, the chlorophyll a concentration decreases. The model over-predicts the chlorophyll a concentration in the upper Itchen Estuary and under-predicts it in Southampton Water.

7.4.1.3 Detrital carbon

In the water quality model, the detrital carbon is mainly derived from phytoplankton mortality. The detrital carbon as particulate matter is assumed to sediment into bottom waters at

Figure 7.19 Seasonal variation of a) surface and b) bottom chllorophyll a (ug l^{-1}) from integrated model (with sedimentation) in the Itchen Estuary and Southampton Water

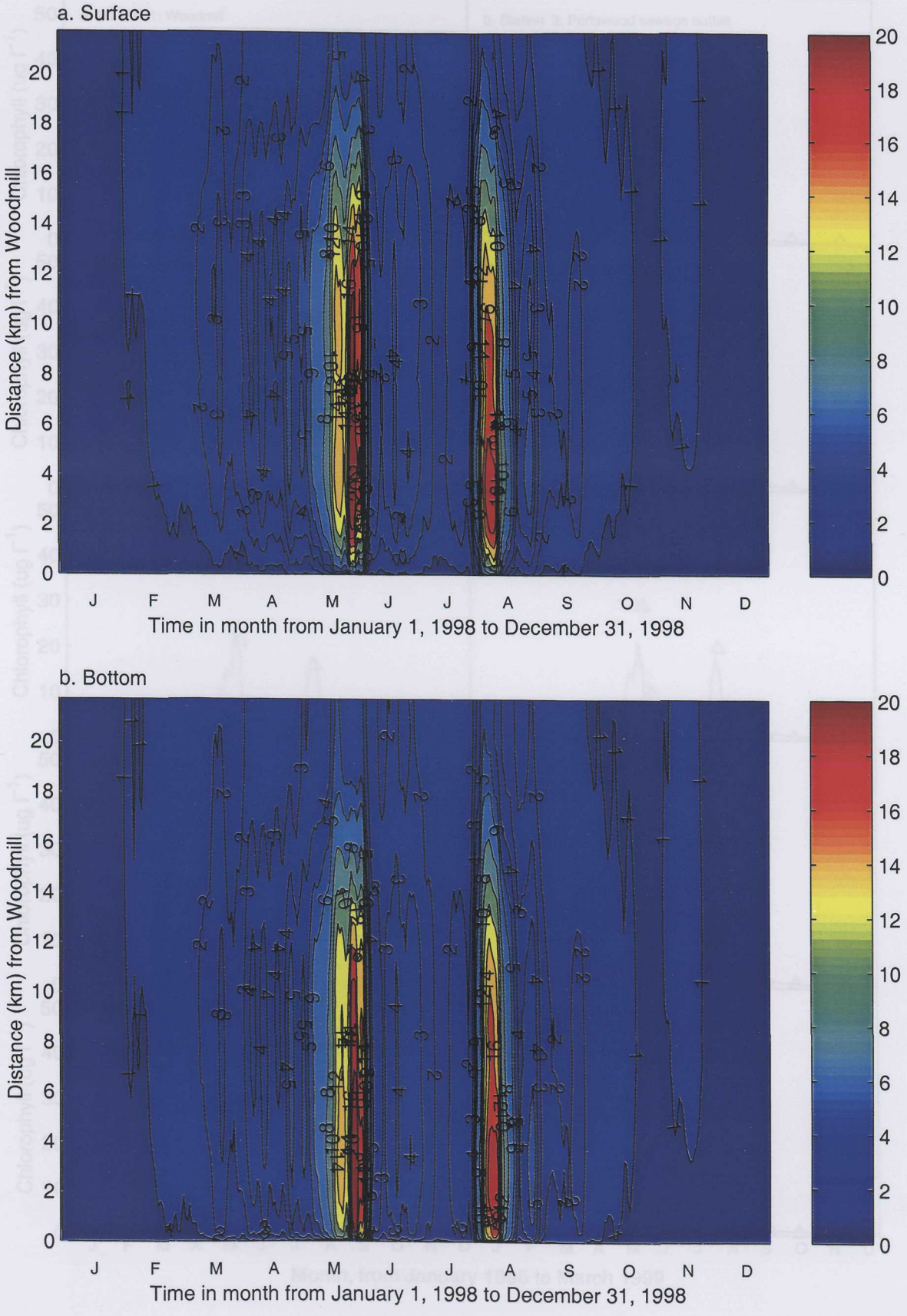

Figure 7.20a–j Seasonal variation of chlorophyll a (ug l^{-1}), comparison between integrated model (with sedimentation) results and observations at 10 survey stations

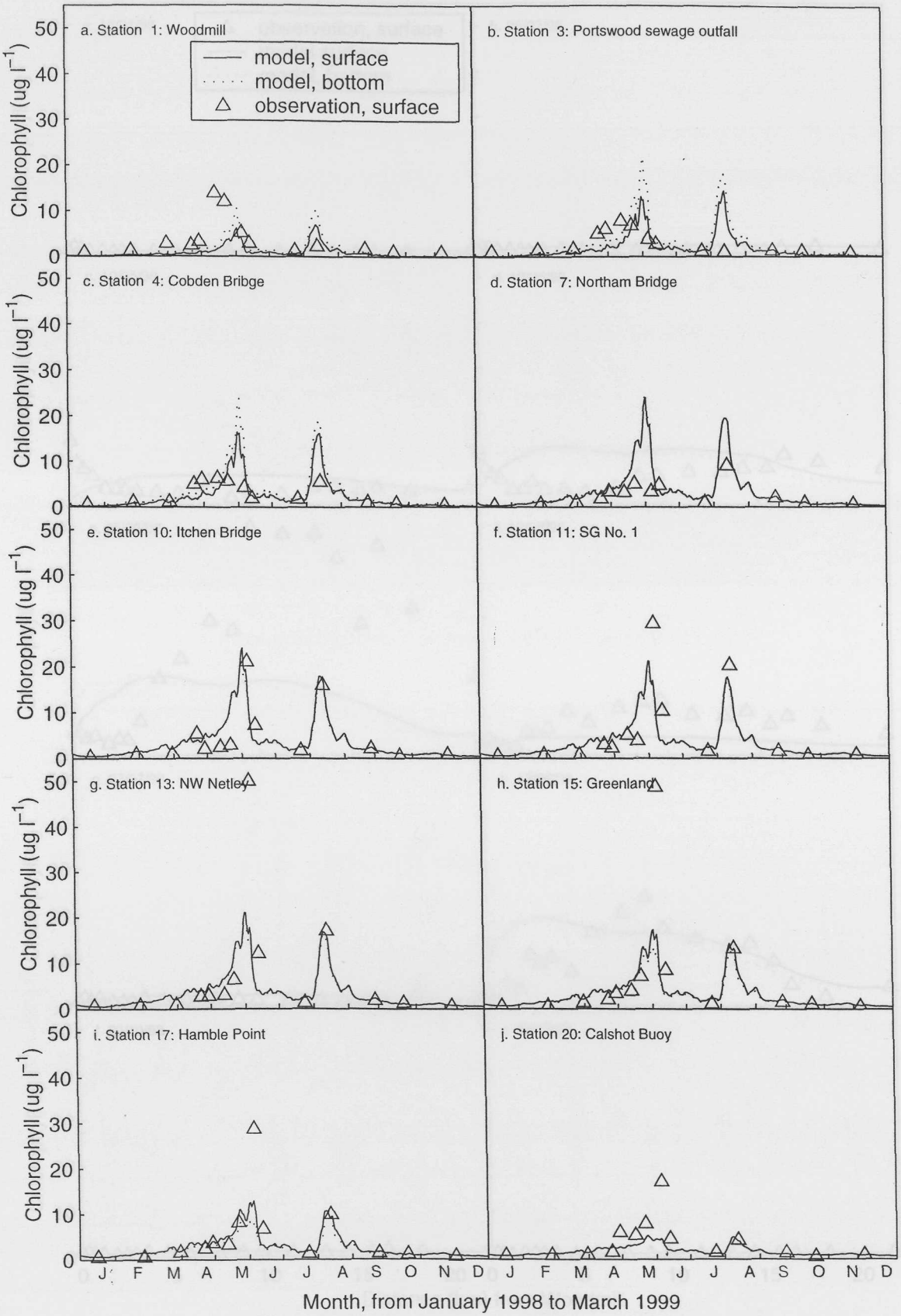

Figure 7.21a–j Longitudinal distribution of chlorophyll a (ug l^{-1}), comparison between integrated model (with sedimentation) results and observations in 1998

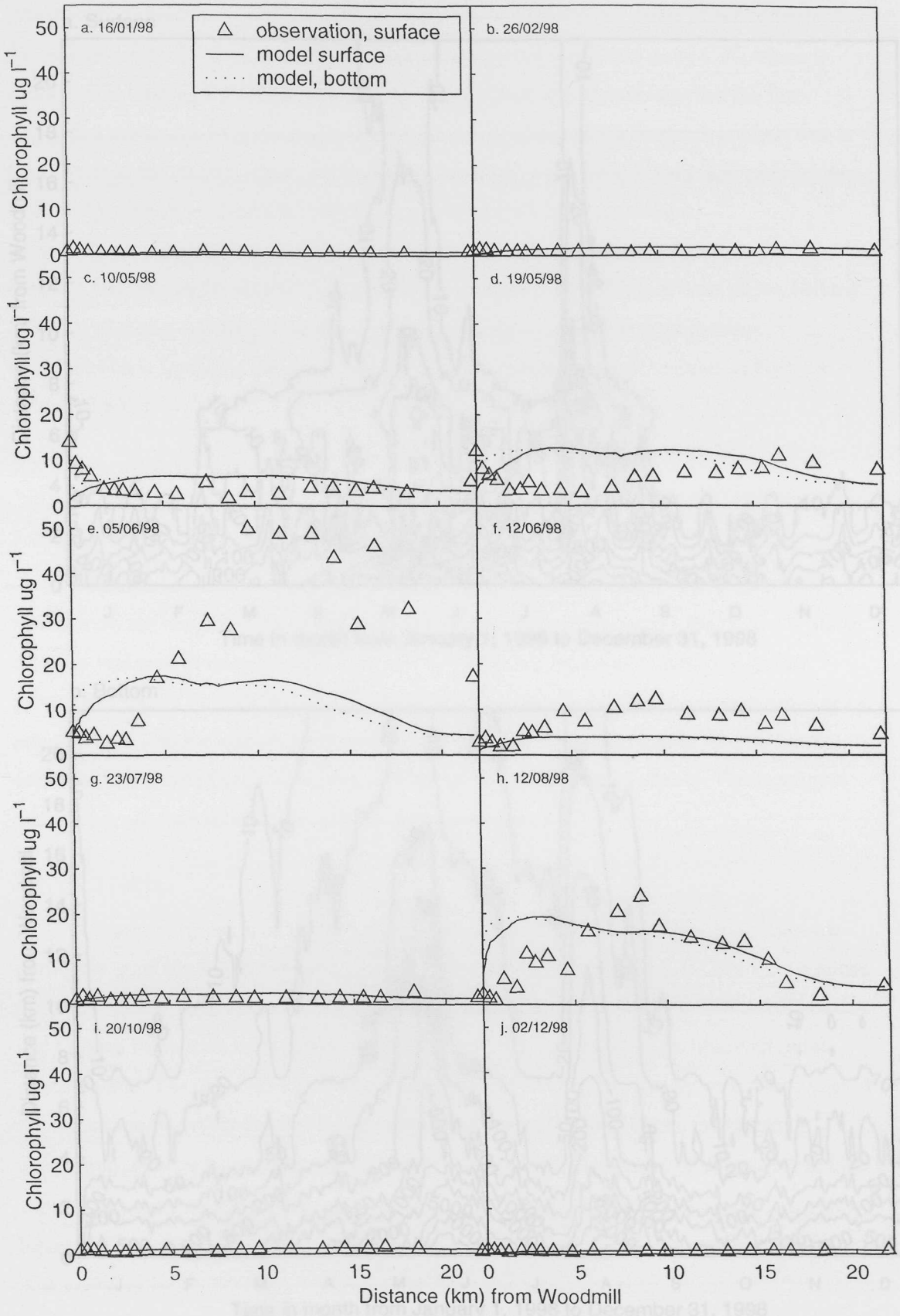

Figure 7.22 Seasonal variation of a) surface and b) bottom detrital carbon (umol C l^{-1}) from integrated model (with sedimentation) in the Itchen Estuary and Southampton Water

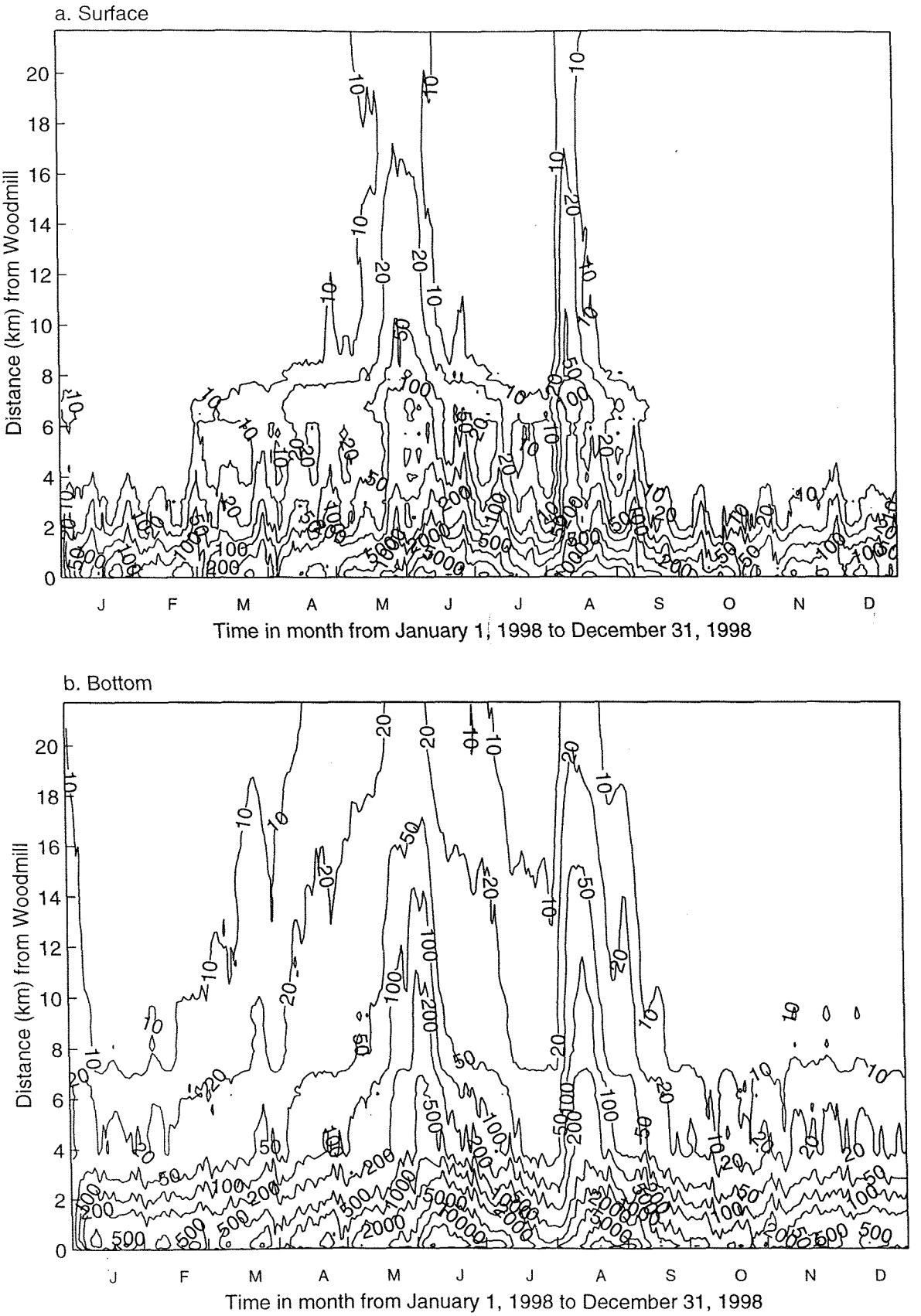

a uniform speed. The distribution of the detrital carbon (Figure 7.22a-b) shows that it is virtually all trapped by the landward bottom flowing water in the estuary, and accumulated in very high concentrations in both bottom and surface layers near the head of the estuary. In this region in the bottom waters the detrital carbon concentration is as high as 20000 μmol C l^{-1}, which is equivalent to 240 mg C l^{-1}. This high detrital carbon concentration indicates that the fine suspended matter has been trapped by the estuarine circulation in the model. It is likely that at some point in the estuary, where the landward circulation ends, there is very high turbidity due to the large amount of suspended matter trapped by the estuarine circulation.

The seasonal variation of the detrital carbon is directly related to the phytoplankton biomass. The maximum detritus concentration is coincident with the maximum phytoplankton chlorophyll a concentration of both bloom events. Longitudinally, the high detritus concentration is limited to the upper part of the Itchen Estuary, from Woodmill to Northam Bridge (2.8 km).

7.4.1.4 Inorganic nutrients

7.4.1.4.1 Ammoniacal nitrogen

Comparing with the ammonium distribution from the external model (Figure 7.9a-b), results from the integrated water quality model (Figure 7.23a-b) show that the relatively stable seasonal variation of ammonium concentration is disturbed by the phytoplankton growth particularly during the algal bloom. When the bloom occurs, firstly there is a sharp decrease of ammonium due to the uptake of nutrient by phytoplankton, then an increase of ammonium concentration occurs from the remineralization of the trapped detrital carbon. The maximum ammonium concentration in the model is about 100.0 μmol l^{-1}.

7.4.1.4.2 Nitrate

Seasonal variation of nitrate concentration (Figure 7.24a-b) shows a sharp decrease during the algal blooms in May and August. Unlike the ammonium (figure 7.23a-b), the nitrite does not show a significant increase subsequent to the bloom. The model results at NW Netley and Calshot Buoy have been plotted (Figure 7.25a-b) in comparison to the observed nitrate concentration. The observed nitrate concentration at NW Netley are mostly within the range of the model results before the first bloom occurs, but during the first bloom, the nitrate concentration drops from a average value of 60.0 μmol l^{-1} to a low value of 20 μmol l^{-1} at high water. The model nitrate concentration recovers very quickly to about 60.0 μmol l^{-1} after the bloom. The observed nitrate did not show such a quick recovery, with the observed nitrate concentration on 23/07/98 prior to the second *Mesodinium* bloom being 30 μmol l^{-1}. The second bloom further depletes the observed nitrate concentration down to about 5.0 μmol l^{-1}, while the

model also simulates a sharp decrease in nitrate concentration. The nitrate concentration in the model can be less than 20 μmol l^{-1} at low water. After the second bloom the observed nitrate concentration recovered to pre-bloom levels (30 μmol l^{-1}), but this is much lower than the model concentration.

The model nitrate data from Calshot Buoy is quite low compared with the observations, and is rarely higher than 10 μmol l^{-1}. The observed nitrate concentration ranges between 20-30 μmol l^{-1}, before the algal bloom, compared with the model value of 5-10 μmol l^{-1}. The observed nitrate concentration dropped to quite low levels during the bloom, but these are higher than the model result with nitrate concentration being less than 0.5 μmol l^{-1}. The observed nitrate concentration increased to 23 μmol l^{-1} in December.

7.4.1.4.3 Phosphate

There is only a small depletion of phosphate (Figure 7.26a-b) in the estuary during the bloom, and this probably indicates that the algal bloom is not phosphate. The decomposition of detrital carbon derived from the algal carbon increases the phosphate concentration in the Itchen Estuary after the bloom collapsed. The increase of phosphate due to remineralization after the bloom can be clearly seen at NW Netley (Figure 7.25c), while the data from the survey shows a depletion of phosphate in the water column. The observed phosphate concentration is about the same magnitude as the model at Calshot Buoy (Figure 7.25d), and the model value is about 2-3 times higher than the observed value at NW Netley.

7.4.1.4.4 Nutrients versus salinity

During the non-phytoplankton growth season, the model nutrient concentration plotted against salinity does not change, because there is little impact of nutrient removal by phytoplankton photosynthesis. The apparent impact of the phytoplankton activity on nutrients can be seen during the phytoplankton bloom. Figure 7.27a show uptake of nitrate by the phytoplankton bloom (i.e. non-conservative removal at high salinity), and this removal of nitrate in the model improves the fit to the observation in comparison to the external model output (Figure 7.14a). Ammonium concentration (Figure 7.27b) is almost double compared with the external model results (Figure 7.14b), due to the remineralization of the detrital carbon. The model data (Figure 7.27b) shows removal of ammonium (non-conservative behaviour) at high salinity (>30). Phosphate (Figure 7.27c) also shows the impact of remineralization, and the model results do not fit the survey data very well. The nutrient model result for12/08/98 bloom (Figure 7.28) also shows the nitrate fits the data well, but for phosphate and ammonium the agreement is poor for a salinity of less than 32.

Figure 7.23 Seasonal variation of a) surface and b) bottom ammonium concentration (umol l^{-1}) from integrated model (with sedimentation) in the Itchen Estuary and Southampton Water

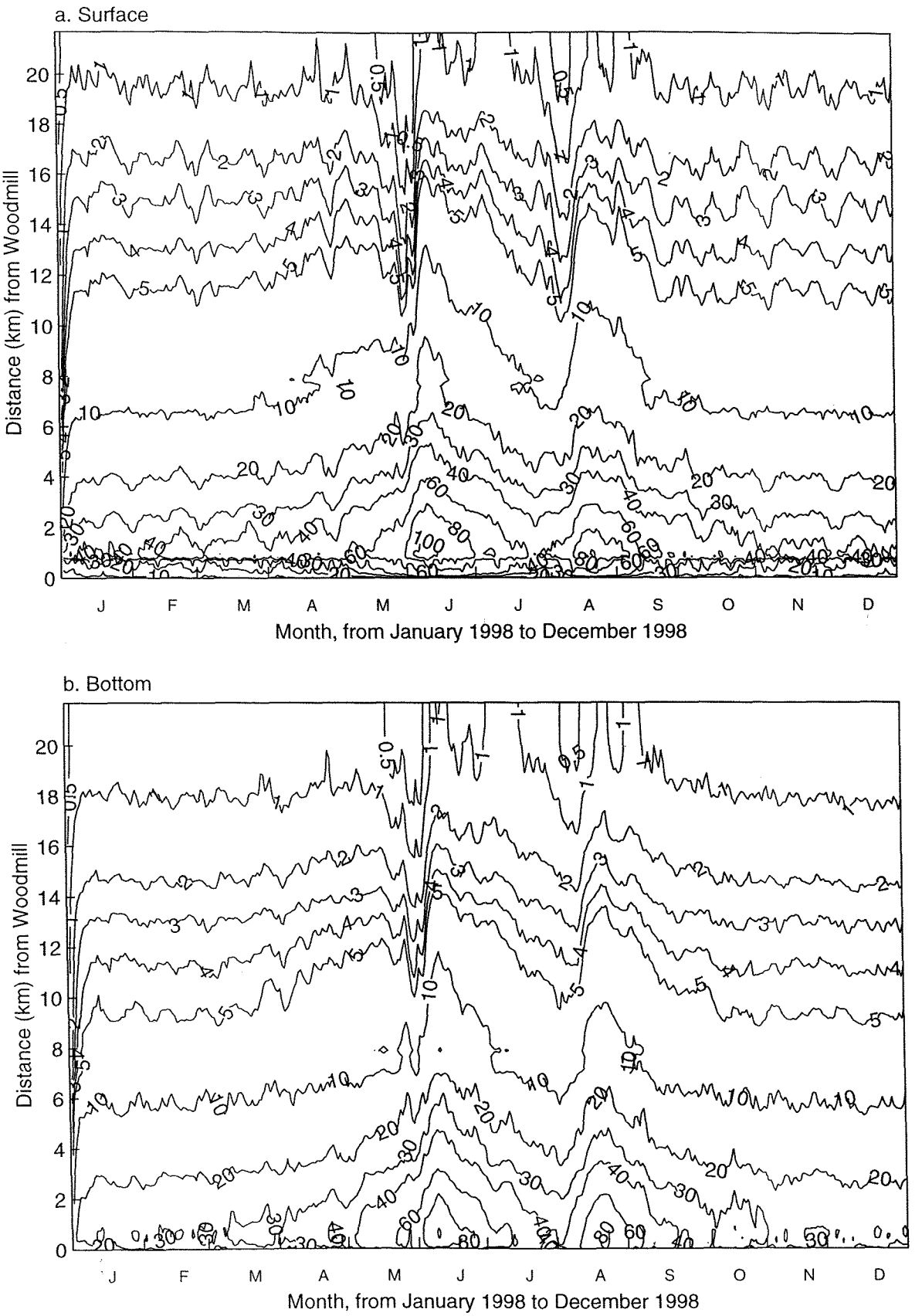

Figure 7.24 Seasonal variation of a) surface and b) bottom nitrate concentration (umol l^{-1}) from integrated model (with sedimentation) in the Itchen Estuary and Southampton Water

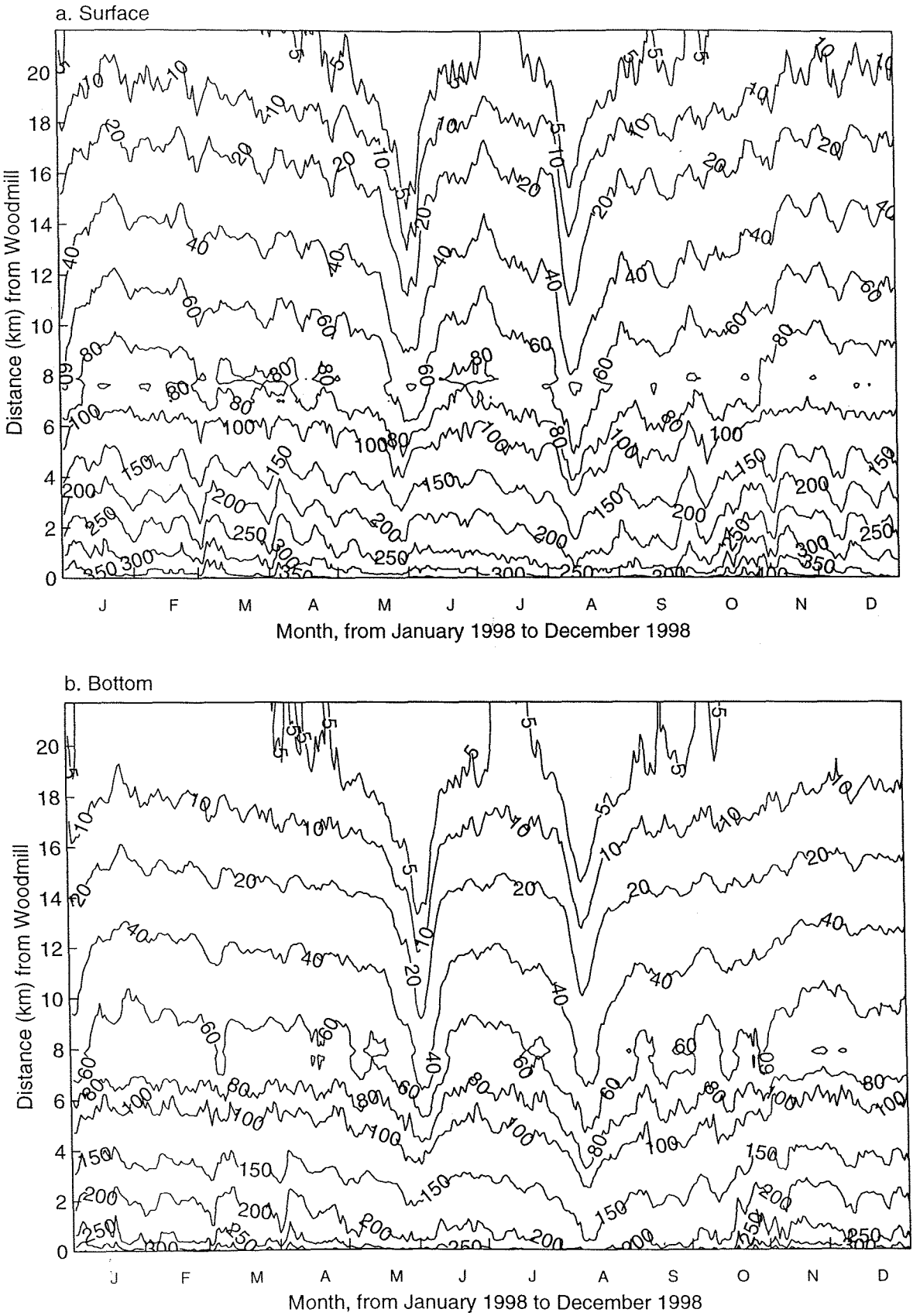

Figure 7.25 Annual variation of the surface nitrate, phosphate concentration at NW Netley and Calshot Buoy: comparison between observations and integrated model (with sedimentation) output

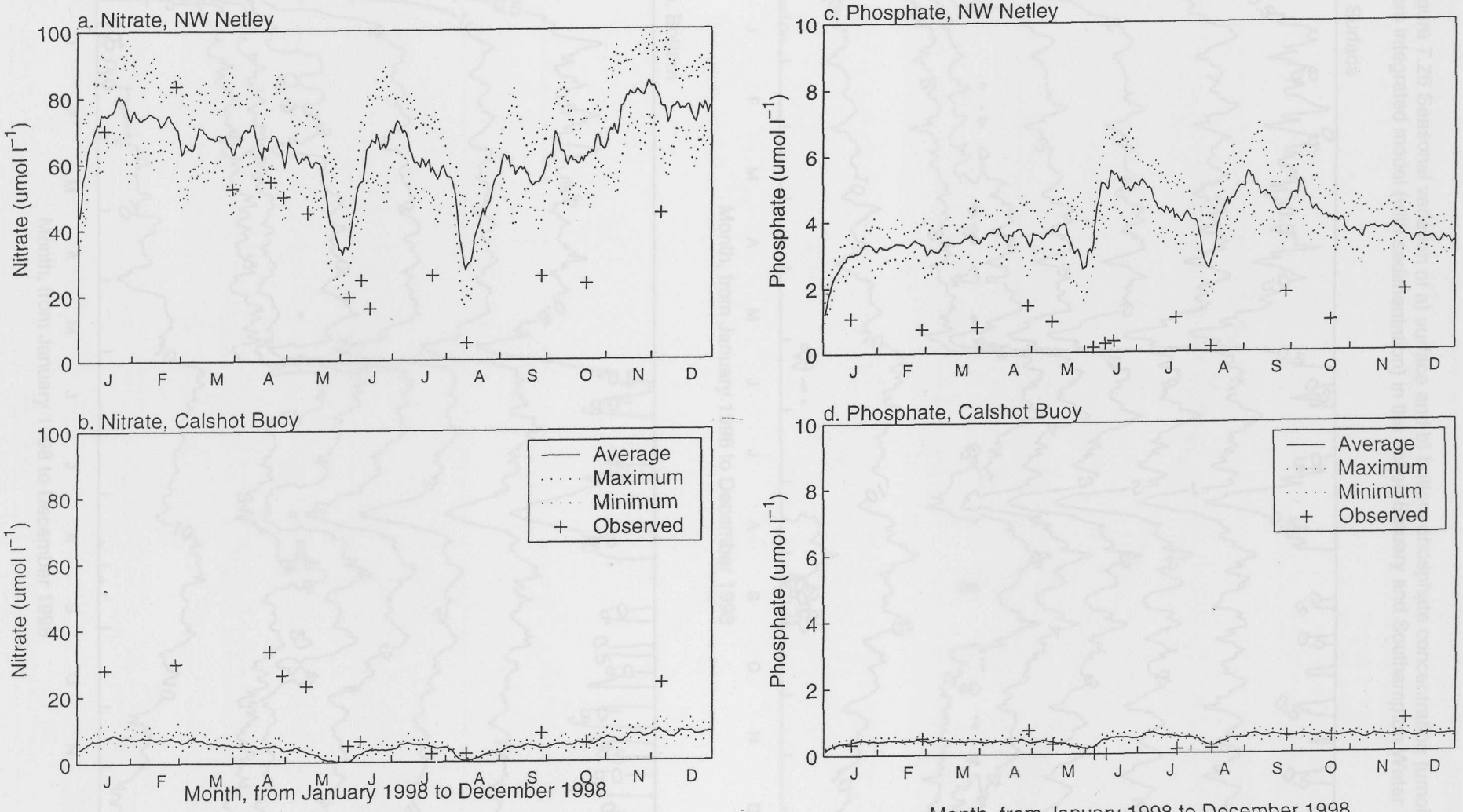

Figure 7.26 Seasonal variation of a) surface and b) bottom phosphate concentration (umol l^{-1}) from integrated model (with sedimentation) in the Itchen Estuary and Southampton Water

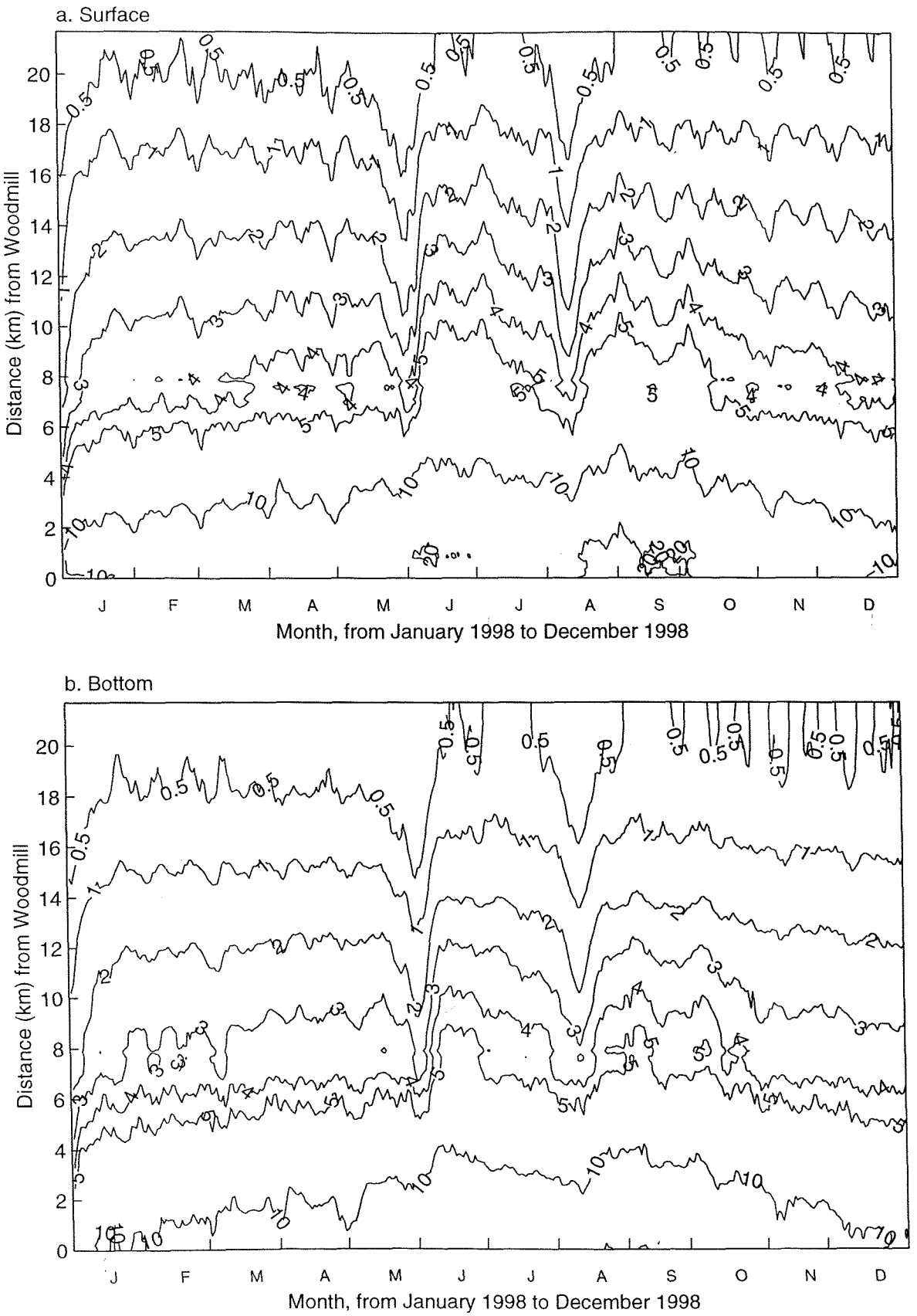

Figure 7.27 Nutrients (daily averaged output (integrated model with sedimentation), observations) plotted against salinity in the Itchen Estuary and Southampton Water, 05/06/98

Figure 7.27a Nitrate against salinity

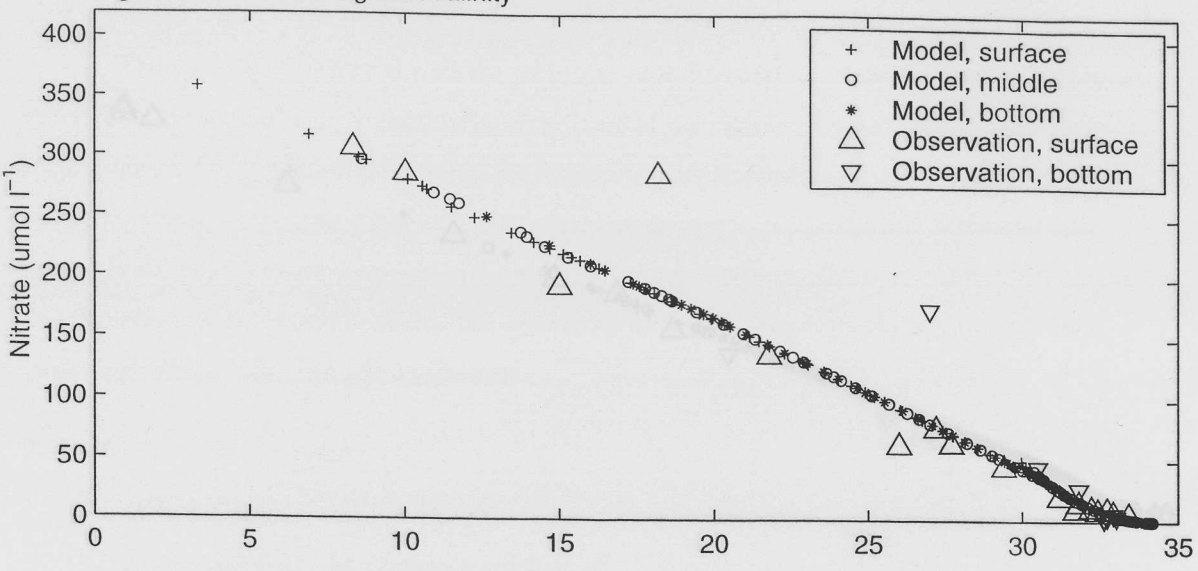

Figure 7.27b Ammonium against salinity

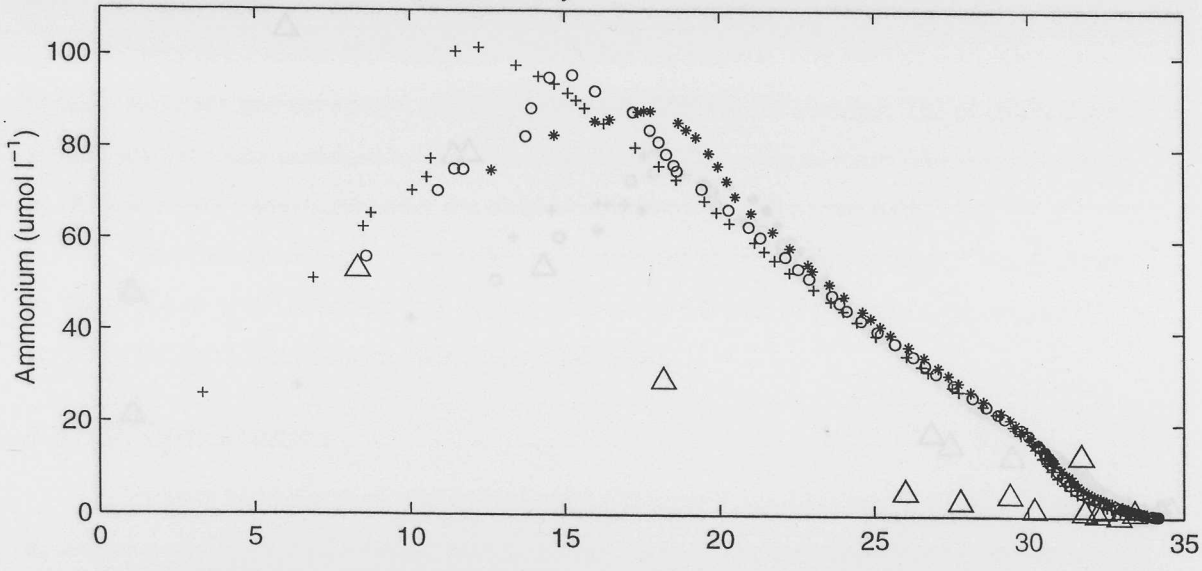

Figure 7.27c Phosphate against salinity

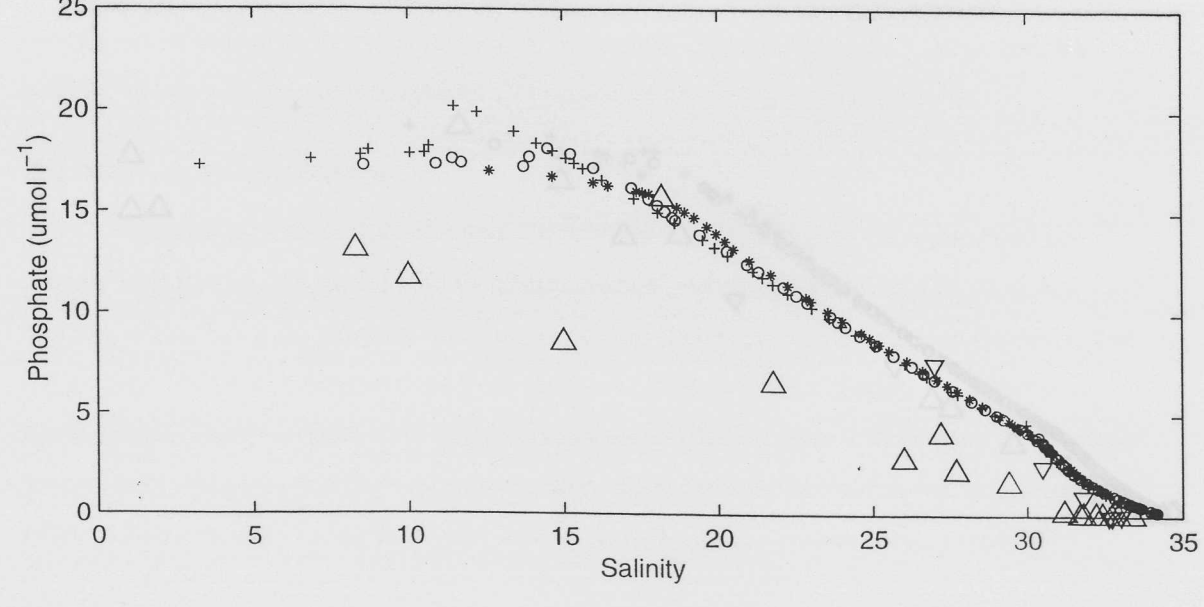

Figure 7.28 Nutrients (daily averaged output (integrated model with sedimentation), observations) plotted against salinity in the Itchen Estuary and Southampton Water, 12/08/98

Figure 7.28a Nitrate against salinity

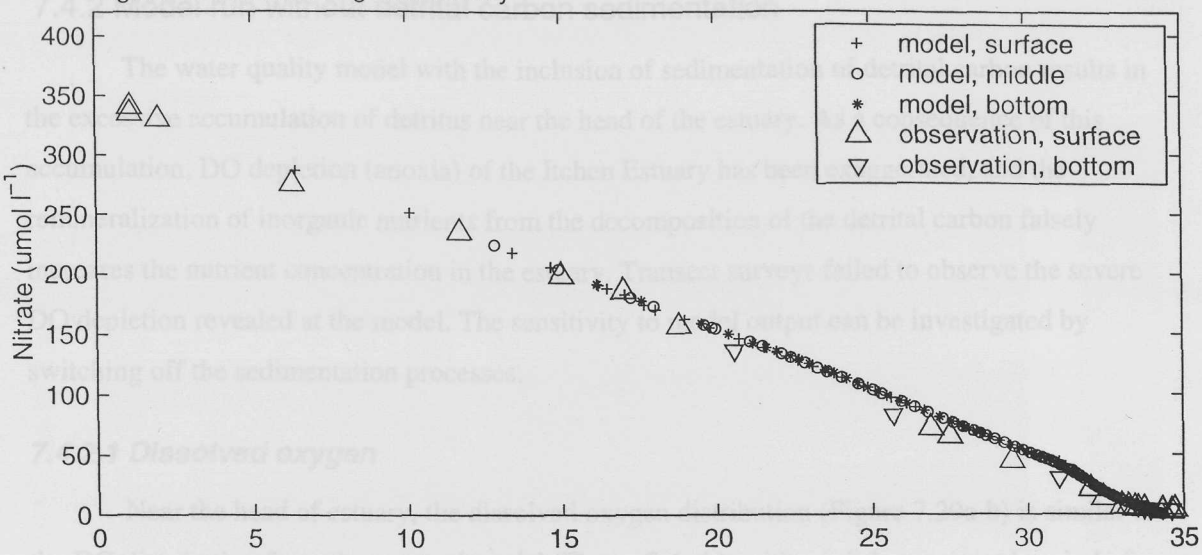

Figure 7.28b Ammonium against salinity

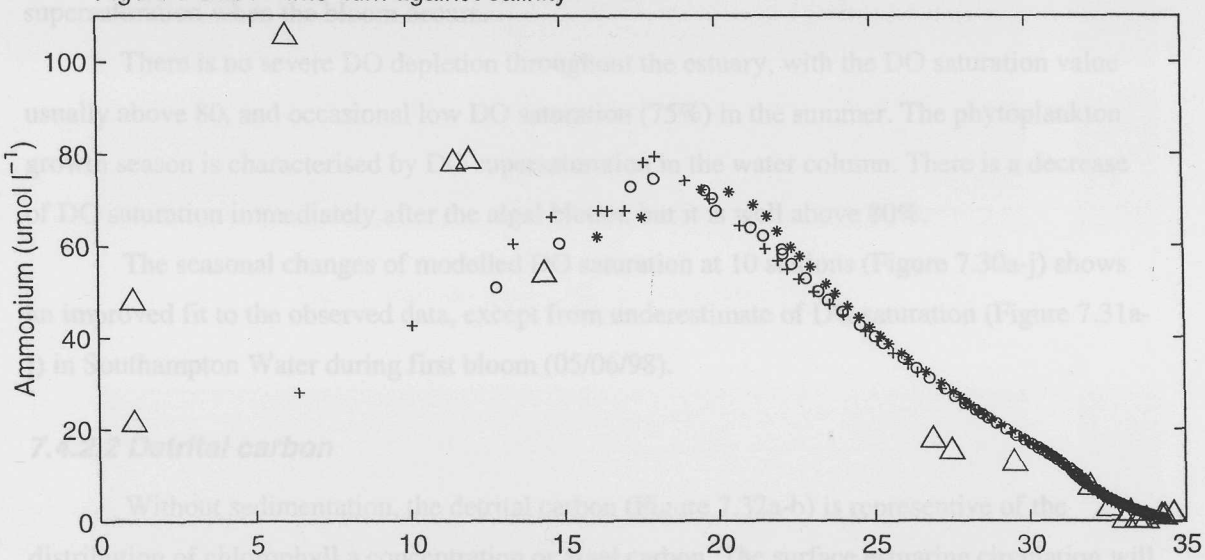

Figure 7.28c Phosphate against salinity

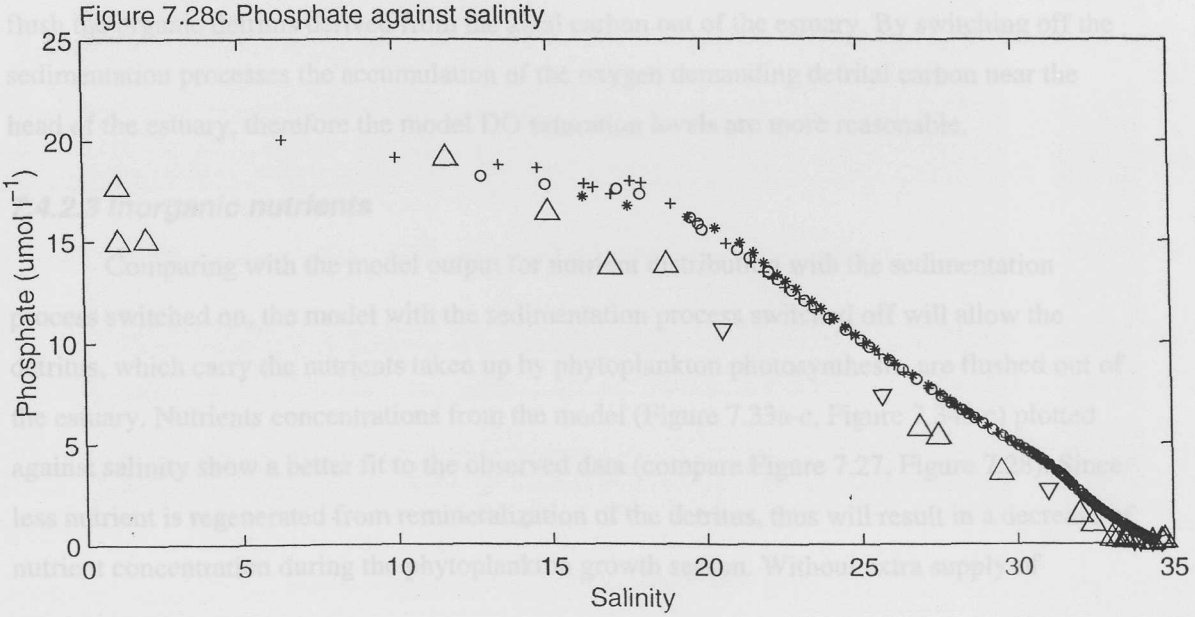

7.4.2 Model run without detrital carbon sedimentation

The water quality model with the inclusion of sedimentation of detrital carbon results in the excessive accumulation of detritus near the head of the estuary. As a consequence of this accumulation, DO depletion (anoxia) of the Itchen Estuary has been exaggerated, and the remineralization of inorganic nutrients from the decomposition of the detrital carbon falsely increases the nutrient concentration in the estuary. Transect surveys failed to observe the severe DO depletion revealed at the model. The sensitivity to model output can be investigated by switching off the sedimentation processes.

7.4.2.1 Dissolved oxygen

Near the head of estuary, the dissolved oxygen distribution (Figure 7.29a-b) is similar to the DO distribution from the external model (Figure 7.4a-b), with a brief exceptional period of supersaturation when the bloom occurs.

There is no severe DO depletion throughout the estuary, with the DO saturation value usually above 80, and occasional low DO saturation (75%) in the summer. The phytoplankton growth season is characterised by DO supersaturation in the water column. There is a decrease of DO saturation immediately after the algal bloom, but it is well above 80%.

The seasonal changes of modelled DO saturation at 10 stations (Figure 7.30a-j) shows an improved fit to the observed data, except from underestimate of DO saturation (Figure 7.31a-j) in Southampton Water during first bloom (05/06/98).

7.4.2.2 Detrital carbon

Without sedimentation, the detrital carbon (Figure 7.32a-b) is representive of the distribution of chlorophyll a concentration or algal carbon. The surface estuarine circulation will flush the organic detritus derived from the algal carbon out of the estuary. By switching off the sedimentation processes the accumulation of the oxygen demanding detrital carbon near the head of the estuary, therefore the model DO saturation levels are more reasonable.

7.4.2.3 Inorganic nutrients

Comparing with the model output for nutrient distribution with the sedimentation process switched on, the model with the sedimentation process switched off will allow the detritus, which carry the nutrients taken up by phytoplankton photosynthesis, are flushed out of the estuary. Nutrients concentrations from the model (Figure 7.33a-c, Figure 7.34a-c) plotted against salinity show a better fit to the observed data (compare Figure 7.27, Figure 7.28). Since less nutrient is regenerated from remineralization of the detritus, thus will result in a decrease of nutrient concentration during the phytoplankton growth season. Without extra supply of

Figure 7.29 Seasonal variation of a) surface and b) bottom DO saturation (%) from integrated model (without sedimentation) in the Itchen Estuary and Southampton Water

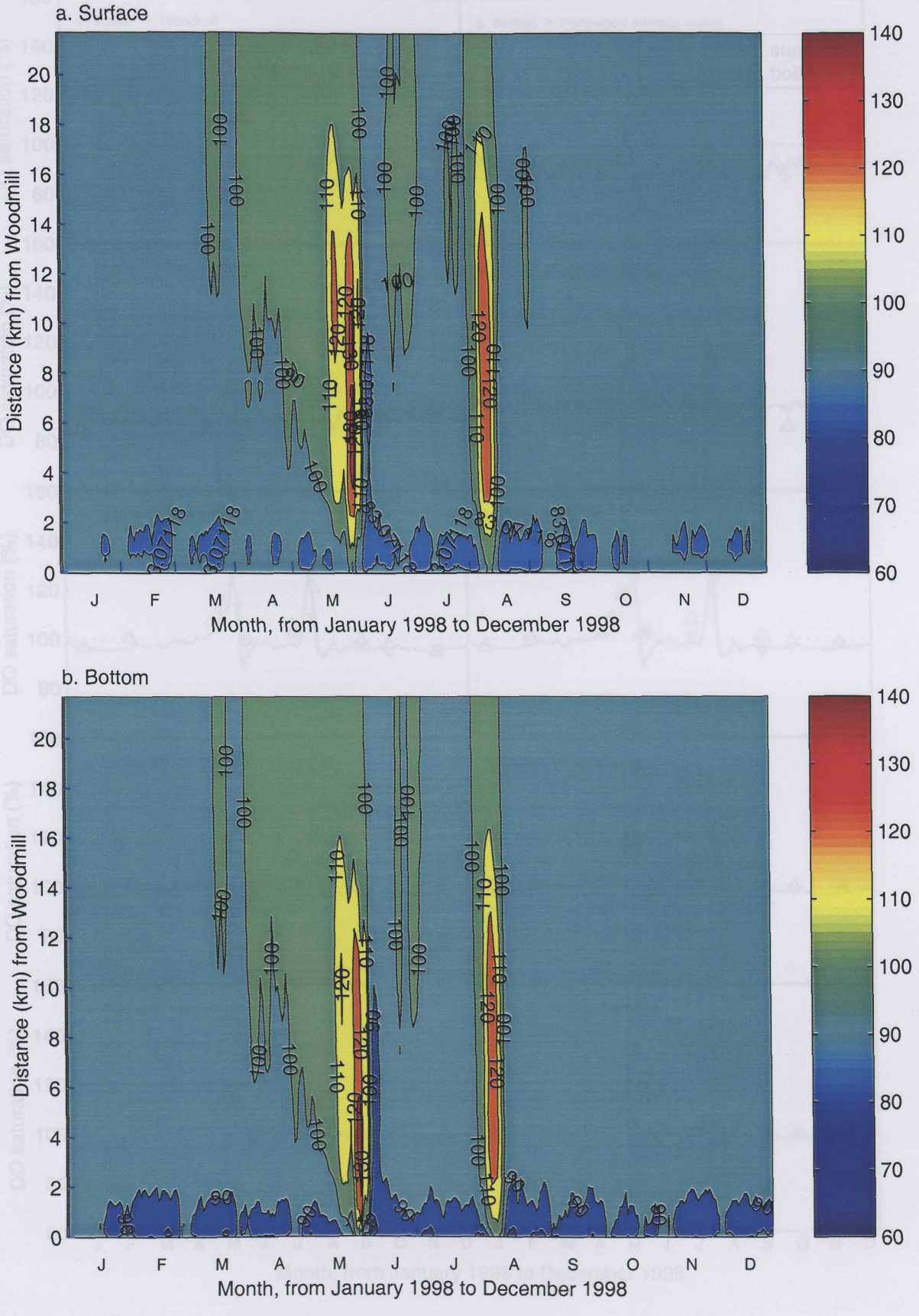

Figure 7.30a–j Seasonal variation of DO saturation (%), comparison between integrated model (without sedimentation) results and observations at 10 survey stations

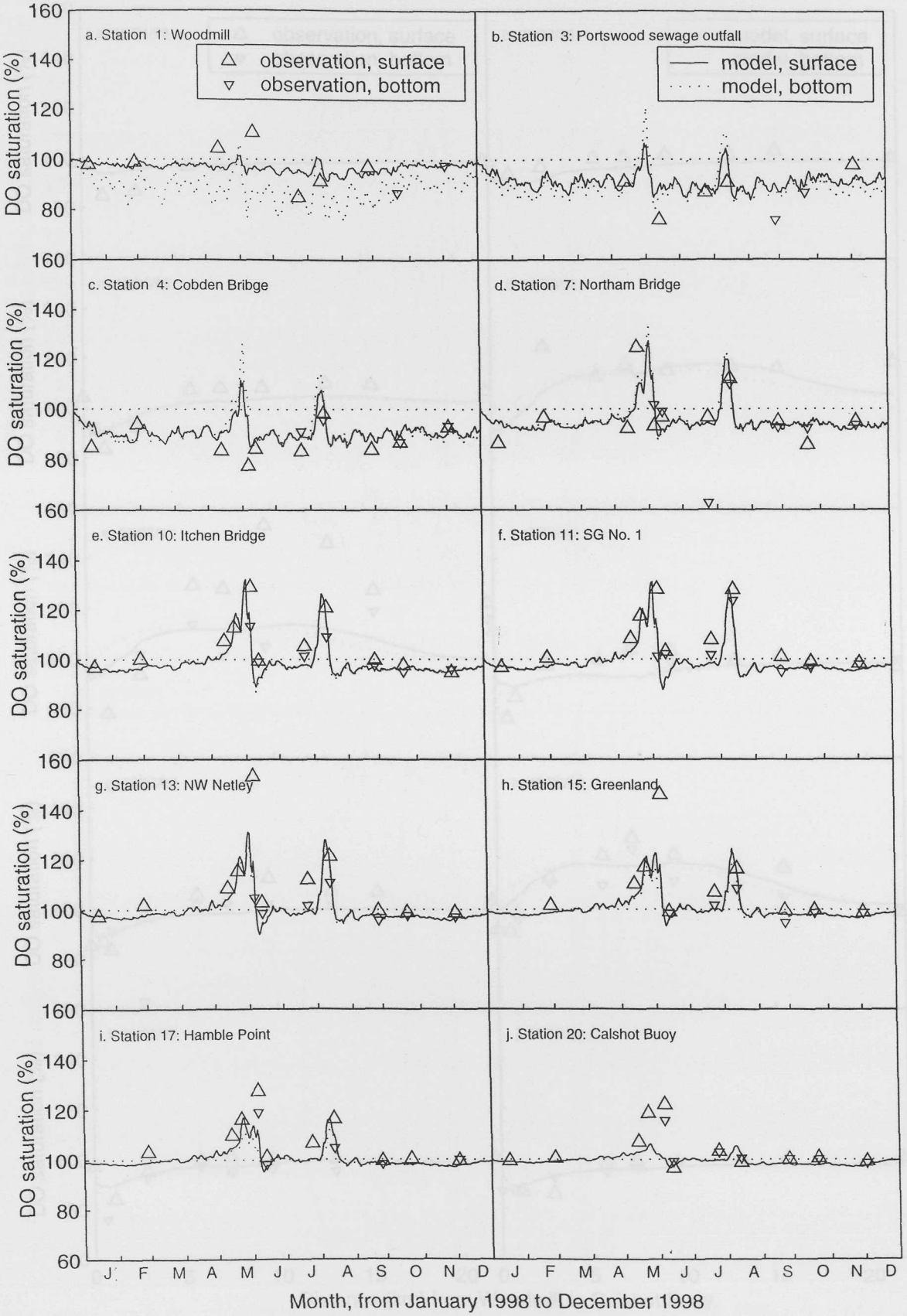

Figure 7.31a–j Longitudinal distribution of DO saturation (%), comparison between integrated model (without sedimentation) results and observations in 1998

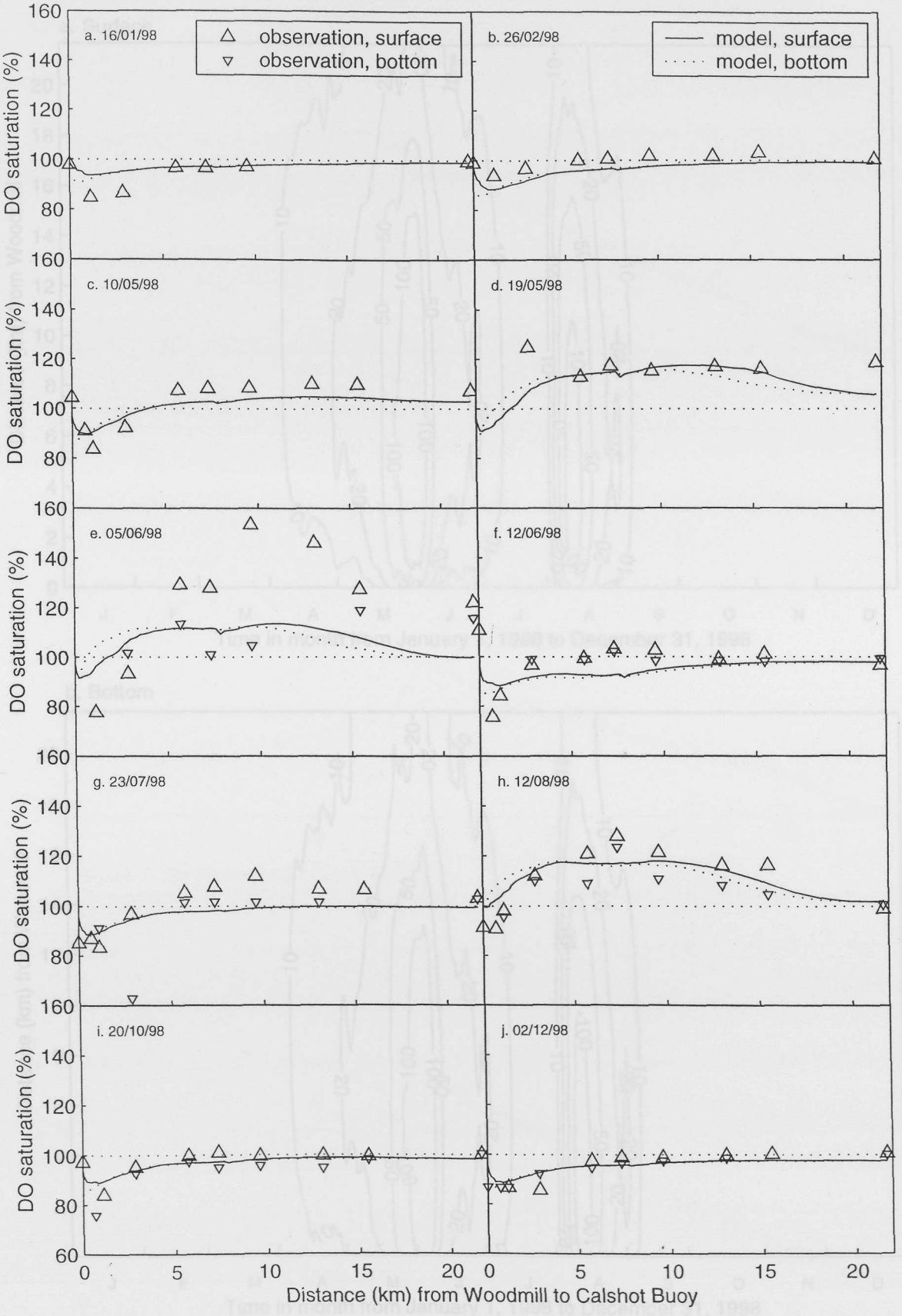

Figure 7.32 Seasonal variation of a) surface and b) bottom detrital carbon (umol C l^{-1}) from integrated model (without sedimentation) in the Itchen Estuary and Southampton Water

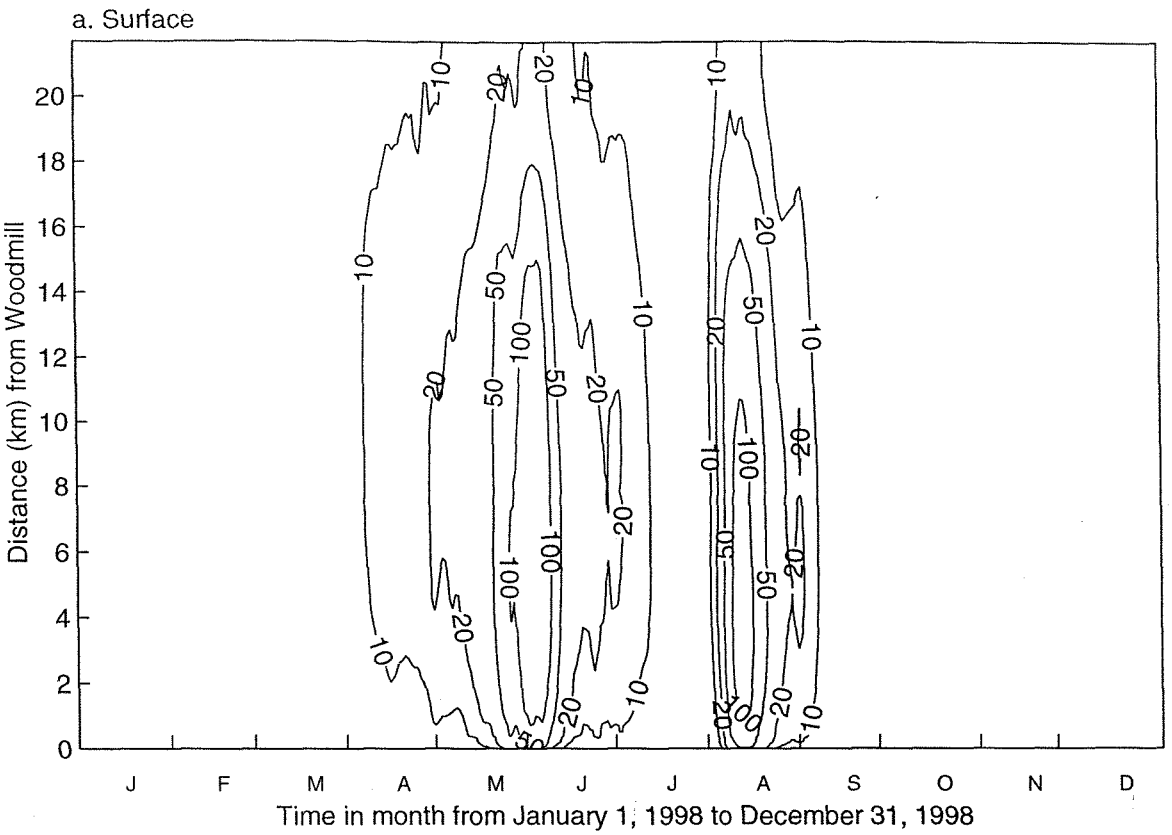

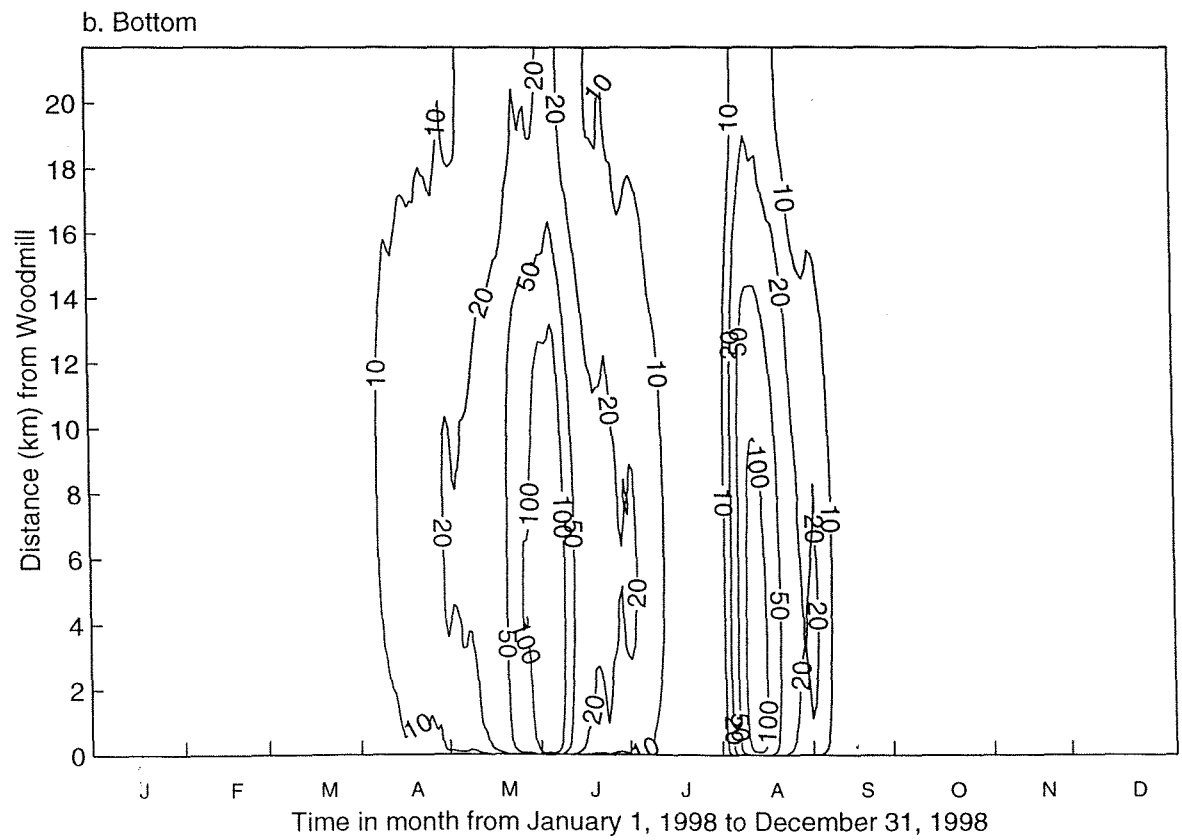

Figure 7.33 Nutrients (daily averaged output (integrated model without sedimentation), observations) plotted against salinity in the Itchen Estuary and Southampton Water, 05/06/98

Figure 7.33a Nitrate against salinity

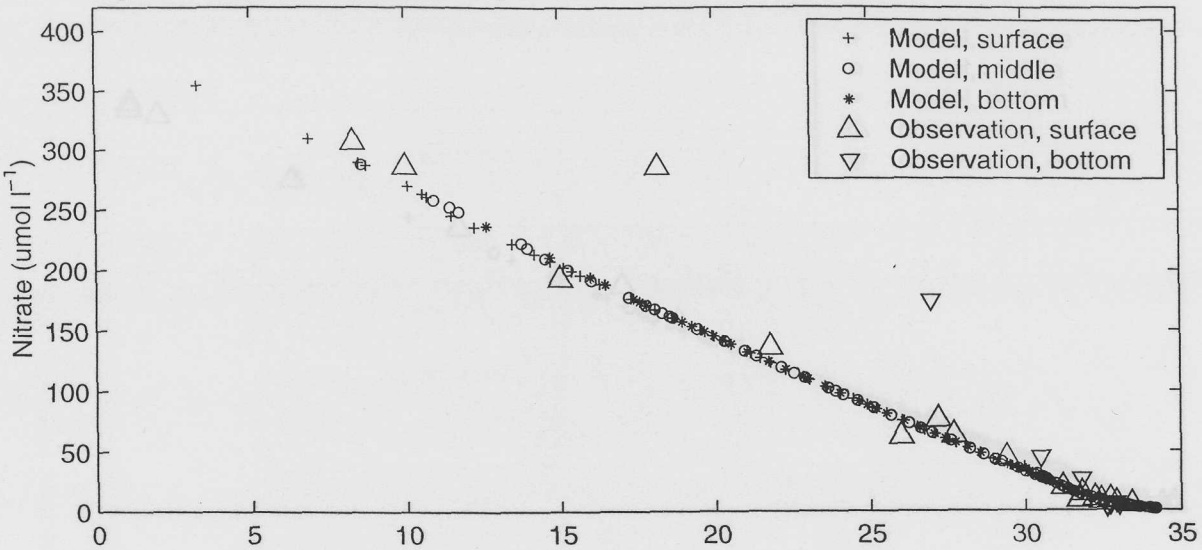

Figure 7.33b Ammonium against salinity

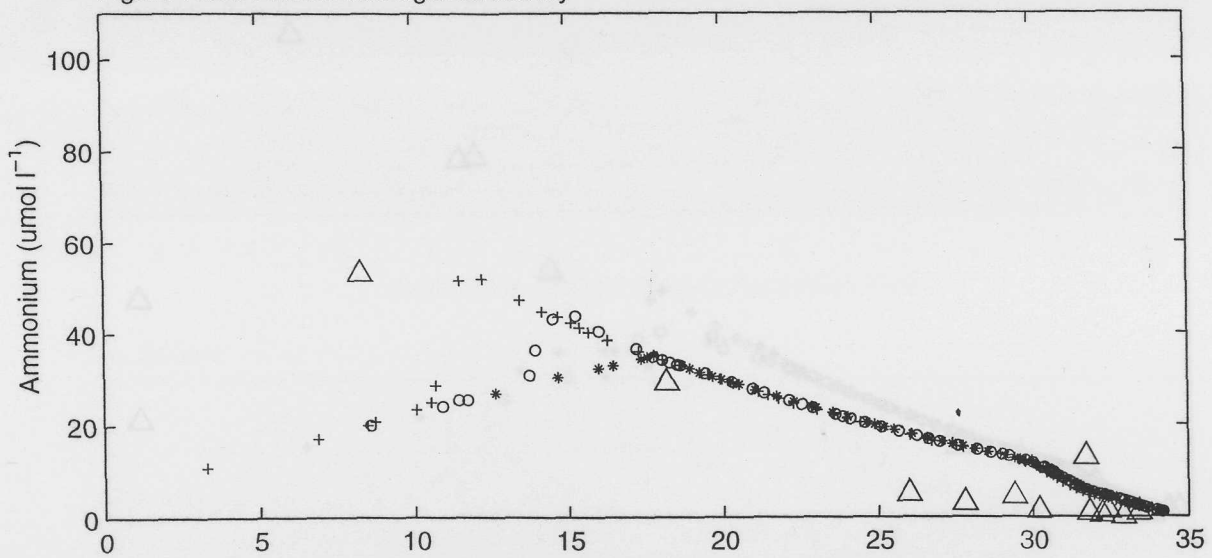

Figure 7.33c Phosphate against salinity

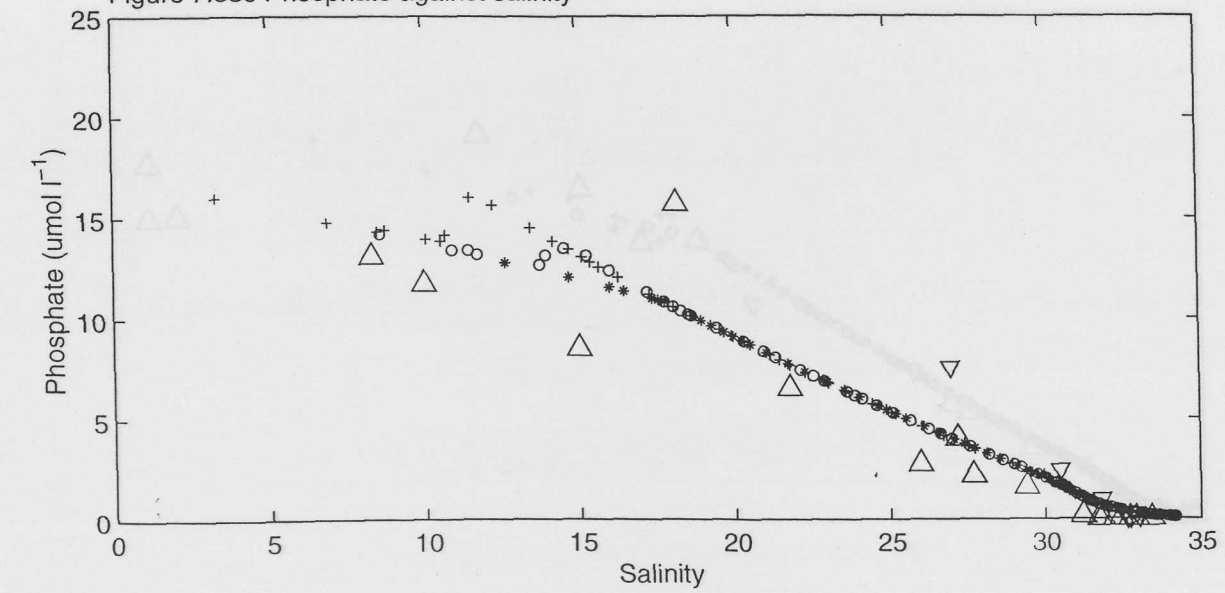

Figure 7.34 Nutrients (daily averaged output (integrated model without sedimentation), observations) plotted against salinity in the Itchen Estuary and Southampton Water, 12/08/98

Figure 7.34a Nitrate against salinity

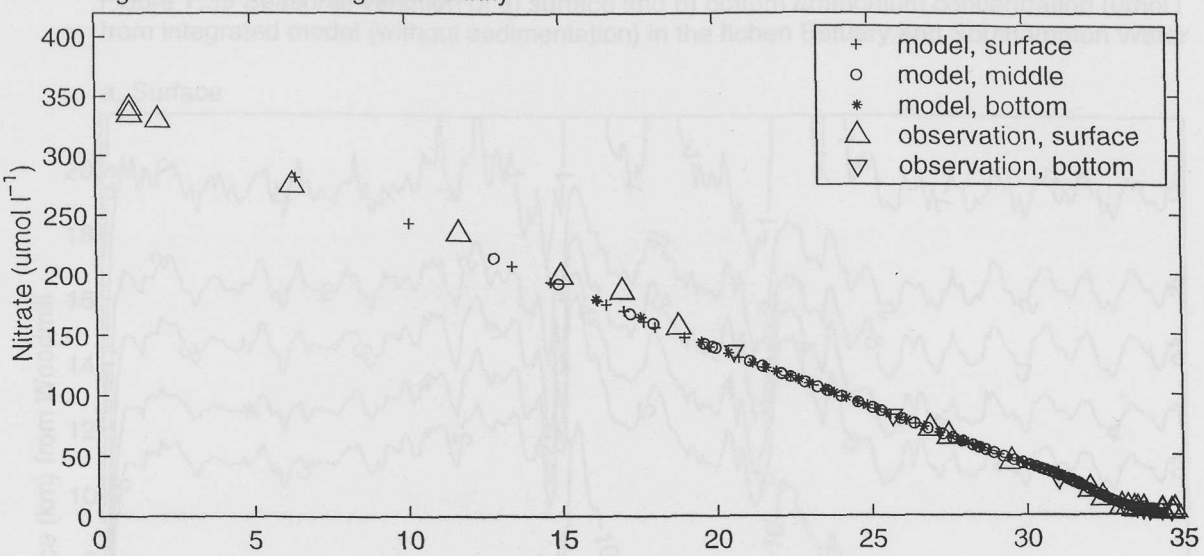

Figure 7.34b Ammonium against salinity

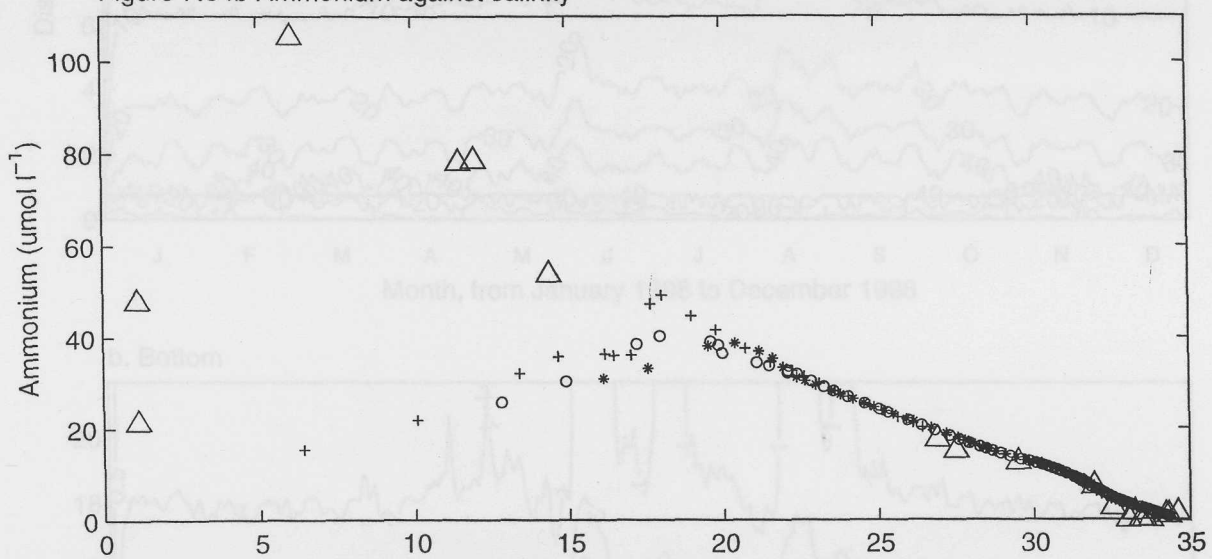

Figure 7.34c Phosphate against salinity

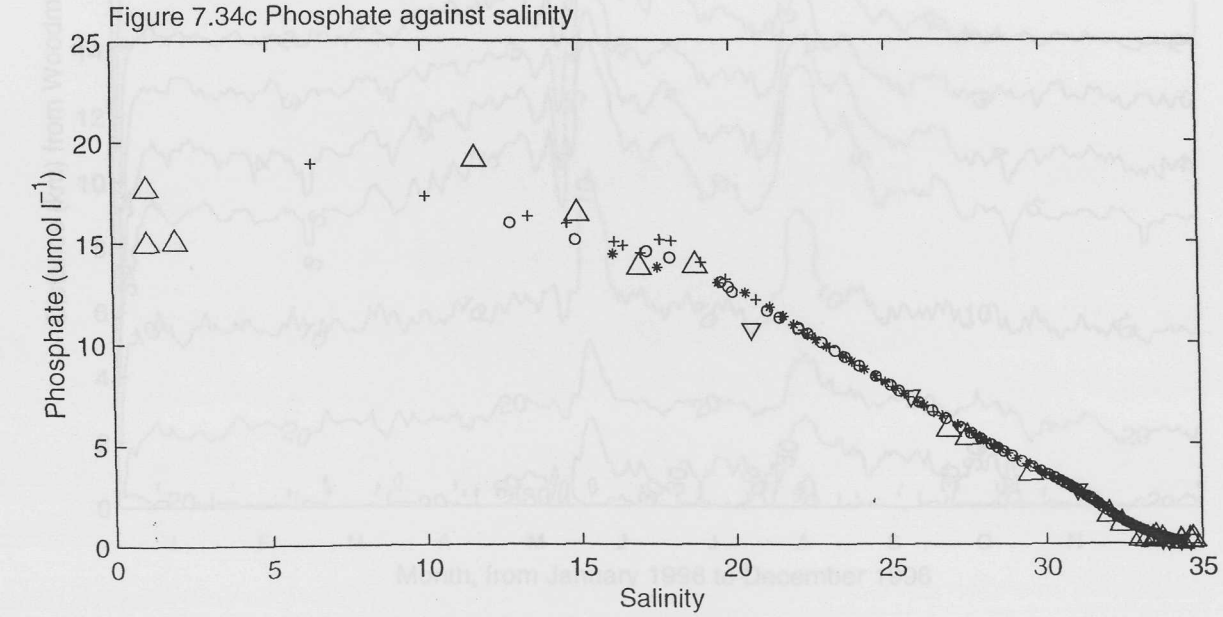

Figure 7.35 Seasonal variation of a) surface and b) bottom ammonium concentration (umol l^{-1}) from integrated model (without sedimentation) in the Itchen Estuary and Southampton Water

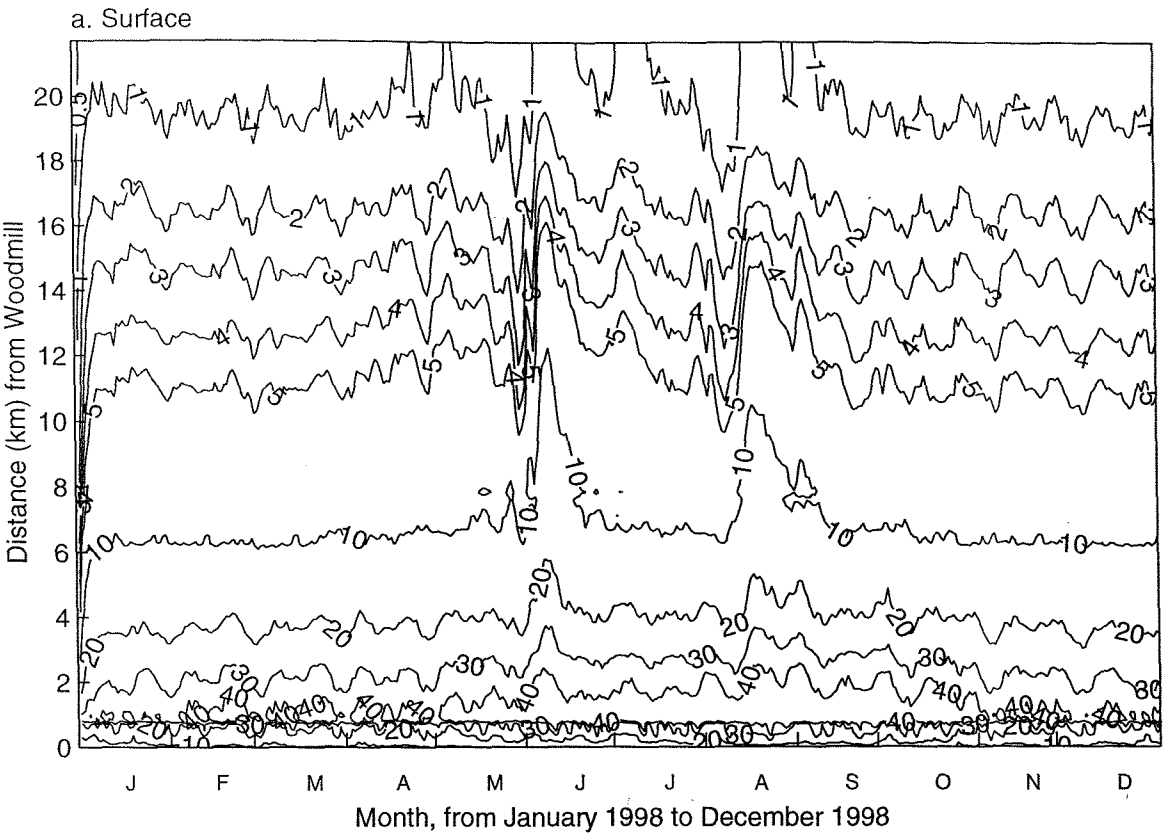

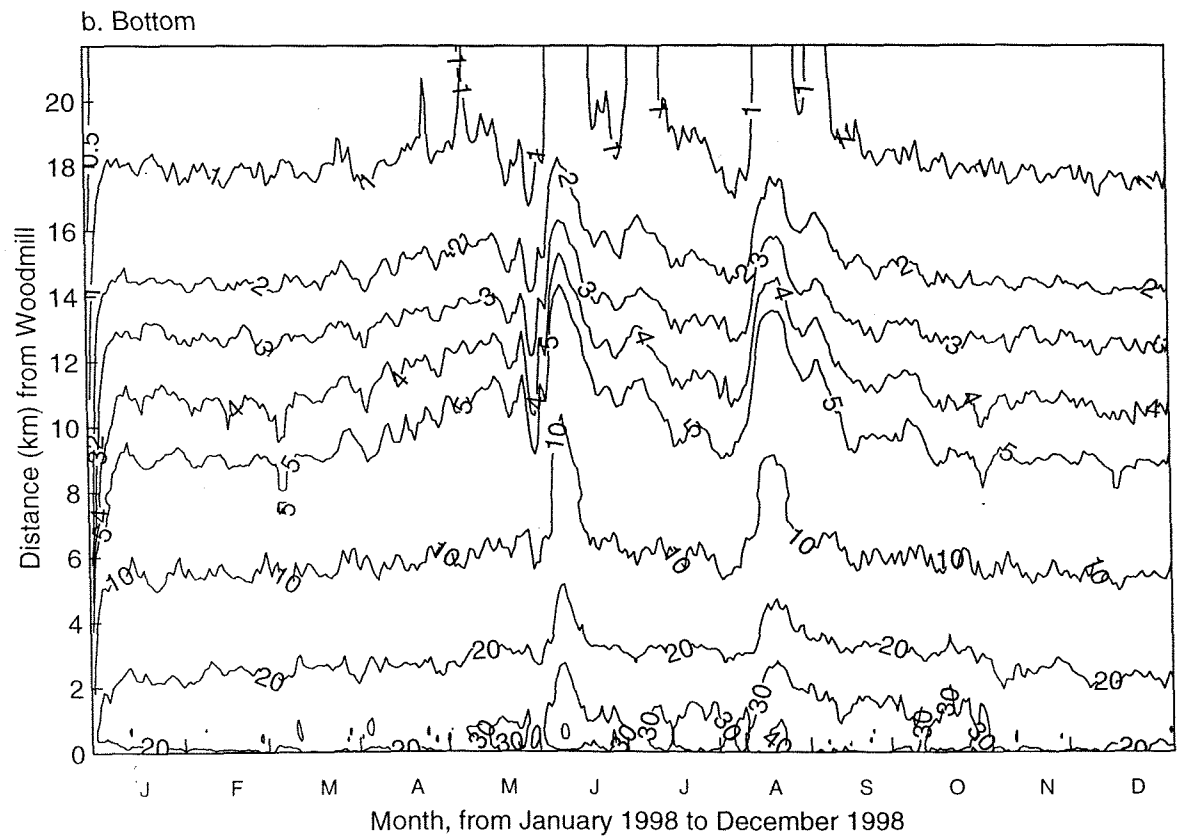

Figure 7.36 Seasonal variation of a) surface and b) bottom nitrate concentration (umol l^{-1}) from integrated model (without sedimentation) in the Itchen Estuary and Southampton Water

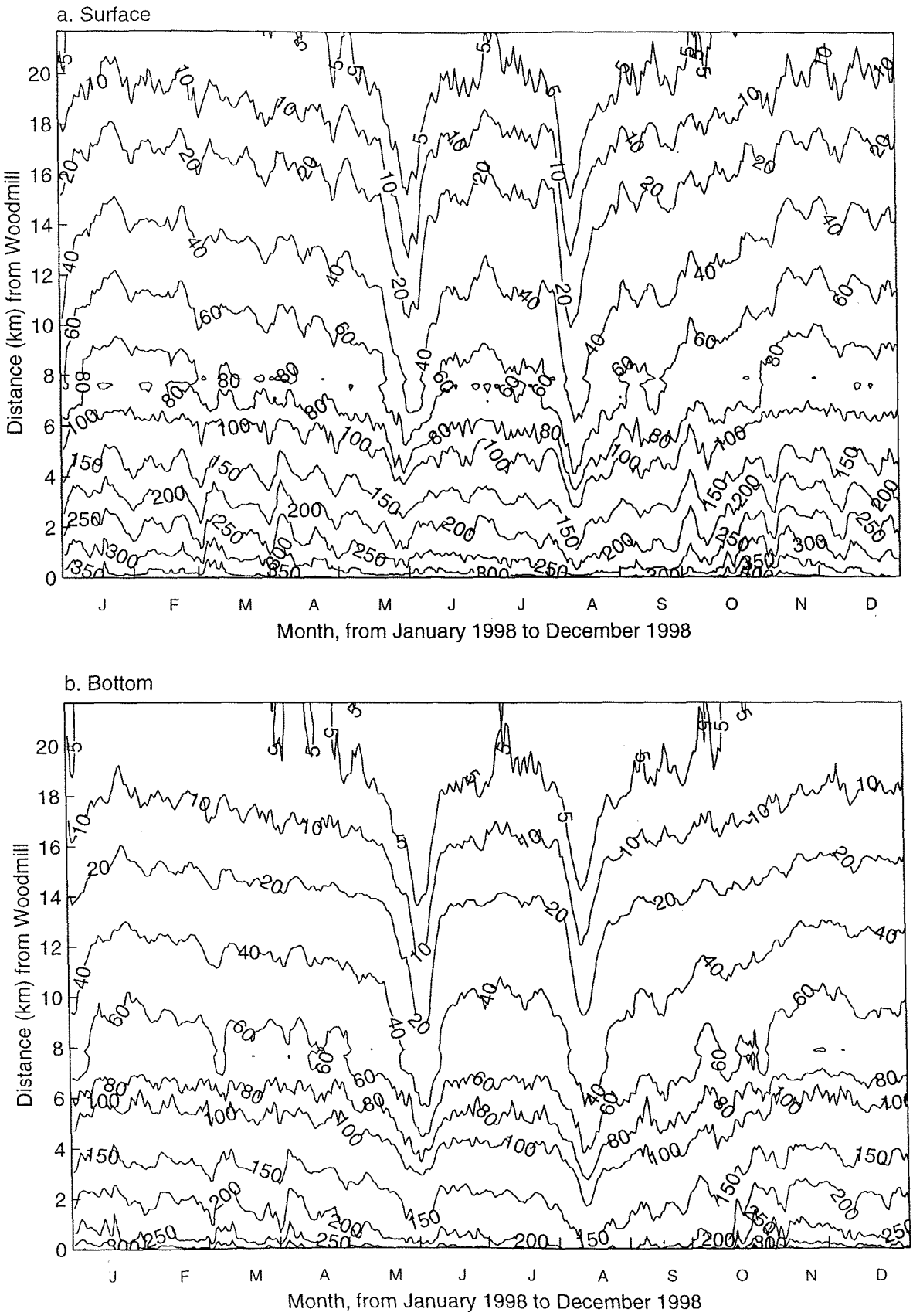

Figure 7.37 Annual variation of the surface nitrate, phosphate concentration at NW Netley and Calshot Buoy: comparison between observations and integrated model (without sedimentation) output

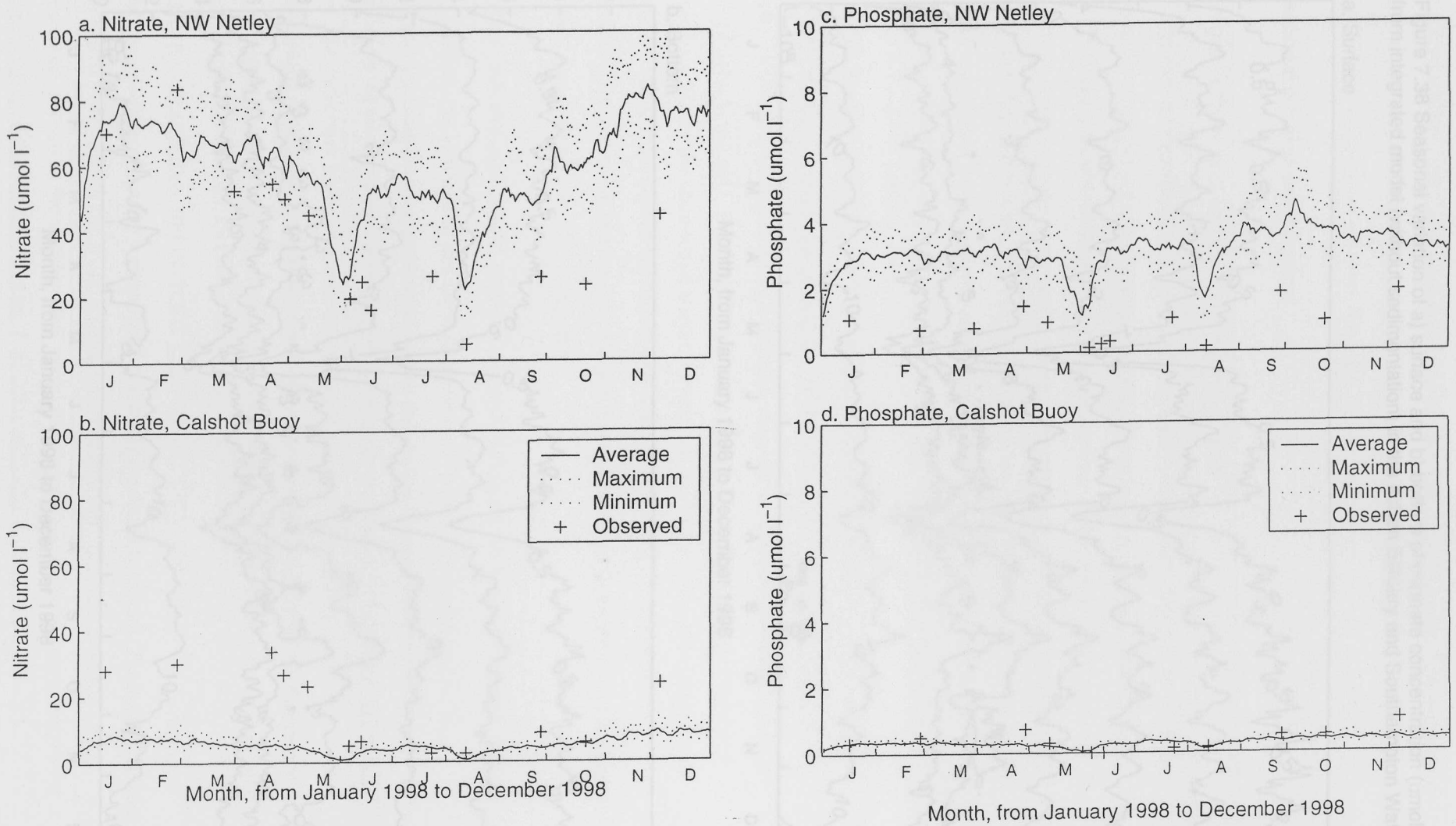

Figure 7.38 Seasonal variation of a) surface and b) bottom phosphate concentration (umol l^{-1}) from integrated model (without sedimentation) in the Itchen Estuary and Southampton Water

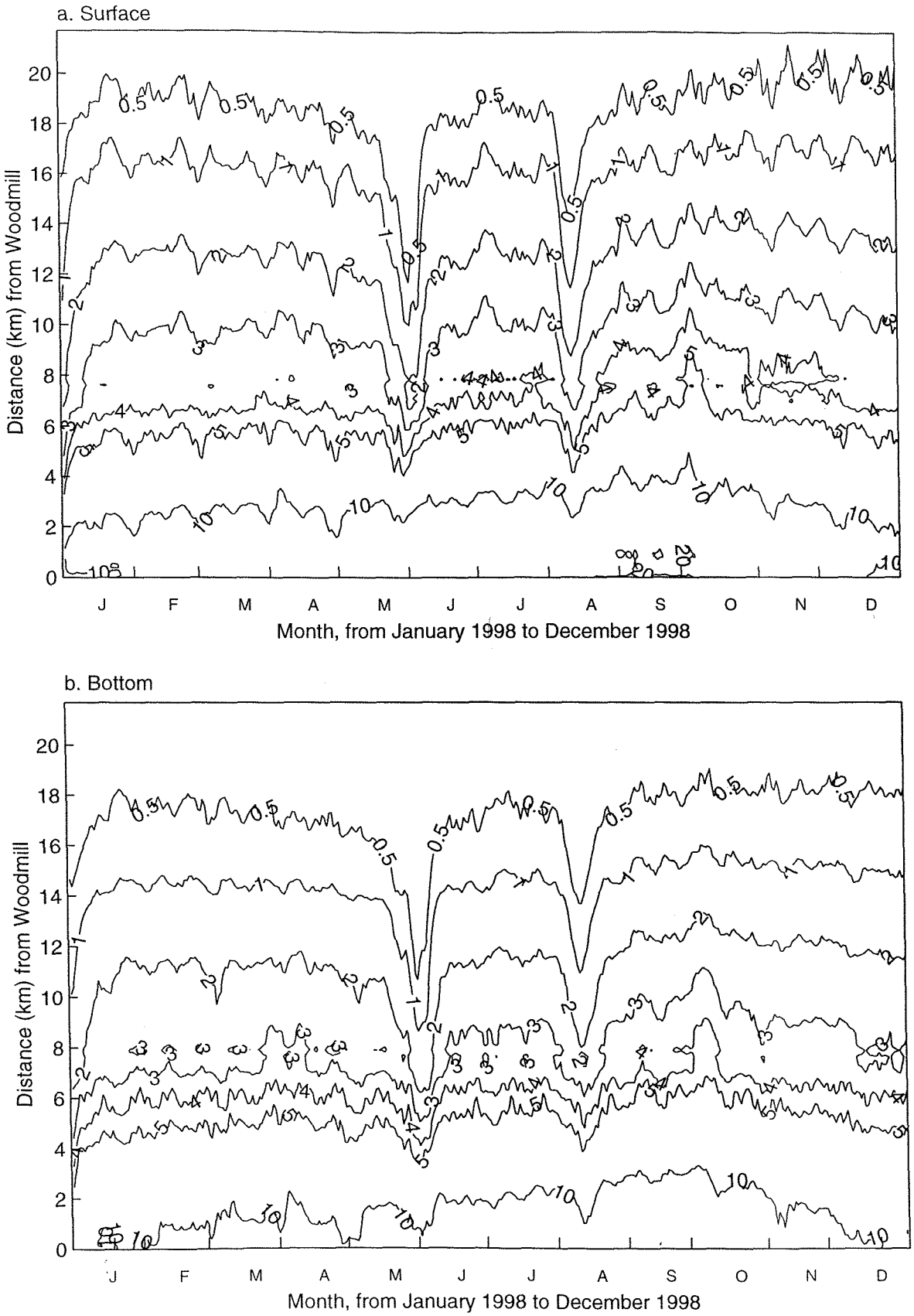

remineralized nutrient, nutrient depletion is more severe (Figure 7.35, Figure 7.36 and Figure 7.38). The model still overestimates the phosphate concentration at NW Netley, and nitrate concentration at Calshot Buoy however (Figure 7.37).

7.5 Discussion and conclusion

7.5.1 Algal carbon and carbon to chlorophyll ratio

The carbon:chlorophyll ratio of the phytoplankton community depends on the light conditions, water temperature, nutrient and individual species. It is reported (Geider, 1987; Geider, 1993) that the carbon:chlorophyll a ratio varies from <0.01 to > 0.1 μg C (μg chl)$^{-1}$ in phytoplankton cultures. In the water quality model developed, an optimal carbon:chlorophyll a ratio (50.0 μg C (μg chl)$^{-1}$) is set. The mechanism in the model, which aims to reduce the diel variation of chlorophyll a concentration due to the sun rise and sun set, does allow the carbon:chlorophyll ratio to change in a very limited range. The carbon:chlorophyll a ratio depends on the specific chlorophyll reproduction rate c_{chl} and the phytoplankton growth rate P. Algal carbon from the model (c_{chl}=0.2 d^{-1}) plotted against the chlorophyll a concentration (Figure 7.39) shows a strong linear correlation (σ^2=0.99) between the algal carbon and chlorophyll a concentration. The linear regression suggests the carbon:chlorophyll a ratio is about 4.92 μmol C (μg chl)$^{-1}$ (equivalent to 59.0 μg C (μg chl)$^{-1}$). From the numerical tests conducted, the higher the chlorophyll a reproduction rate, the higher the carbon:chlorophyll ratio will be. For example, when the chlorophyll reproduction rate c_{chl} is doubled, the carbon:chlorophyll ratio will increase and the new ratio from the linear regression is 5.34 μmol C (μg chl)$^{-1}$ (equivalent to 64.0 μg C (μg chl)$^{-1}$).

7.5.2 Suspended particulate organic matter (detritus) and estuarine circulation

Initially the assumption that the sedimentation of particulate organic matter was necessary in the model caused particulate oxygen demanding organic matter to be trapped in the bottom landward estuarine circulation, and this lead to accumulation in the upper part of the estuary. The extremely high concentration of detrital carbon in the upper estuary, due to the trapping effect of estuarine circulation, results in almost total depletion of DO in this region during the phytoplankton bloom and high remineralization of inorganic nutrients in the water column.

In a partially-mixed estuary like the Itchen Estuary and Southampton Water, where estuarine circulation is well developed, a sophisticated modelling approach is needed. Tuning the descent speed or even switching off the sedimentation processes as was done here produces more realistic model results. In the water quality model developed there is one missing component of the system, the dissolved organic matter. A possible approach is to allow Figure 7.27

Figure 7.39 Algal carbon (umol C/l) plotted against chlorophyll a concentration (ug/l)

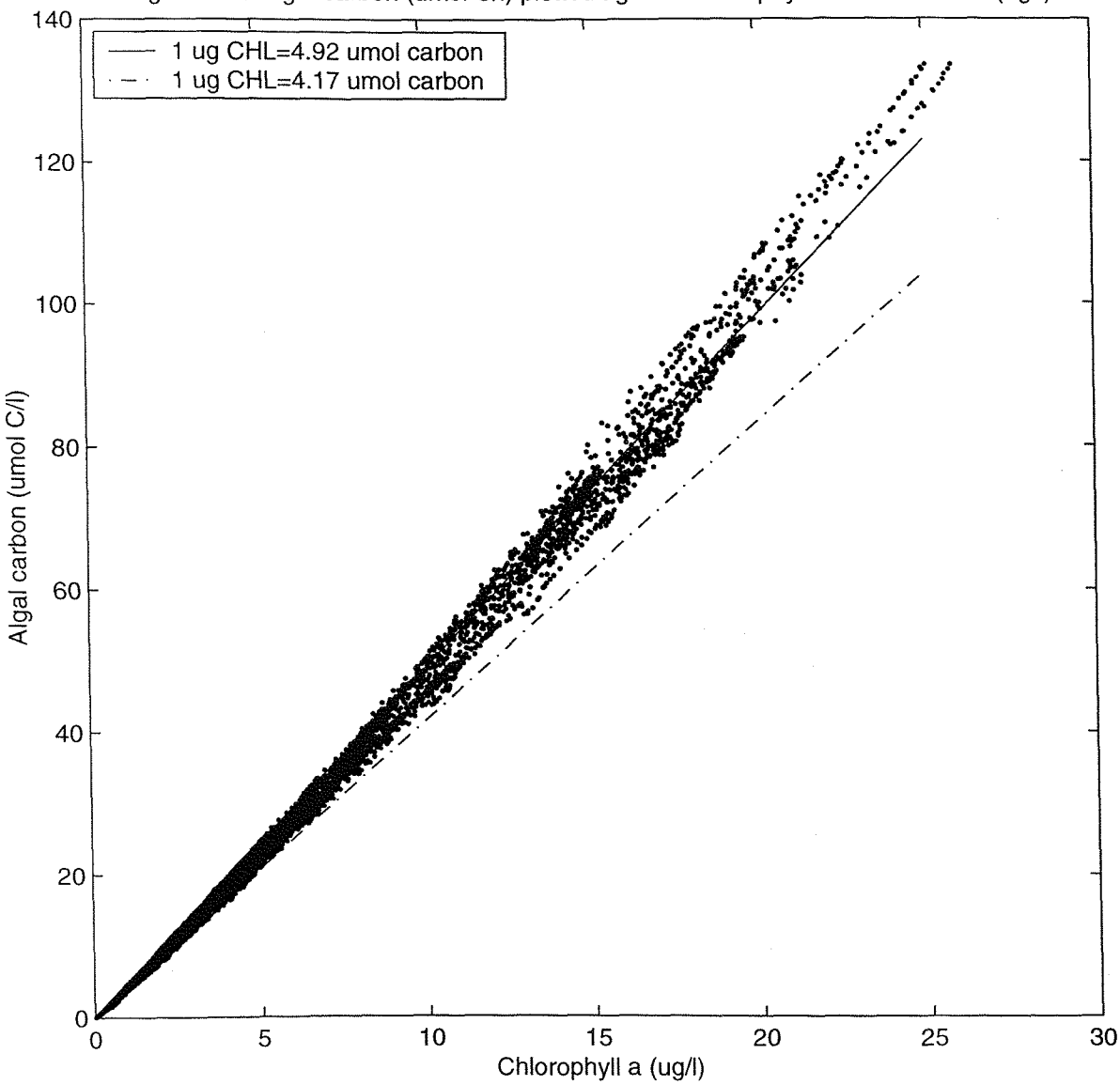

particulate organic matter to be hydrolysed into dissolved organic matter and thus can then escape the trap of estuarine circulation. In addition the model does not include deposition, a processes which may limit the mobility of particulate organic matter. A possible further improvement of the model would be to introduce a sediment layer which allows the deposition of organic matter.

7.5.3 Zooplankton in the model

Zooplankton are not a key factor influencing the balance of phytoplankton dynamics in the model due to the setting of parameters related to zooplankton, although existence of the herbivorous zooplankton will reduce the phytoplankton biomass, and also contribute to the collapse of algal bloom. The main balance in the internal model is the balance among phytoplankton photosynthesis, phytoplankton mortality and phytoplankton respiration.

Since there is a limited zooplankton data for Southampton Water, it is difficult to judge if they are important in controlling phytoplankton dynamics. It is without doubt that when a predator-prey (phytoplankton-herbivore) type model is used to model the seasonal variation of phytoplankton, the model will be very sensitive to the parameters. The highly non-linear interaction of predator-prey (phytoplankton-herbivore) type models causes extremely difficulty in obtaining a reasonable result. Some models (Tett, 1990) did not have the zooplankton as a state variable. Fasham et al. (1994) showed a clear seasonal oscillation of phytoplankton in the Indian Ocean, with the main balance between the phytoplankton photosynthesis and zooplankton. This is probably true for an oceanic station, relatively isolated, but for estuarine and coastal waters, it is less well known.

Further work is needed to better define the role of zooplankton and benthic population in regulating phytoplankton dynamics in Southampton Water.

7.5.4 Conclusion

A 3-D water quality (DO) model, which include both an external model and an internal model, has been developed and has been applied in the Itchen Estuary and Southampton Water. The model has successfully simulated the seasonal variation of the water quality in the Itchen Estuary and Southampton Water. Model results show a reasonable agreement with the observed survey data.

Chapter 8 Discussion and conclusion

8.1 Hydrodynamic model development

8.1.1 Hydraulics in Southampton Water and the Solent estuarine system

The Solent estuarine system includes a number of estuaries along the south coast of England between Poole and Chichester harbours, including the Isle of Wight and Southampton Water. The tides in the Solent estuarine system are dominated by the semi-diurnal M_2 tide. Due to the vicinity of a M_2 tidal node, the tidal regime in the Solent estuarine system is very complex. The Solent estuarine system is relative shallow, and the average water depth is about 20 m. The M_4 and M_6 shallow water constituents, which are generated from the non-linear interaction between the semi-dianual tide constituents propagating from the deep water to shallow water, cause a well known but unusual tidal phenomenon in the Solent including a 'double high water' and other effects to the tides namely, the 'young flood stand' and the short duration of the ebb tide. It was once believed that the unique tidal features in this region are caused by the existence of the two entrances to the Solent around the Isle of Wight. The linear combination of the tidal wave however from different entrances will not generate the shallow wave components. Although the existence of the complex bathymetry in the Solent estuarine system may increase the non-linear interaction of the hydrodynamics to some extent, but it is a minor factor. The modelling work by Townend and his colleague from ABP Research have shown that the 'double high water' and other features will still exist, even if the Isle of Wight was removed from the English Channel (personal communication).

In the Solent, there is prevailing westward tidal induced residual currents from east Solent toward west Solent throughout the year (Dyer & King, 1975), although weather systems may occasionally reverse the direction of the currents.

Since the Solent is a shallow coastal water with a strong tidal currents, the water column tends to be vertically well-mixed. In the absence of a halocline, any vertical stratification caused by surface solar heating will be broken up by vertical turbulence either generated from the tidal induced bottom shear stress or from surface wind stress. In the tributaries of the Solent, where fresh water is discharged from rivers, vertical density stratification will be maintained by the continuous river flow. Southampton Water has been defined (Dyer, 1974) as a partially-mixed estuary, although in the upper Itchen Estuary, water is highly stratified, and at Calshot Buoy well-mixed, where Southampton Water meets the Solent. Solar heating may strengthen the vertical gradient, but is considered to be a minor effect in this region.

8.1.2 The difficulties of Modelling in the Solent estuarine system

Modelling the hydrodynamics in Southampton Water and its tributary estuaries presents following difficulties: 1) the region's complex tidal regime and its unique features; 2) the complex bathymetry, with the scales from hundred km in English Channel to 10's meters in the Itchen Estuary demands a different resolution in different areas. 3) the extensive tidal flats in Southampton Water; 4) the vertical stratification and estuarine circulation adds a third dimension to a horizontal 2-D world.

There are also common concerns in modelling about the mass conservation and upstream scheme which are important in development of a water quality model, but may not be observed in a hydrodynamic model. It could be argued that if a hydrodynamic model is shown to successfully simulate the water movement in Southampton Water, it can be applied to any estuary.

Until now there is no 3-D hydrodynamic model established for the Solent and Southampton Water estuarine system. A 2-D hydrodynamic model developed by Associated British Ports Research (ABP Research) is suitable for tides and tidal current prediction, but obviously it is not appropriate to provide the physical framework for water quality modelling in Southampton Water where the vertical stratification and estuarine circulation is crucial for the pollutants transport and distribution. Sylaios (1994) and HR Wallingford (1995) both have developed independently a similar vertical 2-D hydrodynamic model ignoring the lateral variation across the estuary. These models lack competitiveness and long-term predictive capability, due to the apparent limitation of the vertical 2-D model and their limited prescription of boundary conditions.

8.1.3 The 3-D finite element hydrodynamic model developed

The hydrodynamic model described in Chapter 4 of the thesis was developed from a 2-D finite element hydrodynamic model based on the pioneering work of Wu (1986). The 3-D barotropic model first appeared in 1995 (Shi & Xi, 1995), then in 1996 Shi (1996) introduced a 3-D baroclinic model.

A mass conservation scheme, which is crucial to the success of the further development of the water quality model, has been developed. The upstream mass conservative scheme has replaced a modified characteristic line method. Meanwhile a turbulence closure scheme has been implemented. Although there are different approaches for turbulence closure (Launder & Spalding, 1974; Mellor & Yamada, 1974; Mellor & Yamada, 1982; Luyten, 996; Xing & Davies, 1996), here a level 2.5 two equation Mellor-Yamada q^2-q^2l turbulence closure model (Mellor & Yamada, 1974; Mellor & Yamada, 1982) has been chosen. The model is the quasi-equilibrium version. Deleersnijder & Luyten (1994) have demonstrated the practical advantages

of the quasi-equilibrium version of the Mellor-Yamada level 2.5 turbulence closure which was first modified by Galperin et al. (1988). Finally the model that has been developed is designed to be used in estuaries and coastal waters with a scale from 100s m – 100s km in environment having complex bathymetry, and tides or wind are the dominant force. Beyond this scale the model's competitive ability has not been fully examined. The main characteristic of the modal are:

1) It is three dimensional
2) It is baroclinic
3) It includes dry-wet processes (covering the tidal flats)
4) It uses sigma co-ordinate in vertical
5) It uses a Mellor-Yamada level 2.5 two equation turbulence closure
6) It uses the split mode method
7) It has a mass-conservative upstream scheme for vertical and horizontal advection term and mass conservative scheme for mixing term.

The model as a finite element model however does have two disadvantages:

1) It is expensive on computer time (depend on its application under different circumstance)
2) Data manipulation is relatively difficult compared with conventional finite difference mesh grid

8.1.4 Model results

The hydrodynamic model has been successfully applied to the Solent, Southampton Water, Test Estuary and Itchen Estuary. The model results have been compared against data collected during a field survey campaign and data from other sources. No efforts have been made to tune the model to achieve better results, and the parameters in the hydrodynamic model are all inherited rather than adapted.

The model has successfully simulated the tides and estuarine circulation in the Itchen Estuary and Southampton Water. Tidal induced water exchange at the entrance to Southampton Water from the Solent, water mass transportation, and tidal induced residual currents have also been examined in the estuary.

The seasonal variation of water temperature was not implicitly modelled. Under some circumstance, the modelling of solar heating in the water column is important to predict the vertical stratification and the depth of the thermocline, but this is not important in Southampton Water, a partially mixed estuary. The model underestimated the vertical gradient of salinity in the model, especially when the 3-layer model was used.

8.2 Water quality model development

8.2.1 Overall review of current environmental status of Southampton Water

The surveys conducted during the periods from January 1998 to April 1999 indicated that Southampton Water has few major water quality problems despite the relatively high nutrient concentrations entering the estuary. There was a persistent DO sag in the upper Itchen Estuary throughout the year, but DO % saturation was not detected below 80%, except on one occasion when 64% DO saturation was measured at Northam Bridge. In the lower Itchen Estuary and Southampton Water, the DO concentrations were saturated in the non-phytoplankton growth season, and usually supersaturated during the phytoplankton growth season. No DO depletion was observed following the algal blooms in the Itchen Estuary and Southampton Water in 1998, although pervious researchers (Soulsby et al., 1984; Crawford et al., 1997) have detected DO depletion in the upper Test Estuary and in a semienclosed dock.

In the upper Itchen Estuary, community respiration is dominated by the external input of organic matter, while in the lower Itchen Estuary and Southampton Water, the community respiration rate is dominated by internal autotrophic organic matter. The community respiration rate in the upper Itchen Estuary, maintains a substantial level throughout the year with seasonal variation. In lower Itchen Estuary and Southampton Water, community respiration is generally lower during the non-phytoplankton growth season and increases proportionally to the phytoplankton biomass (chlorophyll a).

The nitrate and silicate data collected during the surveys shows a strong linear correlation (r^2>0.99) with salinity. Phosphate concentration plotted against salinity gives a more scattered distribution due to the sewage effluents discharge. There is little indication of nutrient removal, except in the high salinity (S>30) regions (bulk of Southampton Water) during algal bloom periods.

The algal blooms in Southampton Water are regular events. Usually a spring diatom bloom is followed by a succession of several species dominating the phytoplankton (Kifle & Purdie, 1993) With the most noticeable bloom in summer of *Mesodinium*, which is characterised by a reddish colour. The *Mesodinium* bloom is not toxic, but may have impacts on DO concentration during the summer, especially when the river flow is low. In 1998, two bloom events were observed, a spring diatom bloom on 05/06/98 with maximum chlorophyll concentration of 50 $\mu g\ l^{-1}$, and a summer *Mesodinium* bloom on 12/08/98 with a maximum chlorophyll a concentration of 26 $\mu g\ l^{-1}$.

8.2.2 Water quality (DO) model development

Technically generally the advection-dispersion equation without sink and source term is a water quality model, which describe the conservative distribution of the water quality under the physical processes, mixing and advection. The 3-D hydrodynamic model described in Chapter 4 provided a physical framework for water quality model. Besides the physical processes, Chapter 6 describes chemical and biological processes in the water quality model. The water quality model consists of an external model, which models the impact of external sources of organic matter to the water quality, and an internal model, which models the impact of phytoplankton growth on the water quality.

Unlike the hydrodynamic model which is governed by standardised Navier-Stokes equations, the parameterisation of the water quality model is based on information from the literature (see Appendix 1 and Appendix 2).

8.2.3 Suspended particulate matter (SPM)

Suspended particulate matter (SPM) is the key to water quality modelling in estuaries. In shallow waters, with a strong tidal induced turbulence generated from the bottom current stress and surface wind stress, SPM is brought into the surface layer by turbulence, where it absorbs light and in turn limits algal photosynthesis.

The prediction of the fate of SPM is not easy, because the difficulties of the prescription of the sink and sources terms. The settling velocity will change according to the size, shape and density of the individual particles. It is necessary to classify the SPM into a spectrum defined by its size, shape and density, and to model the SPM separately.

The current work has modelled the particulate organic matter with a uniform settling velocity. Due to lack of observation data, the model does not predict the SPM concentration in the water column. In the model there is no deposition or resuspension of SPM, which is a recognised weakness of the model which needs to be addressed in future work.

8.2.4 Estuarine circulation and its impact on water quality in the estuary

Estuarine circulation results from the baroclinic effects of intersection of density surface with pressure surface, and has a general pattern with a surface seaward flow and bottom landward currents. There are two significant impacts to water quality in the estuary. First, estuarine circulation accelerates the replacement of estuarine water with saltier bottom water. In Southampton Water, the tidal induced Lagrangian residual currents are extremely small, so the water exchange is limited, without the estuarine circulation, except near the entrance to Southampton Water, where the water exchange is more rapid due to the prevailing westward tidal induced residual currents. The water exchange is predominantly affected by the estuarine circulation. The flushing time in the estuary is short, which may limited the impacts of

pollutants. For dissolved oxygen, the bottom saturated water will prevent further deterioration of water quality in the estuary, e.g. when blooms occur.

The second effect of estuarine circulation, is to bring fine particulate suspended matter into the estuary by the landward bottom flow. Finally the fine particulate suspended matter may be trapped near the point where the landward current dwindles, and forms a zone called the 'maximum turbidity zone' with accumulated suspend matter. The accumulation of particulate organic matter may result in the severe depletion of DO.

The following conclusions can be drawn,

1. Estuarine circulation is the main mechanism in a partially-mixed estuary for water transportation.
2. A decrease in the fresh water discharge will reduce the strength of the estuarine circulation, therefore increase the resident time in the estuary. There should be a minimum limit to the fresh water discharge from the estuary, especially in the summer (algal growth, and high temperature therefore high SOD).
3. The deep dredged channel will help the development of the estuarine circulation, by reducing the impact of bottom friction and vertical mixing.
4. Severe DO depletion is more likely to happen in the 'maximum turbidity zone', where the landward current declines.

8.2.5 Sediment oxygen demand (SOD), Bottom boundary layer and sediment layer model

The sediment oxygen demand (SOD) has not been included in the water quality model, because it is very complex in nature and also because of lack of data. Effects of sediment oxygen demand on DO probably are partly compensated for by the high oxygen demand of the particulate matter in the bottom layer of the model.

Sediment processes are very important to the whole community metabolism, in terms of water column oxygen respiration, and the nutrient budget. Free oxygen exchange across the sediment and water column interface has a significant impact on the whole DO budget. Sediment oxygen demand (SOD) has a high variability depending on the temperature, sedimentation etc., and ranges from 10% to 70% of total community respiration. Measurement of SOD normally involves incubation of sediment cores (Rees & Williams, 1982; Rowe & Phoel, 1992; Tahey, 1996) or via the gradient of the DO through the water column (Kemp & Boynton, 1980).

In the Test Estuary, it was estimated (Rees and Williams, 1982) that on average, SOD (using incubation of cores) was about 11% of whole water column respiration. Rees and William (1982) suggested that the DO sag was probably the result of water column respiration rather than sediment respiration. Similarly Soulsby et al. (1984) have modelled some bloom

events in Southampton Water and suggested that oxygen depletion resulted from respiration by the *Mesodinium* ciliate (and presumably bacterioplankton) in the water column, rather than from mass sedimentation of the bloom followed by decomposition.

8.2.6 Comparing different approaches of water quality modelling

In the marine environment there are two influential but different approaches to model ecosystems; one is a nitrogen-based model of the pelagic ecosystem, first described by Fasham et al. (1990); the another developed by Tett (1990), is more relevant to water quality problems in estuarine, and coastal waters. The model developed here has been influenced to some extent by both these approaches. Table 4 gives a comparison of Tett's L3VMF model, and Fasham's nitrogen-based model, and the model developed here.

Table 8.1 Comparison of Tett's L3VMF model, Fasham's nitrogen-based model, and the model developed

	Tett's L3VMF model	Fasham's nitrogen-based model	The model developed (Shi)
phytoplankton	combined	modelled	modelled
planktonic microheterotrophs		modelled	not modelled
zooplankton	implicit grazing pressure	explicitly modelled	explicitly modelled
control of the growth by light and nutrients	threshold-limitation (growth limited either by light or by nutrients)	effects of light limit and nutrient limit multiplied	threshold-limitation (growth limited either by light or by nutrients)
luxury consumption of nutrients	cell-quota approach, allow luxury nutrient consumption	fixed C:N:P:O ratio	fixed C:N:P:O ratio
sediment boundary	consider the bottom boundary flux	upper ocean only	ignore the bottom boundary flux
temporal variation	seasonal	seasonal	diel and seasonal
carbon:chlorophyll ratio	fixed	fixed	changeable

The main reason for using a fixed C:N:P:O ratio in Southampton Water is that the nutrients are usually not a limiting factor to phytoplankton growth, and also the fixed ratio will simplify the model.

8.3 Conclusion and future work

A 3-D finite element baroclinic hydrodynamic model has been developed and successfully applied to Southampton Water and the Solent estuarine system. The Model is able to predict the 3-D currents in estuarine and coastal waters forced by the tides, surface wind stress and baroclinic effects of the density field. A two-equation turbulence closure model has been employed to predict the vertical turbulence mixing coefficients. The 3-D velocity and vertical mixing coefficients in the advection and mixing term water quality model, are provided by the hydrodynamic model, except the horizontal mixing which strongly depends on the model

grid scale and is not explicitly resolved. Temperature prediction has not been implemented at this stage.

A water quality model has been developed and validated using data collected during periods from January 1998 to March 1999. The model was able to simulate the impact of external sources of oxygen demand matter and nutrients to the water quality. A seasonal variation of the water quality impact due to phytoplankton growth was simulated by the internal model. Model results generally agree favourably with the observation.

There are several aspects of the model which could be improved in the future. For the hydrodynamic model, the priority is to predict the water temperature in the model. Inclusion (by parameterisation or coupling in the model) of the wave climate would be another step forward to refining the hydrodynamic model in the near shore region, where waves have a significant impact to the mixing and transport of pollutants. It would also be valuable to quantitatively examine the model performance, to compare the model with other hydrodynamic models used in estuarine and coastal waters, and to evaluate its competitiveness. But for the hydrodynamic model developed itself there really is not much space left for further development.
The main task of the water quality model further development is to develop a sediment layer model which allows the deposition and resuspension of sediment, as well as the chemical and biological processes in the sediment layer, and allow contaminant exchange between the water-sediment interface. A further refinement of the water quality is necessary based on the existing model.

Appendices

Appendix 1 Parameters of the external model

	symbol	description	value	Program name	unit	note
BOD	k_{cs}	Oxygen demanding matter (CES, CPES) degradation rate	5.32×10^{-7}	C12	s^{-1}	HR Warlingford. 1994
	k_{cf}	Oxygen demanding matter (CEF, CPFS) degradation rate	2.66×10^{-6}	C11	s^{-1}	=0.23 d^{-1}, some ref if 0.30 d^{-1} HR Warlingford, 1994
Organic nitrogen	k_{ne}	Organic nitrogen (NE) degradation rate	2.66×10^{-6}	C15	s^{-1}	=0.23 d^{-1}, some ref if 0.30 d^{-1} HR Warlingford, 1994
nitrification	k_{nf}	Nitrification rate	2.66×10^{-6}	Knf	s^{-1}	=0.23 d^{-1} some ref if 0.30 d^{-1} HR Warlingford, 1994
Re-aeration	D_a	Diffusion coefficient of the DO re-aeration on the air-water interface	$D_a = \lambda \frac{(O_{sat} - O)}{O_{sat}}$		mmol O_2 m^{-2} s^{-1}	
	λ	Gas exchange coefficient	$0.5*(1/34)*0.117e^{0.12W10}$		mmol O_2 m^{-2} s^{-1}	Two day, one meter depth water
	W_{10}	Wind speed (m/s) measured on site and converted to a standard height of 10 m with a logarithmic correction.			m s^{-1}	
	O_{sat}	saturation concentration of DO			µmol O_2 l^{-1}	

Appendix 2 Parameters of the internal model

	symbol	description	value	PROGRAM NAME	unit	note
Quanta, energy conversion	Q:W	Energy to quanta conversion rate of solar irradiance (400-700 nm)	2.5×10^{18}~$2.7\ 7\times10^{18}$		Quanta s^{-1} w	Kirk, 1994
Light attenuation	k_0	Irradiance attenuation coefficient $k_0=k_1+k_2+k_3+k_4$		IAC0	m^{-1}	
	k_1	Attenuation coefficient due to sea water, yellowish substances in the sea water and inert particulate matter, $k_1' = k_1 + \alpha_2 SY_s + \alpha_3 SP_i$.			m^{-1}	
	k_2	Light attenuation due to the soluble yellow substance from the fresh water discharge, $k_2' = \alpha_2(\frac{S_b - S}{S_b})(SY_f - SY_s)$			m^{-1}	
	k_3	Light attenuation due to the particulate organic matter, $k_3'=\alpha_3 SP_o$			m^{-1}	
	k_4	Light attenuation due to phytoplankton, $k_4'=\alpha_4 CHL$			m^{-1}	
	α_2	yellow substance absorption coefficient			$m^2\ mg^{-1}$	
	α_{31}	Inert particulate matter absorption coefficient			$m^2\ mg^{-1}$	
	α_{32}	Organic particulate matter absorption coefficient	0.0010	ALPHA32	m^2 (mg C)$^{-1}$	$=\alpha_4/2/r_{cchl}$
	α_4	chlorophyll absorption coefficient	0.0084	ALPHA4	m^2 (mg chl)$^{-1}$	Cullen, 1990
	SP	Particulate suspended matter $SP=SP_i+SP_o$ (they have different specific irradiance absorption rate			$\mu g\ l^{-1}$	

	SP_i	Inert suspended particulate matter			$\mu g\ l^{-1}$	
	SP_o	suspended particulate organic matter, SP_o=CEPS+CEPF+D			$\mu g\ l^{-1}$	
	SY	Soluble yellowish substance $SY=SY_s+SY_f$			$\mu g\ l^{-1}$	
	SY_s	Sea water soluble yellowish substance			$\mu g\ l^{-1}$	
	SY_f	Fresh water soluble yellowish substance			$\mu g\ l^{-1}$	
	S_b	Salinity of sea water (far beyond the fresh water influence)	34.5			
Temporary light attenuation coefficients	k_0+k_{31}		1	IAC031	m^{-1}	Smith, 1997
	$\alpha_2(SY_f-SY_s)$		3	IAC2FS	m^{-1}	Smith, 1997
Photosynthesis rate	ϕ_{max}	Quantum yield	0.074		$\mu mol\ C\ (\mu mol\ quanta)^{-1}$	Cullen, 1990
	P_m	Maximum photosynthesis rate	1.44×10^{-4}	P1MAX	$\mu mol\ C\ (\mu g\ chl)^{-1}\ s^{-1}$	Cullen, 1990
	I_s	Saturation onset parameter	231.5		$\mu mol\ quanta\ m^{-2}\ s^{-1}$	Cullen, 1990
	β	$\beta=(I_s)^{-1}$	0.00432	BETA	$m^2\ s\ (\mu mol\ quanta)^{-1}$	Cullen, 1990
	U_N	Maximum nitrogen uptake rate	2.17×10^{-5}	P2MAX	$\mu mol\ N\ (\mu g\ chl)^{-1}\ s^{-1}$	$=P_m*(16/106)$
	H_{na}	ammonium concentration which allowing half maximum nitrogen uptake rate	0.64	HNA	$\mu mol\ N\ l^{-1}$	$=0.2*H_{nn}$
	H_{nn}	nitrate concentration which allowing half maximum nitrogen uptake rate	3.2	HNN	$\mu mol\ N\ l^{-1}$	$=16*H_{ph}$
	U_P	Maximum phosphate uptake rate	1.36×10^{-6}	P3MAX	$\mu mol\ P\ (\mu g\ chl)^{-1}\ s^{-1}$	$=P_m*(1/106)$
	H_{ph}	phosphate concentration which allowing half maximum phosphate uptake	0.2	HPH	$\mu mol\ P\ l^{-1}$	

Phytoplankton respiration	c_{res}	Specific phytoplankton respiration rate	1.40×10^{-5}	CRES	µmol O_2 (µg chl)$^{-1}$ s^{-1}	=1.206 d^{-1}
Phytoplankton mortality	c_{pmor}	Specific phytoplankton mortality rate	5.79×10^{-7}	CPMOR	s^{-1}	=0.05 d^{-1}
	h_{pmor}	Half-saturation constant for phytoplankton mortality	41.7	HPMOR	µmol C l^{-1}	=10*4.17
Chlorophyll reproduction	r_{cchl}	Optimism carbon chlorophyll ratio (constant)	4.17	RCCHL	µmol C (µg chl)$^{-1}$	=50 µg C (µg chl)$^{-1}$
	r_{chlc}	Optimism chlorophyll carbon ratio (constant)	0.24	RCHLC	µg chl (µmol C)$^{-1}$	
	c_{chl}	Specific chlorophyll reproduction rate	1.16×10^{-5}	CCHLRP	s^{-1}	=1.0 d^{-1}
zooplankton grazing on phytoplankton and detritus	c_{zg}	Specific zooplankton grazing rate	1.16×10^{-5}	CZG	s^{-1}	=1.0 d^{-1}
	p_1	Measure of zooplankton preferences for phytoplankton	0.6	PERF1		
	p_2	Measure of zooplankton preferences for detritus	0.4	PERF2		
	h_{zg}	Half-saturation constant for zooplankton grazing	20.85	HZG	µmol C l^{-1}	=4.17*5
Assimilation (phytoplankton)	c_{za1}	Assimilation rate of zooplankton grazing on phytoplankton Cza1=cza1+	0.3	CZA1	No-dimensional	
Excretion (phytoplankton)	c_{zg1}	Zooplankton excretion coefficient of phytoplankton grazing	0.3	CZG1	No-dimensional	$0<=c_{zg1}<=1-c_{zd1}$
Actual Excretion (phytoplankton)	c_{zg1a}	Actual zooplankton excretion coefficient of phytoplankton grazing, $c_{zg1a}=c_{zg1}\times$oxidiz		CZG1A	No-dimensional	
Digestion (phytoplankton)	c_{zd1}	Zooplankton digestion coefficient of phytoplankton grazing	0.4	CZD1	No-dimensional	$0<=c_{zd1}<=1-c_{zg1}$

Actual Excretion (phytoplankton)	c_{zd1a}	Actual zooplankton digestion coefficient of phytoplankton grazing, $c_{zd1a}=c_{zd1}+c_{zg1}(1\text{-oxidiz})$ $=c_{zd1}+c_{zg1}-c_{zg1a}$		CZD1A	No-dimensional	
Assimilation (detritus)	c_{za2}	Assimilation rate of zooplankton grazing on detritus	0.3	CZA2	No-dimensional	
Excretion (detritus)	c_{zg2}	Zooplankton excretion coefficient of detritus grazing	0.3	CZG2	No-dimensional	$0<=c_{zg2}<=1- c_{zd2}$
Actual Excretion (detritus)	c_{zg2a}	Actual zooplankton excretion coefficient of detritus grazing, $c_{zg2a}=c_{zg2}\times$oxidiz		CZG2A	No-dimensional	
Digestion (detritus)	c_{zd2}	Zooplankton digestion coefficient of detritus grazing	0.4	CZD2	No-dimensional	$0<=c_{zd2}<=1- c_{zg2}$
Actual Excretion (detritus)	c_{zd2a}	Actual zooplankton digestion coefficient of detritus grazing, $c_{zd2a}=c_{zd2}+c_{zg2}(1\text{-oxidiz})$ $=c_{zd2}+c_{zg2}-c_{zg2a}$		CZD2A	No-dimensional	
Zooplankton mortality	c_{zmor}	Zooplankton specific mortality rate	3.47×10^{-6}	CZMOR	s^{-1}	$=0.3\ d^{-1}$
	h_{zmor}	Half-saturation constant for zooplankton mortality	4.17	HZMOR	μmol C l^{-1}	
Detritus decomposition	k_d	Detritus decomposition rate	2.66×10^{-6}	KDCPCO	s^{-1}	$=0.23\ d^{-1}$ some ref if $0.30\ d^{-1}$
Ammonium photosynthetic uptake	r_{na}	Proportion of the ammonia-nitrogen uptake in all nitrogen uptake during photosynthesis	$\frac{NA/h_{na}}{NA/h_{na}+NN/h_{nn}}$	RNAPO	No-dimensional	$0<=r_{na}<=1$
Nitrogen photosynthetic uptake	$1-r_{na}$	Perpetration of the nitrate-nitrogen uptake in all nitrogen uptake during photosynthesis	$\frac{NN/h_{nn}}{NA/h_{na}+NN/h_{nn}}$	RNNPO	No-dimensional	
nitrification	k_{nf}	Nitrification rate	2.66×10^{-6}	KNF	s^{-1}	$=0.23\ d^{-1}$ some ref if $0.30\ d^{-1}$ HR Warlingford, 1994

Oxygen release during phytoplankton (uptake of nitrate nitrogen)	r_{nn}	Ratio of mol free oxygen released from the uptake of nitrate-nitrogen during photosynthesis when 1 mol organic carbon are formed	1.3019	RNNDO	µmol O_2 (µmol C)$^{-1}$	=138/106 Redfield, 1934
Element ratio of the planktonic community	$\frac{N}{CAR}$	Nitrogen carbon ratio	0.1509	NCAR	µmol N (µmol C)$^{-1}$	=16/106 Redfield, 1934
	$\frac{CAR}{N}$	Carbon nitrogen ratio	6.625	CARN	µmol C (µmol N)$^{-1}$	
	$\frac{PH}{CAR}$	Phosphorus carbon ratio	0.0094	PHCAR	µmol P (µmol C)$^{-1}$	=1/106 Redfield, 1934
	$\frac{CAR}{PH}$	Carbon phosphorous ration	106	CARPH	µmol C (µmol P)$^{-1}$	
Oxidisation of organic matter	oxidiz	Specific oxidisation rate of organic matter oxidiz= $\frac{DO^2}{h_{oxid}{}^2+DO^2}$		OXIDIZ	No-dimensional	
	h_{oxid}	The DO concentration which allow the oxidisation rate at half of its maximum	60	HOXID	µmol O_2 l^{-1}	=20% of saturation DO concentration

References

Alvarez-Borrego, S., Guthrie, D., Culberson, C.H. & Park, P.K. 1975 Test of Redfield's model for oxygen relationships using regression analysis. Limnology and Oceanography 20(5), 795-805.

Al-Rasheid, K.A.S. & Sleigh, M.A. 1995 Distribution and abundance of interstitial ciliates in Southampton Water in relation to physicochemical conditions, metal pollution and the availability of food organisms. Estuarine, Coastal and Shelf Science 41, 61-80.

Anning, T. 1995 The expression of photosynthetic genes in natural populations of marine phytoplankton. PhD thesis, University of Southampton.

Awaji, T., Imasato, N. & Kunishi, H. 1980 Tidal exchange through a strait: a numerical experiment using a simple model basin. Journal of Physical Oceanography 10, 1499-1508.

Bach, K. B. & Jensen, J.K. 1994 Modelling of water quality of a proposed impounded lake of a tidally influenced river. Ecological Modelling 74, 77-90.

Barrett, M.J. 1972 The effects of pollution on the Thames estuary. In The estuarine environment (Barnes, R.S.K & Green, J., eds). Applied Science, London, pp. 119-122.

Barrett, M.J. 1978 The Thames model: an assessment. Prog. Wat. Tech. 10, 409-416.

Batelle Columbus Laboratories 1971 Water quality criteria data book, Vol 3. Environmental Protection Agency, Project No. 18050 G.M.V. Contract No. 68-1-0007.

Bender, M., Grande, K., Johnson, K., Marra, J., Williams, P.J.LeB., Sieburth, J., Pilson, M., Langdon, C., Hitchcock, G., Orchardo, J., Hunt, C., Donaghay, P. & Heinemann, K. 1987 A comparison of four methods for determining planktonic community production. Limnology and Oceanography 32(5), 1085-1098.

Bierman, Jr., V.J., Rabalais, N.N., Hinz, S.C., Zhu, D., Turner, R.E. & Wiseman, Jr., W.J. 1994 A preliminary mass balance model of primary productivity and dissolved oxygen in the Mississippi River plume/inner Gulf shelf region. Estuaries 17(4), 886-899.

Billen, G. & Fontigny, A. 1987 Dynamics of a Phaeocystis-dominated spring bloom in Belgian coastal waters. II. Bacterioplankton dynamics. Marine Ecology Progress Series 37(2/3), 249-257.

Billen, G. & Lancelot, C. 1988 Modelling benthic nitrogen cycling in temperate coastal ecosystems. In Nitrogen cycling in coastal marine environments (Blackburn, T.H. & Sorensen, J., eds). pp. 341-378.

Blain, W.R. 1980 Tidal hydraulics of the west Solent. PhD Thesis, University of Southampton, V1:326pp, V2:362pp, V3:374pp.

Blumberg, A.F. & Mellor, G.L. 1987 A descriotion of a three-dimensional coastal ocean circulation model. In: Three-dimensional coastal ocean models (Heaps, N., ed.). American Geophysical Union, New York, NY.

Blumberg, A.F. 1992 A primer for ECOM-si. HydroQual, Inc., Mahwah, NJ, 64pp.

Bowden, K.F. 1967 Circulation and diffusion. In Estuaries (Lauff, G.H., ed.). pp. 15-36.

Bowden, K.F. 1980 Physical factors: salinity, temperature, circulation, and mixing processes. In Cghemistry and Biogeochemistry of Estuaries (Olausson, E. & Cato, I., eds). pp. 37-70.

Boynton, W.R. & Kemp, W.M. 1985. Nutrient regeneration and oxygen consumption by sediments along estuarine salinity gradient. Marine Ecology Progress Series 23, 45-55

Brosnan, T.M. & O'Shea, M.L. 1996 Long-term improvement in water quality due to sewage abatement in the lower Hudson River. Estuaries 19(4), 890-900.

Bryan, J.R. 1979 The production and decomposition of organic material in an estuary-Southampton Water. PhD thesis, Southampton University.

Cammen, L.M. 1991 Annual bacterial production in relation to benthic microalgal production and sediment oxygen uptake in an intertidal sandflat and an intertidal mudflat. Marine Ecology Progress Series 71, 13-25.

Chaudhury, R.R., Sobrinho, J.A.H., Wright, R.M. & Sreenivas, M. 1998 Dissolved oxygen modelling of the Blackstone River (Northeastern United States). Water Research 32(8), 2400-2412.

Chen, C.W. & Orlob, G.T. 1972 Ecological simulation for aquatic environments. Report OWRR C-2044, WRE 1-0500, US Department of the Interior, Washington DC.

Cheng, R.T., Feng, S. & Xi, P. 1986 On Lagrangian residual ellipse. In Physics of Shallow Estuaries and Bays (van de Kreeke, ed.). J. Spring-verlag, pp. 102-113.

Clark, R.B., Frid, C. & Attrill, M. 1997 Marine pollution. Clerendon Press, Oxford, UK.

Collins, K.J. 1978 The fluxes of organic material and nutrients in Southampton Water. PhD thesis, Department of Oceanography, University of Southampton.

Commission of European Communities 1991 Urban waste Water Treatment Directive. Official journal of the European Communities L135.

Conley, D.J. & malone, T.C. 1992 Annual cycle of dissolved silicate in Chesapeake Bay: implications for production and fate of phytoplankton biomass. Marine Ecology Progress Series 81, 121-128.
Conley, D.J., Schelske, C.L. & Stoermer, E.F. 1993 Modification of the biogeochemical cycle of silica with eutrophication. Marine Ecology Progress Series 101, 179-192.
Conley, D.J. 1997 Riverine contribution of biogenic silica to the oceanic silica budget. Limnology and Oceanography 42(4), 774-777.
Crawford, D. W. & Prudie, D.A. 1992 Red tide: Recurrent red-water in Southampton Water. NERC News, January 25-27.
Crawford, D. W. & Prudie, D.A. 1992 Recurrent red-tides in Southampton Water (abstract). ECSA Bulletin 10, 18-19.
Crawford, D.W., Purdie, D.A., Lockwood, A.P.M., Weissman, P. 1997 Recurrent Red-tide in the Southampton Water Estuary caused by the phototrophic cilicate Mesodinium rubrum. Estuarine, Coastal and Shelf Science 45, 799-812.
Cullen, J.J. 1990 On models of growth and photosynthesis in phytoplankton. Deep-Sea Research 37(4), 667-683.
Dauer, D.M., Rodi, Jr., A.J. & Ranasinghe, J.A. 1992 Effects of low dissolved oxygen events on the macrobenthos of the lower Chesapeake Bay. Estuaries 15(3), 384-391.
D'Avanzo, C. & Kremer, J.N. 1994 Diel oxygen dynamics and anoxic events in an eutrophic estuary of Waquoit Bay, Massachusetts. Estuaries 17(1b), 131-139.
D'Avanzo, C., Kremer, J.N. & Wainright, S.C. 1996 Ecosystem production and respiration in response to eutrophication in shallow temperate estuaries. Marine Ecology Progress Series 141, 263-274.
Day, J.H. 1979 Estuarine sediments, salinities and temperatures. In Estuarine Ecology (Day, J.H., ed.). A.A.B. Publishers, Rotterdam, Netherlands.
Delgadillo-Hinojosa, F., Gaxiola-Castro, G., Segovia-Zavala, J.A., Munoz-barbosa, A. & Orozco-Borbon, M.V. 1997 The effect of vertical mixing on primary production in a bay of the Gulf of California. Estuarine, Costal and Shelf Science 45, 135-148.
de Souza Lima, H. & Williams, P.J. leB. 1978 Oxygen consumption by the plankton population of an estuary-Southampton Water. Estuarine and Coastal Marine Science 6, 515-521.
Deleersnijder, E. & Luyten, P. 1994 On the pratical advantages of the quasi-equilibrium version of the Meller and yamada level 2.5 turbulence closure applied to marine modelling. Appl. Math. Modelling 18, 281-287.
de Swart, H.E., de Jonge, V.N. & Vosbeek, M. 1997 Application of the tidal random walk model to caculate water dispersion coeffcients in the Ems Estuary. Estuarine, Costal and Shelf Science 45, 123-133.
DiToro, D.M., O'Conner, D.J. & Thomann, R.V. 1971 A dynamic model of the phytoplankton population in the Scaramento-SanJoaquin Delta. In Nonequilibrium systems in Natural Water Chemistry. American Chemical Society, Washington DC.
Dobbins, W.E. 1964 BOD and oxygen relationships in streams. J. Sanit. Eng. Div. Amer. Soc. Civil Eng. 90, 53-78
Doering, P.H., Oviatt, C.A. Beatty, L.L., Banzon, V.F., Rice, R., Kelly, S.P., Sullivan, B.K. & Frithsen, J.B. 1989 Structure and function in a model coastal ecosystem: solicon, the benthos and eutrophication. Marine Ecology Progress Series 52, 287-299.
Dortch, Q. & Whitledge, T.E. 1992 Does nitrogen or silicon limit phytoplankton production in the Mississipi River plume and nearby regions. Cont. Shelf Res. 12, 1293-1309.
Dortch, Q., Rabalais, N.N., Turner, R.E. & Rowe, G.T. 1994 Respiration rates and hypoxia on the Louisiana Shelf. Estuaries 17(4), 862-872.
Dybern, B.I. 1972 Pollution in the Baltic. In Marine pollution and sea life (Ruivo, M., ed.). FAO, London, UK.
Dyer, K.R. 1973 Estuaries: a physical introduction. John Wiley & Sons, London.
Dyer, K.R. & Taylor, P.A. 1973 A simple, segmented prism model of tidal mixing in well-mixed estuaries. Estuarine and Coastal Marine Science , 411-418.
Dyer, K.R. 1974 The salt balance in stratified estuaries. Estuarine and Coastal Marine Science 2, 273-281.
Dyer, K.R. & King, H.L. 1975 The residual water flow through the Solent, south England. Geophys. J. R. Astr. Soc. 42, 97-106.
Dyer, K.R. 1981 The measurement of fluxes and flushing times in estuaries. In River inputs to ocean systems (Martin, J.M., Burton, J.D. & Eisma, D., eds). UNEP/UNESCO, Paris, pp. 67-76.
Dyer, K.R. 1982 Localized mixing of low salinity patched in partially-mixed estuary (Southampton Water, England). In Estuarine Comparisons (Kennedy, V.S, ed). Academic Press, London.
Egge, J.K. & Aksnes, D.L. 1992 silicate as regulating nutrent in phytoplankton competition. Marine Ecology Progress Series 83, 281-289.

Elliott, A.J., Barr, A.G. & Kennan, D. 1997 Diffusion in Irish coastal waters. Estuarine, Costal and Shelf Science 44(supplement A), 15-23.
Eppley, R. W. 1972 Temperature and phytoplankton growth in the sea. Fishery Bulletin 70, 1063-1085.
Falkowski, P.G. 1981 Light-shade adaptation in marine phytoplankton. In Primary prductivitive in the sea (Falkowski, P.G., ed.). Plenum, New York.
Fasham, M.J.R. et al. 1990 A nitrogen-based model of plankton dynamics in the oceanic mixed layer. J. Mar. Res. 48, 591-639.
Fasham, M.J.R. 1993 Modelling the marine biota. In The global carbon cycle (Heimann, M., ed.). pp. 457-503.
Feng, S. 1986 A three-dimensional weakly nonlinear dynamics on tide-induced Lagrangian residual current and mass-transport. Chinese Journal of Oceanology and Limnology 4(2), 139-158.
Feng, S. 1990 On the Lagrangian residual velocity and the mass-transport in a multi-frequency oscillatory system. In: Residual current and long-term transport (Cheng, R.T., ed.).
Field, C.B., Behrenfeld, M.J., randerson, J.T.. & Falkowski, P. 1998 Primary Production of the Biosphere: Integrating terrestrial and oceanic components. Science 281, 237-240.
Fleming, R. H. 1940 The composition of plankton and units for reporting population and production. Proc. 6th Pafic Sci. Cong. Calif. 3, pp. 535-540.
Galperin, B., Kantha, L.H., Hassid, S. & Rosati, A. 1988 A qusi-equilibrium turbulent energy model for geophysical flows. J. Atmos. Sci. 45, 55-62.
Gameson, ALH, Barrett, MJ & Shewbridge J.S. 1973 Advances in Water Pollution Research 6, 843-850.
Gameson, ALH, Barrett, MJ & Shewbridge J.S. 1975 The aerobic Thames Estuary. In Advances in Water Pollution research (6th Int Conf Jerusalem, June 8-23 1972) (Jenkins, S.H., ed.). Pergamon Press, Oxford, pp. 843-852.
Garber, J.H. 1984 Laboratory study of nitrogen and phosphorus remineralization during decomposition of coastal plankton and seston. Estuarine, Coastal and Shelf Science 18, 685-702.
Garcia, C.A.E., Purdie, D.A. & Robinson, I.S. 1993 Mapping a bloom of the phtosynthetic ciliate Mesodinium rubrum in an estuary from airborne thematic mapper data. Estuarine, Coastal and Shelf Science 37, 287-298.
Garcia, V.M.T. & Purdie, D.A. 1992 The influence of irradiance on growth, photosynthesis and respiration of Gyrodinium cf. aureolum. Journal of Plankton Research 14, 1251-1265.
Garcia, V.M.T. & Purdie, D.A. 1994 Primary production studies during a Gyrodinium cf. aureolum (Dinophyceae) bloom in the western English Channel. Marine Biology 119, 297-305.
Geodigest 1999 The Solent River and how it Disappeared. Geology Today 15(4), 137-138.
GESAMP (GESAMP Working Group Bo. 25 on Coastal Modelling) 1992 A conceptual model of contaminant transport in coastal marine systems. Ambio 21(2), 166-169.
Grenier, Jr., R.R. & Luettich, Jr., R.A. 1996 The influence of turbulance closure strategy on numerical modeling of shallow water tides. In Estuarine and Costal Modeling (Cheng, R.T., ed.). pp.143-155.
Grenney, W.J., Bella, D.A. & Curl, H.C. Jr. 1973 A mathematical model of the nutrient dynamics of phytoplankton in a nitrate-limited environment. Biotechnology and Bioengineering 15, 331-358
Hays, G. 1988 The distribution of ichthyoplankton and ctenophores in Southampton Water: the effect of a Mesodinium bloom. BSc. 3rd Year Project Report, Department of Oceanography, University of Southampton, UK, 127 pp.
Hartman, B. & Hammond D.E. 1985 Gas exchange in San Francisco Bay. Hydrobiologia 129, 59-68.
Hawkins, SJ & Zhai, X. 1999 Recovery and restoration of marine ecosystems. In Wastewater treatment and disposal in coastal areas (Dempsey, P., Xi, P. & Hawkins, S.J., eds). Qingdao, China.
Head. P.C. 1976 Estuarine Chemistry (J. D. Burton and P. S Liss eds). Academic Press, London, 224 pp.
Harrison, W.G., Platt, T. & Lewis, R. 1985 The utility of light-saturation models for estimating marine primary productivity in the field: a comparison with conventional 'simulated' in situ methods. Canadian Journal of Fishery and Aquatic Science 42, 864-872.
Head, P.C. 1985 Data presentation and interpretation. In Practical estuarine chemistry (Head, P.C., ed.). Cambridge University Press, Cambridge, pp. 278-330.
Hecky, R.E. & Vollenweider, R.A. 1988 Nutrient limitation of phytoplankton in freshwater and marine environments: a review of recent evidence on the effects of enrichment. Limnology and Oceanography 33, 796-822.
HMSO 1980 Dissolved oxygen in natural and waste waters. In Methods for the examination of waters and associated materials. Her majesty's Stationery Office, London.
Holligan, P.M., Williams, P.J.leB., Purdie, D.A. & Harris, R.P. 1984 Photosynthesis, respiration and nitrogen supply of plankton populations in stratified, frontal and tidally mixed shelf waters. Marine Ecology Progress Series 17, 201-213.

Horstman, D.A. 1981 Reported red-water outbreaks and their effects on fauna on the west and south coasts of South Africa, 1959-1980. Fisheries Bulletin, Sea Fisheries Institute, Republic of South Africa 15, 71-88.

Howard, A. G., Comber, S., Kifle, D., Antai, E.E. & Purdie, D.A. 1994 Arsenic speciation and seasonal changes in nutrient availability and micro-plankton abundance in Southampton Water, UK. Estuarine, Coastal an Shelf Science 40(4), 435-450.

Howell, P. & Simpson, D. 1994 Abundance of Marine resources in relation to dissolved oxygen in Long Island Sound. Estuaries 17(2), 394-402.

HR Wallingford 1995 Southampton Water and associated estuaries. HR Wallingford Report EX 3253, UK.

Huthnance, J. M. et al. 1993 Towards water quality models. Phil. Trans. R. Soc. London A343, 569-584.

Iriarte, A., Daneri, G., Garcia, V.M.T., Purdie, D.A. & Crawford, D.W. 1991 Plankton community respiration and its relationship to chlorophyll a concentration in marine coastal waters. Oceanologica Acta 14(4), 379-388.

Iriarte, A. 1991 Picophytoplankton: ecological and physiological studies in culture and in natural coastal estuarine waters. PhD thesis, University of Southampton.

Iriarte, A. 1993 Size-fractioned chlorophyll a biomass and picoplankton cell density along a longitudinal axis of a temperate estuary (Southampton Water). Journal of Plankton Research 15(5), 485-500.

Jensen, L.M., Sand-Jensen, K., Marcher, S. & Hansen, M. 1990 Plankton community respiration along a nutrient gradient in a shallow Danish estuary. Marine Ecology Progress Series 61, 75-88.

Johnson, K.M., King, A.E. & Sieburth, J.McN. 1985 Coulometric TCO_2 analyses for marine studies; an introduction. Marine Chemistry 16, 61-82.

Johannesen, T. & Dahl, E. 1996 Declines in oxygen concentrations along the Norwegian Skagerrak coast, 1923-1993 - a signal of ecosystem changes due to eutrophication. Limnology and Oceanography 41(4), 766-778.

Justic, D. 1987 Long-term eutrophication of the Northern Adriatic Sea. Marine Pollution Bulletin 18, 281-284.

Justic, D. 1995 Stoichiometric nutrient balance and origin of coastal eutrophication. Marine Pollution Bulletin 30, 41-46

Justic, D. 1997 When do phytoplankton blooms cause the most intense hypoxia in the northern Adriatic Sea. Oceanologica Acta 20(1), 91-99.

Kawamiya, M., et al. 1995 An ecological-physical coupled model applied to station Papa. Journal of Oceanography 51, 635-664.

Kawamiya, M., et al. 1996 Causes and consequences of spring phytoplankton blooms in Otsuchi Bay, Japan. Estuarine, Coastal and Shelf Science.

Kemp, W.M. & Boynton, W.R. 1980 Influence of biological and physical progresses on dissolved oxygen dynamics in an estuarine system: implications for measurement of community metabolism. Estuarine and Coastal Marine Science 11, 407-431.

Kemp, W.M., Sampou, P.A., Garber, J., Tuttle, J. & Boynton, W.R. 1992 Seasonal depletion of oxygen from bottom waters from Chesapeake Bay: roles of benthic and planktonic respiration and physical exchange processes. Marine Ecology Progress Series 85, 137-152.

Kenney, B.E., Litaker, W., Duke, C.S. & Ramus, J. 1988. Community oxygen metabolism in a shallow tidal estuary. Estuarine, Coastal and Shelf Science 27, 33-43.

Kerr, S.R. & Ryder, R.A. 1993 Effects of culture eutrophication on coastal marine fisheries: a comparative approach. In Marine Coastal Eutrophication: The response of marine transitional systems to human impacts; problems and perspectives for restoration (Vollenweider, R.A., Marchetti, R. & Viviani, R., eds). Science of the Total Environment, Supplement, Elsevier, Amsterdam, pp. 599-614.

Ketchum, H.B. 1951 The exchange of fresh and salt water in tidal estuaries. Journal of Marine Research 10, 18-38.

Kifle, D. 1992 Seasonal and spatial variations in species composition, aboundance, biomass and primary production of phytoplankton in Southampton Water. PhD Thesis, University of Southampton, 309 pp.

Kifle, D. & Purdie, D.A. 1993 The seasonal aboundance of the phototrophic cilicate Mesodinium rubrum in Southampton Water, England. Journal of Plankton research 15, 823-833.

Kilham, P. 1971 A hypothesis concerning silica and the freshwater plankton diatoms. Lomnology and Oceanography 16, 10-18.

Kirk, J.T.O. 1988 Solar heating of water bodies as influenced by their inherent optical properties. Journal of Geophysical Research 93(D90), 10897-10908.

Kirk, J.T.O. 1994 Light and photosynthesis in aquatic ecosystems (2nd ed). Cambridge, UK.

Kovio, A.J. & Phillips, G.R. 1971 Identification of mathematical models for DO and BOD concentrations in polluted streams from noise-corrupted measurements. Water Resources Research 7(4), 853-862.
Kovio, A.J. & Phillips, G.R. 1972 On determination of BOD and parameters in polluted stream models from DO measurements only. Water Resources Research 8(2), 478-486.
Kraines, S., Suzuki, Y., Yamada, K. & Komiyama, H. 1996 Separating biological and physical changes in dissolved oxygen concentration in a coral reef. Limnology and Oceanography 41(8), 1790-1799.
Krause-Jensen, D. & Sand-Jensen, K. 1998 Light attenuation and photosynthesis of aquatic plant communities. Limnology and Oceanography 43(3), 396-407.
Kuhn, W. & Radach, G. 1997 A one-dimensional physical-biological model study of the pelagic nitrogen cycling during the spring bloom in the northern North Sea (FLEX '76). Journal of Marine Research 55, 687-734.
Kuo, A.Y. & Neilson, B.J. 1987 Hypoxia and salinity in Virginia estuaries. Estuaries 10, 277-283.
Kuo, A.Y., Park, K. & Moustafa, M.Z. 1991 Spatial and temporal variabilities of hypoxia in the Rappahannock River, Virginia. Estuaries 14(2), 113-121.
Kuo, A.Y. & Park, K. 1995 A framework for coupling shoals and shallow embayments with main channels in numerical modelling of coastal plain estuaries, 18(2), 341-350.
Kwabe, M. & Kawabe, M. 1997 Temporal and spatial characteristics of chemical oxygen demand in Tokyo Bay. Journal of Oceanography 53, 19-26.
Kwabe, M. & Kawabe, M. 1997 Factors determining chemical oxygen demand in Tokyo Bay. Journal of Oceanography 53, 443-453.
Launder, B.E. & Spalding, D.B. 1974 Comp. Methods Appl. Mech. Eng. 3, p269.
Pomeroy, L.R. & Beibel, D. 1986 Temperature regulation of bacterial activity during the spring bloom in Newfoundland coastal waters. Science 233, 359-361.
Linker, L. 1996 Models of the Chesapeake Bay. Sea Technology, September, 49-55.
Liss, P.S. 1973 progress of gas exchange across an air-water interface. Deep-Sea Research 20, 221-238.
Longuet-Higgins, M.S. 1969 On the transportation of mass by time-varying ocean currents. Deep-Sea Research 16, 31-47.
Lorenzen, C.J. 1967 Determination of chlorophyll and pheopigments: Spectrophotometric equations. Limnology and Oceanography 12, 343-346.
Lynch, D.R. and Werner, F.E. Three-dimensional hydrodynamics on Finite elements, part II: non-linear time-stepping model. Int. J. Numer. Methods Fluids 12, 507-534.
Luyten P.J. et al., 1996 Presentation of a family of turbulence closure models for stratified shallow water flows and preliminary application to the Rhine outflow region. Continental Shelf Research 16(1), 101-130.
Malakoff, D. 1998 Death by suffocation in the Gaulf of Mexico. Science 281(10), 190-192.
Marino, P. & Howarth, R.W. 1993 Atmospheric oxygen exchange in the Hudson River: dome measurements and comparison with other natural waters. Estuaries 3(3A), 433-445.
McClelland, J.W., Valiela, I. & Michener, R.H. 1997 Nitrogen-stable isotope signatures in estuarine food webs: A record of increasing urbanisation in coastal watersheds. Limnology and Oceanography 42(5), 930-937.
Mellor G.L. and Yamada, T. 1974 A hierarchy of turbulence closure models for planetary boundary layers. J. Atmos. Sci. 31, 1791-1806.
Mellor G.L., and Yamada, T. 1982. Development of a turbulence closure model for geophysical fluid problems. Review of Geophysics and Space Physics 20, 851-875.
Mill, D.K. & Tett, P.B. 1990 Use of a recording fluorometer for continuous measurement of phytoplankton concentration. Environment and Pollution Measurement Sensors and Systems 1269, 106/SPIE.
Munekage, Y. & Kimura, H. 1990 Estimation of tidal exchange and dissolved oxygen balance in Uranouchi Bay using a two-layer box model. Coastal Engineering in Japan 33(1), 101-111.
Munekage, Y. & Kimura, H. 1992 Application of a two-layer box model to dissolved oxygen budget in Uranouchi Bay using. Coastal Enginnering in Japan 35(1), 129-145.
Munekage, Y. 1995 Studies on bottom water exchange and dissolved oxygen (DO) budget due to water intrusion in Uranouchi Bay using. Coastal Engineering in Japan 38(1), 129-145.
Murphy, J. & Riley, J.P. 1962 A modified single solution method for determinations of phosphate in nature waters. Anal. Chim. Acta 27, 31-36.
National Rivers Authority 1995 The Mersey Estuary: a report on environmental quality. Bristol, UK.
Nixon, S.W., Kelly, J.R., Oviatt, C.A. & Hale, S.S. 1976 Nitrogen regeneration and the metabolism of coastal marine bottom communities. In The role of terrestrial and aquatic organisms in

decomposition processes (the 17th Symposium of the British Ecological Society) (Anderson, J.M. & MacFadden, A., eds). Blackwell, Oxford, pp. 219-242.
Nixon, S.W., Kelly, J.R., Oviatt, C.A. & Hale, S.S. 1980 Phosphorus regeneration and the metabolism of coastal marine bottom communities. In Marine benthic dynamics. University of South Carolina Press, Columbia, S.C., pp. 219-242.
Nixon, S.W. 1981 Remineralization and nutrient cycling in coastal marine ecosystem. In Estuaries and nurtrients (Neilson, B.J. & Cronin, L.E., eds). Humana Press, Clifton, N.J., pp. 111-138.
Nixon, S.W. 1995 Coastal marine eutrophication: a definition, social causes, and future concerns. Ophelia 41, 199-219.
Nogueira, E., Perez, F.F., Rios, A.F. 1997 Modelling thermohaline properties in an estuarine upwelling ecosystem (Ria de Vigo: NW Spain) using box-Jenkins transfer function models. Estuarine, Coastal and Shelf Science 44, 685-702.
O'Connor, D.J. 1960 Oxygen balance of an estuary. Transaction of the American Society for Civil Engineers, Journal of the Sanitation Engineering Division 86, 35-54
O'Connor, D.J. 1967 The temporal and spatial distribution of dissolved oxygen in streams. Water Resources Research 3(1), 65-79.
O'Connor, D.J., Thomann, R.V. & DiToro, D.M. 1973 Dynamic water quality forecasting and management. EPA-660/3-73-009, 201, EPA, Washington DC.
Officer, C.B. & Ryther, J.H. 1980 Impact of nutrient enrichment on water uses. In Estuaries and nutrients (Neilson, B.J. & Cronin, L.E., eds). Human Press, Clifton, NJ, pp. 247-261.
Officer, C.B., Biggs, R.B., Taft, J.L., Cronin, L.E., Tyler, M.A. & Boynton, W.R. 1984 Chesapeake Bay anoxia: origin, development and significance. Science 223, 22-27.
Olson, D.B., Hitchcock, G.L., Fine, R.A. & Warren, B.A. 1993 Maintenance of the low-oxygen layer in the central Arabian Sea. Deep-Sea Research 40(3), 673-685.
Park, K., Kuo, A.Y. & Neilson, B.J. 1996 A numerical study of hypoxia in the tidal Rappahannock River of Chesapeake Bay. Estuarine, Coastal and Shelf Science 42(5), 563-581.
Parker, C.A. & O'Reilly, J.E. 1991 Oxygen depletion in Long Island Sound: a historical perspective. Estuaries 14(3), 248-264.
Parsons, T.R., Maita, Y. & Lalli, C.M. 1984 A manual of chemical and biological methods for seawater analysis (3rd ed). Pergamon Press, Oxford, 173 pp.
Pietri, F. 1998 The impact of primary production on nutrient concentrations in Southampton Water. M.Sc. dissertation, University of Southampton.
Platt, T. et al. 1980 Photoinhibition of photosynthesis in natural assemblages of marine phytoplankton. Journal of Marine Research 38, 687-701.
Platt, T. 1981 Primary production of the ocean water column as a function of surface light intensity: algorithms for remote sensing. Deep-Sea Research 33, 149-163.
Platt, T. 1983 Remote sensing of phytoplankton in the sea: surface layer chlorophyll as an estimate of water column chlorophyll and primary production. International Journal of Remote Sensing 4, 343-351.
Pomeroy, L.R., Sheldon, J.E., Sheldon Jr., W.M. & Peters, F. 1995 Limits to growth and respiration of bacterioplankton in the Gulf of Mexico. Marine Ecology Progress Series 117, 259-268.
Prandle, D. 1986 Generalised theory of estuarine dynamics. In: Physics of shallow estuaries and bays (J. van de Kreeke, ed.), pp.42-57
Pritchard, D.W. 1989 Estuarine classification - a help or a hindrance. In Estuarine circulation (B.J.Neilson, B.J., Kuo, A. & Brubaker, eds). Humana Press, Clifton, NJ.
Prober, R., Haimes, Y.Y., Teraguchi, M. & Modd, W.H. 1972 Ecosystem model of lake algal blooms. Water-1971, American Chemical Engineering Symposium Series 68(124), 402-412.
Pugh, D.T. 1987 Tides, surges and mean sea-level: a handbook for engineers and scientists. John Wiley & Sons, Chichester, 472pp.
Rabalais, N., Wiseman Jr., W.J. & Turner, R.E. 1994 Comparison of Continuous records of near-bottom dissolved oxygen from the hypoxia zone along the Louisiana coast. Estuaries 17(4), 850-861.
Rabalais, N., Wiseman Jr., W.J., Turner, R.E., Justic, D., Sen Gupta, B.K. & Dortch Q. 1996 Nutrient changes in the Mississippi River and system responses on the adjacent continental shelf. Estuaries 19(2b), 386-407.
Raine, R.C.T. 1985 The effect of nitrogen supply on the photosynthetic quotient of natural phytoplankton assemblages. Bot. Mar. 26, 417-423.
Rajar, R., Cetina, M & Sirca, A. 1997 Hydrodynamic and water quality modelling: case studies. Ecological Modelling 101, 209-228.

Redfield, A.C. 1934 On the proportions of organic derivatives in seawater and their relation to the composition of plankton. In James Johnstone Memorial Volume. University Press, Liverpool, pp. 176-192.
Redfield, A.C., Ketchum, B.H. & Richards, F.A. 1963 The influence of organisms on the composition of sea water. In The Sea (Vol. 2) (Hill, M.N., ed.). Interscience Publishes, London.
Rees, T.A.V., & Williams, P.J. leB. 1982 The role of phytoplankton in the Test Estuary (Report to the Southampton Water Authority). University of Southampton.
Richards, F.A. 1965. Chemical Oceanography, vol(1) (Riley, J.P. & Skirrow, G., eds). Academic Press, London, 508 pp.
Riley, J.P. & Skirrow, G. (eds) 1975 Chemical Oceanography, vol(1). Academic Press, London, pp. 561-562.
Rosenberg, R., Elmgren, R., Fleischer, S., Jonsson, P., Persson, G. & Dahlin, H. 1990 Marine eutrophication case studies in Sweden: a synopsis. Ambio 19, 102-108.
Roson, G., Alvarez-Salgado, A. & Perez, F. 1997 A non-stationary box model to determine residual fluxes in a partially mixed estuary, based on both thermohaline properties: application to the Ria de Arousa (NW Spain). Estuarine, Coastal and Shelf Science 44, 249-262.
Rowe, G.T. & Phoel, W.C. 1992 Nutrient regeneration and oxygen demand in Bering Sea continental shelf sediments. Continental Shelf Research 12(4), 439-449.
Rykiel, E.J. 1996 testing ecological models; the meaning of validation. Ecological Modelling 90, 229-244.
Ryther, J.H. 1956 Photosynthesis in the ocean as a function of light intensity. Limnology and Oceanography 1, 61-70.
Ryther, J.H. & Yentsch, C.S. 1957 The estimation of phytoplankton production in the ocean from chlorophyll and light data. Limnology and Oceanography 2, 281-286.
Ryther, J.H. & Dunstan, W.M. 1971 Nitrogen, phosphorus and eutrophication in the coastal marine environment. Science 171, 1008-1013.
Ryther, J.H. & Officer, C.B. 1980 The possible importance of silicon in marine eutrophication. Mar. Ecol. Prog. Ser. 3, 83-91.
Sakshaug, E., Kiefer, D.A. & Andresen, K. 1989 A steady state description of growth and light absorption in the marine planktonic diatom Skeletonema Costatum. Limnology and Oceanography 34, 198-205.
Sampou, P. & Kemp, W.M. 1994 Factors regulating plankton community respiration in Chesapeake Bay. Marine Ecology Progress Series 110, 249-258.
Sand-Jensen, K., Jensen, L.M., Marcher, S. & Hansen, M. 1990 Pelagic metabolism in eutrophic coastal waters during a late summer period. Marine Ecology Progress Series 65, 63-72.
Sarokin, D. & Schulkin, J. 1992 The role of pollution in large scale population disturbances, Part 1: Aquatic population. Environmental Science and Technology 26, 1477-1484
Schelske, C.L. & Stoermer, E.F. 1971 Eutrophication, silica depletion, and predicted changes in algal quality in Lake Michgen. Science 173, 423-424.
Schelske, C.L. & Stoermer, E.F. 1972 Phosphorus, silica and eutrophication in Lake Michgen. In Nutrients and eutrophication (Likens, G.E., ed.). Am. Soc. Limnol. Oceanogr., Lawrence, KS, pp. 157-171.
Schindler, D. 1977 Evolution of phosphorus limitation in lakes. Science 195, 260-262.
Shi, L. 1996 A three-dimensional baroclinic model for estuarine and coastal waters. Journal of Ocean University of Qingdao 34, 13-25.
Shi, L. & Xi, P. 1995 A hybrid method of fractional steps for numerical solution of three-dimensional hydrodynamic equations. Journal of Ocean University of Qingdao 25(2), 167-172.
Smith, J.C. 1997 Investigation into spatial distribution of SPM in Southampton Water Estuarine system & effects of turbidity on light attenuation. BSc Dissertation, University of Southampton.
Song, Y. and Haidvogel, D. 1994 A semi-implicit ocean circulation model using a generalized topography-following coordinate system. Journal of Computational Physics 115, 2428-2441.
Soulsby, P. G. et al. 1984 The role of phytoplankton in the dissolved oxygen budget of a stratified estuary. Wat. Sci. & Tech. 17, 745-756
Stanley, D.W. & Nixon, S.W. 1992 Stratification and bottom-water hypoxia in the Pamlico River Estuary. Estuaries 15(3), 270-281.
Steele, J.H. & Baird, I.E. 1962 Further relations between primary production, chlorophyll, and particulate carbon. Limnology and Oceanography 7, 42-47.
Stigebrandt, A. & Wulff, F. 1987 A model of dynamics of nutrients and oxygen in the Baltic proper. Journal of Marine Research 45, 729-759.

Strain, P.M., Wildish, D.J. & yeats, P.A. 1995 The application of simple models of nutrients loading and oxygen demand to the management of a marine tidal inlet. Marine Pollution Bulltein 30(4), 253-261.

Streeter, H.W. & Phelps, E.B. 1925 A study of the pollution and natural purification of the Ohio River. Bulletin 146, US Public Health Service, Washington DC.

Sylaios, G. 1994 A numerical investigation into the dynamics of a partially-mixed estuary. PhD thesis, Department of Oceanography, University of Southampton.

Sylaios, G. & Boxall, S. 1998 Residual currents and flux estimates in a partially-mixed estuary. Estuarine, Coastal and Shelf Science 46(5), 671-682

Taft, J.L., Taylor, W.R., Hartwig, E.O. & Loftus, R. 1980 Seasonal oxygen depletion in Chesapeake Bay. Estuaries 3, 242-247

Tahey, T.M., Duineveld, G.C.A., De Wilde, P., Berghuis, E.M. & Kok, A. 1996 Sediment O2 demand, density and biomass of the benthos and phyopigments along the northwestern Adriatic coast: the extent of Po enrichment. Oceanologica Acta 19(2), 117-130.

Tett, P. & Droop, M.R. 1988 Cell quota models and planktonic primary production. In Handbook of laboratory model systems for microbial ecosystem, Vol. 2 (Wimpenny, J.W.T., ed.). CRC, Florida, pp. 177-233.

Tett, P. 1990 A three layer vertical and microbiological processes model for shelf seas, UK Proudman Oceanographic Laboratory Report No. 14, 85 pp.

Tett, P. & Walne, A. 1994 Observation and simulations of hydrography, nutrients and plankton in the southern North Sea. Ophelia 42, 371-416

Thomas, F., Garcon, V. & Minster, J.F. 1990 Modelling the seasonal cycle of dissolved oxygen in the upper ocean at Ocean Weather Station P. Deep-Sea Research 37(3), 463-491.

Tilman, D., Kilham, S.S. & Kilham, P. 1982 Phytoplankton community ecology: the role of limiting nutrients. A. Rev. Ecol. Syst. 13, 349-372.

UNESCO 1973 International Oceanographic Tables, Vol(2). National Institute of Oceanography/UNESCO, Paris.

Velegrakis, A.F., Dix, J.K. & Collins, M.B. 1999 Late Quaternary evolution of the upper reaches of Solent River, Southern England, based upon marine geophysical evidence. Journal of the Geological Society 156(1), 73-87.

Vollenweider, R.A., Marchetti, R. & Vivani, R. (eds) 1993 Marine Coastal Eutrophication: The response of marine systems to human impact; problems and perspectives for restoration. Science of the Total Environment, supplement, Elsevier, Amsterdam.

Vollenweider, R.A. 1993 Coastal marine eutrophication: principles and control. In: Marine Coastal Eutrophication: The response of marine systems to human impact; problems and perspectives for restoration, eds: Vollenweider, R.A., Marchetti, R. & Vivani, R. Science of the Total Environment, supplement, Elsevier, Amsterdam: 1-20

Wanninkhof, R. 1992 Relationship between wind speed and gas exchange over the ocean. J. of Geophys. Res. 97(c5), 7373-7382.

Webber, N.B. 1973 The tidal hydraulics of the Solent and its estuaries. In Pollution criteria for estuaries (Helliwell, P.R. & Bossanyi, J., eds). Pentech Press, London.

Webber, N.B. 1980 Hydrography and water circulation in the Solent. Natural Environment Research Council Publication Series C 22, 25-35.

Weiss, R. F., 1970 The solubility of nitrogen, oxygen and argon in water and sea water. Deep-Sea Research 17, 721-735.

Wells, N.C. 1996 Ocean modelling. OC316 Tutorial Box, University of Soutmapton.

Welsh, B.L. & Eller, F.C. 1991 Meechanisms controlling summertime oxygen depletion in western Long Island Sound. Estuaries 14(3), 265-278.

Westwood, I.J. 1982 Mixing and dispersion in Southampton Water. PhD thesis, University of Southampton.

Williams, P.J.leB., Raine, R.C., Bryan, J.R. 1979 Agreement between the ^{14}C and oxygen methods of measuring phytoplankton production: reassessment of the photosynthetic quotient. Oceanologica Acta 2, 411-416.

Wiiliams, P.J.leB. 1981 Microbial contribution to overall marine plankton metabolism: direct measurements of respiration. Oceanologica ACTA 4(3), 359-364.

Williams, P.J.leB. & Jenkinson, N.W. 1982 A transportable Microprocessor-controlled precise Winkler titration suitable for station and shipboard use. Limnology and Oceanography 27, 576-585.

Williams, P.J.leB., Heinemann, K.R., Marra, J. & Purdie, D.A. 1983 Phytoplankton production in oligotrophic waters: measurements by the ^{14}C and oxygen technique. Nature 305, 49-50

Williams, P.J.leB. 1984 A review of measurements of respiration rates of marine plankton populations. In Heterotrophic activity in sea (Hobbie, J.E. & Williams, P.J.leB., eds). Plenum Press, New York, pp. 357-389.

Wilson, R.E. 1988 Dynamics of partially mixed estuaries. In: Hydrodynamics of estuaries (vol. I): estuarine physics (Kjerfve, B., ed.). CRC Press, Florida, pp 1-16.

Wright, P.N. & Hydes, D.J. 1997 Report on the methods used over the duration of the Southern nutrients (SONUS) Project. Southampton Oceanography Centre.

Wu, J. 1986 Computational fluid dynamics, its theory, method and application. Scientific Press, Beijing, 293 pp.

Xing J. and Davies A.M. 1996 Application of a range of turbulence energy models to the determination of M-four tidal current profiles. Continental Shelf Research 16(4), 517-547.

Yallop, M.L. & Williams, P.J.Leb. 1979. Mathematical sub-model for photosynthesis in the Medway estuary, Kent. Report to the Water Research Centre.

SOUTHAMPTON UNIVERSITY LIBRARY

USER'S DECLARATION

AUTHOR: SHI, LEI TITLE: DEVELOPMENT AND APPLICATION OF A THREE-DIMENSIONAL WATER QUALITY MODEL IN A PARTIALLY-MIXED ESTUARY, SOUTHAMPTON WATER, UK DATE: 2000

To be signed by each user of this thesis

DATE	SIGNATURE	ADDRESS